

Wavelet analysis in the field of coastal engineering

Applications in time series analysis

T.J.P. de Rooij

Delft University of Technology, Deltares

Wavelet analysis in the field of coastal engineering

Applications in time series analysis

by

T.J.P. de Rooij

A master thesis submitted in partial fulfilment
of the requirements for the degree of

Master of Science

in Applied Mathematics

at the Delft University of Technology,

to be defended publicly on Monday October 30, 2017 at 16:00.

Student number 4077903
Specialisation Computational Science and Engineering
Project duration February 1, 2017 – October 31, 2017

Thesis committee	Prof. dr. ir. C. Vuik,	TU Delft, Professor of Numerical Analysis, supervisor
	Prof. dr. ir. A.W. Heemink	TU Delft, Professor of Mathematical Physics
	Ir. J. Kramer,	Deltares, dep. of Coastal Structures and Waves, supervisor
	Ir. A. Capel,	Deltares, dep. of Coastal Structures and Waves

An electronic version of this thesis is available at <http://repository.tudelft.nl/>

Abstract

Time-frequency analysis and digital signal processing are both important tools in the field of coastal engineering. For both, analysts from this field experience a threshold to use wavelet analysis instead of their current methods. This is due to the lack of guidelines in the many choices accompanied by applying wavelets. The continuous wavelet transform is most used for time-frequency analysis. The range of signals that can be analysed more accurately has been increased by adding different signal extension methods and a method to deal with missing data points, based on the wavelets mass distribution. This allows more accurate energy distribution analysis of much more signals than in the Fourier domain. The continuous wavelet coefficients can also be used in separating incident and reflected waves. They outperform current methods based on Fourier coefficients [62] for cases with a changing mean water level. On the other hand, the discrete wavelet transform is mostly deployed in digital signal processing. Due to the wide variety of wavelets and thresholding methods, filtering in the discrete wavelet domain results in better separation of signal elements such as noise and transients for signals that behave non-stationary, like measurements of impacts. Different algorithms to determine the thresholds used in filters have been tested. The soft applied universal threshold was the most effective of the compared algorithm in filtering noise from a non-stationary signal. Wavelet analysis offers many signal processing opportunities due to the wide range of wavelets that can be chosen from.

Preface

Acknowledgements

T.J.P. de Rooij
Delft, October 23, 2017

List of Figures

1.1	Content thesis	2
2.1	Schematic representation of the four different analyses of a signal	6
2.2	Depiction of the fast wavelet transform	11
2.3	Overview of continuous wavelets	12
2.4	Overview of discrete wavelets	12
2.5	Different types of thresholding	17
2.6	Content thesis and research questions	21
3.1	Demonstration 3.1; down-sampling	26
3.2	Signal extension methods for different signals	28
3.3	Demonstration 3.2; effect of missing data points on spectrum	30
3.4	Demonstration 3.4, 3.5, 3.3; evolution from cone of influence to zones of influence	32
3.5	Demonstration 3.6; accuracy of the zones of influence	34
3.6	Measurement set-up in a flume	35
3.7	Effect of placement of gauges on $\sin(k\Delta x)$	37
4.1	Different filter algorithms	47
4.1	Different filter algorithms	49
4.2	Demonstration 4.1; a signal and its decomposition	50
4.3	Demonstration 4.2; coefficients and thresholds	51
5.1	WPS of water height measurements from the Westerschelde	58
5.2	WPS of deviation of water level at first gauge	59
5.3	Cross-wavelet analysis	60
5.4	Residual analysis	62
5.5	Filtered force signal	63
5.6	Haar wavelet reconstruction	64
5.7	Transient filtering	65

List of Tables

2.1	Comparative summary of the Fourier, wavelet and Hilbert-Huang transform	19
3.1	Demonstration 3.7; set-up of measurement gauges	40

Contents

Abstract	iii
Preface	v
List of Figures	vii
List of Tables	vii
Contents	ix
Abbreviations, symbols and maths	xi
1 Introduction	1
1.1 Research	2
1.2 Overview	2
2 Background	3
2.1 Time Series and Signal Analysis	3
2.1.1 Time Series	3
2.1.2 Signal Analysis	4
2.2 Fourier Analysis.	6
2.2.1 Continuous Fourier Transform.	7
2.2.2 From Continuous to Discrete	7
2.2.3 Short Term Fourier Transform	8
2.3 Wavelet Analysis	9
2.3.1 Continuous Wavelet Transform for Discrete Signals	9
2.3.2 Discrete Wavelet Transform	10
2.3.3 Wavelets	11
2.4 Time-frequency Analysis using Fourier and Wavelet Coefficients	13
2.4.1 Amplitude	13
2.4.2 Phase	14
2.4.3 Averaging Wavelet Coefficients.	14
2.4.4 Cross Spectral Information.	14
2.4.5 Coherence	15
2.5 Digital Signal Processing	16
2.5.1 Filters	16
2.5.2 Elements of a Signal	17
2.5.3 Other techniques	18
2.6 Coastal Engineering Challenges.	20
2.6.1 Research questions	21
3 Continuous Wavelet Transform	23
3.1 Expansion.	23
3.1.1 Down-sampling	24
3.1.2 Wavelet Coefficients near the Boundaries	26
3.1.3 Missing Data Points	28
3.1.4 Wavelet Mass Distribution	30
3.2 Separation of Incident and Reflected Waves (2D)	35
3.2.1 Gauge Distance and Wavenumber	36
3.2.2 Expanding to N Gauges	37
3.2.3 Error Analysis and Reduction	39
3.2.4 Linearity, stationarity and noise	42
3.2.5 Residual signal analysis	44

3.3 Guidelines	45
4 Discrete Wavelet Transform	47
4.1 Filter Algorithms	47
4.1.1 Implementation	48
4.2 Test Signals	48
4.2.1 Different wavelets	52
4.2.2 Signal Extension Modes	52
4.2.3 Different Dilation Factor	52
4.3 Results	53
4.3.1 Low Pass Filter and DWD Algorithms	53
4.3.2 Wavelet comparison	53
4.3.3 Discussion	54
4.4 Recommendations Noise Filters	54
5 Added Value of Wavelet Analysis	57
5.1 Spectral Information	57
5.1.1 Missing Data Points	57
5.1.2 Continuous Wavelet Coefficients.	58
5.2 Discrete Wavelet Decomposition Filtering	63
5.3 Computation	65
5.4 Discussion	66
6 Conclusion and Recommendations	67
6.1 Conclusions.	67
6.2 Recommendations and Future Research	69
List of Demonstrations	71
Bibliography	73
Appendices	A1
A MSc thesis assignment	A3
B Fourier transforms	A5
C Sampling theory	A7
D Multi resolution analysis	A11
E Wavelets	A27
F Separation of incident and reflected waves	A31
G Filter results	A51
H Compare techniques	A67

Abbreviations, symbols and maths

List of abbreviations

Abbreviation	Definition	Explanation
CFT	Continuous Fourier Transform	Section 2.2.1
CWT	Continuous Wavelet Transform	Section 2.3.1
COI	Cone of Influence	Page 26
DCWT	Discretised Continuous Wavelet Transform	Equation 2.20
DFT	Discrete Fourier Transform	Section 2.2.2
DTFT	Discrete Time Fourier Transform	Section 2.2.2
DTWT	Discrete Time Wavelet Transform	Equation 2.19
DSP	Digital Signal Processing	Page 16
DWD	Discrete Wavelet Decomposition	Page 10
DWT	Discrete Wavelet Transform	Page 10
FA	Fourier Analysis	Section 2.2
FFT	Fast Fourier Transform	Page 8
flop	Floating Point Operation	Section 5.3
FT	Fourier Transform	Section 2.2.1
FWT	Fast Wavelet Transform	Section 2.3.2
GWN	Gaussian White Noise	Section 2.5
GWS	Global Wavelet Spectrum	Section 2.4.3
ICWT	Inverse Continuous Wavelet Transform	Section 2.3.1
IDWT	Inverse Discrete Wavelet Transform	Section 2.3.2
IFFT	Inverse Fast Fourier Transform	Section 2.2.3
ISTFT	Inverse Short Term Fourier Transform	Section 2.2.3
MAD	Median of Absolute Deviation	
MRA	Multi Resolution Analysis	Appendix D
PSD	Power spectral density	Section 2.2.2
PSR	Peak-to-sum ratio	Equation 4.1
SAWP	Scale Averaged Wavelet Power	Section 2.4.3
SNR	Signal-to-noise ratio	Equation 2.37
std	Standard deviation	Equation 3
STFT	Short Term Fourier Transform	Equation 2.16
WA	Wavelet Analysis	Section 2.3
WC	Wavelet Coherence	Section 2.4.5
WES	Wavelet Energy Spectrum	Equation 2.28
WFT	Windowed Fourier Transform	Section 2.2.3
WPS	Wavelet Power Spectrum	Equation 2.27
XWT	Cross Wavelet Transform	Section 2.4.4
ZOI	Zones of Influence	Section 3.1.3

List of symbols

Symbol	Explanation
Capital	Fourier or Wavelet Transform of signal, e.g. $X(\omega)$, $X(a, b)$
Bold	A vector, e.g. $\mathbf{x} = \{x_j\}_{j=0, \dots, N-1}$
a	Scale parameter in continuous wavelet domain
a_i	i^{th} level of approximation coefficients (Discrete Wavelet Transform)

Symbol	Explanation
A	Set of scales for the DCWT
b	Translation parameters in continuous wavelet domain
$C_{a,j}$	Separation coefficient at scale a and gauge j
d_i	i^{th} level of detail coefficients (Discrete Wavelet Transform)
dB	Decibel: $10 \log_{10}(\cdot)$
f	Frequency variable [Hz = s^{-1}]
f_s	Sampling frequency [Hz]
f_N	Nyquist frequency [Hz], i.e. $f_N = f_s/2$
f_ψ	Wavelets centre frequency [Hz], $f_\psi = 1/\lambda_\psi$
g	Gravitational acceleration parameter [m/s^2]
h	Water depth parameter [m]
$H(x)$	Heaviside Step function (see (13))
i	$i^2 = -1$, imaginary unit
j, ℓ, m, p	Integer variables
k	Wave number [1/m] (see Section F.1)
n	Discrete time variable
N	Maximum length of discrete variable
m	Unit for meters
rad	radians
t	Time variable [s]
s	Unit for seconds
S	Sparsity based on PSR
$S()$	Smoothing operator
$S_{xx}^f(\omega)$	Energy spectral density (ESD) of $x(t)$ $^2/\text{Hz}$
$S_{xx}^w(a, b)$	Wavelet energy spectrum (WES) of $x(t)$ $^2/\text{Hz}$
w	Wavelet coefficient in discrete wavelet domain
$W(a, b)$	Wavelet coefficient in continuous wavelet domain, can be function of scale a and translation b
W^{xy}	Cross wavelet transform (XWT) of signals x and y
$x(t)$	Signal function in continuous time
$x[n]$	Signal function in discrete time
$\delta(x)$	Delta Dirac function (see equation 11)
δ_{ij}	Kronecker delta function (see equation 12)
γ_{xy}^2	Coherence between signal x and y (2.31)
Δt	Sampling interval [s]
Δx	Spacing difference [m]
ϵ	Residual
$\zeta(t)$	Analytic wave function, i.e. $\text{Re}(\zeta(t)) = \eta(t)$
$\eta(t)$	Real wave function
$\theta(t)$	Phase, can be function or constant [rad]
θ_{xy}	Phase difference between signal x and y (??)
$\kappa(t)$	Scale Averaged Wavelet Power, SAWP
λ	Wave length [m]
λ_ψ	Equivalent wavelength of wavelet, $\lambda_\psi = 1/f_\psi$; linear relationship scale a : $\lambda_{\psi_a} = a\lambda_\psi$
μ	Mean
σ	Standard deviation
σ^2	Variance
$\phi(t)$	Refinable function
$\psi(t)$	Wavelet function for scale $a = 0$ and translation $b = 0$
$\psi_a(t)$	Wavelet function at scale a , with translation $b = 0$
$\psi_{ab}(t)$	Wavelet function at scale a , with translation b
τ_a	e -folding time of a wavelet (see Section 3.1.2)
ω	Radial frequency variable [rad/sec], $\omega = 2\pi f$
Ω	Sum of weighing factors

Mathematics

Complex Numbers

The imaginary number i is defined as $i^2 = -1$. A complex number $z = x + iy$ consists of a real part $\text{Re}(z) = x$ and an imaginary part $\text{Im}(z) = y$. The modulus of this complex number z is defined by $|z| = \sqrt{x^2 + y^2}$ and the argument $\theta = \arg(z)$ by

$$\arg(z) = \arctan\left(\frac{\text{Im}(z)}{\text{Re}(z)}\right), \tag{1}$$

such that the complex number can be written in polar form as $z = |z|e^{i\theta}$. The complex conjugate of a complex number is defined as $z^* = \text{Re}(z) - i\text{Im}(z)$.

Mathematical operators

Operator	Operation
$(\cdot)^*$	Complex conjugate
$\langle x_1, x_2 \rangle$	Inner product operation $\int_{-\infty}^{\infty} x_1(t)(x_2(t))^* dt$
$*$	Convolution
\otimes	Circular convolution
$\arg(\cdot)$	Argument function
$\hat{\cdot}$	No clue
$\tilde{\cdot}$	Estimator of (\cdot)
$\bar{\cdot}$	Mean value; $\bar{x} = \frac{1}{N} \sum_{j=0}^{N-1} x_j$
$\text{Re}(\cdot)$	Real part of \cdot
$\text{Im}(\cdot)$	Imaginary part of \cdot
$\mathcal{F}\{\cdot\}(\omega)$	Continuous Fourier Transform
$\mathcal{F}^{-1}\{\cdot\}(t)$	Inverse Continuous Fourier Transform
$\mathcal{G}\{\cdot\}(\omega)$	Windowed Fourier Transform
$\mathcal{O}(\cdot)$	Landau's \mathcal{O} -symbol
$\mathcal{W}\{\cdot\}(a, b)$	Continuous Wavelet Transform
$\mathcal{W}^{-1}\{\cdot\}(t)$	Inverse Continuous Wavelet Transform

Functions

Expected value

$$E[x(t_0)] = \lim_{N \rightarrow \infty} \frac{1}{N} \sum_{i=1}^N x_i(t_0) \tag{2}$$

Variance

$$\text{Var}(x(t_0)) = \sigma^2(t_0) = E[(x(t_0) - E[(x(t_0))])^2] = E[(x(t_0))^2] - E[x(t_0)]^2 \tag{3}$$

Convolution

The convolution of two signals $x(t)$, $y(t)$ is defined by

$$(x * y)(t) := \int_{-\infty}^{\infty} x(\tau)y(t - \tau) d\tau = \int_{-\infty}^{\infty} x(t - \tau)y(\tau) d\tau = (y * x)(t). \tag{4}$$

It is important to notice that the convolution of two signals in the time domain is equivalent to the multiplication of their transforms in the frequency domain [43]. This is known as the *convolution property*:

$$\mathcal{F}(x * y)(\omega) = X(\omega) \cdot Y(\omega). \tag{5}$$

The (discrete) convolution of two discrete time signals $x[n]$ and $y[n]$ (assume both length N) is given by:

$$(x * y)[n] = \sum_{k=-\infty}^{\infty} x[k]y[n - k], \quad \text{for } 0 \leq n < N. \tag{6}$$

To compute the discrete convolution, information from $x[n]$, $n \geq N$ is needed, but the signal does not exist there. The *circular convolution* considers these two signals as periodic, such that $x[N] = x[0]$, $x[N+1] = x[1]$ etc. The computation (6) can be abbreviated to

$$(x \otimes y)[n] = \sum_{k=0}^{N-1} x[k]y[n-k], \quad (7)$$

where the \otimes denotes the *circular* or *cyclic* convolution.

Cross correlation

The *cross correlation* of two complex signals $x(t)$ and $y(t)$ is defined by [21]

$$(x \star y)(t) := \int_{-\infty}^{\infty} \overline{x(\tau)}y(t+\tau) d\tau = \overline{x(-t)} * y(t). \quad (8)$$

The *auto correlation* of a function $x(t)$ is the cross correlation of this function with itself,

$$(x \star x)(t). \quad (9)$$

In the Fourier domain the cross correlation satisfies $\mathcal{F}\{x \star y\}(\omega) = X(\omega) * Y(\omega)$. The autocorrelation thus satisfies $\mathcal{F}\{x \star x\}(\omega) = X(\omega) * X(\omega) = |X(\omega)|^2$.

In statistics the autocorrelation expressed as the expected value of two signals, i.e.

$$E[x(t_1)x(t_2)]. \quad (10)$$

Delta Dirac function

The Delta (Dirac) function is a theoretical function with a support reduced to $t = 0$, but with an integral of 1. This theoretical function simplifies computations, leaving convergence issues aside [38]. The Delta function $\delta(t)$ associates any continuous function $f(t)$ to its value at $t = 0$:

$$\int_{-\infty}^{\infty} \delta(t-t_0)f(t) dt = f(t_0). \quad (11)$$

Note that by this property that

$$f * \delta(t) = f(t).$$

The Kronecker delta function is the discrete counterpart of the Delta Dirac function. It is defined by:

$$\delta_{ij} = \begin{cases} 1 & \text{if } i = j \\ 0 & \text{elsewhere} \end{cases}. \quad (12)$$

Heaviside Step function

$$H(x) = \begin{cases} 0 & x < 0 \\ 1/2 & x = 0 \\ 1 & x > 0 \end{cases} \quad (13)$$

Introduction

Time-frequency analysis is the study of the behaviour of signals in the time-frequency space. Knowledge of this behaviour allows researchers to characterise it and filter unwanted elements. Time-frequency analysis was introduced in 1946 by Dennis Gabor. He came up with the idea to place a window over the signal and apply the Fourier transform to the windowed signal, to provide insight in the time-frequency behaviour of a signal [19]. Fourier analysis, along with its transform, was introduced in the early 1800's, which allowed the study of signals in the frequency domain. From the 1960's researchers from different disciplines started to adjust the window that was introduced by Gabor, by changing its size depending on the frequency of interest. Meyer¹, Daubechies and Mallat unified this work in the mid-eighties, marking the birth of wavelet analysis [14, 37].

Wavelet analysis has strong similarities with Fourier analysis. The advantage of wavelet analysis over Fourier analysis is that there is no fixed base (i.e. sines and cosines) as in Fourier analysis, but there are many bases to choose from, called wavelets, hence the name wavelet analysis [30, 31, 55]. This offers a wider range of applications and therefore wavelet analysis is adopted in many different fields, such as electrical engineering, ecology, finance, etc. [2, 10, 43]. In civil engineering, the wavelet transform became more and more popular since turn of the century [30]. However, guidelines are missing for the application of wavelet analysis in different fields of civil engineering [30]. One such field is the field of coastal engineering.

Bosboom and Stive [8, p.1], experts from the field, describe coastal engineering as: "[...] the branch of civil engineering concerned with the planning, design, construction and maintenance of works in the coastal zone." These works are divided into soft and hard measures. Soft measures make use of natural coastal material, such as beach nourishments, while hard measures consist of man-made structures, for instance breakwaters. The purposes of these measures are plentiful: from the development of harbours to the control of shoreline erosion. The most important ones are defence structures against floodings [8]. These floodings can be caused by natural effects such as storms, tides and tsunamis. Above all the long-term sea-level rise is a thread for low-laying areas all over the world. Thus coastal engineering deals with relevant social-economic problems.

In the field of coastal engineering different kinds of signals are investigated. These signals are always digital, i.e. they are sampled with a certain frequency and stored on a computer. These signals can be the result of simulations, measurements in the field and (scale) experiments, of both soft and hard measures [16, 35]. This results in a wide variety of challenges: from time-frequency analysis for measurements with missing data points to filtering pressure sensor measurements plagued by noise. The filtering of (digital) signals is one of many components of digital signal processing. Digital signal processing is the application of a wide variety of signal processing operations by digital means, for instance a computer [47]. Signals from the field of coastal engineering have some unique characteristics, such as large amplitude differences in a short amount of time, that are better fit to analyse and process using wavelet analysis than current methods [43]. Wavelets are not often applied in practice yet. The abundance of choices in wavelet analysis, such as a choice of base, creates a high threshold to apply it in coastal engineering. Guidelines regarding the use of wavelet analysis in the field of coastal engineering are needed, in order to decrease this experienced threshold.

¹This years Abel Prize is appointed to Yves Meyer for his work in wavelet analysis [5].

1.1. Research

The goal of this thesis is to derive guidelines for practical applications of wavelet analysis in the field of coastal engineering. Application of these guidelines by coastal engineers could contribute in the knowledge to cope with the unique characteristics of signals seen in the field of coastal engineering and thus could assist in the future creation of coastal infrastructure. Because there is such a wide ranges of signals, the scope of this thesis is limited to time-series. Hence, the main research question of this thesis is:

*How can wavelet analysis improve time-series analysis and processing
in the field of coastal engineering?*

It is important to note that wavelet analysis is divided into two categories. The first category uses continuous wavelet coefficients to do time-frequency analysis and some basic signal processing [30, 53]. Time-frequency analysis based on the continuous wavelet transform has already been applied much in coastal engineering, often based on the guidelines from other research fields [16, 17, 23, 30, 53]. An interesting feature of the continuous wavelet coefficients is that they can be used in digital signal processing instead of Fourier coefficients [22, 35]. This offers opportunities for problems where the behaviour in the frequency domain depends on time.

The second category is the discrete wavelet transform, which is applied in digital signal processing only [29, 43]. An example of the application of the discrete wavelet transform is the JPEG-format [15, 43]. The coefficients in the discrete wavelet decomposition have many applications in digital signal processing, from denoising and compression to filtering specific signal elements. The focus of this thesis lies in application of wavelet analysis in general. Therefore the sub questions are divided into the application of the discrete and the continuous branch. Another sub question will address the added value of wavelet analysis onto coastal engineering signals. These questions are presented at the end of the next chapter, Chapter 2 Background.

1.2. Overview

The next chapter will provide background with respect to coastal engineering time-series, Fourier and wavelet analysis. The first sub question is addressed in Chapter 3 and the second one in Chapter 4. These chapters both provide some additional theory to the background and present comparisons between Fourier and wavelet based methods. In Chapter 5 the added value of wavelet analysis for signals from the field of coastal engineering is addressed. Lastly the research questions will be answered in Chapter 6, followed by recommendations for future research. The appendices contain some theoretical additions and results that could not be presented in the main part of this thesis. The content of the appendices is summarised on page A1.

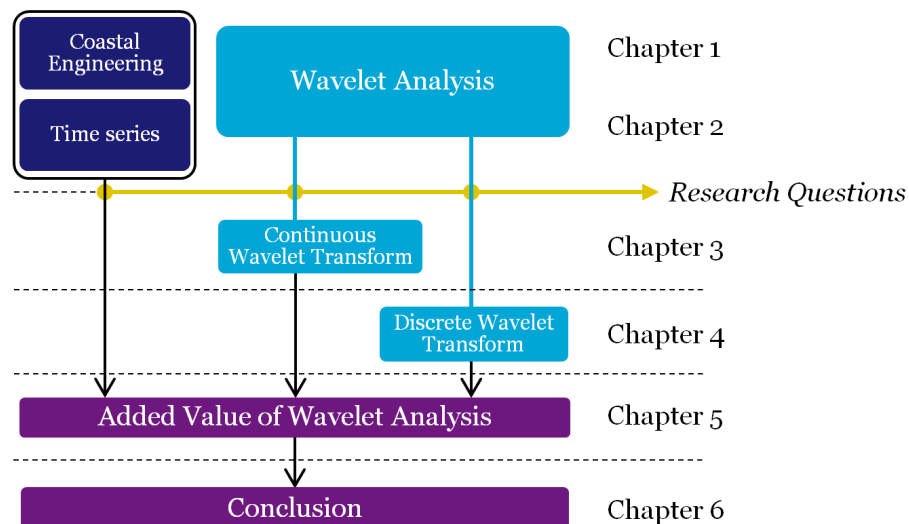
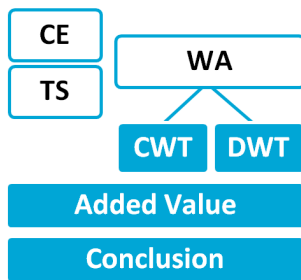


Figure 1.1: A schematic overview of the content of this thesis.



2

Background

As addressed in the introduction, the aim of this research to de guidelines with respect to the application of wavelet analysis in the field of coastal engineering. This chapter provides the background for these guidelines. Therefore it starts with the definition of a time series and what different analyses there are. Moreover, specific coastal engineering examples will be presented. Two types of analysis will be explained more elaborate. These are Fourier Analysis (Section 2.2) and Wavelet Analysis (Section 2.3). Applications of signal processing are discussed in Section 2.4 and 2.5. At the end of this chapter, the research questions supporting the main research question will be presented.

2.1. Time Series and Signal Analysis

In the field of coastal engineering many different time series are analysed and processed. These time series are the result of simulation and measurements, which are conducted in the field or in an experimental environment. The most common measured quantities in coastal engineering are distances, forces and pressures. The measurements are often analysed, processed, or a combination of these two. In Section 2.1.1 some general characteristics of time series are discussed. This is followed by different types of signal analysis, which are elucidated in Section 2.2 and 2.3. At the end of this chapter the challenges with respect to coastal engineering time series are discussed in Section 2.6

2.1.1. Time Series

Time series are generally divided into two categories. *Deterministic signals* can be modelled completely as a function of a variable, for instance time. A deterministic signal has a known and unambiguous value at every point in time [12, 21]. These signals are composed of additions, subtractions, delays, derivations and integrals of deterministic parts. *Random* or *stochastic signals* are non-deterministic signals [21]. These are modelled using probability theory.

Most signals in coastal engineering are considered random, they are the result of a so-called *random process*. Such a process can produce an entirety of random signals, this entirety is called an *ensemble*. One signal from such an ensemble is known as a *sample function* in mathematics or as a *realisation* in signal analysis. Random signals cannot be described deterministically. They are characterised by characteristics that are valid for the whole ensemble [21]. The whole ensemble is the set of realisations $\{x_i(t)\}$, consisting of the individual random signals $x_1(t)$, $x_2(t)$, etc.

Two important properties of ensembles are the expected value (2) and the variance (3) (or its square root: the standard derivation). Often, these characteristics are time dependent. Note that the *time average* of a signal is the average over the whole time domain, which can be computed for every ensemble member individually. The quadratic average of an ensemble, $E[x^2(t)]$, is used to describe the average power of a random process. The expected value and variance are often sufficient to describe common random signals. The more general formulation of the expected value and the variance of an ensemble at a certain time t_0 is [12]

$$E[f(x(t_0))], \quad (2.1)$$

where for the expected value: $f(x) = x$ and for the variance we choose $f(x) = (x - E[x])^2$. A probability density function is a description of a characteristic (2.1) for the whole time t . Advanced models of stochastic process

can become very complicated, using *higher-order statistics*, such as $f(x) = x^3$ in (2.1) [21].

Random processes, which result in random signals, have a lot of different classifications. Two important classes are stationary processes and linear processes. Such a process always relates two (or more) signals to each other. An example of a process is 'a megaphone': in one end you talk, the process in the megaphone amplifies your voice and the horn will broadcast this.

Stationary and ergodic random processes

A random process is called *stationary* if its statistical properties do not change over time. So in the example of the megaphone your voice is amplified with the same factor at all times. This is considered a stationary process. An ensemble can be stationary as well: this implies that the statistical properties of the ensemble do not change over time: for instance its mean and variance are the same for all times. An ensemble is *stationary to the order N* if [12]:

$$E[f(x(t_1), x(t_2), \dots, x(t_N))] = E[f(x(t_1 + \Delta t), x(t_2 + \Delta t), \dots, x(t_N + \Delta t))] \quad (2.2)$$

for all Δt . All signals from this ensemble are stationary as well. This expression is hard to use, therefore often a random process is stationary if its second-order expected values only depend on the difference of observed time points $t_1 - t_2$ [21], mostly checked using the autocorrelation function (9). Note that this mathematical description excludes finite random signals and deterministic functions other than constant functions as stationary [21]. A random process is called *weak stationary* if only the autocorrelation and the expected value of a signal are stationary [9, 12], respectively if $\forall \Delta t$

$$E[x(t_1)x(t_2)] = E[x(t_1 + \Delta t)x(t_2 + \Delta t)], \quad E[x(t_1)] = E[x(t_1 + \Delta t)].$$

For a stationary random process for which all time averages are the same as all ensemble averages, the process is an *ergodic* random process [12, 21]. This holds for all function $f(\mathbf{x})$ from (2.2). A signal is again called *weak ergodic* if the autocorrelation and expected value of the signal are the same as their time averages [21]:

$$\lim_{T \rightarrow \infty} \frac{1}{2T} \int_{-T}^T x_i(t)x_i(t - \Delta t) dt, \quad \lim_{T \rightarrow \infty} \frac{1}{2T} \int_{-T}^T x_i(t) dt.$$

Linearity

A process or function $f(\mathbf{x})$ is a *linear process* if the following relationship holds [12]:

$$f(A\mathbf{x} + B\mathbf{y}) = Af(\mathbf{x}) + Bf(\mathbf{y}). \quad (2.3)$$

For instance if two people talk through the same megaphone at the same time, both their voices are equally amplified. If one of them starts to talk louder, the result will be louder as well. However, if the megaphone is limited to a certain maximum output volume, it could be that this louder person is amplified less than the other person. Then the process is classified as *non-linear*. Important is that a signal can be the result of a non-linear process, but cannot be non-linear on its own. The relationship (2.3) cannot be applied to a single signal. If a signal is the result of a non-linear process, it is often referred to as non-linear as well.

Time invariance

The last important characteristic of a system is its *time invariance*. This holds that *the response to a delayed input signal results in a corresponding delayed output signal* [21]. Systems that are both linear and time invariant are abbreviated to *LTI* systems.

2.1.2. Signal Analysis

There are different methods to analyse the time-frequency behaviour of a signal. This section will present different 'observation options' of temporal information. These 'data types' could also be applied to spatial information, but that is outside the scope of this thesis. The goal is to find an easy retrieval of both temporal and frequency information of a signal $x: \mathbb{R} \rightarrow \mathbb{C}$, a function of time t . An important theme in analysis is the representation of a known or unknown function (or signal, time series) $x(t)$ by special known functions [7]. Often the function is referred to as (*time*) *signal* or *time series*, which is a broader concept of a *function or sequence that represents information* [21].

For the representation of the function, a set of functions is chosen. This set always has a mathematical correspondence. The analytical properties of a set tend to show the evident or hidden symmetries of the considered function $x(t)$. This family is known as the *basis functions*. In general, the set is given by

$$\{e_\alpha | \alpha \in I\} \quad \text{with the basis functions } t \mapsto e_\alpha(t). \quad (2.4)$$

The index set I can be discrete, but also continuous. An arbitrary function $x(t)$ then can be represented in the form

$$x(t) = \sum_{\alpha \in I} c_\alpha e_\alpha(t) \quad (2.5)$$

in the discrete case. This expression (2.5) is called a *representation*. In the continuous case the representation is expressed as an integral:

$$x(t) = \int_I c(\alpha) e_\alpha(t) d\alpha.$$

Here the c_α , or $c(\alpha)$, is the coefficient belonging to the basis function $e_\alpha(t)$. The set of coefficients $\{c_\alpha | \alpha \in I\}$ is called the *analysis* of x with respect to the family $\{e_\alpha | \alpha \in I\}$. The inverse operation that takes a given coefficients as input and returns the function itself as output is called the *synthesis* of x by means of e_α . There are tons of different families of basis functions to choose from. The Taylor polynomial for instance uses higher and higher derivatives of the function $x(t)$. In this thesis two different families will be addressed. These are known respectively as the complex exponentials in Fourier analysis (FA, Section 2.2) and wavelets in wavelet analysis (WA, Section 2.3). First a brief overview of these techniques is presented, using an example comprehensible for readers with different backgrounds: a guitar player striking three strings separately. Thereafter these techniques will be elaborated more.

Time Domain

The receiver of a time signal, for instance an ear receiving sound waves, a cellphone receiving the 4G signals or laser equipment measuring wave heights at Deltares, always receives an amplitude at a given time. Mathematically this is seen as a function: $x(t)$, mostly being referred to as a (*time*) *signal* in signal analysis. From this signal a lot of properties of the transmitter, transmission and receiver can be derived using the right techniques. However, in transmission the signal $x(t)$ can be disturbed, making it hard to draw the right conclusions based on the time signal.

Fourier Transform

The signal $x(t)$ does contain more information than just the amplitude at a given time. With the right mathematical transformations, an insight in the different frequencies of the signal can be given. The *Fourier transform* (FT) is a common and much used transformation to derive the energy density per frequency of a signal. This transformation represents the signal in the Fourier or frequency domain. Remember the guitar player? If only the time domain signal of the sound is considered, one cannot know which notes were played. However we do know at what times the strings were struck, by observing the amplitude differences in time. If only the Fourier transform of the signal is considered, the representation of the signal in the frequency domain, one can tell exactly which notes were played, but not in which order. The Fourier transform is addressed in Section 2.2.

Short Term Fourier Transform

A (practiced) listener, however, can tell both the notes and the order in which these notes were played! This is impossible when only the time domain or in the frequency domain of the signal is reviewed. A visual representation of the shortcomings of these domains is shown in Figure 2.1. In the early twentieth century Gabor [7] was the first to act on these shortcomings, developing the Gabor transform. He used the combination of a window function and the Fourier transform to derive a coupling of the temporal and frequency domain. Hence, this method gives insight in the occurrence of frequencies in distinct time intervals. Later his work was placed in the framework of the *short term Fourier transform* (STFT, Section 2.2.3). A disadvantage of this method is the relative large loss of both temporal and frequency information, which is explained by the uncertainty principle (see Section C.2.1).

Wavelet Analysis

The introduction of wavelet analysis minimises these losses. Wavelet analysis is a tool that cuts the function $x(t)$ up into different frequency components, studying each component with a resolution matching its scale [15]. So it is alike the STFT, but more optimised. In the 1960's the basis of the wavelet transform was developed in both mathematics and physics. In the late 1980's the approaches from different disciplines were combined, which led to the theory of wavelet analysis as known today. As shown in Figure 2.1d, for different frequencies the time spacings are different, this again finds its explanation in the uncertainty principle. The simpler explanation is that it takes longer for a low frequency wave to complete a full cycle, therefore one will have to 'listen longer' to detect it. A high frequent wave can be detected in much less time, however, then it is harder to determine which frequency it is.

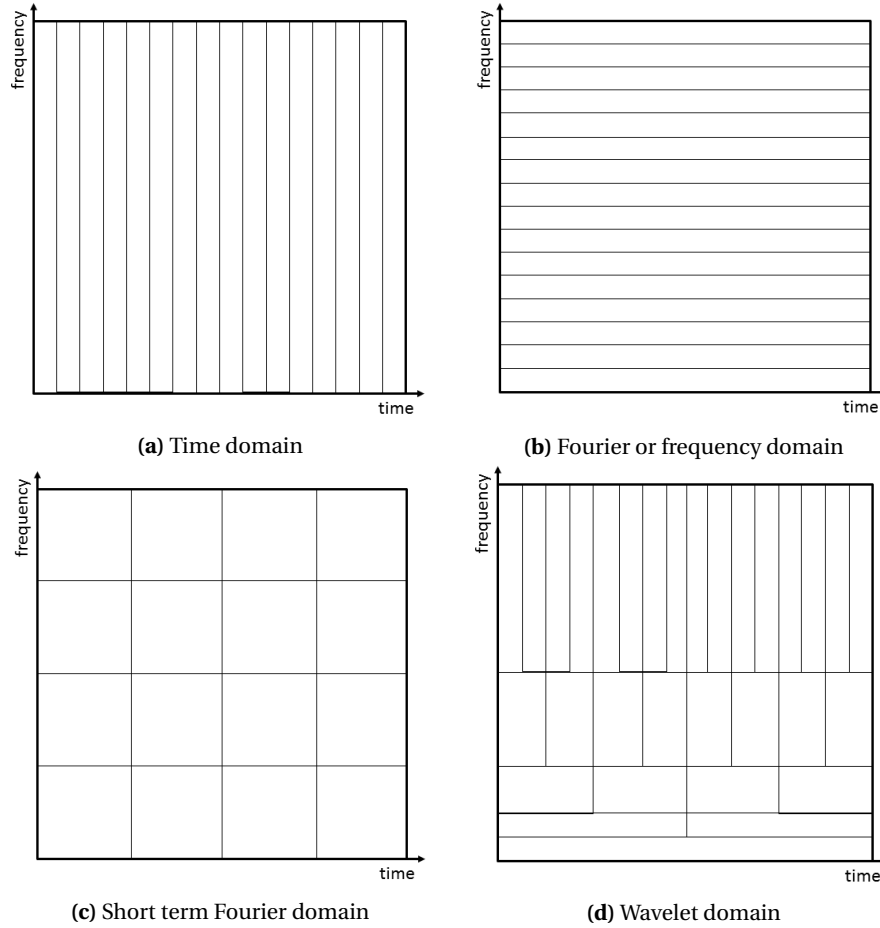


Figure 2.1: Schematic representation of the four different analyses of a signal.

2.2. Fourier Analysis

In the formal Fourier analysis, the basis functions as described in equation 2.4 are from the family of complex exponentials:

$$t \mapsto e^{ikt} = \cos(kt) + i \sin(kt), \quad k \in \mathbb{Z}. \quad (2.6)$$

This is a family of 2π -periodic, orthonormal functions. For any $f \in L^2(\mathbb{R}/2\pi)$, measurable functions $f: \mathbb{R} \rightarrow \mathbb{C}$, the formal definition of the Fourier transform can be applied. This theory expanded to cover not only these specific functions, but all functions on \mathbb{R} . This results in the Fourier series representation of $x(t)$:

$$x(t) := \sum_{k=-\infty}^{\infty} c_k e^{ikt}. \quad (2.7)$$

2.2.1. Continuous Fourier Transform

The Fourier transform (abbreviated to FT, or CFT where the C stands for continuous) of a time signal, or function, $x \in L^1$ is defined by the integral [?]

$$\mathcal{F}\{x(t)\}(\omega) = \mathcal{F}x(\omega) = X(\omega) := \int_{-\infty}^{\infty} x(t)e^{-i\omega t} dt, \quad \omega \in \mathbb{R}.$$

Here ω denotes the angular frequency in rad/s, i.e. $2\pi f$. This transform gives a representation in the complex domain of the frequency content of the time signal $x(t)$. Often the modulus of the Fourier transform is displayed against the frequency ω to indicate the energy density over the spectrum. As discussed before, information concerning time-localization cannot be read off from $X(\omega)$. So it is hard to determine at what time, which frequencies are present in the signal. However when one is looking out for one frequency, like radars which respond to very specific frequencies, this characteristic of the Fourier transform is very convenient.

$X(\omega)$ is also known as the two-sided spectrum of $x(t)$. The original time signal can be calculated from this spectrum by using the inverse Fourier transform

$$x(t) = \frac{1}{2\pi} \int_{-\infty}^{\infty} X(\omega)e^{i\omega t} d\omega, \quad (2.8)$$

the linear combination of the pure oscillations of all frequencies $\omega \in \mathbb{R}$. Note that for a periodic, continuous time signal the CFT is discrete in frequencies, because the CFT will exist of a finite set of basis coefficients. But for a general non-periodic signal this will not hold. An important characteristic of a stationary signal is that its frequency content does not change over time, i.e. its Fourier coefficients are time-invariant [43]. This implies that both the power spectral density and the autocorrelation of the signal are time invariant too.

The Fourier transform of a signal consists of a real and an imaginary part. The decomposition $\mathcal{F}\{x\}(\omega) = X(\omega) = Y(\omega) + iZ(\omega)$ is known as the *Cartesian* or *quadrature form* [12]. An other well known form is the *polar form*: $X(\omega) = |X(\omega)|e^{i\theta(\omega)}$. This is also known as the *magnitude-phase form*, where the real functions $|X(\omega)|$ and $\theta(\omega)$ denote the magnitude and the phase of the signal. The quadrature Fourier series uses the property that the complex exponential can be written as a sum of a sine and a cosine, which leads to another representation of any physical waveform $x(t)$ (over the interval $a < t < a + T$) [12]:

$$x(t) = \sum_{n=-\infty}^{\infty} a_n \cos n\omega_0 t + b_n \sin n\omega_0 t \quad (2.9)$$

$$\text{where } a_n = \begin{cases} \frac{1}{T} \int_a^{a+T} x(t) dt & n = 0 \\ \frac{2}{T} \int_a^{a+T} x(t) \cos n\omega_0 t dt & n \geq 1 \end{cases} \quad \text{and } b_n = \begin{cases} 0 & n = 0 \\ \frac{2}{T} \int_a^{a+T} x(t) \sin n\omega_0 t dt & n \geq 1 \end{cases}.$$

2.2.2. From Continuous to Discrete

As stated before, most signals in the field of coastal engineering are discrete. The continuous Fourier transform is therefore not applicable to these signals. The sampling theory describes how these so-called *sampled signals* can be transformed using the discrete Fourier transform (DFT). In Appendix C this theory and some advantages and disadvantages are discussed more elaborate.

A sampled signal can be represented as a sum of delta functions. For this we assume a *uniform sampling*, sampled with the *sampling frequency* $f_s = \Delta t^{-1}$ [Hz]. Assume a continuous signal $x(t)$ is being sampled, then the uniform sampling of this signal is described as

$$x_{\text{sampled}}(t) = \sum_{k=-\infty}^{\infty} x(t)\delta(t - k\Delta t) = \sum_{k=-\infty}^{\infty} x(kT)\delta(t - k\Delta t).$$

Now determine the Fourier transform of $x_{\text{sampled}}(t)$, using the linearity property (B.1) of the Fourier transform and the Fourier transform of the Delta function (B.9) to derive the *discrete time Fourier transform* (DTFT, discrete in time, continuous in frequency):

$$\mathcal{F}\{x_{\text{sampled}}\}(\omega) = X_{\text{sampled}}(\omega) = \sum_{k=-\infty}^{\infty} x(k\Delta t)e^{-i\omega k\Delta t}.$$

Most sampled signals $x(kT) = x[k]$ are finite. For now, we will work with the abbreviated expression for a signal of length N

$$X(\omega) = \sum_{k=0}^{N-1} x(k\Delta t) e^{-i\omega k\Delta t}. \quad (2.10)$$

Discrete Fourier Transform

Expression (2.10) can be simplified further, by discretisation of the frequency domain. In the discrete Fourier transform (DFT) the following set of orthogonal basis functions is used [38]:

$$\left\{ e_n[k] = \exp\left(\frac{i2\pi nk}{N}\right) \right\}_{0 \leq n \leq N}. \quad (2.11)$$

Using this basis, the *discrete Fourier transform* (DFT) is defined. This transform is discrete in both time and frequency. Now again consider a discrete time signal, given by $x[k]$, with $k \in \mathbb{N}$ and finite with a duration of time T , then the DFT becomes

$$\mathcal{F}\{x[k]\}[n] := X[n] = \sum_{k=0}^{N-1} x[k] e^{-i2\pi nk/N}, \quad \text{where } n = 0, 1, 2, \dots, N-1, \quad (2.12)$$

and the inverse operation is given by

$$\mathcal{F}^{-1}\{X[n]\}[k] := x[k] = \frac{1}{N} \sum_{n=0}^{N-1} X[n] e^{i2\pi nk/N}, \quad \text{where } k = 0, 1, 2, \dots, N-1. \quad (2.13)$$

From now on the index k is used for indexing the discrete time domain and the index n for the discrete frequency domain. Note that the basis functions (2.11) are independent of the sampling frequency or the total duration of the signal $x[n]$. The resulting DFT has domain $[-f_{\text{sample}}/2, f_{\text{sample}}/2]$.

Fast Fourier Transform

The fast Fourier transform (FFT) is a faster implementation of the DFT algorithm. The direct computation of the DFT is of $\mathcal{O}(N^2)$ arithmetic operations [47]. The FFT algorithm brings this number down to $\mathcal{O}(N \log N)$ operations by breaking the large convolution from equation 2.12 into shorter convolutions, lowering the number of operations [47]. The terms are interchangeable because the DFT and FFT algorithm both result in the same Fourier coefficients.

2.2.3. Short Term Fourier Transform

In order to apply time-frequency analysis, a connection between time and frequency information has to be extracted from a time signal. The WFT makes use of a so-called *window function* $g: \mathbb{R} \rightarrow \mathbb{R}_{\geq 0}$ to connect time and frequency [7]. This window function should have the property that it has compact support containing 0, or at least a maximum at $t = 0$, decaying fast for $|t| \rightarrow \infty$ and $\int_{-\infty}^{\infty} g(t) dt = 1$. A widely used window is the *Gabor window*, after the physicist mentioned in the introduction. He remarked that the window $\mathcal{N}_{\sigma,0}$ is optimal to extract time-frequency information using the Fourier transform. This Gabor transform window is given by

$$g(t) = \mathcal{N}_{\sigma,0}(t) := \frac{1}{\sqrt{2\pi}\sigma} e^{-t^2/2\sigma^2}, \quad \text{with } \sigma \text{ constant.} \quad (2.14)$$

The choice for a window like (2.14) instead of a rectangular pulse for instance is obvious to the reader familiar with Fourier transform properties. The sharp cut off by a rectangular window, will lead to rippling effects, described in Section C.1. These contributions will disturb the results. The WFT is the CFT of the signal $x(t)$ multiplied with the window function $g(t)$.

The chosen window g will be slid over the signal $x(t)$ to not select the full signal, only parts of it. Therefore the *window transform* is defined as

$$g_s: t \mapsto g(t-s), \quad (2.15)$$

a translation by $s \in \mathbb{R}$ of the window g . Note that for $s > 0$ the window is translated to the right. Now define:

$$\mathcal{G}\{x\}(\omega, s) := \int_{-\infty}^{\infty} x(t) g(t-s) e^{-i\omega t} dt = \int_{-\infty}^{\infty} x(t) g_s(t) e^{-i\omega t} dt. \quad (2.16)$$

This use of the translated window transform is widely known as the *short term Fourier transform* (STFT) because the multiplication by $g(t - s)$ localizes the Fourier integral in the neighbourhood of $t = s$ [38]. The value of $\mathcal{G}\{x\}(\omega, s)$ represents again the complex amplitude by which the pure harmonic $e^{i\omega t}$ is present in the signal $x(t)g_s(t)$ for that particular s . By the redundancy of information of the signal $x(t)$ in the STFT $\mathcal{G}\{x\}(\omega, s)$, there are many inverse transformations defined [7]. The representation of this transformation is often given by a *spectrogram*. The spectrogram is a measure of the energy of $x(t)$ in the time-frequency neighbourhood of (ω, s) . This neighborhood is specified by its so called Heisenberg box $h_{\omega,s}$ (see Section C.2.1). For large signals the spectrogram can be come quite hard to read. The two most applied enhancers are window overlapping and bin averaging. This last one, however, decreases time frequency resolution even further.

Discrete Short Term Fourier Transform

As for the DFT and DTFT, the discrete STFT and discrete time STFT, respectively DSTFT and DTSTFT, are defined. The derivation is following the same steps as the derivation of the DTFT and DFT. In the discrete case a *discrete window* or *window sequence* $g[n]$ is chosen. Most of the time this is a symmetric discrete signal of period N , with unit norm $\|g\| = 1$ [38]. For the DTSTFT the discrete signal $x[n]$ is multiplied with the shifted *window sequence* $g[n - k]$, resulting in the expression

$$X(\omega, k) = \sum_{n=-\infty}^{\infty} x[n]g[n - k]e^{-i\omega n} = x[n]e^{i\omega n} * g[n].$$

The same step as for the DFT (Section 2.2.2) is done, leading to the expression for the DSTFT [38]:

$$X[n, k] = \sum_{\ell=0}^{N-1} x[n]g[n - k] \exp\left(\frac{-i2\pi n\ell}{N}\right).$$

2.3. Wavelet Analysis

In wavelet analysis a different set of basis functions is chosen. Instead of using the complex polynomials, a so-called wavelet $\psi(t)$ is used. The wavelet transform of a continuous time signal $x(t)$ is defined by [63]

$$\mathcal{W}\{x\}(a, b) = W(a, b) = \int_{-\infty}^{\infty} x(t)\psi_{ab}^*(t) dt, \quad (2.17)$$

where ψ_{ab}^* is the complex conjugate of a *daughter wavelet*. This expression denotes the autocorrelation (9) of the signal $x(t)$ with this daughter wavelet. This daughter wavelet is derived by scaling and translating the wavelet $\psi(t)$ by respectively a *scaling factor* a and a *translation* b :

$$\psi_{ab}(t) = \frac{1}{\sqrt{a}}\psi\left(\frac{t-b}{a}\right). \quad (2.18)$$

A wavelet function is characterized by a finite support and a zero mean value. This is where the term *wavelet* originates from; because a function with these two characteristics will be of a short wavelike shape. For further admissibility conditions for functions to classify as wavelet the reader is referred to Mallat [38].

Wavelets can be both real or complex valued. This leads to respectively real or complex valued coefficients. It is important to note that a continuous wavelet is often a composition of a wave and a window. Different continuous wavelets are presented in Section E.1. Observe the Complex Morlet wavelet as an example (see Table E.1). It is the product of a wave described by $e^{i\omega_0 t}$ and a Gaussian window, $e^{-t^2/2}$. The wavelet transform is therefore very similar to the STFT, however, due to the scaling, the size of the window changes per frequency. This allows the investigation of a larger range of frequencies.

2.3.1. Continuous Wavelet Transform for Discrete Signals

For the discrete case we consider signals that are samples with a constant sampling interval Δt . To compute the wavelet transform of a discrete signal, the integral has to be discretised. This discretisation can be written as a sum:

$$W^{\text{DT}}(a, b) = \sum_{m=0}^{N-1} x[m] \cdot \sqrt{\frac{\Delta t}{a}} \psi^*\left(\frac{t-b}{a}\right). \quad (2.19)$$

The factor $\sqrt{\Delta t}$ has been added to assure that $|W^{\text{DT}}(a, b)| \approx |W(a, b)|$, so that the discrete coefficients are a good approximation of the continuous ones. By maintaining a continuous translation, this transformation has a lot of abundant information. By discretising b with the sampling frequency f_s we find the discretised continuous wavelet transform as

$$W(a, n\Delta t) = W[a, n] = \sum_{m=0}^{N-1} x[m] \cdot \sqrt{\frac{\Delta t}{a}} \psi^* \left(\frac{(m-n)\Delta t}{a} \right) = x[n] * \sqrt{\frac{\Delta t}{a}} \psi^* \left[\frac{n\Delta t}{a} \right]. \quad (2.20)$$

This discretised expression approaches the continuous wavelet transform very well and therefore this expression is referred to as the continuous wavelet transform in most modern literature [1, 16, 35, 53]. In this thesis, however, it the term *discretised continuous wavelet transform* (DCWT) is preferred.

The fastest way to compute the coefficients is through the Fourier domain [53]. This can be divided into four steps:

1. Compute the Fourier transform $\mathbf{X} = \mathcal{F}\{\mathbf{x}\}$ using the FFT.
2. Choose a wavelet function ψ (with $\Psi = \mathcal{F}\{\psi\}$) and a set of scales to analyse.
3. For each scale, construct the normalised wavelet function using

$$\Psi(a\omega_k) = \sqrt{\frac{2\pi a}{\Delta t}} \Psi_0(a\omega_k), \quad \omega_k = \begin{cases} \frac{2\pi k}{N\Delta t} & : k \leq N/2 \\ \frac{2\pi k}{N\Delta t} & : k > N/2 \end{cases}. \quad (2.21)$$

4. Find the wavelet transform at all scales a using the the inverse FFT:

$$W(a, n\Delta t) = \mathcal{F}^{-1} \{ \mathbf{X}(\omega_k) \Psi^*(a\omega_k) \} = \sum_{k=0}^{N-1} \mathbf{X}(\omega_k) \Psi^*(a\omega_k) e^{i\omega_k n\Delta t}. \quad (2.22)$$

Reconstruction

By the redundancy of the DCWT coefficients in time and scale the reconstruction is less arbitrary than the reconstruction of a signal from the Fourier domain. However, it is possible to reconstruct the time series with a completely different wavelet function [53]. The most easy function possible would be the Delta function $\delta(t)$. Assume a discrete number of scales $A = a_1, a_2, \dots$, logarithmically scaled with distance $a_{i+1} - a_i = \log(\Delta a)$. In that case the reconstructed real valued time series becomes [53]:

$$x[n] = \frac{\Delta a \sqrt{\Delta t}}{C_\delta \psi(0, 0)} \sum_{j=0}^J \frac{\text{Re}[W(a_j, n)]}{a_j^{1/2}}, \quad (2.23)$$

with C_δ a constant defined by: (2.24)

$$C_\delta = \frac{\Delta a \sqrt{\Delta t}}{\psi(0, 0)} \sum_{j=0}^J \frac{\text{Re}[W_\delta(a_j)]}{a_j^{1/2}}, \quad \text{where } W_\delta(a) = \frac{1}{N} \sum_{k=0}^{N-1} \Psi^*(a\omega_k).$$

The result $x[n]$ is known as an analytical signal. When the decomposed signal was real, the real value of this analytical signal represents the reconstruction of the original signal.

2.3.2. Discrete Wavelet Transform

The Discrete Wavelet Transform (DWT) is a powerful tool to decompose a signal. Discrete signals can be decomposed to the same number of elements as the original signal, therefore it is much less abundant than the continuous wavelet transform. There are two ways to derive the discrete wavelet transform. The derivation through multi resolution analysis (MRA) is the most common, of which a more elaborate explanation is presented in Appendix D. The other is through special windows in the Fourier domain [7].

Fast Wavelet Transform

This derivation lead to the definition of the fast wavelet transform, an algorithm that reduces the number of coefficients to a maximum of N , the length of the signal. The algorithm is based on filters, first described in the late 1980's by Daubechies [14]. In the DWT the signal is decomposed into a detail level using wavelets and an approximation level (the left-over). Thereafter both can be down-sampled to save space.

So the signal, sometimes referred to as sum, at level n , s_n , is filtered using a wavelet, which results in d'_{n+1} , the detail signal at the next level. The approximation signal at that same level is determined by subtracting: $a'_{n+1} = s_n - d'_{n+1}$. Both the detail and approximation signal are then down-sampled by a factor 2 to determine the final detail and approximation *coefficients* at level $n + 1$: d_{n+1} and a_{n+1} . They are referred to as coefficients, because they represent the detail and approximation signals, but are not the same. By combining the information in these two sets of coefficients, the original signal can be reconstructed (see Figure 2.2a). By cascading the algorithm; using the approximation coefficients as input for the next step, more levels of coefficients are determined. To reconstruct the original input the last set of approximation coefficients and all detail coefficients are used (see Figure 2.2b).

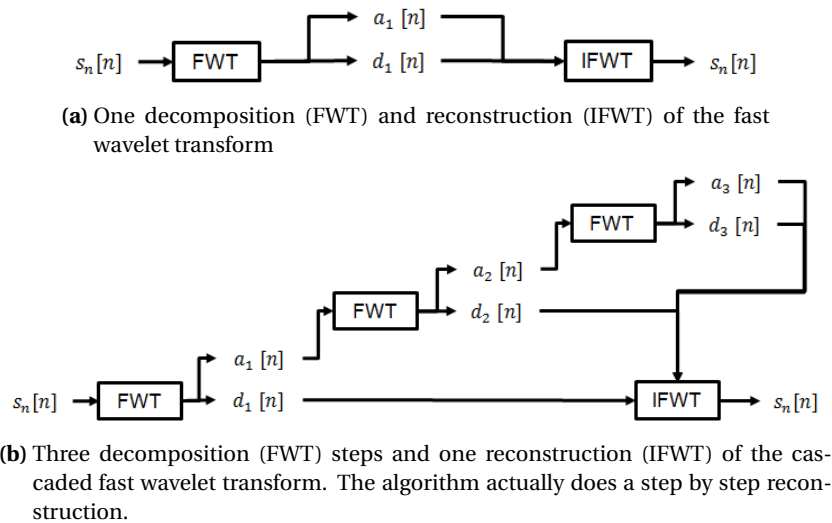


Figure 2.2: Fast Wavelet Transform, the a_i are the approximation coefficients, the d_i the detailed coefficients at level i .

2.3.3. Wavelets

In the previous sections both the continuous and discrete wavelet transform are presented. There is also discussed that there are many different wavelets available, these are discussed here. In Appendix E a more elaborate description of a lot of different wavelets is given, in Appendix D the Haar wavelet is even derived.

In this section a little overview of the different wavelets is given. The realm of wavelets is divided in two types of wavelets: continuous and discrete wavelets. This difference is due to the fact that both transforms discretise scale differently. In the discrete wavelet transform uses in general an exponential scale with base 2, whereas the continuous wavelet transform uses a much smaller base. Therefore different wavelet characteristics are preferred in the different transforms. A sparse representation that is created by the DWT is not possible using most continuous wavelets¹ The continuous wavelet coefficients based on discrete wavelets will often not result in information that is comprehensible in time-frequency analysis. If discrete wavelets are used for the continuous wavelet transform, they are often of relative high order: a small frequency bandwidth is preferred.

Continuous Wavelets

There are very many continuous wavelet, of which only a hand full are often used in time-frequency analysis. They are divided into complex and real wavelets, as presented in Figure 2.3. Real wavelets in combination with real signals lead to real coefficients, so they do not convey information about the phase of the signal. Edges in signals are often detected using wavelets with a relative short time support. This as all to do with the

¹Only the discretised Meyer wavelet is sometimes used in the DWT, see Table E.2.

time-frequency distribution is of the wavelet. For a wavelet to be applicable in time-frequency analysis, it has to have a relative short bandwidth in the frequency domain [31]. This is a characteristic that a lot of discrete wavelets lack and therefore they are not used much in the continuous wavelet transform.

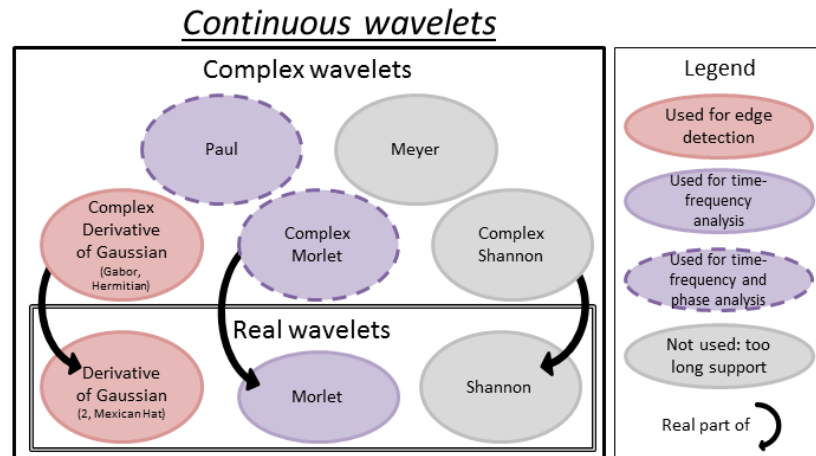


Figure 2.3: An overview of the most used continuous wavelets. See Section E.1 for a more elaborate description of these wavelets.

Discrete Wavelets

In the discrete wavelet transform much more wavelets are used than in the continuous wavelet transform. In Figure 2.4 an overview of the most commonly used wavelets are presented. The most important wavelet characteristics are described at the end of this section. For more information about these characteristics, the reader is referred to Appendix D. If one would want to merge the continuous and discrete wavelets shown in Figure 2.3 and Figure 2.4², the continuous wavelets would be addressed as 'non-orthogonal'. The lack of orthogonality makes them less suited for discrete wavelet transformation. Techniques such as lifting can be used to create an unlimited amount of new discrete wavelets based on these wavelets [29].

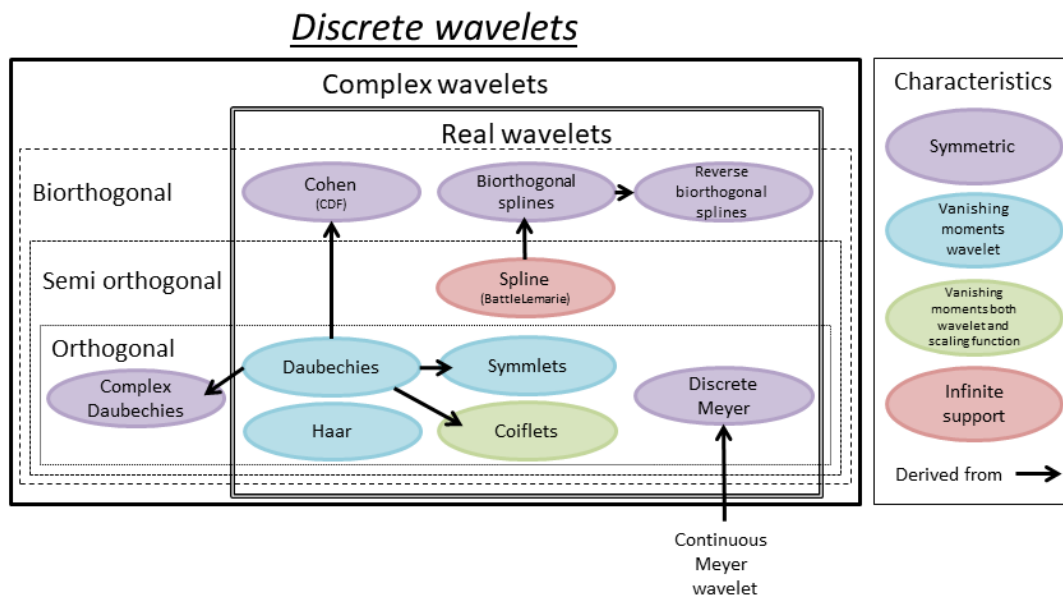


Figure 2.4: An overview of the most used discrete wavelets. See Section E.2 for a more elaborate description of these wavelets.

²Both figures are based on the work of van Berkel [55] and expanded with some extra information.

Filter Most discrete wavelets have the advantage that they can be written as a filter, i.e. they can be implemented using the FWT. This is beneficial in computations, these can be done by low level electronics. The filter length ℓ_f of the wavelet determines the size of the wavelet and the maximum decomposition level: $2^{\text{max.level}} \cdot \ell_f = N$, where N is the length of the signal. To ensure $\text{max.level} \in \mathbb{N}$ different signal extension modes can be applied, these will be discussed later.

Orthogonality A wavelet decomposition is characterized by a scaling function $\phi(x)$ and a wavelet $\psi(x)$ (for more information: Appendix D). In the orthogonal case these two functions are orthogonal to each other. In the bi orthogonal case there is a set of two refinable functions ϕ and $\tilde{\phi}$, such that

$$\langle \phi(x), \tilde{\phi}(x - k) \rangle = \delta_{0k}.$$

An orthogonal wavelet family is also bi orthogonal, i.e. the family is its own dual.

Symmetry A family is known as symmetric if the wavelet function is a symmetric function. An orthogonal family of real wavelets cannot be symmetric.

Moments The number of vanishing moments influences the support in time and frequency space of the wavelet and the scaling function. If there is a larger support in the time domain a smaller support in frequency domain can be achieved and vice versa. For more information about moments, read Appendix D.

2.4. Time-frequency Analysis using Fourier and Wavelet Coefficients

Fourier and wavelet coefficients are applied in many engineering fields. The magnitude and phases of the coefficients are often used as a measure of the energy density of a signal. How this is applied is discussed first. Thereafter some different time-frequency analysis tools are discussed.

2.4.1. Amplitude

To determine which (time-)frequency components are present in a signal, often the *magnitude spectrum* is analysed. Expressed by $|X(\omega)|$ in the continuous Fourier domain and by $|W(a, b)|$ in the continuous wavelet domain.

Energy Spectral Density

The energy spectral density of a signal describes the distribution of the energy of a signal over the frequencies. The energy of a signal $x(t)$ (in seconds) is defined by [47]

$$E = \sum_{t=-\infty}^{\infty} |x(t)|^2. \quad (2.25)$$

The energy of a signal can be finite or infinite, however for discrete signals, the energy is always infinite. The energy before and after the transformation to the frequency domain have to be equal, this is known as Parseval's relation. From this the *energy density spectrum* (EDS) of $x(t)$ can be derived as [47]:

$$S_{xx}^f(\omega) = |X(\omega)|^2. \quad (2.26)$$

The EDS represents the distribution of the energy of the signal over the frequency domain. The unit of energy clearly is the unit of the original sample squared, for instance η^2 , which makes the units of the EDS η^2/Hz . The EDS is often used as estimator for the *power spectral density* (PSD).

Wavelet Power Spectrum

The *scalogram* or *wavelet power spectrum* (WPS) is often defined as the square of the modulus of the wavelet coefficients [20, 53]. In the same manner as the ESD for Fourier coefficients:

$$|W(a, b)|^2 = WW^* = (\text{Re}[W(a, b)])^2 + (\text{Im}[W(a, b)])^2. \quad (2.27)$$

The resulting scalogram shows bias with respect to the ESD of the signal. Liu et al. [33] show that this definition is not a physically consistent definition of energy, in an average sense. It should be the transformation coefficient squared divided by the scale it is associated to, i.e.

$$S_{xx}^w(a, b) = \frac{|W(a, b)|^2}{a}. \quad (2.28)$$

This quantity, denoted as the Wavelet Energy Spectrum (WES) has the units η^2/Hz at a certain time b . The frequency depends on the scale a .

2.4.2. Phase

The argument (1) of both the Fourier and Wavelet coefficient, respectively $\arg(X(\omega))$ and $\arg(W(a, b))$, contains the phase difference of the complex waveform with respect to the signal. In the Fourier transform this is the complex exponential $e^{i\omega t}$ and for the wavelet transform it is the wavelet $\psi(a, b)$. Note that this wavelet has to be complex in order to determine the argument. The phase difference between two signals is often assessed in cross spectral form, this is discussed in Section 2.4.4.

2.4.3. Averaging Wavelet Coefficients

By averaging the two dimensional result of the wavelet transform in time or scale, this comparison can be made. The key features of these two averages will be discussed briefly. By averaging the wavelet spectrum in time the so-called global wavelet spectrum (GWS) is created. This global wavelet spectrum provides an unbiased and consistent estimation of the true power spectrum of a time series [33, 53]. The global wavelet spectrum could provide a useful measure to base the background spectrum on. By smoothing the wavelet spectrum in time, the significance of the peaks in the wavelet power can be increased [53]. Instead of averaging over all times, also bands of be used to average over, this is not often used though.

The scale averaged wavelet power (SAWP) is used to examine fluctuations in power over a range of scales, also referred to as a band. The SAWP between two scales a_0 and a_1 is defined by [53]

$$\kappa(t) = \frac{\Delta a \Delta t}{C_\delta} \sum_{a=a_0}^{a_1} \frac{|W_a(t)|^2}{a}. \quad (2.29)$$

This results in a time series containing the average variance of the wavelet coefficients in a certain frequency band. It can therefore be used to examine modulation of one time series by another of the modulating effects frequencies mutually in one time series. When further examination is needed, the cross wavelet spectrum is used.

2.4.4. Cross Spectral Information

The relation between different time series is also often of interest of data analysts. Both in the Fourier as the wavelet domain this can be studied. The continuous wavelet coefficients are therefore employed in the cross-wavelet tools. The three best known are: the cross-wavelet power spectrum, the wavelet phase difference and the wavelet coherency [2]. These know different applications in for instance ecology [10, 11, 48], finance [2] and meteorology [53]. All three will be discussed shortly. Significance testing for these cross-wavelet tools is almost always done via Monte Carlo simulations [2].

The cross-wavelet transform (XWT) of two time series $x(t)$ and $y(t)$ is defined as [2, 53]

$$S_{xy}^w = W\{x\}W^*\{y\}. \quad (2.30)$$

The XWT exposes region with high common power and reveals information about the phase relationship [23]. Again if the quantity W^{xy} has to make any physical sense, it should be divided by the scale it is associated with. The cross-wavelet power spectrum is defined by the modulus of the given product, $|W^{xy}|$, and illustrates the local correlation between the two time series at each scale. The complex argument $\arg(W^{xy})$ can be interpreted as the local relative phase between x and y . Normalisation of both time series will result in a different cross wavelet spectrum if they are of different magnitudes. By normalising both series, the regions of high power correlation are not dominated by the time series with the larger variance any more. This will not have any effect on the phase behaviour that can be extracted from the XWT. The *cross-power spectral density*, the equivalent of the XWT in the Fourier domain, is defined as the Fourier transform of the cross-correlation (2.30) of two signals and denoted by S_{xy}^f . This however is always real and therefore only indicates frequencies of common high power [47].

The phase difference of two wavelet transforms indicates the delay of the oscillations between two time series as a function of time and scale and is defined as the argument of the XWT (1) [2, 53]. Different values point to lagging or leading phase of the function x or y as:

$$\theta_{xy} \in \begin{cases} (0, \pi/2) & \text{series are in phase, } y \text{ is leading with phase } \phi_{x,y}, \\ (-\pi/2, 0) & \text{series are in phase, } x \text{ is leading with phase } -\phi_{x,y}, \\ \{-\pi, \pi\} & x \text{ and } y \text{ are in anti phase,} \\ (\pi/2, \pi) & x \text{ is leading,} \\ (-\pi, -\pi/2) & y \text{ is leading.} \end{cases}$$

2.4.5. Coherence

Another measure for correlation between two time series is the coherence. Two waves are said to be coherent if they have the same wavelength and there is a constant phase difference [42]. Where the cross spectra correlates regions of high power, the coherence correlates regions of constant phase difference. The term coherence is used in the Fourier domain as well, which is just called coherence. Coherence in the wavelet domain will be referred to as wavelet coherence. The coherence (in the Fourier domain) between two continuous functions $x(t)$ and $y(t)$ is defined as [49]

$$\gamma_{xy}^2(\omega) = \frac{|S_{xy}^f(\omega)|^2}{S_{xx}^f(\omega)S_{yy}^f(\omega)}. \quad (2.31)$$

For this value holds $0 \leq \gamma_{xy}^2(\omega) \leq 1$.

This value can be read as the fractional portion of the output power that is (linearly) contributed by the input power. So if $x(t) = y(t)$ the coherence equals 1. This value of 1 implies that the two signals are linearly related. If the signals are uncorrelated, then $S_{xy}(\omega) = 0$ and so will the coherence be. Any value in between 0 and 1 indicates a partially linear relationship. This difference has three main contributors [23]

1. In both signals noise can be present;
2. The two signals are not completely linearly related, there is some non linear relation between the two;
3. The signal $y(t)$ is determined not only by $x(t)$ but also by other input signals.

When this coherence function is directly implemented in the for discrete functions, all values will be one. So when samples signals are used, the estimates of the smoothed power and cross-spectral density functions should be used:

$$\tilde{\gamma}_{xy}^2(\omega) = \frac{|\tilde{S}_{xy}^f(\omega)|^2}{\tilde{S}_{xx}^f(\omega)\tilde{S}_{yy}^f(\omega)}. \quad (2.32)$$

If no smoothing is applied the sampled coherence function $\hat{\gamma}_{xy}^2$ will be one for all ω [49], this even holds for unrelated signals. By smoothing the three different variables of the sampled coherence function $\tilde{\gamma}_{xy}^2$, the coherence will be close to the real coherence γ_{xy}^2 . The smoothing, however, will result in a reduced frequency resolution. For more considerations regarding this smoothing, the reader is referred to Shin and Hammond [49].

Wavelet Coherence

The described coherence functions results are only valid for stationary signal cases [59]. Then non-stationary signals need to be addressed, the wavelet coherence is used. The continuous wavelet coherence (WC) of functions x and y for scale a and translation b is defined as [23]

$$\gamma_{xy}^2(a, b) = \frac{|S(a^{-1}S_{xy}^w(a, b))|^2}{S(a^{-1}|S_y^w(a, b)|^2) \cdot S(a^{-1}|S_x^w(a, b)|^2)}, \quad (2.33)$$

where S is a smoothing operator. This smoothing operator consists of a smoothing in time and in scale: $S(W) = S_{\text{time}}(S_{\text{scale}}(W))$. Again, without smoothing operator, the wavelet coherence will be 1 everywhere, just as in the Fourier case [53]. The wavelet coherence can be seen as a localized correlation coefficient in the time frequency space, i.e. when there is little power in the CWT coherence can still be detected. To find this relation, some time and frequency information is lost by smoothing. For further considerations of this wavelet coherence smoothing and a suitable smoothing operator for the Morlet wavelet, the reader is referred to Grinsted et al. [23]. There are two main advantages of the WC over the XTW. The first is that the WC is a normalized value, the second one is that the WC is less disturbed by spurious coincidences than the XTW. Though there are some redundancies between the XWT and WC, they do complement each other [23].

Linearity

When a signal is transformed to the Fourier or wavelet domain, it is assumed to be a linear combination of different basis functions. The coherence function therefore can only rate the linear dependence between two signals with a number between 0 and 1. The mathematical description using harmonic components or

wavelets of such a non-linear signal does have a mathematical meaning, however, they do often not have a physical meaning [26]. What this means is that a non-linear signal is 'identified' as a sum of harmonics (mathematical), but actually it is for instance one wave with a changing harmonic (physical). This is a characteristic that should be kept in mind when analysing signals; non-linear signals are not recognised in these methods.

2.5. Digital Signal Processing

All presented methods, Fourier, short term Fourier, (discretised) continuous wavelet and the discrete wavelet transform have a decomposition and a reconstruction formula, i.e. the transformations from one domain to the other. The application of the reconstruction allows to apply signal processing these domains, by decomposing, adjusting the coefficients and reconstructing Signal processing using the DCWT not addressed much, because filtering in the discrete wavelet domain is more efficient. A numerical experiment using the CWT results in a reconstruction error of 1.4%, when using the Delta function. Which is not so bad, but much worse than the reconstruction error of the FFT or DWT, which are often only affected by the rounding error of the computer. This is normally in the absolute range of 10^{-15} .

2.5.1. Filters

Different signal elements are often filtered from the signal. For instance, noise filtering or denoising is a much applied in signal processing. The goal of denoising is to filter the noise present in the measurement without distorting the underlying signal. In the Fourier domain a filter removes energy from some frequency bands. In general they there are two types of filters: low-pass filters and high-pass filters, respectively filtering out high and low frequencies from the signal. Combinations of these filters lead to band-pass, band-stop and more kinds of filters [47].

As discussed before, discrete wavelet coefficients are mainly used in signal processing, especially filtering. The difference with the filters in the Fourier domain is that the discrete wavelet filters can filter out some elements in a frequency band, while other elements pass. This is impossible for a Fourier filter: all elements in a frequency band are damped with the same factor.

The first level of the discrete wavelet approximation coefficients addresses the highest frequencies present in the signal. As the levels of decomposition rise, the addressed frequencies are lower. So in the low scale detail levels, a lot of high frequency components of the signal are caught. Noise can be present in all frequency levels, however often there is much noise in the high frequencies, with respect to the signal power. Only some of the coefficients are important in supporting discontinuities or other high frequency signal components. This assumption lies at the basis of FWT filtering: by applying a threshold to the coefficients in the low scales, noise is reduced.

The two most used ways of thresholding are hard and soft thresholding, though there are a lot of 'intermediate' thresholding possibilities [3]. These are shown in Figure 2.5. Hard thresholding for a threshold T is defined by (w is the discrete wavelet coefficient):

$$w_{\text{new}} = \begin{cases} 0 & |w| < T \\ w & \text{else} \end{cases}, \quad (2.34)$$

and soft thresholding by

$$w_{\text{new}} = \begin{cases} 0 & |w| < T \\ w - T & w \geq T \\ w + T & w \leq -T \end{cases}. \quad (2.35)$$

Applying the thresholds is a simple process, the crux lies in determining the thresholds. The most used threshold is the so-called universal threshold [50]:

$$T = \sigma_1^{\text{noise}} \sqrt{2 \log(N_1)}. \quad (2.36)$$

This universal threshold is based on the standard deviation of the noise of the first detail level σ_1^{noise} . N_1 is the number of elements of the first detail level. The standard deviation of the noise is often replaced by an estimator based on the Median of Absolute Derivation (MAD) of the detail level d_i , $\bar{\sigma}_i^{\text{noise}} = \text{MAD}(d_i)/0.675$ [43] based on a Gaussian White Noise (GWN) assumption.

By using different thresholds, different types of signal can be taken out. These are addressed in the next section. The results of filtering in the wavelet domain can be even further improved by using techniques like:

1. Shifting [29] uses the not shift invariant characteristic of the FWT. By shifting the original signal and averaging the denoised copies, a better approximation of the underlying signal can be reached.
2. Cycle spinning [29] is a process that shifts the approximation coefficients at every step.
3. A combination of different algorithms, or cascading different algorithms by using the output of one algorithm as input for another.

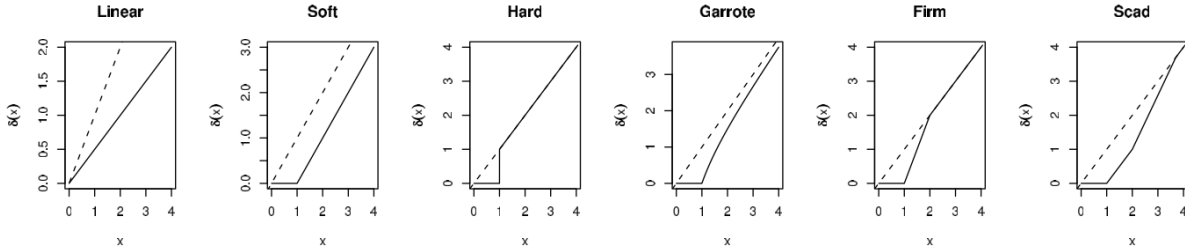


Figure 2.5: Different types of discrete wavelet thresholding. From Antoniadis [3, Figure 1].

2.5.2. Elements of a Signal

Filters are used to separate different elements in the signal from the rest of the signal. These different elements are addressed shortly.

Noise

A received waveform $x(t) = s(t) + v(t)$ usually consists of two parts: a desired part $s(t)$, containing the information, and the undesired part $v(t)$ [12]. The desired part is referred to as the *signal*, the undesired part as *noise*. The sum of these parts is then referred to as the *noisy signal* or *received signal*. This is noise in the most broad sense of the word and it has all kinds of shapes and sizes: it can be 'added' to the desired signal by the sender, the measurement equipment or other processes. Often noise is assumed to be of constant power in all frequencies, *white noise*, but could also be contained in specific frequencies, which is known as *coloured noise*. These names are in convention with light, where white light contains photons of all frequencies and coloured light only those of specific frequencies. Noise does not always have to be of constant power, it can for instance fade out or build up. This is known as *non stationary noise*. The amount of noise on a signal is often described using the signal-to-noise ratio, SNR for short (sometimes denoted as S/N) [12]. It is the ratio between the power of the signal and the power of the noise:

$$\text{SNR} = \frac{P_{\text{signal}}}{P_{\text{noise}}}, \quad (2.37)$$

often expressed in decibels. If the variance of the signal and noise are known and the signal is of zero-mean, the SNR is also expressed by

$$\text{SNR} = \frac{\sigma_{\text{signal}}^2}{\sigma_{\text{noise}}^2}. \quad (2.38)$$

Transients and Discontinuities

The detection of transients and discontinuities (or edges in signal analysis) is very important in most engineering fields. Any discontinuity measured by a sensor may characterize an event [43]. *Transients* are always of short duration and unpredictable nature, changing frequency over time and they often decay fast: the parameters of the transient and its arrival time are unknown. In the Fourier domain the STFT is used to determine the location of the transient. The trade-off between time and frequency chosen beforehand influences the detection of a certain transient. The time frequency representation of the WT on the other hand enables exact localization of any abrupt change, impossible for the STFT. This is not only applicable to transients, but also to discontinuities. Transients usually only appear in the lower scales of the WT, whereas the higher scales represent the low frequency basis of the signal. The choice of wavelet is very important in the detection of transients: remember the WT coefficients represent the correlation between the transient and the wavelet function used. The detection will improve when the the shape of the transient and wavelet are similar [43].

The scales that need to be considered for detecting transients are dependent on the size of these transients. The amplitude of a transient often is rather low in comparison to the signals amplitude. This brings down the computational load for transient detection; only a few scales have to be computed. The lowest scales contain information about the discontinuities and high frequency noise of the signal, transient detection most of the time is done from scale 4 and up [43]. But for shorter signals this might be in higher scales. To detect transients in the presence of noise can be difficult, it may be necessary to first apply some thresholding and then do transient detection on the reconstructed signal. Discontinuities are recognizable by their high detail coefficients over a lot of decomposition levels, as mentioned before [29]. Especially the Haar wavelet had good discontinuity recognizing properties, because it is a discontinuous wavelet.

Amplification or delay

The noise theory discussed till now concerns noise as an addition to the signal: additional noise. Often a large share of the mutation of a signal consists of this additional noise [12]. However noise can also adjust or adapt the signal in other ways: noise can also be a distort the amplification and delay of (specific frequencies) the signal. Amplification (or damping) and the delay of parts of the signal may have different causes. If the whole signal has been amplified or delayed with the same factor, this does not affect the signal analysis that much. These two noise effects are often modeled as filters. Damping is often a result of the range of the measurement equipment. For instance the detection of sounds by the human ear rapidly decays under 50 Hz, which can be modeled as a damping. In a spectrum or scalogram this can be noted from the amplification or damping of specific frequencies or detail coefficients.

Delays can have a lot of different causes, also often modeled as a filter. As addressed before, delay is modeled as a phase change in the Fourier domain (B.2). Therefore it is also known as *phase noise*. Phase noise is generally hard to detect, because it is a non linear effect. E.g. $\sin(\omega_0 t + \theta(t))$ has a basis frequency of $2\omega_0\pi$, however this might be altered by the phase change $\theta(t)$. Because both the wavelet and Fourier transform are linear transforms, some phase changes $\psi(t)$ might be hard to detect: by the linearity they are modelled as different frequencies instead of one phase changing frequency.

Linearity and Stationarity

Linearity and stationary are characteristics of a signal, not 'an element'. Both Fourier and wavelet analysis are linear analyses, they decompose the signal into a sum of linear combinations. Elements that can be filtered, have to be an element in this sum. As discussed above, non-linear elements cannot be filtered by either the Fourier or wavelet transform, because they are not described by a linear combination.

Fourier analysis is only suited for stationary signals; the frequency content of a signal cannot change over time. The magnitude of a Fourier coefficient $|X(\omega)|$ is either 0 or larger than that, i.e. the frequency is present in the signal or not. So if a frequency component is filtered out, it is filtered from the signal at all times. In the wavelet transform the magnitude of a wavelet with scale a_1 and translation b_1 can be larger than zero, while $|X(a_1, b_2)|$, where $b_2 \neq b_1$ can be. Signals with a changing frequency content, which are non-stationary signals, are better filtered using the wavelet transform. One can decide to not address a certain frequency at a certain time, but at another time it can be filtered.

2.5.3. Other techniques

Time frequency analysis and (digital) signal processes are not only implemented in the Fourier and wavelet domain. Of course the behaviour of the signal in the time domain gives information about the signal as well. Filtering signals without transformations is applied often, i.e. filtering in the time domain. The advantage of this type of filtering is that less calculations are needed, because the signal does not have to be transformed (twice). These filters are often referred to as signal smoothing filters, for they optically make the signal smoother. The most used filters are [40]: the (weighted) moving average filter and the Savitsky-Golay filter. Another type of filter is the Kalman filter, which is much more computationally intensive. This filter filters signals based on a model prediction of the signal and the signal itself [60]. It can be applied on temporal information, but also in the Fourier or wavelet domain. Multi-channel filters use multiple inputs to reduce noise or detect signal elements like transients.

Multi-channel Approach

The focus of this thesis lies in noise reduction that is called a *single-channel* noise reduction method. In this method is assumed that there is just one sensor available. In *multi-channel* noise reduction methods, the input of different sensors is used to suppress noise [61]. A good example is a modern mobile phone,

which often has two or more microphones to record your voice when calling, to be able to suppress noise better. This method is most used in speech enhancement, however multi-channel noise reduction can have some application in the field of coastal engineering as well. The multi-channel approach can be applied in all different kinds of domains, among which the wavelet domain.

Hilbert-Huang Transform

In time-frequency analysis there are more options than the STFT of the wavelet transform. The Hilbert Huang transform has been developed by NASA in the late 90s, to specifically analyse non-linear, non-stationary data [28]. Applications of this transform emerged around 2005 [27, 45]. This method combines an empirical mode decomposition with Hilbert spectral analysis [26]. The signal is first decomposed in so-called empirical modes: simple harmonic components which can have variable amplitude and frequency in time. These modes are then analysed using Hilbert spectral analysis, which computes instantaneous frequencies easily. The Hilbert transform of a signal $x(t)$, $\mathcal{H}\{x\}(i\omega)$ is defined by[21]:

$$\mathcal{H}\{x\}(\omega) := \frac{1}{\pi} \mathcal{F}\{x(t)\}(\omega) * \frac{1}{\omega} = \frac{1}{\pi} \int_{-\infty}^{\infty} \frac{X(\eta)}{\omega - \eta} d\eta.$$

In contrary to the Fourier and wavelet transform, the basis of this decomposition, the empirical modes, is adaptive. The instantaneous frequency is a controversial definition, and inceptive: when something is instantaneous, it is localized in time. However, time and frequency are inverse quantities, resulting in the ambiguity [18]. The resulting algorithm, the called the Hilbert-Huang transform has a lot of empirical support [26, 27, 45]. An overview of the comparison of the three methods is given in Table 2.1. The most important improvement of the Hilbert-Huang transform with respect to the Fourier and wavelet transform is that it is a non-linear transform, allowing better analyse of non-linear systems.

This all sounds very promising, however the great drawback of this method is the lack of (mathematical) theoretical base. Due to its adaptive base, one element of the basis could counteract another element, resulting in a false energy distribution in time-frequency. This is in large contrast with Fourier and wavelet analysis, which both have an elegant mathematical framework, very suitable for model building [18]. Huang and Shen [26] sums up a lot of challenges, among others: non linear system identification, optimization and approximation problems.

Table 2.1: Comparative summary of the Fourier, wavelet and HH transform. From [26, Tab. 1].

	Fourier	Wavelet	Hilbert-Huang
<i>Basis</i>	a priori: $e^{i\omega t}$	a priori: $\psi(t)$	adaptive
<i>Frequency</i>	convolution: global uncertainty	convolution: regional uncertainty	differentiation: local, certainty
<i>Presentation</i>	energy frequency STFT: energy-time-frequency	energy-time-frequency	energy-time-frequency
<i>Non linear</i>	no	no	yes
<i>Non stationary</i>	no	yes	yes
<i>Feature extraction</i>	no	discrete: no, continuous: yes	yes
<i>Theoretical base</i>	theory complete	theory complete	empirical base
<i>Computation time</i>	FFT: $\mathcal{O}(N \log_2 N)$ STFT: $\mathcal{O}(N^2 \log N)$	CWT: no fast algorithm DWT (all scales): $\mathcal{O}(N^2 \log N)$	$\mathcal{O}(N \log N)$

2.6. Coastal Engineering Challenges

This chapter started with the description of time series. Important characteristics were discussed, such as stationarity and linearity. Thereafter the field of signal analysis was explored. The different domains, to know the time, frequency and wavelet domain are summarised in Figure 2.1.

Fourier analysis and wavelet analysis are elaborately explored in respectively Section 2.2 and 2.3. The main difference between the two methods is that Fourier analysis correlates the signal with infinite complex exponentials with a certain specific frequency, whereas wavelet analysis correlates the signal with finite functions, that can be real or complex. This allows time-frequency analysis through wavelet coefficients. In the Fourier domain only frequencies can be studied. The discrete wavelet transform is a 'compact form' of the continuous wavelet transform, which gives other insight into signals.

In Section 2.4 different applications of both the continuous and discrete wavelet coefficients are addressed. Moreover, a clear overview of the different continuous and discrete wavelets and their different characteristics is given (in respectively Figure 2.3 and 2.4). In this last section, different coastal engineering challenges are coupled to possible solutions based on wavelets. Based on this outline, the sub questions to answer the research question are presented.

In the field of coastal engineering many time series are recorded. These measurements concern both soft or hard measures. Measurements on hard measures (structures) are often conducted in an experimental setting. This often results in time-series containing pressures and forces. Soft measures are measured both in the field and in experimental settings, resulting in pressures, distances, velocities, temperatures. Sometimes quantities are derived from each other. For instance the water level, based on the pressure at a fixed point. Furthermore wind speeds, water temperature etc. are recorded and often used as input for models.

Time-frequency Analysis

Time-frequency analysis allows analysts to get an overview the behaviour of a signal, which sometimes is not directly observed from the time series or the spectrum. Especially when signals are non-stationary, i.e. some frequency components can dominate a time-series at some time, while at another time they are not present, the Fourier spectrum is not worth much. Missing data points or other (known) disturbances often appear in long-term soft measure measurements, for instance due to deterioration of the equipment or power failure. A lot of experience with these signals is needed to correctly analyse them. Wavelet analysis might provide solutions concerning these problems.

A threshold in the use of wavelet analysis in many fields is the different concept of 'energy' in the WPS and the regular spectrum. The correction per scale by Liu et al. [33] presented in Section 2.4.1 addresses this problem. By applying this, the concept of energy distribution is equal to the one in the Fourier domain. This measure will be used throughout this thesis.

Separating Waves

Time-frequency analysis is often based on the energy distribution, which are based on the magnitudes of the coefficients. An example of the use of phase information (Section 2.4.2) in coastal engineering is the separation of incident and reflected waves. Measurements record a superposition of the two, and therefore they have to be separated. This information is important for testing constructions. Constructions, or scaled models of them, are tested on different characteristics such as stability and overtopping. In order to determine these characteristics the reconstruction of the wave pattern as close to the construction as possible is indispensable. The reconstruction of the incident wave is used to determine whether the imposed spectrum is met. Based on the reflected wave a measure of absorption is created.

The most used method to separate these waves is based on Fourier coefficients and was proposed by Mansard and Funke [39]. Their method uses information of three gauges, which is an expansion to the analysis of Goda and Suzuki [22], who solved the problem using two measurement gauges. The expansion to N gauges was done in the early 1990's by Zelt and Skjelbreia [62]. The use of wavelet coefficients in this application is rather new. In 2010 a method was proposed by Ma et al. [35] using two gauges to separate waves. An expansion to multiple gauges is indispensable to show comparable results to the Fourier coefficients based methods. This subject will be treated more elaborate in Section 3.2.

Noise Reduction

The testing of constructions often includes the effect of impacts on these structures. These impacts are measured through force and pressure sensors. The impacts result in non-stationary elements in the recordings. Examples of recordings of impacts are shown in Section H.1.3. These signals are subject to a lot of noise.

Due to their non-stationary nature, it is expected that filters that apply thresholding in the discrete wavelet domain would perform better than filters in the time or frequency domain.

2.6.1. Research questions

All in all it can be concluded that there is a lot of potential for wavelet analysis in the field of coastal engineering. The main research question of this thesis is:

*How can wavelet analysis improve time-series analysis and processing
in the field of coastal engineering?*

Four research questions have been drafted in order to answer this question. They concern the application of both amplitude and phase determined in the continuous wavelet transform, the application of the discrete wavelet transform in denoising and the added value over the current methods.

1. What improvements are necessary in the (discretised) continuous wavelet transform to improve time-frequency analysis for time series in the field of coastal engineering?
2. Does the separation of incident and reflected waves based on wavelet coefficients for N gauges perform better than the separation based on Fourier coefficients?
3. Which discrete wavelet based algorithm is best suited to remove noise from coastal engineering signals?
4. What is the added value of wavelet analysis over current time series analysis methods in coastal engineering?

The thesis overview in Figure 1.1 has been expanded with these research questions to Figure 2.6. The next chapter focusses on the continuous wavelet transform, in order to answer first two sub questions. In Chapter 4 different wavelet based noise filter algorithms are compared. The added value of both continuous and discrete wavelet transform is discussed for some coastal engineering time series in Chapter 5. The conclusions and the answer to the main research question are presented in Chapter 6.

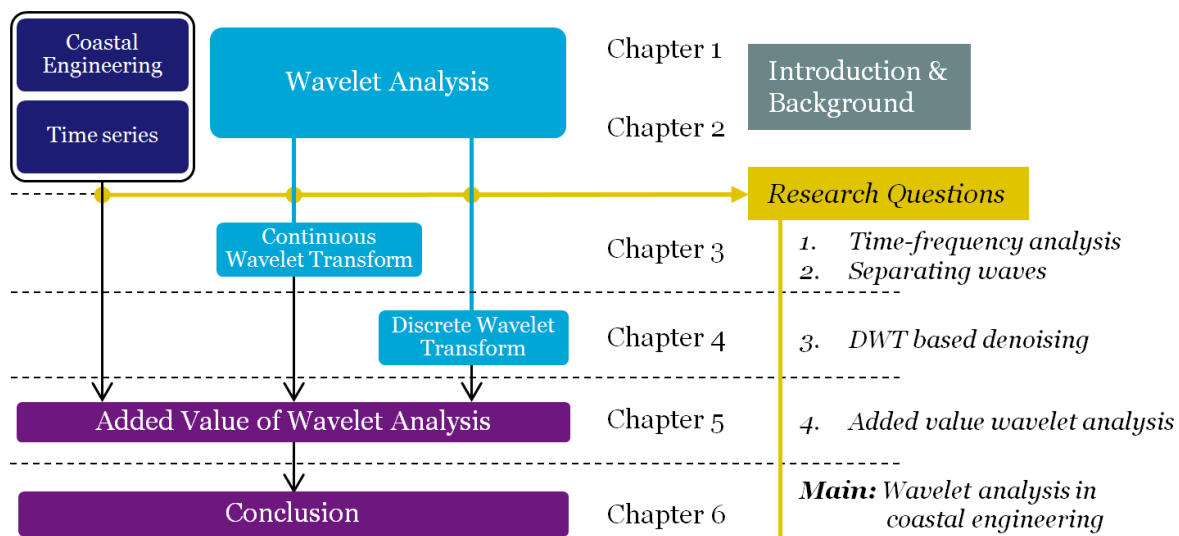
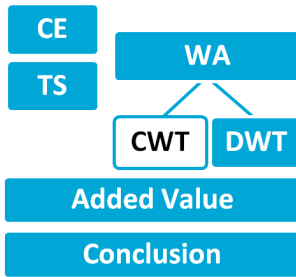


Figure 2.6: The schematic overview of the contents of this thesis expanded with the four research questions.



3

Continuous Wavelet Transform

In the last chapter background information with respect to time series and different analysis methods is given. The objective of this thesis is to investigate the added value of wavelet analysis over current methods. The current methods are often Fourier based, especially when it comes to spectral information. This chapter focusses on application of the continuous wavelet transform, CWT for short, see equation 2.17. To determine the continuous wavelet coefficients, the discretised continuous wavelet transform, DCWT (2.20), is used.

First, the most used and freely available algorithm to determine the DCWT of a signal by Torrence and Compo [53, 54] is presented. Their algorithm is the basis for over 5800 scientific publications (Scopus, 9 May 2017), among which some of Deltares [16, 17]. This algorithm is expanded in order to allow better analysis of time series, with special interest in challenges in coastal engineering time series (Section 3.1). This section is followed by a section with an important coastal engineering application of the continuous wavelet coefficients: the separation of 2D waves. The errors of this algorithm can be analysed using both traditional and wavelet based measures. The added value of these expansions and improvements will be discussed in Chapter 5.

To calculate the coefficient via the DCWT (2.20) it is most efficient to utilise the the convolution property (5). Torrence and Compo [53] have proposed a protocol around the algorithm to determine the reliability of the coefficients as well. The protocol is given below. To the reader unknown terms are discussed after the algorithm. Furthermore, expansions and improvements are discussed per algorithmic step as well. The discrete time series $x[n]$ with N values is expressed as vector $\mathbf{x} = \{x[j]\}_{j=0,\dots,N-1}$.

1. Apply signal extension, by padding zeros, if necessary, this results in the signal \mathbf{x} .
2. Compute the Fourier transform $\mathbf{X} = \mathcal{F}\{\mathbf{x}\}$ using the FFT.
3. Choose a wavelet function ψ (with $\Psi = \mathcal{F}\{\psi\}$) and a set of scales to analyse.
4. For each scale, construct the normalised wavelet function using equation 2.21.
5. Find the wavelet transform at all scales a using the the inverse FFT (2.22).
6. Determine the cone of influence and the Fourier wavelength at that scale. The cone of influence shows which coefficients are effected because the wavelet crosses the edge of the signal.
7. Remove any padding and contour plot the wavelet power spectrum.
8. Determine the confidence contour of the scalogram. Plot this contour and the cone of influence on top of the scalogram.

3.1. Expansion

The above described protocol does little explanation. Some steps can be expanded in order to improve analysis of the DCWT results, specifically for time series from the field of coastal engineering. These expansion of the original algorithm are discussed in the subsections. The computational resources are discussed in Section 5.3.

1. Extending the discrete signal over its boundaries is has two reasons. The first one is the circularity assumption made in the convolution through the FFT. The convolution (4) is an infinite sum. The

signal is not infinite because of its discrete nature. In the circular convolution (7) the signal is assumed to be periodic. This will lead to edge effects in the wavelet coefficients.

Furthermore, the FFT algorithm is most effective for signals of length 2^k , $k \in \mathbb{N}$. If signal extension is applied, it is best to pad a signal with a length $2^{k-1} < L \leq 2^k$ to a length of 2^{k+1} instead of 2^k ($k \in \mathbb{N}$). In Section 3.1.2 different extension methods are added to the just one method discussed by Torrence and Compo [53], zero padding.

2. The computation of the Fourier transform of a function in general is not hard, but when data points are missing, it is impossible to compute the Fourier transform. By adding dummy values at the missing data points, the effects on the spectrum are hard to predict. Missing data points is a frequent defect in coastal engineering time series. In Section 3.1.3 a solution is proposed, together with two methods to access the reliability of the calculated wavelet coefficients. For cyclic time series there will not be a cone of influence and extending is therefore not needed.
3. The choice of wavelet and set of scales influences ones analysis. Different types of continuous wavelets are already addressed in Section 2.3.3. Therefore this will be addressed only shortly in Section 3.1.1. For long signals or a large set of scales, the number of wavelet coefficients will be huge. This is addressed in the same section as the wavelets.
5. Whether the FFT algorithm is still the best way to go for signals with missing data points is addressed in Section 3.1.3.
6. The cone of influence is based on the e -folding time of the wavelet Section 3.1.2. In Section 3.1.3 other reliability measures are addressed, that do not only address the edges of the signal, but also the missing datapoints.
8. The significance contour is not addressed in this research. The significance can be determined analytically or using Monte Carlo methods [53].

3.1.1. Down-sampling

For long signals the discrete wavelet transform might become to large to store in memory, or takes a lot of time to compute the continuous wavelet coefficients. When there is only an interest in relative low frequencies, down-sampling can be applied in order to speed up the process. Down-sampling is the process of reducing the sampling rate of a time series. A down-sampled time series contains less data points, which reduces the CWT computation time and the memory needed to store the result. Down-sampling is a sampling rate conversion process [47]. The focus here lies on the sampling rate conversion in the digital domain and how this effects the CWT coefficients. Consider a signal $x[n]$ with a sampling frequency $f_x = 1/\Delta t_x$ which is down-sampled to signal $y[m]$ with $f_x > f_y = 1/\Delta t_y$. Only rational sampling rate conversion will be addressed, i.e. $f_x/f_y \in \mathbb{Q}$. First an integer conversion factor is addressed, followed by a more general rational factor.

Down-sampling with an integer factor d , can be done by simply selecting every d^{th} value of the time series. This is known as decimating and will lead to major aliasing effects¹. To avoid aliasing, the bandwidth of the signal $x[n]$ has to be reduced to $f_{\max} = f_x/d$. The signal can be decimated after applying the low pass filter $h[n]$, to cut off the high frequencies inducing the aliasing, i.e.

$$y[m] = \sum_{k=0}^{\infty} h[k]x[md - k]. \quad (3.1)$$

This combination of filtering and decimating is called down-sampling and it results in a time-variant system: if $x[n]$ produces $y[m]$, then $x[n - n_0]$ does only result in $y[n - n_0]$ if n_0 is a multiple of d . For the spectra of the original signal $x(t)$ and the resulting spectrum of $y(t)$ the following relationship holds:

$$Y[\omega] = \frac{1}{d} X\left[\frac{\omega}{d}\right].$$

From this relationship can be concluded that the resulting spectrum is a scaled variant of the original spectrum. Note that this scaling does not preserve energy. The energy in the time series is reduces with a factor $1/\sqrt{d}$. This makes sense because the filtering of high frequency components takes energy out of the signal.

When a signals sampling rate is converted by a rational factor i/d , it first has to be interpolated by a factor i , and then decimated by a factor d . The interpolation process by a natural factor i converts the signal $x[n]$

¹For more information about aliasing see Section C.1

to the signal $w[m]$, where $f_w = i f_x$. This is obtained by first adding $i - 1$ zeros between successive values of $x[n]$ to obtain $v[m]$:

$$v[m] = \begin{cases} x[m/i] & m \in \{i\ell \mid \ell \in \mathbb{N}\}, \\ 0 & \text{elsewhere.} \end{cases}$$

The spectrum of the new signal $v[m]$ has the same shape as the spectrum of $x[n]$: $V[\omega] = X[\omega i]$. The spectrum is an i -fold periodic repetition of the original spectrum. These repetitions however are non-unique, thus the signal $v[m]$ has to be passed through a low pass filter $g[m]$. This filter ideally cuts off all repetitions and scales the result by a factor i so that $w[m] = x[m/i]$ for $m \in \{i\ell \mid \ell \in \mathbb{N}\}$. This results in the interpolation

$$w[m] = \sum_{k=-\infty}^{\infty} g[m-k]v[k] = \sum_{k=-\infty}^{\infty} g[m-ki]x[k].$$

When the sampling rate by a factor i/d is considered, first the signal has to be interpolated by a factor i , because this keeps the original spectral shape in tact. Then the signal can be decimated in order to find the signal with a new sampling rate of $f_y = f_x i/d$. The interpolation term already has a normalization term, but the decimation does not. Therefore a signal that has been resampled with a rate of i/d , will have an energy reduction of $1/\sqrt{d}$ as well. For other non rational sampling rate conversions, different techniques can be used, those are not within the scope of this study.

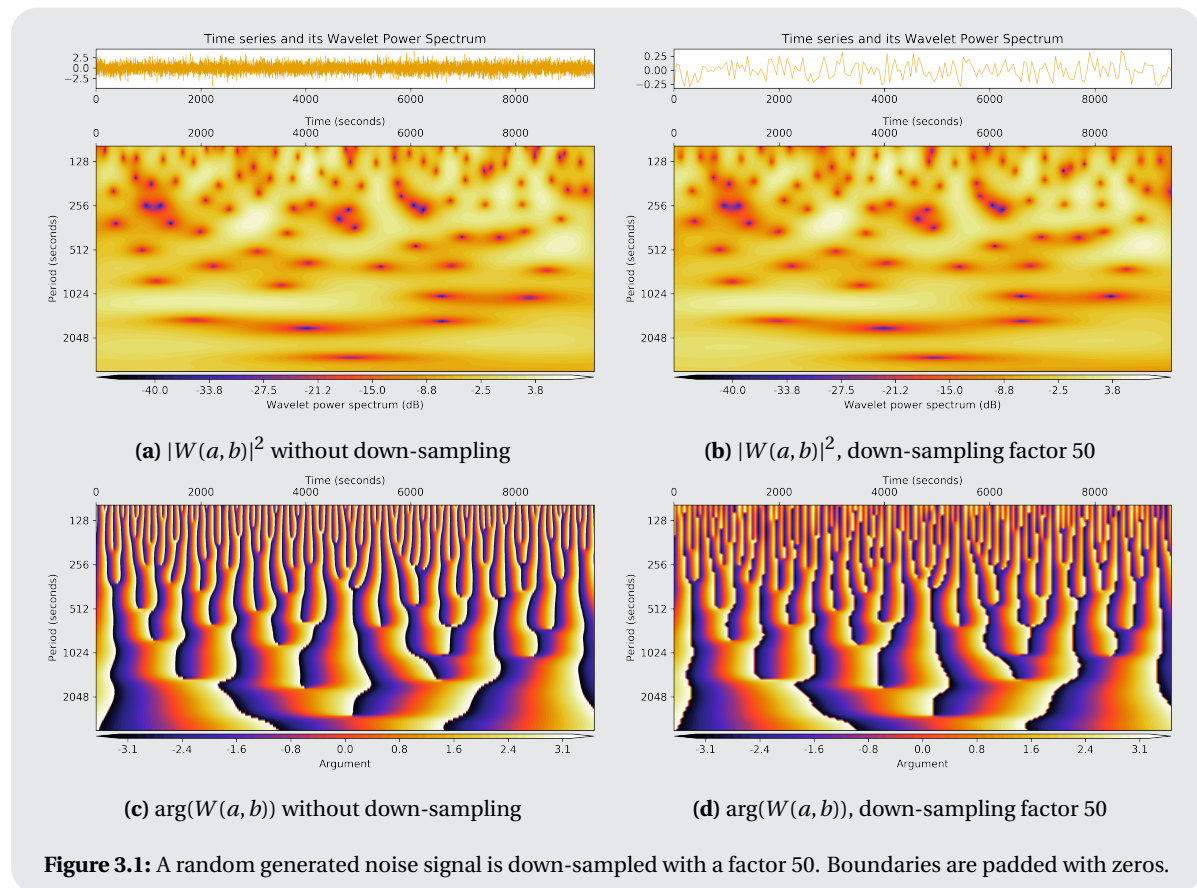
Down-sampling affects the frequency content of the signal by filtering high-frequencies and preserving low frequencies. This operation therefore does not affect the mean of the signal, but the standard deviation of the signal will decay as the new sampling frequency increases. The discrete wavelet coefficients of a down-sampled signal have to be scaled with a factor \sqrt{d} to ensure that the coefficients are equal to the original coefficients. This can be shown by substituting the original signal spectrum $X[\omega]$ for the down-sampled signals spectrum $Y[\omega]$ into equation 2.22. For $\ell = n/d$ holds:

$$W(\ell, a) = \mathcal{F}^{-1} \{ Y(\omega_k) \Psi^*(a\omega_k) \} = \mathcal{F}^{-1} \left\{ \sqrt{d} \frac{1}{d} X\left(\frac{\omega_k}{d}\right) \Psi^*(a\omega_k) \right\}. \quad (3.2)$$

The spectrum $\frac{1}{\sqrt{d}} X\left(\frac{\omega_k}{d}\right)$ is a scaled version of the original spectrum $X(\omega)$, with the energy preserved. Note that this is not the spectrum belonging to the down-sampled signal, but it is only used to not change the wavelet coefficients due to down-sampling. The smaller number of samples in the time series due to down-sampling will result in a smaller number of samples in the wavelet approximation. In Figure 3.1 two different signals are compared.

Demonstration 3.1 (Down-sampling) In Figure 3.1a the wavelet power spectrum of a random signal is presented. The wavelet power spectrum of the down-sampled signal multiplied with a factor $\sqrt{50}$ is found in Figure 3.1b. From the signal at the top it is clear that the down-sampling has influenced a lot of high frequencies. These are therefore not shown, both wavelet power spectra are based on the same set of scales.

In Figure 3.1c and 3.1d, the argument of the wavelet coefficient for both signals is given. Again the same pattern arises as before, however, note the arguments of the down-sampled signal is much coarser. This is especially clear for small periods. This is due to the decrease in resolution. The signal has 9500 data points and the down-sampled signal has less than 200. This leads to a resolution difference visible in the figures.



3.1.2. Wavelet Coefficients near the Boundaries

As explained in Section 3.1, the signal is extended in order to prevent edge effect from distorting the time-frequency analysis near the edges of the signal. At low scales, wavelets have a small support in the time domain, so the number of affected wavelet coefficients will be small. The higher the scale, the larger the support of the wavelet in the time domain and the more wavelet coefficients are affected.

Cone of Influence

The cone of influence (COI) is the name of a line that shows which wavelet coefficients are and are not influenced by the boundaries, in theory. Outside the cone, the coefficients are expected to be influenced by the boundary. In general holds: the closer to the boundary, the more affected a coefficient will be. This cone is based on the e -folding time τ_a of the autocorrelation of the used wavelet [53]. This is the time in which the wavelet power of a Delta Dirac peak at the edge of a signal has decreased by a factor e^{-2} . The cone shows the distance between the edge of the signal and the e -folding time at that scale. This is a linear relationship. This cone of influence is a guideline and not a strict border. There will still be coefficients affected by the signal extension within the cone. Strictly speaking, all coefficients within the compact support of the wavelet are influenced by the signal extension. This compact support is larger than the e -folding time. In the following paragraphs the cone will be expanded and the effect of missing data points on the wavelet coefficients will be added to the cone of influence.

Signal Extension

So the reliability of wavelet coefficients near the edges of the signal depends on the choice of signal extension. So what are the options to pad the time series and which ones are the best? In DWT practice a number of paddings are proposed and implemented [52]. Some of these have also been implemented in the CWT algorithm. After itemising these different extensions, including some advantages and disadvantages, some recommendation for different kinds of signals are presented. Figure 3.2 presents an overview of common signal behaviour and different ways to extend such signals. A number of different paddings are given below.

- No padding:

$$\left| x_0 \quad x_1 \quad \cdots \quad x_{N-2} \quad x_{N-1} \right|$$

No padding is the most obvious and easy choice to make. As mentioned before, some FFT algorithms perform optimal when a signal of length $\ell_{\text{optimal}} \in \{2^k \mid k \in \mathbb{N}\}$ is used. So when padding has to be applied, it makes sense to lengthen the signal up to a length in $\{2^k \mid k \in \mathbb{N}\}$. For the signals we use, the time efficiency is negligible. The FFT algorithm has another characteristic. This is also known as circular convolution [12]. When a convolution is computed through the Fourier transform, the signal is treated like a periodic signal. This could lead to unexpected behaviour at the begin and end of the signal. When padding is applied, it is convenient to make sure that the signal is not extended with just a few data points, but with many, that way the circularity will have little influence on the result. Of course padding is superfluous when handling a cyclic signal.

- Zero padding:

$$\cdots \quad 0 \quad 0 \quad \left| x_0 \quad x_1 \quad \cdots \quad x_{N-2} \quad x_{N-1} \right| \quad 0 \quad 0 \quad \cdots$$

This type of padding is never advised. At a first glance the zeros do not contribute anything to the coefficients near the edge. This is true, however, this can create large jumps in the signal, which leads to unwanted high and low scale behaviour near the edges of the signal.

- Constant padding: repeating the values x_0 and x_{N-1} at the edges of the signal

$$\cdots \quad x_0 \quad x_0 \quad \left| x_0 \quad x_1 \quad \cdots \quad x_{N-2} \quad x_{N-1} \right| \quad x_{N-1} \quad x_{N-1} \quad \cdots$$

This type of padding will not lead to high coefficients at low scales, but might lead to high coefficients in the high scales. Advised to use when $|x_{N-1} - x_0|$ is relatively large.

- Symmetric padding: the series is mirrored in the edges

$$\cdots \quad x_1 \quad x_0 \quad \left| x_0 \quad x_1 \quad \cdots \quad x_{N-2} \quad x_{N-1} \right| \quad x_{N-1} \quad x_{N-2} \quad \cdots$$

- Reflect padding: the series is mirrored in the points x_0 and x_{N-1}

$$\cdots \quad x_2 \quad x_1 \quad \left| x_0 \quad x_1 \quad \cdots \quad x_{N-2} \quad x_{N-1} \right| \quad x_{N-2} \quad x_{N-3} \quad \cdots$$

- Periodic padding: the signal is assumed periodic

$$\cdots \quad x_{N-2} \quad x_{N-1} \quad \left| x_0 \quad x_1 \quad \cdots \quad x_{N-2} \quad x_{N-1} \right| \quad x_0 \quad x_1 \quad \cdots$$

Periodic padding would lead to almost the same scalogram as when no padding is applied. The padded signal is longer than the original signal, which also lengthens the wavelet used in the analysis. For high scales, the support of the wavelet can be important to improve the analysis.

Symmetric, reflect and periodic padding all are best applicable to periodic signals. The difference of between symmetric or reflect padding is the repetition of the value at the edge of the signal. This will mostly affect the low scale coefficient behaviour. When $|x_{N-1} - x_0|$ is relatively large, reflect and symmetric padding are chosen above periodic padding. E.g. periodic padding will then lead to high coefficients in the low scales.

- Linear padding: the end points of the signal are connected linearly:

($\Delta = x_{N-1} - x_0$, h is the number of data points to add)

$$\cdots \quad \left(x_0 - 2\frac{\Delta}{h} \right) \quad \left(x_0 - \frac{\Delta}{h} \right) \quad \left| x_0 \quad x_1 \quad \cdots \quad x_{N-2} \quad x_{N-1} \right| \quad \left(x_{N-1} + \frac{\Delta}{h} \right) \quad \left(x_{N-1} + 2\frac{\Delta}{h} \right) \quad \cdots$$

This type of padding may result in high low scale coefficients, because of the abrupt change of derivative at the edges. For a relatively large value of Δ also high scale coefficients will increase.

- Linear continuation: the ends are extended using the first derivatives in the ends ($d_1 = x_0 - x_1$, $d_N = x_{N-1} - x_{N-2}$)

$$\cdots \quad (x_0 - 2d_1) \quad (x_0 - d_1) \quad \left| x_0 \quad x_1 \quad \cdots \quad x_{N-2} \quad x_{N-1} \right| \quad (x_{N-1} + d_N) \quad (x_{N-1} + 2d_N) \quad \cdots$$

This type of padding is not advised to use. The derivative bases on two neighbouring points can be very large due to the erratic behaviour of (noisy) measurements.

- Smooth padding: instead of using the first order derivative (linear continuation), higher order derivatives are used.
- Smooth padding: in stead of using the derivative based on the edge values, the derivative is based on the difference over the whole signal, i.e. $x_0 - x_{N-1}$. For signals with a trend (i.e. non stationary) this might be very effective.

- Mean value padding: $\bar{x} = \frac{1}{N} \sum_{i=0}^{N-1} x_i$

$$\cdots \quad \bar{x} \quad \bar{x} \quad | \quad x_0 \quad x_1 \quad \cdots \quad x_{N-2} \quad x_{N-1} \quad | \quad \bar{x} \quad \bar{x} \quad \cdots$$

This type of padding has the same effect as zero-padding on a normalized signal. It might lead to some spurious low scale coefficients, but for the high scales it will be an effective estimator of the signal. Do not use when the signal has a trend.

- Noise padding: add noise to both ends, this could be from a Gaussian distribution or a random walk.

$$\cdots \quad \mathcal{N}(\bar{x}, \text{var}) \quad \mathcal{N}(\bar{x}, \text{var}) \quad | \quad x_0 \quad x_1 \quad \cdots \quad x_{N-2} \quad x_{N-1} \quad | \quad \mathcal{N}(\bar{x}, \text{var}) \quad \mathcal{N}(\bar{x}, \text{var}) \quad \cdots$$

On high scale coefficients the effects will be more or less the same as for the mean value padding. The noisy behaviour will result a unpredictable effect at all scales and is not implemented therefore.

Most of these different paddings have been implemented through matrix vector multiplication such that $\mathbf{x}_{\text{padded}} = \mathbf{A}\mathbf{x}$, where

$$\mathbf{A} = \begin{bmatrix} L \\ I \\ R \end{bmatrix}.$$

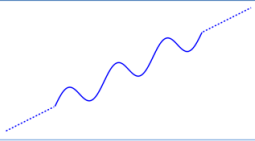
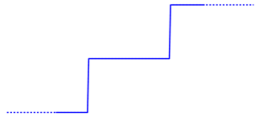


Stationary	Behaviour	Padding	Result
Non stationary	Trend	Smooth* <small>*derivative based on $x_{N-1} - x_0$</small>	
	Large differences	Constant	
Stationary	Periodic behaviour	<ul style="list-style-type: none"> • Symmetric • Reflect • Periodic 	
		Mean	

Figure 3.2: Different signals and the preferred signal extension method. For more explanation of the pro's and con's of a method, consult the more elaborate overview above.

3.1.3. Missing Data Points

Time series in coastal engineering often have some missing data points. These defects are caused by many different causes, for instance an equipment-damaging storm or power failure at sea. When the equipment has been restarted, the measurements are often continued. When applying Fourier analysis, it is only valid to asses the spectrum when the signal is stationary. Missing data points cannot be part of a stationary signal. When these missing data points are replaced by values to apply the Fourier Transform, the signal stays non stationary. The spectrum therefore does not reflect the frequencies of uninterrupted signal. A set of consecutive missing data points is called a gap. Often, a gap is filled with NaN's². When there is a NaN in a time series, a lot of computations return NaN's as well, resulting in a large disturbance in the analysis. Therefore these have to be addressed, there are two relatively simple ways:

²NaN is short for 'not any number'

- Implement the convolution form of the CWT algorithm. When a NaN appears in the computation the coefficient will become a NaN as well, which will lead to a scalogram with blank spots. However, the most efficient convolution algorithms will result in all NaN coefficients, even if the NaN is not in the time support of the wavelet. Moreover, blank spots do not have any indication of reliability or whatsoever. It is just a yes or no: a NaN has or has not been part of the computation.
- When using the FFT form of the CWT algorithm, there cannot be any NaN's in the signal, because this will lead to a full NaN FFT. To use this implementation of the algorithm, missing data points have to be filled in. This will lead to a full scalogram, however, the cone of influence has to be adapted in such a way that it shows the influence of not only the boundary, but also of the NaN's.

The second option has been implemented and tested with coastal engineering data. There are different ways to fill the black spaces. We will consider two cases, the NaN values are depicted with a dash (-):

- NaN('s) at the edge of the signal:
 $\mathbf{x} = [- \dots - x_k \ x_{k+1} \ \dots \ x_{N-1}]$ or $\mathbf{x} = [x_0 \ x_1 \ \dots \ x_k \ - \ \dots \ -]$.
 These are best addressed by the different signal extension modes discussed before; i.e. omit the missing data points near the edges before applying signal extension.
- NaN('s) not at the edge of the signal: $\mathbf{x} = [x_0 \ \dots \ x_k \ - \ \dots \ - \ x_\ell \ \dots \ x_{N-1}]$, which cannot be addressed by the different signal extension modes.

Of course multiple gaps can occur in a signal. Again there are many ways to replace the missing data points:

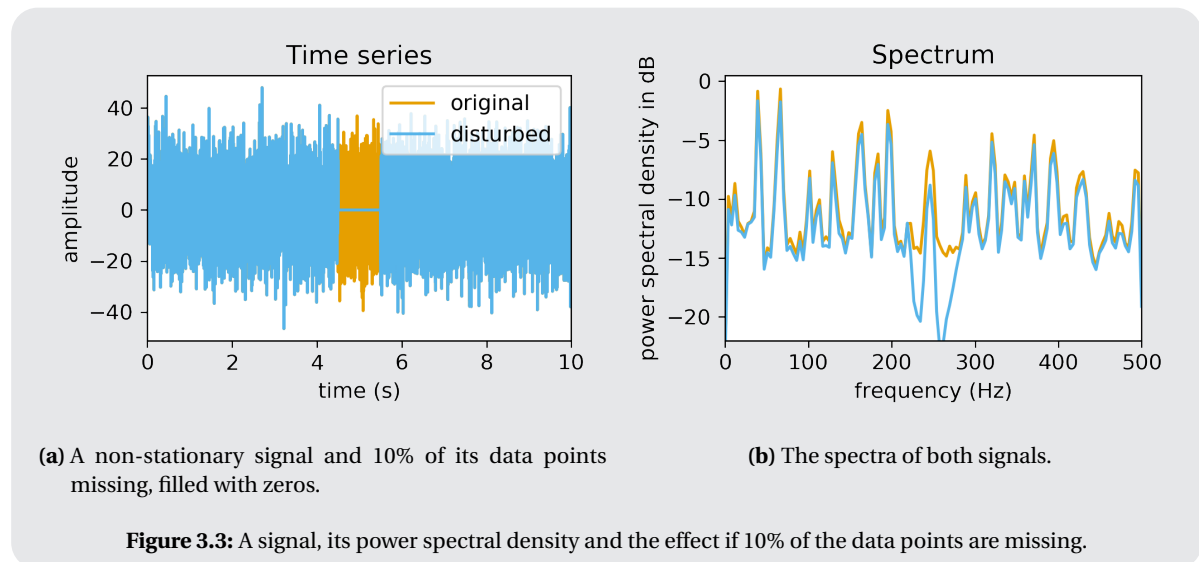
- Zero filling: replace the missing values by 0's.
- Linear filling: fill the gap with a linear interpolation between the values adjacent to the gap.
- Noise filling: replace the missing values with random noise.
- Mean value filling: replace the missing values by the mean value of the time series.
- Median filling: replace the missing values by the the median of the time series.
- Higher order interpolation methods can be used to fill values within gaps. However for these methods to work, there have to be enough values at the edges of the gap. This cannot be assured for field data, where effects like $[\dots - x_i - \dots]$ can occur.

Note that the Fourier transform can be applied to time series where the missing data points are filled as well. The filled data points are non-stationary signal elements, this causes unwanted effects in the resulting spectrum. For a signal with constant frequency content over the whole time, a decrease in power over the whole spectrum is expected when a number of data points is eliminated, plus some effects of the jumps at the edges of the filling. The effect on a signal with a changing frequency content is addressed in Demonstration 3.2.

Demonstration 3.2 (Effect of missing data points on spectrum) In Figure 3.3a two signals are plotted. The original signal consists of 100 random real waves plus a non-linear element: a waveform with a linear increasing frequency from 0 to 500 Hz over the whole duration. In the other signal 10% of the data points are swapped for zeros. If the spectra are compared, we note that for a lot of frequencies the energy indeed is approximately 1 dB less than the energy of the original signal. However in the band 200 - 350 Hz this is not true. The non-linear element loses more power than the waves and thus the spectrum is affected. This effect cannot be predicted when the underlying signal element are unknown.

Expanding the Cone of Influence

In the case of the wavelet power spectrum, some of the coefficients near the gap are affected, but definitely not all coefficients as is the case for the spectrum. Some coefficients, such as low scale, with a time support within the gap, will be affected severely. The same wavelet with a time support completely outside the gap will not be affected at all. So, a lot coefficients are affected a bit and therefore an expression for the degree of affectedness will be derived. If the edges of the gaps are interpreted as beginnings and ends of signals, the cone of influence can be divided into multiple cones of influence.



Demonstration 3.3 (Cones of influence) For the coming demonstrations gaps are made into a signal with zeros. This signal is shown in Figure 3.4a. It contains only zeros and some gaps. The gaps from left to right have a length of 100, 10, 50, 217, 1 data point. The sampling frequency of this signal is 1 Hz.

In that same Figure, the expansion based on the cone of influence is shown. Expected is that the missing of one data point (last gap) should influence a little number of wavelet coefficients. However, in the figure is shown that the effect of one missing data point is enormous. Therefore, a different solution has to be found.

Zones of Influence

Consider a wavelet at scale a . The cone of influence is based on the fact that a certain part of the wavelet extends over the border, based on the e -folding time. Assume this part to be q . If one data point is missing from the signal, the wavelet at scale a is affected less than this part q , however by the expansion of the cone of influence, it is ruled out. Therefore a better measure can be developed. This measure is expressed in the fraction g :

$$g = \frac{\text{number of known data points in time series for } t \in [n - \tau_a, n + \tau_a]}{\text{total number of datapoints in } t \in [n - \tau_a, n + \tau_a]}. \quad (3.3)$$

If this fraction g is 1, there are no missing data points in the 'significant' time support of the wavelet. If this fraction is 0, all data points within this time support are missing. The example presented in Demonstration 3.3 is expanded using this method and presented in Demonstration 3.4. Note that the shapes are not cones any more and therefore the term 'Zones of Influence' will be used from now on (abbreviated to ZOI).

Demonstration 3.4 (Zones of influence 1.0) In Figure 3.4b the contours based on a value of $g = 0.9$ is shown. If the value of g is equal to 1, the cones of influence from Figure 3.4a are retrieved. As the period increases, the time support of the influence increases until there is a vertical line and the influence stops. Even a non-connected area is created at about (5000, 1000). The vertical line is the result of the increasing time support of the wavelet. The fraction g crosses the limit (0.9 in this case) from one to the other scale. For the non-connected area holds the same, where the combination of the two gaps left and right from the $t = 5000$ seconds influence the number of known data points in g (3.3). The solid vertical lines are remarkable and do not seem very natural. A different path therefore is explored in the next section.

3.1.4. Wavelet Mass Distribution

The results presented in Demonstration 3.4 can also be derived in another way. Therefore we define the wavelets mass by the following integral:

$$m_{\psi_a} = \int_{-\infty}^{\infty} (\psi_a(t))^2 dt$$

Assume this mass be to equally distributed over the time interval between the centre of the wavelet (translation n) minus the e -folding time and plus the e -folding time. In other words, the mass of the wavelet between two points t_0 and t_1 is estimated by

$$\int_{t_0}^{t_1} (\psi_a(t))^2 dt \approx \tilde{m}_{\psi_a}(t_0, t_1) = \int_{t_0}^{t_1} \left[\mathbf{1}_{[n-\tau_a, n+\tau_a]}(t) \cdot \frac{m_{\psi_a}}{2\tau_a} \right] dt. \quad (3.4)$$

And so $\tilde{m}_{\psi_a}(n - \tau_a, n + \tau_a) = m_{\psi_a}$. The fraction g from (3.3) can be expressed using these values as well:

$$g = \frac{m_{\psi_a} - \sum_{\text{gaps}} \tilde{m}_{\psi_a}(t_{\max(n-\tau_a, \text{begin gap})}, t_{\min(n+\tau_a, \text{end gap})})}{m_{\psi_a}}. \quad (3.5)$$

This approach thus does not address the place of the gap with respect to the translation of the wavelet. Wavelets have finite support, their amplitude decays to zero and most have the characteristic $|\psi(0)| \geq |\psi(t)| \forall t$. In (3.5) is shown that the fraction g presented in (3.3) does not take these characteristics in account. So a better approximation than (3.4) can be used to determine the effect of missing data points. An improvement can be to use the real wavelets mass between two points in time:

$$\int_{t_0}^{t_1} (\psi_a(t))^2 dt. \quad (3.6)$$

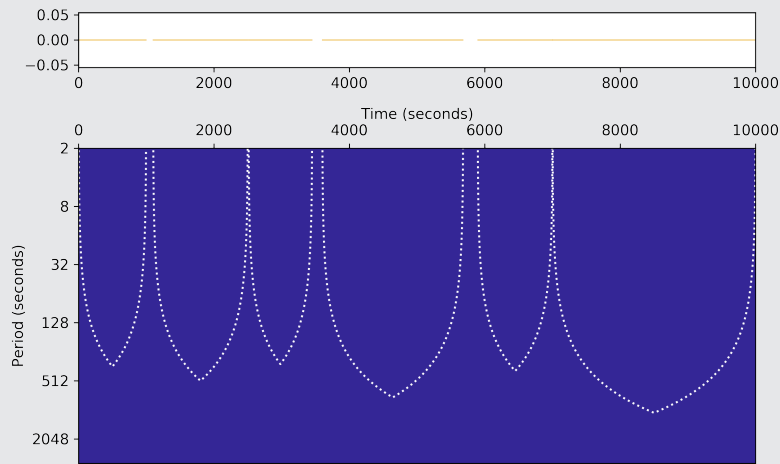
To efficiently compute this integral for discrete time series and possibly multiple gaps, this integral is computed by convolving the normalized mass distribution of the wavelet with a vector \mathbf{x}^{NaN} that is derived³ from the original time series \mathbf{x} :

$$x_i^{\text{NaN}} = \begin{cases} 0 & \text{if } x_i \text{ is a NaN,} \\ 1 & \text{elsewhere} \end{cases}.$$

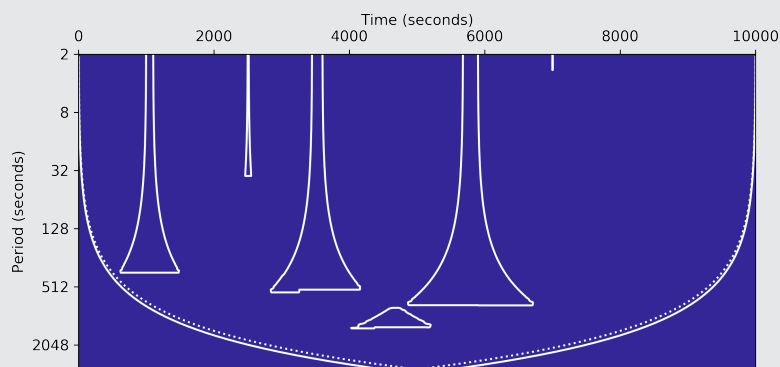
For a signal with some gaps the vector \mathbf{x}^{NaN} is convolved with the vector with function values of $(\psi_a(t))^2$. When the compact support of the wavelet is completely within a gap, the result of the convolution will be 0. When it is completely outside a gap, the result is 1. Other values are within this range. The value represents the relative mass of the wavelet used in computing the coefficient. At the edges of the time series, these values are close to 0.5, because half the wavelet is within the boundaries and half the wavelet is outside. The zones of influence derived from this wavelet mass distribution are expected to be more of a droplet shape, because the wavelets mass is other centred in its centre. The example from Demonstration 3.3 is discussed in Demonstration 3.5. In Demonstration 3.6 the accuracy of the determined values are compared to the real change of the coefficients.

Demonstration 3.5 (Zones of influence 2.0) In Figure 3.4c and 3.4d two contours based on the wavelet mass distribution are presented. The first is based on a significance value of 0.9, the second of 0.95. By comparing the first one with the first attempt from Figure 3.4b, some clear improvements are visible. The vertical stops are not there, and more droplet like shapes are presented. The significance of 0.95 (Figure 3.4d) clearly decreased the number of reliable coefficients. However, compared to the expansion of the cone of influence in Figure 3.4a, below the short gaps there is much improvement.

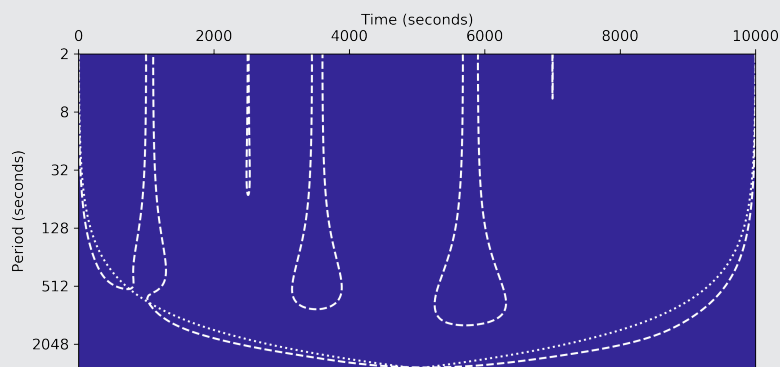
³Use the Python function `x_nan = 1. * numpy.isnan(x)`



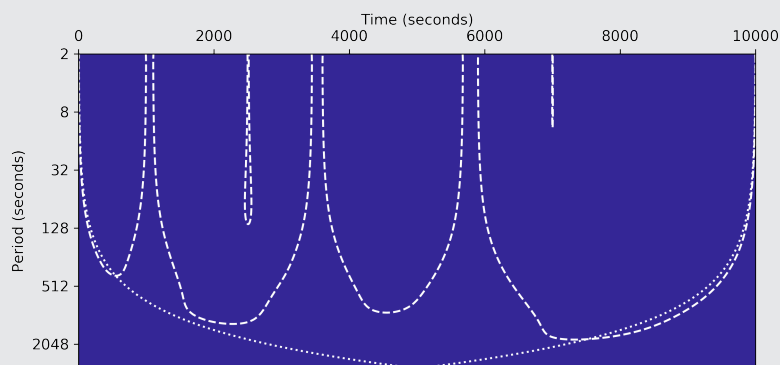
(a) On top: zero signal filled with gaps, below: multiple cones of influence: the begin and end of gaps are interpreted as respectively the end and begin of a signal.



(b) Zones of influence based on the fraction g from (3.3). Solid contour shows $g = 0.9$.



(c) Zones of influence based on the wavelets mass distribution. Dashed contour shows significance 0.9 based on wavelet mass distribution.



(d) Zones of influence based on the wavelets mass distribution. Dashed contour shows significance 0.95 based on wavelet mass distribution.

Figure 3.4: From cone of influence to zones of influence, in three steps. All figures are based on the Morlet 6 wavelet. The dotted line in (b)-(d) shows the cone of influence of the boundaries based on the e -folding time.

Demonstration 3.6 (Accuracy of the zones) The most important question regarding the zones of influence is whether the estimate of this influence is correct. I.e. consider a zone of influence of 95%: the coefficients within this zone should be disturbed at most 5%, but are they?

To find out, an artificial signal is created. The signal consists of a number of sines, cosines and a small noise contribution. First the clean scalogram is created, denoted by S^{signal} (Figure 3.5a). The signal extension method used is the zero padding. Then a number of NaN's are introduced, which results in the scalogram S^{NaN} in Figure 3.5b. This scalogram is extended using the smooth signal extension method, based on the first derivative at the edge of the signal.

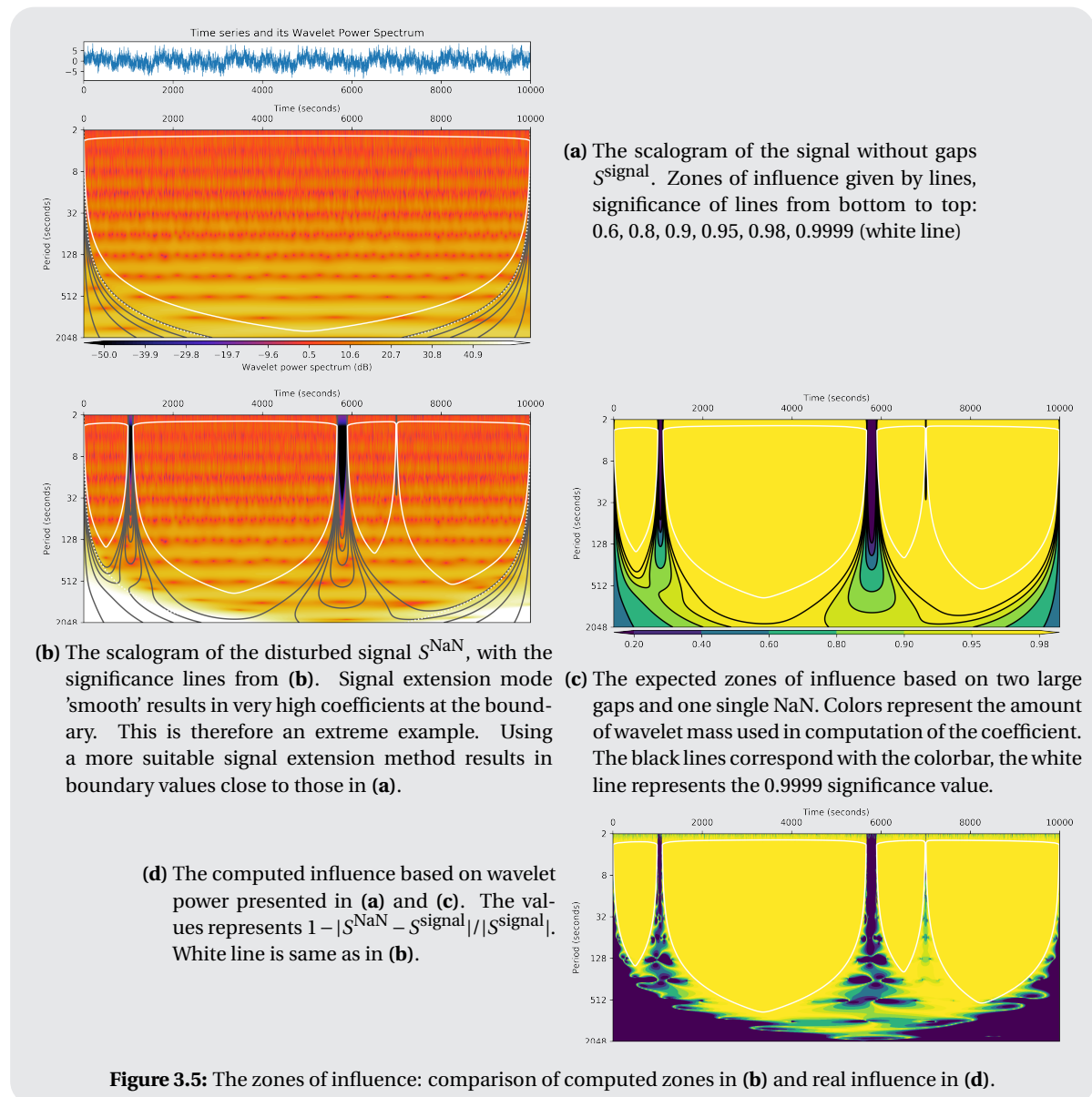
First look at the computed significance levels of the zones of influence of the signal with gaps in Figure 3.5c. As expected the influence of the gaps decreases as the scales increase (as do the periods). The scalogram of the disturbed signal S^{NaN} shows that the gaps and the different signal extension method have major effects on the wavelet coefficients. At the borders, the coefficients increase, due to the extreme boundary condition. The coefficients in the gaps have not uniformly increased or decreased with respect to the coefficients in Figure 3.5a. We note that the red line, the 0.9999 significance border contains most of the changes, but not all. Now we compute the relative change of the scalograms: $|S^{\text{signal}} - S^{\text{NaN}}|/|S^{\text{signal}}|$. To compare this to the computed zones of influence in Figure 3.5c, the value $1 - |S^{\text{signal}} - S^{\text{NaN}}|/|S^{\text{signal}}|$ is shown in Figure 3.5d. This way the value 1 denotes a 100% match between the original and adjusted coefficient and the 0 a complete mismatch. The predicted zones of influence differs a lot from the real zones of influence.

The influence can be split into contributions of the boundary and of the gap. First consider the contribution of the boundary. Here the most striking feature is that the wavelet coefficient is affected severely by the signal extension method, although a small part of the wavelet is expected to be determined by the signal extension. The effect of the gaps is a lot closer to the computed zones of influence, however, still there is some unwanted behaviour. In the low scale range the highly disturbed wavelet coefficients are well predicted. For the larger scales, there are many spots where the difference is much larger than expected. For instance around the period of 512 seconds, under the second gap at 5800 seconds, large differences are present. Compare these spots in the scalograms in Figure 3.5a and 3.5b and note that these spots occur mostly where the wavelet coefficients are relatively low. The absolute difference (figure not included) shows that the absolute change of the high and low valued coefficients around this point is very close. Therefore the relative change is much worse for coefficients with a small modulus.

At the lowest scales an interesting effect arises: wavelet coefficients of the lowest scales at the edges of the signal and the gaps, belonging to wavelets that theoretically should not be influenced by the gaps are inside the computed zone of influence in Figure 3.5c. In Figure 3.5b and 3.5d it is clear that the low scale coefficients are very much affected by the gaps and the different signal extension. These figures are created using the Morlet wavelet, $\omega_0 = 6$. This effect does also show for other wavelets. This effect is independent of the gaps in the signal, or with the signal extension method: it is the result of the approximation of the low scale wavelet. For very low scales, the approximation of the wavelet function has just a few values that are not close to zero, and all the others are close to zero, but not exactly zero. This results in a large effect of the time series values outside the theoretical compact support of the wavelet on the low scale coefficients.

The definition of the cone of influence is based on the effect of a discontinuity at the edge of the signal [53], not the wavelet mass distribution. This definition cannot be used for gaps in the signal. Moreover, most users will have more feeling for the wavelets mass distribution. In Demonstration 3.6 the real disturbance and the disturbance based on the wavelets mass distribution have been compared. Three important things are shown. Firstly, the zone(s) of influence have to be interpreted with great care, they do give a general insight into changes of the coefficients by gaps and the boundaries, but they do not predict the influence very well. And secondly, the choice of signal extension method has a large influence on the scalogram. It is important to choose a suitable signal extension method. From these effects of the extensions, we may conclude that better filling methods may reduce the influence of the gaps on the scalogram enormously. When the filling of the gap is close to the original signal, the theoretical zones of influence are a much better approximation of the real influence. For instance, when a single NaN is replaced by an average of the two neighbouring values, it is very hard to spot the differences between the original and the signal with gaps.

The detection and correction of missing data is not only a challenge in this engineering area. Especially in data transmission and storage this is a frequent problem [6]. The most used solutions are known as linear



codes. These codes impose a strong structural property to data before being transmitted or stored. Checks are built in to help detect and restore errors in the data, supported by these structural properties. These techniques depend on a fully known signal to start with, which is not the case for data points that have not been present at all. Better estimates for wavelet coefficients can be reached by filling the data points using data at other moments, or data from other measurement points (in combination with a model). Fourier analysis can then also be applied again, however, there will not be a cone of influence which shows the analyst which coefficients are expected to be affected by the filling.

Finally, the minimum scale advised to use differs per wavelet. The low scale coefficients might be dominated by the signal values outside the theoretical compact support of the wavelet instead of the values within. The assumption of $2\Delta t/\lambda$ may not be sufficient. λ is the Fourier wavelength, which relates the centre period T of the wavelet with its scale a through $\lambda a = T$. By using a minimum scale of $4\Delta t/\lambda$ the problem is definitely solved.

- Different types of filling have different effects on the scalogram.
- Already known from theory, and very clear from the figures: sharp edges result in changes of coefficients at all scales. The filling of a gap introduces behaviour that does not belong to the original signal.

- The length of the missing data points and the effects of (different types of) filling at certain scales are correlated.
- Significance testing can be used to interpret the filled parts of the time series.

3.2. Separation of Incident and Reflected Waves (2D)

In Section 2.4.2 is explained why the separation of incident and reflected waves is of special interest in the field of coastal engineering. A much used solution to this problem was published by Mansard and Funke [39], who recover the separated waves based on three points of measurement. This method was generalised to N points by Zelt and Skjelbreia [62]. Both these methods use amplitude and phase information in Fourier coefficients to separate these waves. Throughout the rest of this chapter, the method of Zelt and Skjelbreia [62] will be referred to, because for two or three gauges in the system, their solution is equal to the solution as published by respectively Goda and Suzuki [22] and Mansard and Funke [39]. This section starts with the general theory about how to separate incident from reflected waves, based on the method developed by Ma et al. [35]. They proposed a wavelet coefficient based method using two gauges. An expansion of this method will be presented in Section 3.2.2, followed by all kinds of factors influencing the results of the separation.

Let us first start with the theory. A general experimental set-up in which incident and reflected waves are to be separated is shown in Figure 3.6. On the far left, there is a wave maker which creates waves. These waves propagate through the flume and bump onto the construction at the far right of the channel. For simplicity assume that they are being (partially) reflected or absorbed at this point. So there are waves travelling from left to right, and from right to left, i.e. in one dimension. Let us assume that the mean water level is h meters above the floor. If this mean water level changes (over time or over space) this problem becomes a two dimensional problem.

Throughout the flume wave gauges are placed, which measure the water level, which is constantly changing due to the waves travelling back and forth. In the sketch in Figure 3.6 two gauges are depicted, later a scenario with more than two gauges will be addressed. The waves created by the wave maker are assumed to be a linear combination of harmonics. A wave gauge will therefore also measure a linear combination of harmonics, i.e. the wave gauges measures

$$\sum_{i=-\infty}^{\infty} a_I \cos(\omega_I t + \theta_I). \quad (3.7)$$

All these waves have an individual amplitude a_I , frequency ω_I and phase θ_I . This assumption of linearity allows us to separate all waves independently and sum the reconstructed incident and reflected waves.

So, from now on one single wave propagating from left to right through the channel will be considered:

$$\eta_{\text{incident}}(t) = W^I \cos \omega t + \theta_I. \quad (3.8a)$$

This is the wave created by the wave maker at the left of the channel. This point, i.e. $x = 0$, will be the point of reference for now. This wave has amplitude W^I , radial frequency ω and phase θ_I . At the end of the channel the wave is being partially reflected or absorbed. The reflected wave as observed from the reference point (wave maker) is described by

$$\eta_{\text{reflected}}(t) = W^R \cos(\omega t + \theta_R). \quad (3.8b)$$

Typically $W^R \leq W^I$ holds for the amplitude of the reflected wave. However, this is not a necessary condition. The phase of the reflected wave, θ_R , depends among others on the length of the channel, the original phase θ_I and the reflection properties of the construction on the other end.

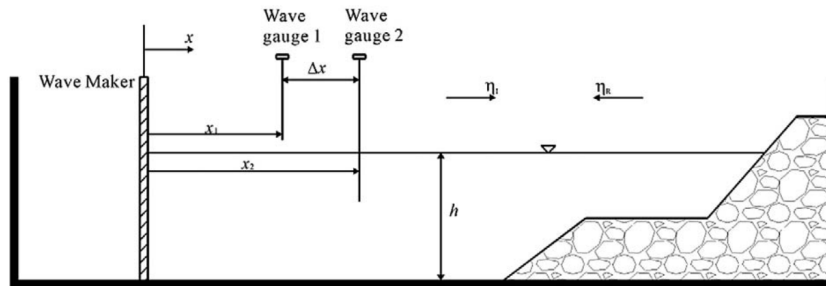


Figure 3.6: Measurement set-up in a flume for separating incident and reflected waves, two gauges are depicted [35, fig.1].

Now, assume there are two gauges in the channel, one on a distance of x_1 from the wave maker and the second one at a distance $x_2 > x_1$. Define $x_2 - x_1 = \Delta x$, as depicted in Figure 3.6. The surface elevation as recorded at point x_1 is the sum of the incident and reflected wave at that point:

$$\eta_1(x_1, t) = W^I \cos(\omega t - kx_1 + \theta_I) + W^R \cos(\omega t + kx_1 + \theta_R). \quad (3.9a)$$

The incident and reflected wave were defined at the reference point, so at point x_1 a phase shift is introduced. This phase shift is expressed in $-kx_1$, for the reflected wave it is $+kx_1$ because it is travelling in the other direction. This phase shift depends on the wavenumber k , more theory about this number is presented in Section F.1. It is important to know that the wavenumber depends on the depth of the water the wave is travelling in, the frequency of the wave and the gravitational acceleration, which in general is assumed constant on earth. At point x_2 , the measured water level is thus described by

$$\begin{aligned} \eta_2(x_2, t) &= W^I \cos(\omega t - kx_2 + \theta_I) + W^R \cos(\omega t + kx_2 + \theta_R) \\ &= W^I \cos(\omega t - kx_1 - k\Delta x + \theta_I) + W^R \cos(\omega t + kx_1 + k\Delta x + \theta_R). \end{aligned} \quad (3.9b)$$

Reconstructing the incident and reflected waves through these equations directly is hard, therefore their analytic forms are being used. The real part of these analytic wave descriptions are the waves described by (3.9).

$$\zeta_1(x_1, t) = W^I e^{i(\omega t - kx_1 + \theta_I)} + W^R e^{i(\omega t + kx_1 + \theta_R)} \quad (3.10a)$$

$$\begin{aligned} \zeta_2(x_1, t) &= W^I e^{i(\omega t - kx_1 - k\Delta x + \theta_I)} + W^R e^{i(\omega t + kx_2 + k\Delta x + \theta_R)} \\ &= W^I e^{i(\omega t - kx_1 + \theta_I)} e^{-ik\Delta x} + W^R e^{i(\omega t + kx_2 + \theta_R)} e^{ik\Delta x}. \end{aligned} \quad (3.10b)$$

The incident and reflected wave can be reconstructed from these equations through the following relationship⁴ [35]:

$$W^I e^{i(\omega t - kx_1 + \theta_I)} = \operatorname{Re} \left(\frac{\zeta_1(x_1, t) e^{ik\Delta x} - \zeta_2(x_1, t)}{2i \sin(k\Delta x)} \right), \quad (3.11a)$$

$$W^R e^{i(\omega t - kx_1 + \theta_R)} = \operatorname{Re} \left(\frac{\zeta_1(x_1, t) e^{-ik\Delta x} - \zeta_2(x_1, t)}{-2i \sin(k\Delta x)} \right). \quad (3.11b)$$

These equations can be extended to a sloping bathymetry and obliquely incident waves [35, 36].

So, instead of using the analytical expressions of the waves in (3.11), the continuous wavelet coefficients are used, as published by Ma et al. [35]. When these two equations are solved, the coefficients of respectively the incident and reflected wavelet transformed waves are recovered. The time series of the incident and reflected waves can then be reconstructed through the reconstruction equation (2.24). Ma et al. [35] use numerical examples, simulations with large numbers of waves in stationary and non-stationary situations, to show that the method is independent of the length of the channel. They find an average reflection coefficient error of 3.3%. A comparable error is found in the verification presented in Figure F.1.

3.2.1. Dependency of Gauge Distance Δx and Wavenumber k

The largest influence on the correctness of the recovered separate waves is the distance between the gauges. The reconstruction formulas (3.11a) and (3.11b) both depend on the factor $\sin(k\Delta x)$. Remember that the wavenumber k actually depends on the frequency f , i.e. from (E.1) $k(f, h, g)$ can be derived. Figure 3.7 shows the effect of the distance between the gauges on that factor $\sin(k\Delta x)$. The value of this factor sometimes is zero or a value very close to zero. Computational errors are caused by values of $\sin(k\Delta x)$ close to or equal to 0. These errors result in the wrong estimation of the separate waves. For values where $\sin(k\Delta x) = 0$ the solution cannot be derived analytically either.

The best solution is to place the gauges in such a way that the factor $\sin(k\Delta x) > 0$ for all frequencies of interest. This can however be impossible for a large frequency bandwidth. This problem can be solved by combining measurements from gauges at multiple distances. The Fourier counterpart of this algorithm, developed by Goda and Suzuki [22], has this same shortcoming. This algorithm has been expanded twice, once for three gauges (by Mansard and Funke [39]) and the last time to N gauges (by Zelt and Skjelbreia [62].)

⁴In Section E.2 the derivation of this result is given.

This expansion is applied for the wavelet coefficients in Section 3.2.2. An other solution would be to carefully choose the spacing of the scales. This option, however, is not explored in this thesis.

Another important assumption has been made in the derivation process. That assumption is that the wavenumber based on the centre frequency of the wavelet at scale a , $f_c = f_\psi \cdot a$, is representable for all frequencies in the bandwidth of the wavelet $\psi_a(t)$. Clearly this is not true and this assumption cannot be without side effects. This and a comparison to the method using the Fourier transform by Zelt and Skjelbreia [62] will be addressed after expanding the method to N gauges.

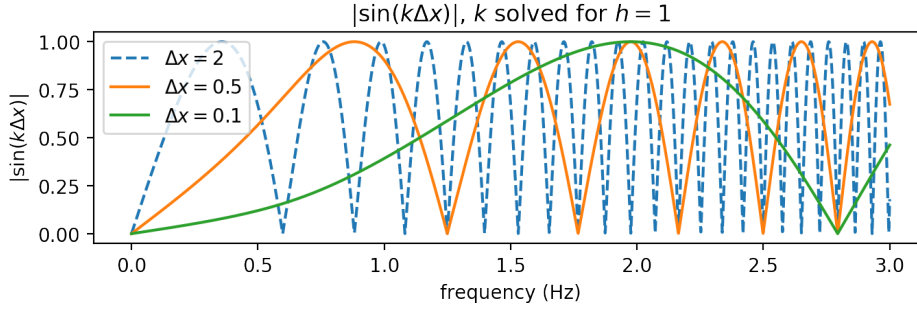


Figure 3.7: The effect of the placement of the gauges on the factor $\sin(k\Delta x)$. The wavenumber is based on the solution of the dispersion equation for a water depth of 1 meter.

3.2.2. Expanding to N Gauges

As described in the last section, the information of multiple gauges can be used to separate the incident and reflected wave more accurately over larger bandwidths. This section starts with a mathematical derivation for a number of $N \geq 2$ gauges. This derivation is followed by a verification that shows that the $N = 2$ case results in the same equations as Ma et al. [35]. Then the error of the solution is analysed.

So now assume that, instead of two, there are N gauges in the system: at different distances $x_1 < x_j < x_N$. Again assume the incident and reflected wave are described by (3.8). Define the distance between gauge m and n as $\Delta x_{mn} = x_n - x_m$. Gauge m is used as a reference point, then the analytical form, based on the wavelet transform at scale a , of the wave height measured at gauge j becomes

$$\zeta_{a,j}(t) = W_{a,j}^I e^{i(\omega_a t - k_a x_m + \theta_a^I)} e^{-ik_a \Delta x_{mj}} + W_{a,j}^R e^{i(\omega_a t + k_a x_m + \theta_a^R)} e^{ik_a \Delta x_{mj}}, \quad j = 1, \dots, N. \quad (3.12)$$

This is a generalisation of the step from (3.9a) to (3.9b). The modulus operator has been left out for simplicity. Where k_a is the wavenumber for the centre frequency of the wavelet at scale a . First we substitute the analytical representation of the incident and reflected wave at the reference point m with

$$W_{a,j}^I e^{i(\omega_a t - k_a x_m + \theta_a^I)} = Z_a^I, \quad W_{a,j}^R e^{i(\omega_a t + k_a x_m + \theta_a^R)} = Z_a^R.$$

For $N = 2$ this system of equations from (3.12) is solved by (3.11), as will be shown later. For larger N , this system becomes overdetermined. The linear least squares method is applied to solve this. Instead of solving Z_a^I and Z_a^R , equations for the estimates, respectively \widetilde{Z}_a^I and \widetilde{Z}_a^R , will be solved. Therefore the residual $\epsilon_{a,j}$ is defined as the difference between the estimated water level at gauge j minus the measured water level at gauge j (both for scale a):

$$\epsilon_{a,j} = \left(\widetilde{Z}_a^I e^{-ik_a \Delta x_{mj}} + \widetilde{Z}_a^R e^{ik_a \Delta x_{mj}} \right) - \zeta_{a,j}. \quad (3.13)$$

The system is solved for \widetilde{Z}_a^I and \widetilde{Z}_a^R by minimizing the sum of the moduli of the residuals. For reasons discussed later, a weighing factor $w_{a,j} > 0$ is added per gauge. Define the sum of the weighing factors as $\Omega_a = \sum_j w_{a,j}$. The objective is to determine the minimum of

$$\sum_{j=1}^N w_{a,j} |\epsilon_{a,j}|^2 = \sum_{j=1}^N w_{a,j} \epsilon_{a,j} \epsilon_{a,j}^* \quad (3.14)$$

The minimum of (3.14) is found when [62]:

$$\sum_{j=1}^N w_{a,j} \epsilon_{a,j} e^{ik_a \Delta x_{mj}} = \sum_{j=1}^N w_{a,j} \epsilon_{a,j} e^{-ik_a \Delta x_{mj}} = 0. \quad (3.15)$$

Substituting (3.13) into (3.15) yields the two equations:

$$\begin{aligned} \sum_{j=1}^N w_{a,j} \left(\widetilde{Z}_a^I e^{-ik_a \Delta x_{mj}} + \widetilde{Z}_a^R e^{ik_a \Delta x_{mj}} - \zeta_{a,j} \right) e^{ik_a \Delta x_{mj}} = 0 &\Rightarrow \sum_{j=1}^N w_{a,j} \zeta_{a,j} e^{ik_a \Delta x_{mj}} = \widetilde{Z}_a^I \Omega_a + \widetilde{Z}_a^R \sum_{j=1}^N w_{a,j} e^{2ik_a \Delta x_{mj}}, \\ \sum_{j=1}^N w_{a,j} \left(\widetilde{Z}_a^I e^{-ik_a \Delta x_{mj}} + \widetilde{Z}_a^R e^{ik_a \Delta x_{mj}} - \zeta_{a,j} \right) e^{-ik_a \Delta x_{mj}} = 0 &\Rightarrow \sum_{j=1}^N w_{a,j} \zeta_{a,j} e^{-ik_a \Delta x_{mj}} = \widetilde{Z}_a^I \sum_{j=1}^N w_{a,j} e^{-2ik_a \Delta x_{mj}} + \widetilde{Z}_a^R \Omega_a. \end{aligned}$$

This can be written as a matrix-vector product:

$$\begin{bmatrix} \Omega_a & \sum_{j=1}^N w_{a,j} e^{2ik_a \Delta x_{mj}} \\ \sum_{j=1}^N w_{a,j} e^{-2ik_a \Delta x_{mj}} & \Omega_a \end{bmatrix} \begin{bmatrix} \widetilde{Z}_a^I \\ \widetilde{Z}_a^R \end{bmatrix} = \begin{bmatrix} \sum_{j=1}^N w_{a,j} \zeta_{a,j} e^{ik_a \Delta x_{mj}} \\ \sum_{j=1}^N w_{a,j} \zeta_{a,j} e^{-ik_a \Delta x_{mj}} \end{bmatrix}. \quad (3.16)$$

This matrix-vector product has a unique solution if the matrix is non-singular. Singularity should thus be avoided, this will be addressed later. \widetilde{Z}_a^I and \widetilde{Z}_a^R are solved as:

$$\widetilde{Z}_a^I = \frac{1}{D} \left(\Omega_a \sum_{j=1}^N w_{a,j} \zeta_{a,j} e^{ik_a \Delta x_{mj}} - \sum_{j=1}^N w_{a,j} e^{2ik_a \Delta x_{mj}} \sum_{j=1}^N w_{a,j} \zeta_{a,j} e^{-ik_a \Delta x_{mj}} \right), \quad (3.17a)$$

$$\widetilde{Z}_a^R = \frac{1}{D} \left(\Omega_a \sum_{j=1}^N w_{a,j} \zeta_{a,j} e^{-ik_a \Delta x_{mj}} - \sum_{j=1}^N w_{a,j} e^{-2ik_a \Delta x_{mj}} \sum_{j=1}^N w_{a,j} \zeta_{a,j} e^{ik_a \Delta x_{mj}} \right), \quad (3.17b)$$

with the discriminant

$$D = \Omega_a^2 - \sum_{j=1}^N w_{a,j} e^{-2ik_a \Delta x_{mj}} \sum_{j=1}^N w_{a,j} e^{2ik_a \Delta x_{mj}}. \quad (3.17c)$$

Note that the discriminant D is a real quantity and can be rewritten to [62]:

$$D = \Omega_a^2 - \left(\sum_{j=1}^N w_{a,j} \cos(2k_a \Delta x_{mj}) \right)^2 - \left(\sum_{j=1}^N w_{a,j} \sin(2k_a \Delta x_{mj}) \right)^2 = 4 \sum_{j=1}^N \sum_{\ell < j} w_{a,j}^2 \sin^2(k_a \Delta x_{\ell j}). \quad (3.18)$$

Verification for Two Gauges

First is shown that the N gauge expression for $N = 2$ is equal to the method of Ma et al. [35]. By manipulating (3.17a), we can express the separation coefficient at scale a , $C_{a,j}$, as

$$\widetilde{Z}_a^I = \sum_{j=1}^N C_{a,j} \zeta_{a,j} = \sum_{j=1}^N \zeta_{a,j} \frac{w_{a,j}}{D} \underbrace{\left(\Omega_a e^{ik_a \Delta x_{mj}} - e^{-ik_a \Delta x_{mj}} \sum_{\ell=1}^N w_{\ell} e^{2ik_a \Delta x_{m\ell}} \right)}_{=C_{a,j}}. \quad (3.19)$$

The coefficient $C_{a,j}$ can be simplified to:

$$\begin{aligned} C_{a,j} &= \frac{w_{a,j}}{D} \left(\Omega_a e^{ik_a \Delta x_{mj}} - e^{-ik_a \Delta x_{mj}} \sum_{\ell=1}^N w_{\ell} e^{2ik_a \Delta x_{m\ell}} \right) \\ &= \frac{w_{a,j}}{D} \left(\sum_{\ell=1}^N w_{\ell} e^{ik_a \Delta x_{mj}} - e^{-ik_a \Delta x_{mj}} \sum_{\ell=1}^N w_{\ell} e^{2ik_a \Delta x_{m\ell}} \right) \\ &= \frac{w_{a,j}}{D} \sum_{\ell=1}^N w_{\ell} \left(e^{ik_a \Delta (x_j - x_m)} - e^{ik_a \Delta (2x_{\ell} - 2x_m)} e^{-ik_a \Delta (x_j - x_m)} \right) \\ &= \frac{w_{a,j}}{D} \sum_{\ell=1}^N w_{\ell} e^{-ik_a (x_m - x_{\ell})} 2i \sin(k_a (x_j - x_{\ell})) \quad \left[\text{use } e^{i(a-b)} - e^{-i(a-b)} = e^{i(2c-2b)} - e^{-i(b-c)} 2i \sin(a-c) \right] \\ &= 2i \frac{w_{a,j}}{D} e^{-ik_a x_m} \sum_{\ell=1}^N w_{\ell} e^{ik_a x_{\ell}} \sin(k_a \Delta x_{\ell j}) \end{aligned}$$

Now assume there are two gauges at a distance $x_1 < x_2$, and the equations are solved at x_1 (thus $m = 1$). The weights of the two gauges are both equal to 1, i.e. $w_1 = w_2 = 1$. Then the discriminant (3.18) simplifies to:

$$D = 4 \sin^2(k_a \Delta x_{12}).$$

$C_{a,1}$ and $C_{a,2}$ are then solved as:

$$\begin{aligned} C_{a,1} &= 2i \frac{1}{D} e^{-ik_a x_1} \sum_{\ell=1}^2 e^{ik_a x_\ell} 2i \sin(k_a \Delta x_{\ell 1}) = 2i \frac{1}{D} e^{-ik_a x_1} \left(e^{ik_a x_1} \sin(k_a \Delta x_{11}) + e^{ik_a x_2} \sin(k_a \Delta x_{21}) \right) \\ &= 2i \frac{1}{D} e^{-ik_a x_1} \left(-e^{ik_a x_2} \sin(k_a \Delta x_{12}) \right) = -2i \frac{1}{4 \sin^2(k_a \Delta x_{12})} e^{-ik_a x_1} e^{ik_a x_2} \sin(k_a \Delta x_{12}) \\ &= \frac{e^{ik_a \Delta x_{12}}}{2i \sin(k_a \Delta x_{12})} \end{aligned}$$

and

$$\begin{aligned} C_{a,2} &= 2i \frac{1}{D} e^{-ik_a x_1} \sum_{\ell=1}^2 e^{ik_a x_\ell} 2i \sin(k_a \Delta x_{\ell 2}) = \frac{2i}{D} e^{-ik_a x_1} \left(e^{ik_a x_1} \sin(k_a \Delta x_{12}) + e^{ik_a x_2} \sin(k_a \Delta x_{22}) \right) \\ &= \frac{2i}{4 \sin^2(k_a \Delta x_{12})} \sin(k_a \Delta x_{12}) \\ &= \frac{-1}{2i \sin(k_a \Delta x_{12})}. \end{aligned}$$

When these values for C_1 and C_2 are substituted into equation 3.19 equation 3.11a is recovered. For the reflected wave, the same similarity with equation 3.11b can be shown, using the relationship [62]

$$\widetilde{Z}_a^R = \sum_{j=1}^N C_{a,j}^* \zeta_{a,j}. \quad (3.20)$$

Numerical test also result in exactly the same results using the analytic solution (3.11) or the least squares approximation (3.17) for $N = 2$.

3.2.3. Error Analysis and Reduction

The residual at scale a is defined by (3.13). This can be rewritten such that

$$\zeta_{a,j} = \widetilde{Z}_a^I e^{-ik_a \Delta x_{mj}} + \widetilde{Z}_a^R e^{ik_a \Delta x_{mj}} - \epsilon_{a,j}.$$

If this expression is filled into (3.19) and (3.20) an expression of the error for both the incident and reflected wave is found as

$$\widetilde{Z}_a^I = Z_a^I - \sum_{j=1}^n C_{a,j} \epsilon_{a,j}, \quad \widetilde{Z}_a^R = Z_a^R - \sum_{j=1}^n C_{a,j}^* \epsilon_{a,j}.$$

If the residual signal is zero the 'exact' coefficients are obtained⁵. This is de case for $N = 2$. Otherwise the error at gauge j for scale a , $\epsilon_{a,j}$, is amplified by the coefficient $C_{a,j}$. This amplification of the error is represented by the factor

$$|C_{a,j}| = \left| \frac{\partial \widetilde{Z}_a^I}{\partial \epsilon_{a,j}} \right| = \left| \frac{\partial \widetilde{Z}_a^R}{\partial \epsilon_{a,j}} \right| = 2 \frac{w_{a,j}}{D} \left| \sum_{\ell=1}^N w_{a,\ell} e^{ik_a x_\ell} \sin(k_a \Delta x_{\ell j}) \right|. \quad (3.21)$$

The error is worst when $D = 0$. For N arbitrarily placed gauges, this occurs if $k_a \Delta x_{mn} = \ell \pi$ ($\ell \in \mathbb{Z}$). The error can be reduced by influencing the weight $w_{a,n}$, $n \in \{1, \dots, n\}$. Zelt and Skjelbreia [62] have introduced a weighting that should reduce the error, which is discussed on page 42.

In numerical experiments without noise and with a constant wave number the residual signal will contain mainly errors due to discretisation. These will be present near the boundaries of the signal due to signal extension and the circularity of the convolution. In real experiments the residual signal accounts for effects like [62]

⁵These coefficients are not necessarily the exact coefficients, but the relationship $\widetilde{Z}_a^I + \widetilde{Z}_a^R = Z_a^I + Z_a^R$ will hold when the residual signal is zero for all scales.

- Discretisation errors;
- Noise;
- Non-linear hydrodynamic effects;
- Deviations from the linear dispersion relation (E.1);
- Wave motions in the third dimension, i.e. over the width of the channel (also known as cross modes);
- Viscous effects;
- Energy dissipation (for instance by friction or wave breaking).

In this section factors such as gauge placement and weighing and how they affect the error will be discussed. The next section explores the effect of the characteristics of the signals on the result. This will all be based on numerical experiments. Chapter 5 present an example of the separation of a time series from the field of coastal engineering. These numerical examples are based on the signals described in Demonstration 3.7.

Demonstration 3.7 (Separate coastal engineering time series) Numerical simulated waves will be separated using wavelet coefficients. These results will be compared to the results from the Fourier algorithm from Zelt and Skjelbreia [62]. Note that this algorithm for $N = 2$ is equal to Goda and Suzuki [22] and for $N = 3$ to Mansard and Funke [39] [62]. The signals are based on a general measurement set-up in a flume at Deltares. On one end there is a wave maker, on the other end there is some kind of structure that is being tested. The gauge placement is given in Table 3.1. This is the standard set-up at Deltares, based on the optimally criterion from Zelt and Skjelbreia [62]. In the comparison is worked with the deviation of the mean water height, because we know for frequencies close to 0 (extreme example: $\omega = 0$) the algorithm will not be able to separate the waves.

The wave spectrum is based on a much used spectrum in coastal engineering, a JONSWAP spectrum [25]. The peak frequency lies at 0.8 Hz. Random frequencies in the range $[0.01, f_N]$ are picked. The sample frequency $f_s = 12$ Hz is used, so the Nyquist frequency is 6 Hz. The assumed water depth is 0.7 meter, and the wavenumbers are based on the solution of the linear dispersion equation (E.1).

Number of gauges	Distances from wave maker
2	39.382, 40.1
3	39.382, 39.83, 40.1
4	35.742, 39.382, 39.83, 40.1
5	35.742, 38.726, 39.382, 39.83, 40.1

Table 3.1: Distance of gauges used in the demonstrations

Gauge Placement

As mentioned the determinant is non-zero if for all gauges m and n $k_a \Delta x_{mn} = \ell \pi$ ($\ell \in \mathbb{Z}$). This is the same as $2|\Delta x_{mn}|/a\lambda_\psi \in \mathbb{Z}$ for each combination of $m, n \in \{1, \dots, N\}$. This is observed most easily by checking the behaviour of $\sin(k\Delta x)$ as shown in Figure 3.7. Wave gauge positions should be chosen carefully to ensure that this criterion is not approached near frequencies of interest.

Demonstration 3.8 (Wave number) Before considering different numbers of gauges, the wavenumber is shortly addressed. When the wavenumber is set equal for all frequencies, an almost perfect reconstruction of the incident and reflected wave is achieved, shown in Figure E.3. The error in the reconstruction of the incident and reflected wave is in the order of magnitude of the error of the reconstruction of the signal from the wavelet coefficients. When the wavenumber is based on the solution of the linear dispersion equation (E.1), the error of the reflection coefficient based on the wavelet coefficients is approximately 5% (see Figure E.2).

This error is mostly due to the very low frequencies and the frequencies above 1.5 Hz. The error in the low frequencies and at the spikes visible in the Fourier spectrum are due to the critical gauge placement, addressed in Demonstration 3.9. Note that in the frequencies above 3.5 Hz the recovered

spectrum based on the wavelet coefficients is worse than the one based on the Fourier coefficients. This is discussed more elaborate in Demonstration 3.10.

Demonstration 3.9 (Critical gauge placement, number of gauges) It is known from the mathematics that the gauge placement is very important for the results. A combination of the right distance and number of gauges ensures the best result. The improvement between the case using two gauges (Figure E2) and three gauges (Figure E4) is very large. The estimate of the reflection coefficient in the Fourier case decrease from 79% to 6% and for the wavelets from 5% to 0.2%. The addition of more gauges (five: Figure E5) does not improve the result as much as the addition of one gauge to the two gauges case (Fourier: 0.53%, wavelets: 0.35%). The Fourier method is much more plagued than the wavelet method by low frequencies when a little number of gauges is used. This is because the wavelet method has a maximum period, limiting the contribution of low frequencies.

Different Wavelets, Number of Scales

On the first eye changing wavelets would not effect the results of the separation. That is does, is shown in Demonstration 3.10.

Demonstration 3.10 (Different wavelets) In Figure E2 the Morlet 60 wavelet has been used, and in Figure E7 the Morlet 6 wavelet. These wavelets are both depicted in Section E.1.1. The Morlet 6 wavelet is performing over 15 times worse than the Morlet 60 wavelet. Increasing the number of gauges does not change this fact, as can be observed in Figure E5 and E8. Note that for low frequencies, they both reconstruct the same spectra, but for higher frequencies this does not hold. If the wavenumber is again assumed equal, there is little to no difference between the separation using these two wavelets, as can be seen in Figure E3 and E9.

So answer to this problem consists of three factors: the wavelet, the frequency of the wave and the wavenumber. As mentioned before in Section 3.2.1, the separation depends on the assumption that the wavenumber is valid for all frequencies within the band of the wavelet. Because the Morlet 60 wavelet has a much smaller bandwidth than the Morlet 6 wavelet, this assumption is valid for more frequencies. This however will have major effects when higher frequencies are studies. In coastal engineering these higher frequencies do not occur frequent, which allows this method to be used. Other wavelets with smaller bandwidth can be implemented in order to avoid this problem for higher frequencies.

Another influencer is the number of scales. For a too small number the reconstruction will start deviating more from the original signal: the combined bandwidth of the wavelets of all scales do not cover the bandwidth of the signal as described before. For good results it is important to take the guidelines in Section 3.1.1 into account. By increasing the number of scales, the errors due to the estimate of the wavenumber are not expected to decrease drastically. The error might even increase, because a higher number of scales results in a more dense set of frequencies. A more dense set of frequencies results in more solutions with a determinant close to zero.

Demonstration 3.11 (Number of scales) The general setting of 200 scales (Figure E5) is compared to two other numbers of scales. By decreasing the number of scales, the *reconstruction error* of the separated waves increases much (Figure E10): from 0.001% to about 12%. This results in estimates of the incident and reflected wave that are very erroneous. Notable is that, although the reconstruction error is large, the estimate of the reflection coefficient is still quite accurate. Increasing the number of scales to 1000 does not decrease the reconstruction error (Figure E11), it is also around 0.001% and therefore the estimates of the values are comparable to the estimates using 200 scales.

Determinant Limiter

Finding the right gauge placement is one way to ensure that the results are less disturbed by a close-to-zero valued determinant. However, this is not always possible. In measurements it may happen that the gauges are wrongly placed, or that there is just a limited amount of gauges available. By introducing a limiter based on the determinant, the frequencies or scales (in respectively the Fourier or wavelet based solutions) for which the determinant is under a certain limit are eliminated. The reconstructed wave values are set to 0^6 .

⁶This is already used in practice at Deltares.

This has the opposite effect as dividing by close-to-zero values. As could be observed, this resulted often in more energy in both separated waves. The disposal of energy by using the determinant limiter is expected to result in a bit weaker resulting signal: some energy is left out of the reconstruction that is in both original signals. In wavelet analysis another option is to limit the maximum period used in determining the wavelet coefficients. For low frequencies this results in the same effect as omitting the frequencies for which the determinant is under the limit.

Demonstration 3.12 (Determinant limiter, p_{\max}) A determinant limiter has been added, and the results are improved very much. Both algorithms without determinant limiter do overestimate the reflection coefficient quite severely in the 2 gauges case (Figure E2). However, by adding a determinant limiter of 0.1, the estimation of the reflection coefficient for both algorithms is around 1% off, instead of 80% and 5% in respectively the Fourier and wavelet cases. This is shown in Figure E6. From the recovered spectra it is clear that the spikes at the erroneous frequencies are not present any more.

If the determinant limiter is increased more, more energy is taken from the separated waves. The results of the use of a determinant limit of 0.5 is shown in Figure E12. For estimating the reflection coefficient, this is not that big of a problem if the relative energy change in the reconstructed incident and reflected wave is approximately the same. However, the introduction of this determinant limiter may lead to other underestimation problems when other wave characteristics are studied. So, this limiter has to be used with care.

More or less the same results are found in the wavelet algorithm by limiting the maximum period p_{\max} of the decomposition. This, however, does only effect the low frequencies and not the high frequencies for which the determinant is close to 0. The limitation of p_{\max} can be used to suppress the effect discussed in Demonstration 3.8.

Weighing

As mentioned before, the error can be reduced by introducing the weighting factor into the equations. Zelt and Skjelbreia [62] propose a weighing coefficient based on two characteristics. The first characteristic is the quantification of the phase difference associated with the spacing between gauge j and the other gauges. Multiples of one-half the wavelength associated with scale a are undesirable. The second characteristic is the spacing relative to the wavelength: a large spacing is undesirable. The resulting weighing coefficients of Zelt and Skjelbreia [62] are defined as:

$$w_{a,j} = \sum_{\ell=1}^n G(k_a \Delta x_{\ell j}) \quad \text{with } G(k_a \Delta x_{\ell j}) = \frac{\sin^2(k_a \Delta x_{\ell j})}{1 + (k_a \Delta x_{\ell j} / \pi)^2}. \quad (3.22)$$

This weighing will result in an estimate for the incident and reflected wave that is the same (aside from a phase shift) for all reference points. A more simple weighing, such as $|\sin(k_a \Delta x_{mn})|$, will result in small differences in the result per reference point. It is expected that the addition of the distance in (3.22) will result in a better reconstruction of incident and reflected waves.

Demonstration 3.13 (Weighing) The effects of the addition of the weights from (3.22) is higher when the number of gauges is little. The higher the number of gauges, the less need there is for the weights. For three gauges, the error of the Fourier case reduces from 6% to about 3%, in the wavelet case there is little difference (see Figure E4 and E13). The more simple weights based on only the sine actually increase the error with a factor 4 for both methods.

3.2.4. Linearity, stationarity and noise

As both the Fourier and wavelet transform are linear operations, they are not fit to analyse non-linear signals with. The separation of waves is a perfect example of where this analysis would fail. Again assume two gauges for simplicity. The assumption on which the whole analysis is build is that both gauges measure the same linear combination of waves, different by only a phase shift. If for instance a wave changes frequencies between two points (i.e. a non-linear relationship), this assumption is not valid. Non-linear effects will therefore result in a larger residual signal and thus an underestimation of both separated waves. Linear relations, such as a sloping bathymetries [35] and oblique incident waves [36] can be added to the separation algorithms.

Furthermore Ma et al. [35] note that this method is not suitable for breaking waves, because energy is dissipated in the wave breaking. This loss of energy due to breaking reduces the energy measured at the

gauges, for both incident and reflected waves. This will cause wrong estimates for the reflection behaviour of the structure. Whether the estimate increases or decreases depends on whether the incident or reflected waves lose more energy in this process. This however will be a problem for every method that determines the energy in the wave at a certain distance from the reflecting area.

Stationarity

Fourier analysis in theory is not applicable to non-stationary waves, and wavelet analysis is. Remember that a signal is non-stationary if the statistical properties of the ensemble it belongs to change over time (see page 4). For the demonstrations above this is not true, the statistical properties of the ensemble used are constant in time. To create a non-stationary signal, it is most easy to change the mean or the variance of the signal.

Changing the mean has a nasty side-effect: the wavenumber is dependent on the water level and this becomes a variable of time. This causes the following time dependencies in (3.17) as follows:

$$\widetilde{Z}_a^I(t) = \frac{1}{D(t)} \left(\Omega_a(t) \sum_{j=1}^N w_{a,j}(t) \zeta_{a,j}(t) e^{ik_a(t)\Delta x_{mj}} - \sum_{j=1}^N w_{a,j}(t) e^{2ik_a(t)\Delta x_{mj}} \sum_{j=1}^N w_{a,j}(t) \zeta_{a,j}(t) e^{-ik_a(t)\Delta x_{mj}} \right), \quad (3.23a)$$

$$\widetilde{Z}_a^R(t) = \frac{1}{D(t)} \left(\Omega_a \sum_{j=1}^N w_{a,j}(t) \zeta_{a,j}(t) e^{-ik_a(t)\Delta x_{mj}} - \sum_{j=1}^N w_{a,j}(t) e^{-2ik_a(t)\Delta x_{mj}} \sum_{j=1}^N w_{a,j}(t) \zeta_{a,j}(t) e^{ik_a(t)\Delta x_{mj}} \right), \quad (3.23b)$$

with discriminant

$$D(t) = \Omega_a(t)^2 - \sum_{j=1}^N w_{a,j}(t) e^{-2ik_a(t)\Delta x_{mj}} \sum_{j=1}^N w_{a,j}(t) e^{2ik_a(t)\Delta x_{mj}}. \quad (3.23c)$$

The effect of non-stationary signals on the algorithm is discussed in Demonstration 3.14, 3.15 and 3.16.

Demonstration 3.14 (Change reflection coefficient over time) By changing the reflection coefficient over time, the variance of the signal changes over time. Because the water level remains equal, this problem can be solved using (3.17). The results are presented in Figure F.14. Clearly the changing variance has little effects on both algorithms. Their performance is comparable to the stationary reflection coefficient case (Figure F.5).

Demonstration 3.15 (Sloping signal) In this demonstration a water level variation of 0.5 meter over 8 minutes has been added to the signal. The water depth therefore changes from 1 meter to 1.5 meter. The effect of this slope on both methods is directly clear from the results presented in Figure F.15.

The Fourier method is disturbed by two effects. The first effect is the changing water depth, which effects the wavenumber through time. As the water level rises, the error of the Fourier separated waves becomes more variable. The other effect is the presence of low frequencies that are the result of the non-stationarity.

The result is that the wavelet separated waves are much closer to the original incident and reflected wave than the Fourier separated waves. The deviations of the wavelet separated important values are in the same order of magnitude as the case without slope (Figure F.5).

Demonstration 3.16 (Jumps) For this example the wavenumber was assumed to be for the depth of 1 meter, jumps of 0.5 meter were added as non-stationary elements. As known from Fourier analysis a jump is build of all frequencies (see equation B.10). But the CWT is limited both at the lower frequencies because of boundary effects and on the higher end due to discretisation. The Fourier transform in general has a lower lowest frequency and a higher highest frequency. The results can be observed in Figure F.16. Both the separation in Fourier and wavelet domain cannot (fully) reconstruct the jump. When the signal is extended, it becomes clear from the error of the wavelet reconstruction that both the high and low frequencies close to the jump are missing to reconstruct the jump. The shape of the used wavelet, the Morlet 60 wavelet, is clearly visible the plot. In the Fourier case there are also some expected Gibbs ripples at the edges of the jump.

Noise

The last signal element to discuss is noise. Noise can be present in the measurement, but can also be the result of processes in the flume. Assume on both measurements uncorrelated noise is present. In this ideal case it is expected that the noise does not affect the separation, i.e. it will all be directed to the residual signal. This type of noise is addressed in Demonstration 3.17. By filtering the signal before separating the waves, the effects of the noise on the signal is decreased.

Correlated noise on the other hand can be the result of processes in the flume for instance resonance of the structure or due to the digital processing of the signals. When there is a correlation between the noise of the gauges, it is expected that the error of the separation will increase.

Demonstration 3.17 (Noise) In this demonstration different amounts of noise have been added to the simulated measurements. White Gaussian noise has been added with powers of 1/100, 1/10, 1, 10 and 100 times the power of the incident wave. The determinant limiter is set to 0.1. Both the two and five gauges cases are discussed here. The no noise reconstruction is comparable to the reconstruction in the case of added noise powers of 1/100, 1/10 and 1 times the power of the incident wave. The noise is spread over the whole spectrum, whereas the main power of the signal is in the frequency band [0.5, 2] Hz. In the frequencies outside this band some disturbance is detected, but this does not significantly affect the results (i.e. reflection coefficient, m_0 etc.).

As the noise power increases, the separation is disturbed more and there is a significant difference between the two and five gauges cases. In the extreme case of 100 times the power of the incident wave, both results based on Fourier or wavelet coefficients are not near the original incident and reflected wave. Both, however, perform better in the five gauges case than in the two gauges case. The addition of the number of gauges has two effects. The first is that the estimate is better for a higher number of gauges, described in Demonstration 3.9. The second reason is that there will be less random correlations between five different noise signals than between two. Therefore more noise is filtered when there are more gauges in the system.

The results are shown in the appendix for a noise power of 10 times the incident wave power in both the two and five gauges case (respectively Figure F.17 and F.18). By observing the spectra, it is clear that the noise in the high frequencies disturbs the resulting separation: noise on the signal is added to both incident and reflected wave. The main power bandwidth (0.5-2 Hz) of the separated waves is recovered well: the noise has little effect on the separated waves in this bandwidth.

In the five gauges case correlated noise has been added to all gauges, resulting in no difference at all with the uncorrelated noise case. This effect can be subscribed to the lack of phase difference between the noise. In order to distort the analysis, the noise has to have a correlation with a phase difference. Noise present in the flume, such as resonance behaviour, will be correlated with the right phase difference, which will affect the results.

From this demonstration may be concluded that filtering is not necessary for high SNR signals. The least squares method is able to filter low power noise very well. The more gauges there are in the system, the better the noise can be filtered. Signals with an SNR < 0 dB will distort the algorithm and filtering on beforehand is advised.

3.2.5. Residual signal analysis

For real signals the separated signals cannot be compared to a 'known' original incident and reflected wave. How well the estimate is, has to be based on the residuals. These can be computed by subtracting the sum of the recovered incident and reflected wave from the original signal. The residuals can be investigated in three different domains. These are the time domain, the frequency (Fourier) domain and the wavelet (time-frequency) domain.

If waves are compared in the time domain, the difference between the crest and trough height per wave is often analysed [25]. A wave is then defined as the signal between two up or down-crossings. Characteristics such as the height of the 1% highest waves of a set of waves are often based on these values. These values can be used to investigate the error over time.

In the frequency domain the error per frequency is investigated. Moreover, the reflection coefficient often depends on the frequency. Therefore the frequency domain is the most common domain to analyse the separated waves in.

The residual coefficients in the wavelet domain can be analysed as well. These are defined by (3.13). Averaging the wavelet coefficients in scale is an estimator for the spectrum of the error, which can also be

computed using the Fourier transform. The global wavelet spectrum thus has no added value over the Fourier method.

The time domain method based on the crossings has the disadvantage that the residual wave often contains a different amount of zero-crossings than the original wave, which makes it hard to determine the (relative) error 'per wave'. A solution is to determine the maximum difference between the zero (up or down) crossings of the other wave. Here the scale averaged wavelet power spectrum (2.29) is used. A measure for the error over time can be made by dividing the SAWP of the original signal by the SAWP of the residual signal, resulting in:

$$\epsilon_{\text{rel}}(t) = \frac{\sum_a \frac{|\mathcal{W}\{\eta_j - \widetilde{\eta}_j^I - \widetilde{\eta}_j^R\}(a, t)|^2}{a}}{\sum_a \frac{|\mathcal{W}\{\eta_j\}(a, t)|^2}{a}}. \quad (3.24)$$

Residual analysis using this measure is applied in Chapter 5.

3.3. Guidelines

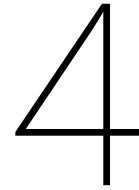
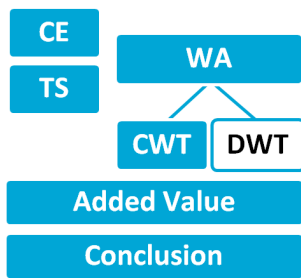
In this chapter two main subjects are discussed. The first subject was the improvement of time-frequency analysis through the wavelet transform. The second subject is the application of continuous wavelet coefficients to separating incident and reflected waves travelling in one axis. The additions to the original algorithm are best summarised in the form of the algorithm.

1. Apply signal extension to the signal. This results in the signal \mathbf{x} . There are many different signal extensions possible (see Section 3.1.2) of which the most important ones are summarised in Figure 3.2.
2. Compute the Fourier transform $\mathbf{X} = \mathcal{F}\{\mathbf{x}\}$ using the FFT. Computing the wavelet coefficients in the time domain takes $\mathcal{O}(N^2)$ operations, while in the frequency domain this takes $\mathcal{O}(N \log N)$ operations. Missing data points affect both convolution in the time domain as the FFT. Therefore these have to be filled, different methods are presented in Section 3.1.3.
3. Choose a wavelet function ψ and a set of scales to analyse the signal. The most used continuous wavelets are summarised in Figure 2.3. Pick a wavelet based on the research objective. The order of the wavelet determines its time-frequency spacing. When using the coefficients to separate waves, it is important to pick complex wavelet, with a small bandwidth. Discrete wavelets (Figure 2.4) are sometimes also used in the DCWT as well. This is not explored in this thesis.
4. For each scale, construct the normalized wavelet function using (2.21).
5. Find the wavelet transform at all scales a using the the inverse FFT, see equation 2.22.
6. Determine the zones of influence. For a signal without missing data points, the cone of influence based on the e -folding time suffices. However, if a signal is missing some data points, the zones of influence allows for more insight in the time-frequency behaviour of the signal. It is important to remember that the coefficients depend on the signal, the signal extension and the filling used. Different choices will lead to different coefficients. The COI and ZOI are only guidelines for the reliability of the coefficients, not strict borders.
7. The last two steps remain unchanged, i.e. remove any padding and contour plot the wavelet power spectrum;
8. and determine the confidence contour of the scalogram. Plot this contour and the cone of influence on top of the scalogram.

The second main subject of this chapter was the separation of incident and reflected waves. Ma et al. [35] separates waves based on wavelet coefficients for two gauges. Zelt and Skjelbreia [62] use Fourier coefficients to separate the waves for N gauges. In this chapter a combination of these method is presented: wavelet coefficients of measurements from N gauges are used to separate waves. In Section 3.2.3 all influencing factors on the error of the separation are discussed. Numerical demonstrations of these factors are shown. To remind: the wavenumber, critical gauge placement and the number of gauges, the used wavelet, the number of scales, the implementation of the determinant limiter, weightings and the properties of the signals all influence the final separated waves. Separation based on wavelets does not perform better than separation based

on Fourier coefficients, except for non-stationary signals as described in Demonstration 3.15. Analysing the residual using the relative error in time based on the SAWP (3.24) allows analysis of the error over time.

The added value of these two subjects is addressed in Section 5.1. First, the application of the discrete wavelet transform to signals in the coastal engineering field is discussed.



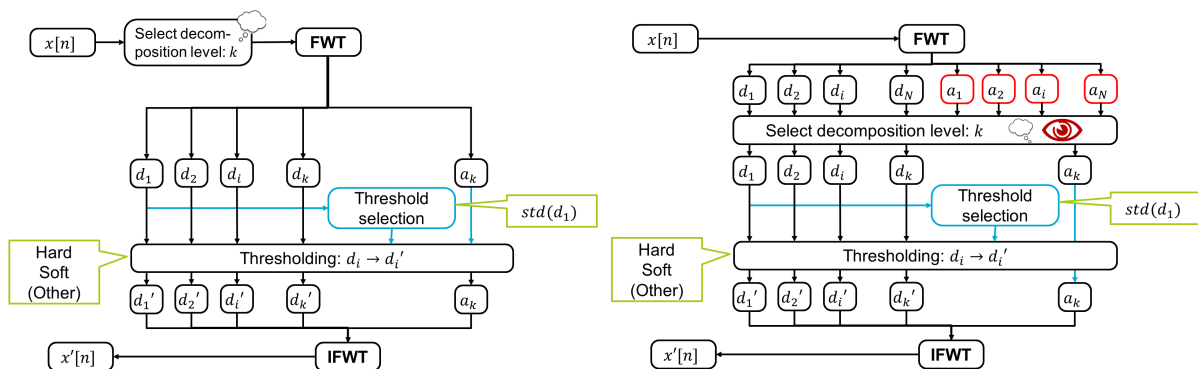
Discrete Wavelet Transform

In the previous chapter the computation and application of the continuous wavelet transform is discussed. This chapter concentrates on the application of the discrete wavelet transform (DWT) in noise filtering. Other applications of the applicability of the DWT are discussed in Chapter 5. In Section 2.3.2 the computation of the discrete wavelet decomposition was addressed, the basics of filtering using these discrete wavelet coefficients is discussed Section 2.5.1. This chapter starts with a more elaborate overview of the different algorithm, followed by a description of the test cases. Thereafter, the performance of the different filters for these cases is presented in Section 4.3. The chapter is concluded with the discussion of the results.

4.1. Filter Algorithms

In Section 2.5.1 the basics of wavelet filtering are addressed. In Figure 4.1 (a-d) a number of different wavelet filter algorithms are shown in a more detailed schemes. The performance of these algorithms is compared in this chapter. A traditional wavelet filter algorithm is shown in Figure 4.1a. At the start of the filtering protocol a choice for a decomposition level k is made, resulting in k sets of detail coefficients and one set of approximation coefficients after applying the DWT. To filter the signal, thresholds have to be picked. This threshold is often based on the standard deviation (abbreviated to std) of the first detail level, d_1 . An example of such a threshold is the universal threshold, presented in (2.36). Thresholds at a certain level can also be based on the coefficients in that level, instead of the coefficients in the first level. When the thresholds are determined, they can be applied using hard, soft or other types of thresholding methods (more are shown in Figure 2.5). The thresholded coefficients are then inverse transformed, resulting in a filtered signal.

A disadvantage of this traditional filtering is the choice of decomposition level selection before applying the filter. This is a very subjective method that will lead to trial-and-error experiments to determine the cor-



(a) Traditional wavelet filtering. Thresholds are often based on the standard deviation (std) of the first level. Another possibility is a per level threshold. (b) Subjective wavelet filtering, changes with respect to traditional wavelet filtering (see (a)) in red.

Figure 4.1: Different filter algorithms

rect levels. To improve the accessibility of subjective level selection, the decomposition level k is selected after all detail and approximation levels are visually judged. The judgement is discussed in Demonstration 4.1. This visual (subjective) level selection is shown in Figure 4.1b by the addition of the eye.

In this chapter, the results of this traditional filtering method, using both soft and hard thresholding, is compared to the results of two other threshold determination methods. Both these methods were presented by Srivastava et al. [50]. The first method is based on the fact that there is a period in the signal where there is no underlying signal: the measurement equipment is already turned on, but the experiment has not started yet. The recordings therefore only contain noise. The discrete signal $x[n]$ is assumed to consist of two parts: a part in which is known there is no signal present, $x_{\text{idle}}[n]$ and a part in which the signal is present, $x_{\text{signal}}[n]$. First the whole signal is decomposed to select a decomposition level. The signal $x_{\text{idle}}[n]$ is then padded with zeros until it has the same size as $x[n]$. This padded signal is decomposed and the detail coefficient thresholds are based on the maximum and minimum values in this decomposition. These thresholds are applied by soft thresholding, (2.35). The support of the choice for soft thresholding follows from the question: what if hard thresholding is used? Then noise just a bit above the threshold will have a large impact on the filtered result, which is an unwanted effect. Therefore soft thresholding is used. This algorithm is denoted as the 'signal free' algorithm.

The last algorithm is named after Srivastava [50]. There are three main differences between this algorithm and those already discussed. All three differences are highlighted in Figure 4.1d. The first one is the use of an objective measure to select the decomposition level. This measure is based on the peak-to-sum ratio (PSR) of the coefficients. The peak-to-sum ratio for a vector \mathbf{x} is defined as

$$\text{PSR}(\mathbf{x}) = \frac{\max_n(|x_n|)}{\sum_n |x_n|}. \quad (4.1)$$

This ratio is not only used to select the decomposition level, but also to determine the lower and upper thresholds, which is the second difference. In the original thresholding there is one threshold for the absolute value of the coefficients, not one for coefficients above and below zero. This change has also been applied within the signal free based filter. The last one is the use of hard filtering of the approximation coefficients at level k , to also address the low frequency noise in the signal [50].

4.1.1. Implementation

To determine the detail coefficients, a convolution of the wavelet and the signal has to be computed. Convoluting two signals is a rather computational expensive operation. The multiplication of their Fourier transforms is less computational expensive and the result is the same [29, 38]. For implementation of the DWT filtering, the PyWavelets package of Python has been used. Notable is that this package uses the convolution operation in the time domain, instead of the Fast Fourier Transform (FFT).

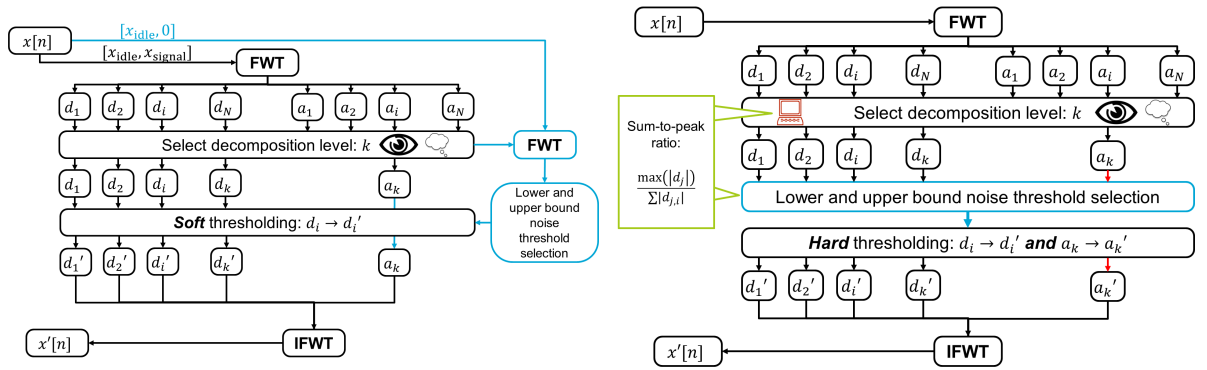
It has been discussed before that most of the algorithms rely on a subjective level selection to denoise the signal. Only the Srivastava algorithm has an objective level selection method. To be able to subjectively select a level a clear overview of all approximation and detail levels have to be presented. In Figure 4.1e the different colours refer to the different colours used for lines in plots discussed in the demonstrations in this chapter. Blue lines represent the original detail and approximation coefficients up to k levels, the grey signals represent the computed coefficients that are not used in the filtered reconstruction, and the orange signals are the filtered coefficients. The thresholds are shown by dashed red lines; long dashes show the lower threshold, short dashes the upper.

4.2. Test Signals

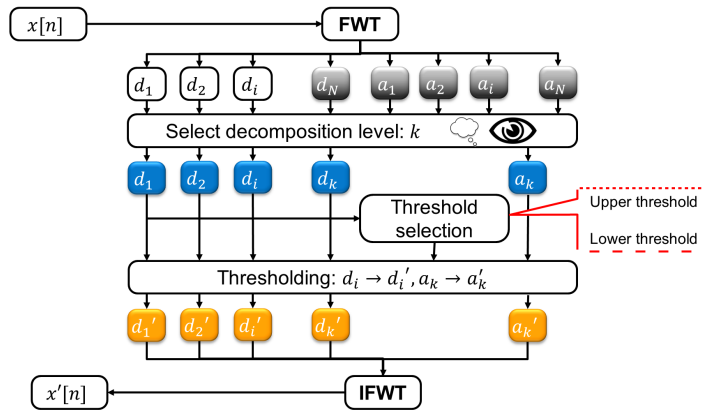
In the last section the different algorithms that are being tested were discussed. In this section the signals on which they are tested are presented. For this the discrete signal $s[n]$ is defined as the sum of three signals:

$$s[n] = x[n] + w[n] + v[n].$$

Here x is the basis signal, this can be a stationary or a non-stationary signal. The non-stationary signal is based on the impacts present in the force measurement presented in Section H.1.3. w denotes the measurement noise, such as resonance behaviour, only added in the non-stationary signal case. At last v contains environmental noise, this can be white noise, red noise and noise at very specific frequencies, for instance originating from the power supply. Moreover, non-stationary environmental noise such as nearby cellphone



(c) Wavelet filtering based on a signal free period in the signal; threshold selection based on this period. (d) Wavelet filtering by Srivastava [50], level selection possible via subjective and objective methods.



(e) Colours of the coefficients match colours in the plots containing the filters.

Figure 4.1: Filtering algorithms and implementation. The d_i denote the detail coefficients in level i , the a_i the approximation coefficients. By thresholding they are adjusted to d_i' and a_i' respectively.

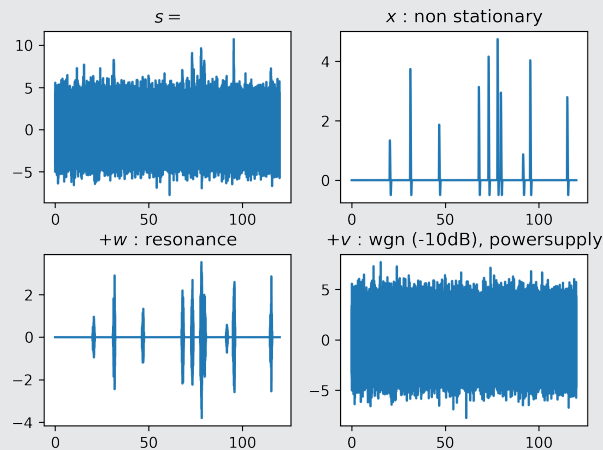
calls are not simulated. The noise will be scaled with different signal-to-noise ratios (SNRs). The test signals have a duration of 2 minutes, with a sampling frequency of 3 kHz.

Demonstration 4.1 (Test signal and discrete wavelet coefficients) The three different elements of one of the test signals are depicted in Figure 4.2a. The four signals $s[n]$, $x[n]$, $w[n]$ and $v[n]$ are shown separately in this figure. The Symmlets 8 wavelet is applied to decompose the signal s . This wavelet is advised for natural signals [50]. The effect of different wavelets in noise reduction will be discussed later.

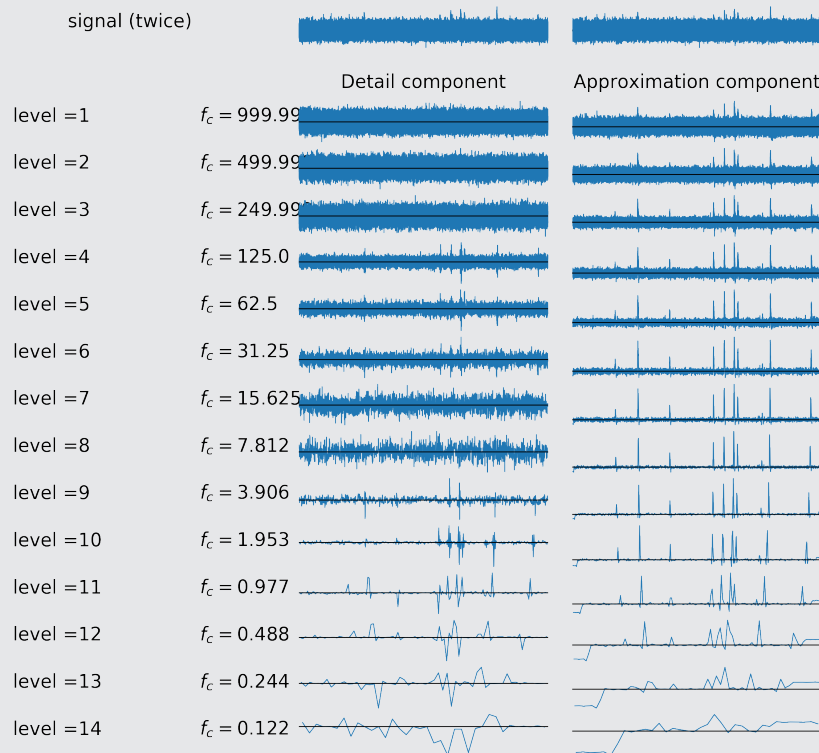
All the approximation and detail levels of this signal are shown in Figure 4.2b. In this demonstration, most noise is contained in the high frequency range; i.e. the non-stationary signal is of relative low frequency. This can be seen very clearly in the approximation coefficients; the contribution of the noise drastically decreases as details are omitted. This characteristic is used to choose the maximum level to filter: in levels 1-7 noise is identified in the approximation component, for levels 8 and 9 this becomes harder, for levels 10 and up the noise is not distinguishable from the approximation coefficient.

A decomposition level of 9 is chosen for all algorithms except the Srivastava [50] algorithm based on the results presented in Demonstration 4.1. Note that this is a subjective choice. After implementing the algorithms, some fine tuning can be applied. Often this concerns changing thresholds or threshold methods. This, however, is not done for every test signal because the objective is to find the best fitting algorithm, not the best data analyst. As explained before, this algorithm bases some choices on the PSR (4.1). Srivastava [50] claims that this ratio is a good universal measure, however after some tests with longer signals, different conclusions have to be drawn. This discrepancy in thresholds is due to the fact that the Srivastava test signals contain 4096 sampling points, signals in the field of coastal engineering easily contain over 3 million sampling points, which blows up the sum term in the PSR (4.1). Therefore the adjusted version contains a limited

PSR, which is the maximum of the peak-to-sum ratios of segments of 4096 samples of the full length input.



(a) The three signals and their sum



(b) The approximation and detail coefficients for the signal s from Figure 4.2a using the Symmlets 8 wavelet. On the left of the coefficients the levels and the centre frequencies f_c of the wavelets are given. Note that all x -scales are the same, the y -scales are different. The black line shows the line $y = 0$.

Figure 4.2: Signal from Demonstration 4.1

Demonstration 4.2 (Srivastava filtering) The result of the Srivastava algorithm using the adjusted PSR is shown in Figure 4.3. The S denotes the PSR of the detail coefficients. For $S < 0.01$ the detail coeffi-

coefficients are all considered noise, for $0.01 \geq S < 0.2$, there is noise present, but peaks contain information about the signal. For $S \geq 0.2$ there is almost no noise in the detail coefficients, so these are not filtered. Therefore the decomposition level is chosen as the last level with $S < 0.2$. Both these values are empirically based and can be adjusted for different signals. The automated threshold computation shows fairly good results. In level 4-6 the contribution of w in the signal is recognized and filtered out. The upper threshold of these approximation component is to high and will filter to much out. This can be adjusted manually.

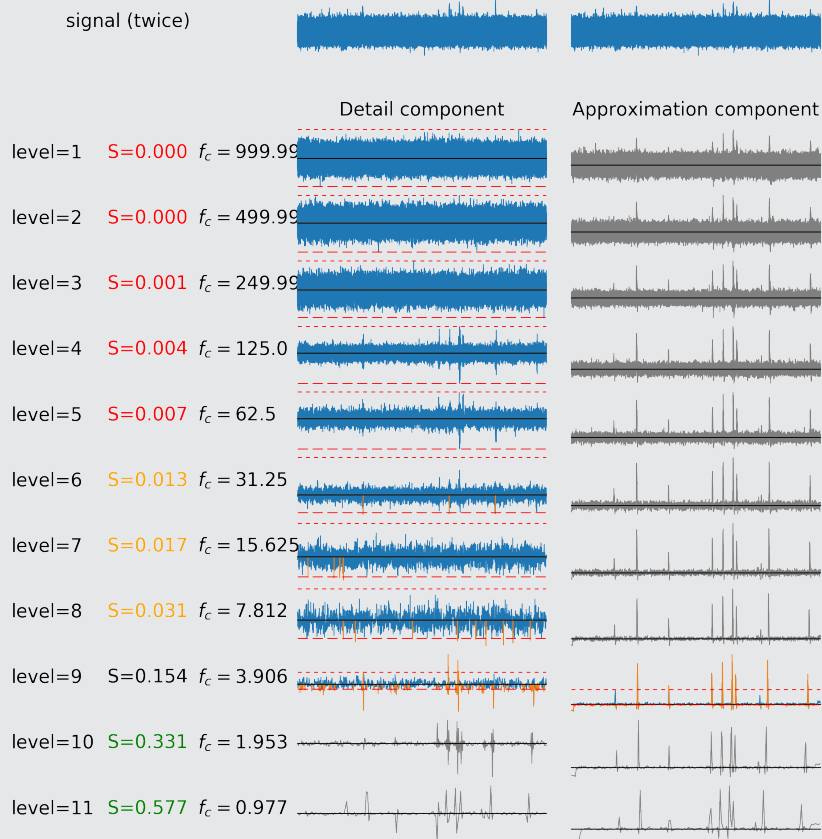


Figure 4.3: The approximation and detail coefficients and their thresholds, as by the Srivastava algorithm. The colours correspond with the colours in Figure 4.1e. The S denotes the PSR (or sparsity) of the detail coefficients at that level.

When we compare the results from Demonstration 4.2 to for instance hard thresholding result (Figure G.4) and the signal free approach (Figure G.3), a maximum decomposition level 9 is subjectively selected. The different thresholds result in different filtered results. The thresholds based on the signal free period let some part of w through in level 4-6. Because there is no approximation coefficient filtering, both these filters did not filter any peaks from the stationary basis signal x , in contrast to the Srivastava algorithm. The results will be discussed in Section 4.3.

Comparison: Fourier Filtering

The performance of the wavelet filtering algorithms is being compared to the performance of a low pass filter. The filter has not been optimized per signal, neither are the wavelet filters. Some fine-tuning could increase the performance of the Fourier filter, which also holds for the wavelet filters. A low pass filter with a band pass frequency of 10 Hz and a band stop frequency of 15 Hz is applied in both the stationary and non-stationary basis signal case. When the measurement noise w was not intended to be filtered out, a band pass frequency

of 100 Hz and a band stop frequency of 150 Hz has been applied. The Fourier filter has been implemented via Matlab. In Chapter 5 some examples using coastal engineering data are discussed.

4.2.1. Different wavelets

Until thus far the different choices of algorithms have been presented. There are, however, more choices that influence the filter result. The choice of wavelet, for instance, also effects the performance of the algorithms. In the Appendix E, in Table E.2, an overview of the different wavelets available in the PyWavelets package is presented. These are also depicted in Figure 2.4. A total number of 75 wavelets that can be used the PyWavelets package [52]. From these a set of five wavelets has been chosen to compare. These are:

Haar The Haar wavelet is expected to show poor results: its discontinuous behaviour in time or spectrum do not match any of the signals. This does also result in discontinuous behaviour in the filtered result.

Symmlet 8 Advised by Srivastava [50] for natural signals.

Coiflet 3 Its spectrum is close to the Symmlet 8 wavelet spectrum. Little difference is expected.

Bior 2.8 A bi orthogonal, symmetric wavelet. The spectrum of this wavelet has high resemblance with spectrum of the stationary signal than the others: it has a faster decay toward high frequencies. The numbers denotes respectively the number of vanishing moments of the wavelet and scaling function. (For more information see Appendix D.)

Daub 20 The Daubechies 20 wavelet is a wavelet with a long support in comparison to the others. Because of its high number of vanishing moments it has a short support in the frequency space.

These wavelets and their spectra are depicted in Section G.3. The choice of wavelet influences the choice of threshold, the reconstruction of the underlying signal and much more. The attentive reader notes that the tested wavelets are all real wavelets. This can be justified by the fact that the test signals, but also the ones from the field of coastal engineering are real as well. This leads to real coefficients, that can be used in the different algorithms. If a complex wavelet is used, the coefficients contain magnitude and phase information. This phase information is not needed for any of the algorithms and thus only the magnitude information is of use. The algorithm based on a universal threshold applied with hard thresholding, from level 9 and up, is used to compare the results per wavelet. These results are discussed later.

4.2.2. Signal Extension Modes

To apply the DCWT, signal extension methods are often applied. This idea originated from DWT theory, where it is already used much. Here too, signal extension modes have to be applied to most signals. It is very important that the right signal extension mode is chosen before applying a filter. The thresholds are often based on the wavelet coefficients. If these coefficients are distorted by signal extension, this might lead to wrong threshold choices. Especially the thresholds based on a signal-free time are sensitive to poor signal extension mode choices. The PyWavelets packages [52] possesses 6 different signal extension modes:

- Zero-padding;
- Constant-padding;
- Symmetric padding;
- Reflect-padding;
- Periodic: signal is treated periodic, a special mode to compute the least possible number of coefficients is called 'periodization';
- Linear extension.

The standard setting of the PyWavelets decomposition function is the symmetric extension. This setting has been used for all test cases. The coefficients near the boundaries in Figure 4.2b do not show any remarkable behaviour in the detail coefficients. However in the approximation coefficients, the boundary seems to have some effects, at the right boundary it seems to lower and on the left it rises.

4.2.3. Different Dilation Factor

In the derivation of the DWT through multi resolution analysis has been done with the dilation factor 2. Generally speaking, the use of this factor 2 results in the wavelet in the next level being twice as long and the

bandwidth of that same wavelet is halved. Another dilation factor can be used as well [29]. With a dilation factor $m > 2$, for one scaling functions, there are $m - 1$ different wavelets. The use of different dilation factors may have its advantages [4]. A dilation factor of 2 results in a shift variant transform, with another factor the transform can become more or less shift invariant and a larger set of smooth wavelet families can be used. These families can possess characteristics like both symmetry and orthogonality, which is cannot be in the case of $m = 2$. The use of a larger dilation factor will, however, not necessarily result in better algorithms. It will complicate the filtering steps, because it results in more coefficients, leading to more thresholds and more filters, which is not user-friendly at all.

4.3. Results

In this section the results of the performance of the different filter are compared to the results of the low pass filter. First the results of the different algorithms are discussed, followed by the effect of the different wavelets. The results are discussed in difference in signal-to-noise ratio (SNR) in dB.

4.3.1. Low Pass Filter and DWD Algorithms

When one takes a look at the signal-to-noise ratio increase and decrease in Figure G.1, the first thing to note is the lack of improvement in any red noise case. The red noise that is added to the signal has a slope of -6 dB per octave, which originates from sound signal processing. An example of a signal and its red noise can be found in the Attachments, Figure 14. This has high power for low frequencies, decreasing as the frequency increases. This results in much disturbance of the signal in and below the range of frequencies it consists of (1-10 Hz). Therefore the red noise is not filtered by these filters. Moreover, this kind of noise is not present often in coastal engineering time series. A different filter design is needed to filter this type of noise, but that is outside the scope of this thesis. This will therefore not be discussed any further.

In the stationary cases the low-pass filter outperforms all wavelet filter algorithms, although for the higher SNR, the signal free and universal hard threshold method approach the performance of the low pass filter. This result is to be expected because the low pass filter is very effective in filtering higher frequencies. If we compare the different wavelet filtering algorithms in the stationary cases, the Srivastava algorithm performs the worst, in the high SNR case it even distorts the signal more. The Srivastava algorithm was not to expected to perform well in the stationary signal case; i.e. the PSR is effective to filter peaks from the rest of the signal. In the stationary case, there are no real peaks, therefore this a poor measure.

In the non-stationary basis signal case, it is the other way around: the wavelet filter algorithms perform better than the low pass filter. In general it is noted that the filters have more effect when there is more noise on the signal. This is consistent with the low pass filter performance in all cases as well. First the filtering of both measurement and environmental noise is addressed. This has been tested twice, once where when there was measurement noise on the signal, once when there was not. Most remarkable is the difference between the hard and soft automated thresholding methods, which both perform way worse in the case when there is measurement noise present. Furthermore, the algorithm based on a signal free period does not only affect the environmental noise, but also the measurement noise. If a user changes the thresholds of a few levels, it functions much better in the objective is to filter only environmental noise.

From the results presented in Figure G.1 it is concluded that in the high SNR cases there is little difference between low pass and wavelet filtering for the stationary case. When the noise increases, especially the universal soft, hard and signal free based algorithms perform much better than the low pass base case. The performance of the Srivastava algorithm stays behind, even with the adapted PSR.

In Figure G.17 the result of different filters is shown. This is for the non-stationary case, with much noise, SNR = -10 dB and measurement noise. From this figure it is clear that the low pass filter leaves too much noise on the signal, the other signals show a nice reconstruction of the jump in the signal. They all show some deviations at different places. From this figure one cannot derive which of the four algorithms performs the best overall. However it is clear that the soft and the signal free based best reconstructs the maximum peak. The application of soft or hard thresholding, based on the MAD do have almost exactly the same filter result, this is due too high thresholds. Therefore there is little difference between soft and hard thresholding.

4.3.2. Wavelet comparison

In the comparison of the five different wavelets, the hard thresholding based on the universal threshold was used. Due to the poor results for filtering red noise, only the white noise cases are compared. The results in terms of difference of SNR are presented in Figure G.2. The results per wavelets are addressed here:

Haar Was expected to show the worst results, because of the discontinuities. In the stationary basis signal case the Haar wavelet was outperformed by all other wavelets. In the non-stationary, high SNR case it seems to perform slightly better than the others in filtering w . The Haar-wavelet is a relative short wavelet (filter size 2), therefore the addition of an extra decomposition level could increase its performance. The downside of the Haar wavelet is that the reconstruction shows jumps.

Symmlet 8 In the stationary signal case this wavelet has a comparable performance with the Coiflet 3 and Daubechies 20 wavelet. In the non-stationary case it performs best in filtering both the measurement noise and the environmental noise from the signal.

Coiflet 3 This wavelet has a spectrum that is very similar to the Symmlet 8 wavelet. This is also directly observed from the results: their performances differs just slightly. It is outperformed by one of the other wavelets in all cases.

Bior 2.8 The bi orthogonal wavelet is able to increase the SNR at least 0.5 dB with respect to the other wavelets in the stationary x case. In the non-stationary base case it performs best in filtering the environmental noise. Other wavelets are better for filtering both the environmental and the measurement noise. The bi orthogonal wavelet is the only symmetric wavelet in this comparison. The stationary signals and the measurement noise w both have symmetric characteristics. This is why these are addressed best by the bi orthogonal 2.8 wavelet.

Daub 20 The Daubechies 20 wavelet results in comparable noise reduction with respect to the Symmlet 8 and Coiflet 3 wavelets.

4.3.3. Discussion

When dealing with stationary signals and white noise, the use of standard low pass filtered is advised over the use of wavelet filtering. This is consistent with the Fourier theory, which is well-suited to stationary signal situations. For non-stationary signals, especially signals containing peaks and discontinuities, the Fourier theory is not applicable any more.

Wavelet analysis is better applicable to these non-stationary basis signal cases. Filtering in the wavelet domain shows much better results than the use of the low pass filter. However, in this domain there are much more choices to make than in the frequency filter domain. What wavelet to choose? What signal extension mode to pick? Which decomposition level to use? It is shown that different wavelets result in different outcomes of the algorithms. From theory it is known that the resemblance of the wavelet in time and frequency domain with the signal is a good estimator of its effectiveness. This theory is consistent with the results of the comparison presented in this chapter. The signal extension mode has to fit the data and has to prevent large jumps or other discontinuous behaviour to affect the coefficients as little as possible. A subjective and objective measure to pick the decomposition level have been presented, a combination of these two will be a good guide for an analyst.

There are many fine-tuning elements that differ per used signal, such as finding a filter that does filter the environmental noise, but does not filter the measurement noise. A general objective method does not seem to exist, it is probably easier, faster and more precise to apply some subjective fine-tuning to the thresholds for a whole set of similar signals. The Srivastava conclusions are well-drawn for the short signals they address, but they do not hold for the 30 minute 3 kHz sampled signals from the coastal engineering field.

4.4. Recommendations Noise Filters

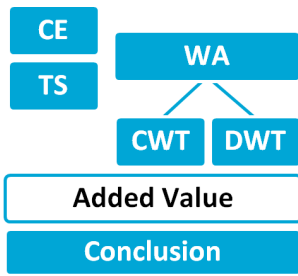
At the end of this thesis some recommendations will be discussed. These are focussed on the application of the discrete wavelet transform in the field of coastal engineering. Therefore some recommendations concerning the compared wavelet based noise are addressed here. For starters, red noise cases will have to be challenged with different algorithms. The algorithms compared in this chapter are not suitable in these situations.

The signal free algorithm does show high noise reduction, however, there are some improvements to this algorithm. First note that the signal free period is zero-padded, however we know from DWT theory this might lead to high coefficients at the boundary between the signal free period and the zero-padded part. Therefore other signal extension modes can be evaluated. Moreover, a mean-value of the signal containing part of the signal could be used as well. Further more it is interesting to consider whether approximation level filtering can be part of the signal free based algorithm.

The Srivastava algorithm did not work as well as predicted. Another measure of the peak-to-signal ratio could solve some problems. Furthermore the approximation level filtering is not always necessary. It often disturbs the signal more than the same algorithm without the approximation level filtering. The use of the peak-to-signal ratio to select the right decomposition level has proven itself useful and could be used in different algorithms. A separate threshold for coefficients above and below zero is another improvement which can be used in other algorithms.

Most wavelet filter algorithms show great improvements in SNR in stationary noise situations. non-stationary noise situations have not been addressed, but the performance is predicted to drop. The thresholds are stationary, and when applied to non-stationary noise, this cannot result in non-stationary noise filtering. This also has been seen in the coastal engineering signals, where some non-stationary noise is present. Moreover, a different thresholding technique (see Figure 2.5) may show some improvements as well.

On the computational side of the algorithms there are many improvements possible, however, not much time will be gained for the signals discussed. The computers are fast enough to change from time to discrete wavelet domain and back in little time. If there is need for improvements, one can think of the use of the fast Fourier transform instead of the convolution, and to implement a DWT algorithm without down sampling to speed up the shifting algorithm.



5

Added Value of Wavelet Analysis

Multiple applications of wavelet analysis have been addressed and expanded in the two previous chapters, in order to improve signal analysis and signal processing in the field of coastal engineering. In Chapter 3 the different applications of the continuous wavelet transform are discussed. The interpretation of coastal engineering data is improved by adding different signal extensions and zones of influence offer guidance for missing data points. Long signals can be down-sampled in order to analyse faster. Furthermore the separation technique for incident and reflected waves in the wavelet domain has been expanded and compared to the current Fourier method by Zelt and Skjelbreia [62]. Section 5.1 addresses the added value with respect to these applications of the continuous wavelet coefficients.

Section 5.2 focusses on applications of the discrete wavelet transform, discussed in Chapter 4. In this chapter a comparison is made mainly between Fourier and wavelet filters. However, in this chapter these two will be compared to the filter technique used at Deltares. Furthermore some other applications of filtering will be addressed. At the end of the chapter the computational intensity of the two methods is compared.

5.1. Spectral Information

In this section the use of regular (Fourier) spectral information is compared to the spectral information expressed by the continuous wavelet coefficients. These are determined in discretised form using (2.20). In Section 3.1.1 is described that for long or oversampled signals, down-sampling can be applied. The down-sampling procedure, however, removes energy from the signal. To compare the wavelet coefficients based on down-sampling with the coefficients based on the original signal, they should be multiplied by a factor \sqrt{d} , as described in equation 3.2. This also offers opportunities to calculate the wavelet coefficients faster, because less scales are needed for a smaller frequency range.

In Section 3.1.2 it has been made clear that the continuous wavelet coefficients near the boundaries are sensitive to the signal extension that is used. In Figure 3.2 the most common signal shapes are tied to preferred signal extension methods. Important is to take the drawbacks of the signal extension method into account. The signal extension method should be chosen with care, based on the objective of the information.

5.1.1. Missing Data Points

Missing data points disturb standard frequency analysis. For a stationary signal, the effects of some missing data points are fairly predictable, i.e. the power in the spectrum is expected to reduce with the same factor for all frequencies. Filling gaps could lead to sharp edges in the signal disturbing both low and high frequencies. A comparison of two energy spectra (one disturbed, the other not) is given in Demonstration 3.2. The introduction of sharp edges by filling the data results in disturbance over all frequencies. This is due to the frequency contribution of the sharp edge (see equation B.10). If the signal is non-stationary or contains non-linear signal elements, these effects are even much more unpredictable.

As the wavelet coefficients are dependent on translation (time), the effect of the gap onto the coefficients can be taken into account. This is done by determining the amount of wavelet mass disturbed by the missing data points (see equation 3.6). In Figure 5.1 the so called zones of influence are depicted with dashed lines. They show the wavelets that are disturbed more than 95%. In the 8 to 16 Hz area some areas are marked as

significant that are outside the cone of influence based area's (dotted lines). This expansion results in more insight into time-frequency behaviour, that was not available before.

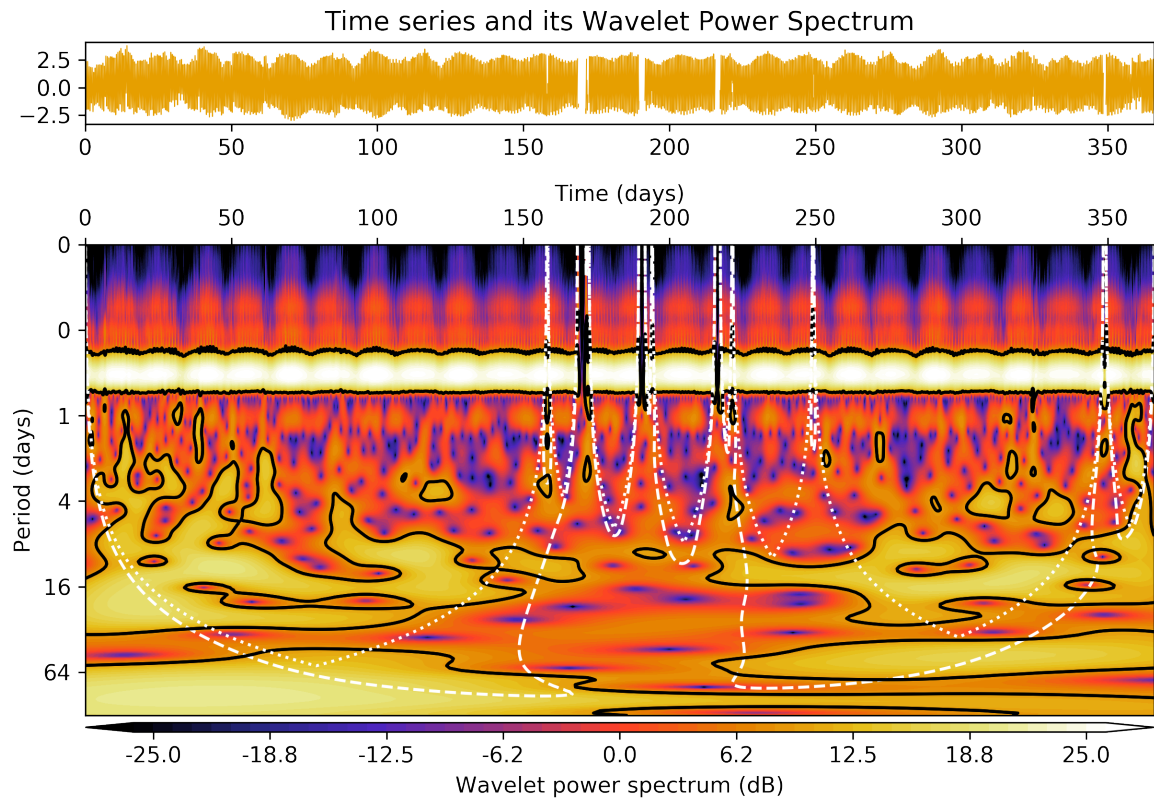


Figure 5.1: Wavelet power spectrum of water height measurements from the Westerschelde (see Section H.1.1). WPS based on Morlet 6 wavelet, mean signal extension and mean NaN filling applied. COI: dotted line; 95% ZOI: dashed line; 95% confidence area based on WGN assumption: black line.

Wavelet Applications

Regular coherence and correlation of spectra based on missing data time series are not used because they are unreliable. The wavelet cross spectrum can be calculated and its reliability could be determined by multiplying the zones of influence of the two signals. In the wavelet coherence the smoothing operator has to be taken into account when using the zones of influence to determine reliability. Averaging of the wavelet power spectrum would not lead to any useful information. The separation of waves can be computed both in the Fourier as in the wavelet domain for signals which gaps are filled. The Fourier separate waves will all be affected by the filled gap. How much the wavelet separated waves are affected can be assessed by the zones of influence.

5.1.2. Continuous Wavelet Coefficients

In the standard wave separating techniques, Fourier coefficients are used to separate the incident and reflected wave. In Section 3.2.4 is shown that wavelet coefficients are more effective to use in separating non stationary signal cases than Fourier coefficients. Fortunately a lot of signals in coastal engineering have stationary characteristics, which allow analysis through the Fourier coefficients [25]. In the following example a non-stationary wave from the field of coastal engineering is discussed. Not only the separation of the incident and reflected wave is discussed; other wavelet applications will be addressed as well.

The non-stationary case that is addressed in the following example is an experiment where the water level in the flume is increased by 20 cm over 72 minutes and then decreased again, to mimic the effects of the tide. A more elaborate signal description is given in Section H.1.2. This increase in water level influences the wavenumber k . There are two options to apply the method of Zelt and Skjelbreia [62] on this signal. The first is to apply the short term Fourier transform, i.e. apply wave separation on different time intervals with a more

or less stationary water level. This however results in separated waves with discontinuities. The other option is to use the mean water level for the whole signal, as is done in Section 3.2. This does result in separated continuous waves. That is the case that is compared with the separation using wavelet coefficients in this section.

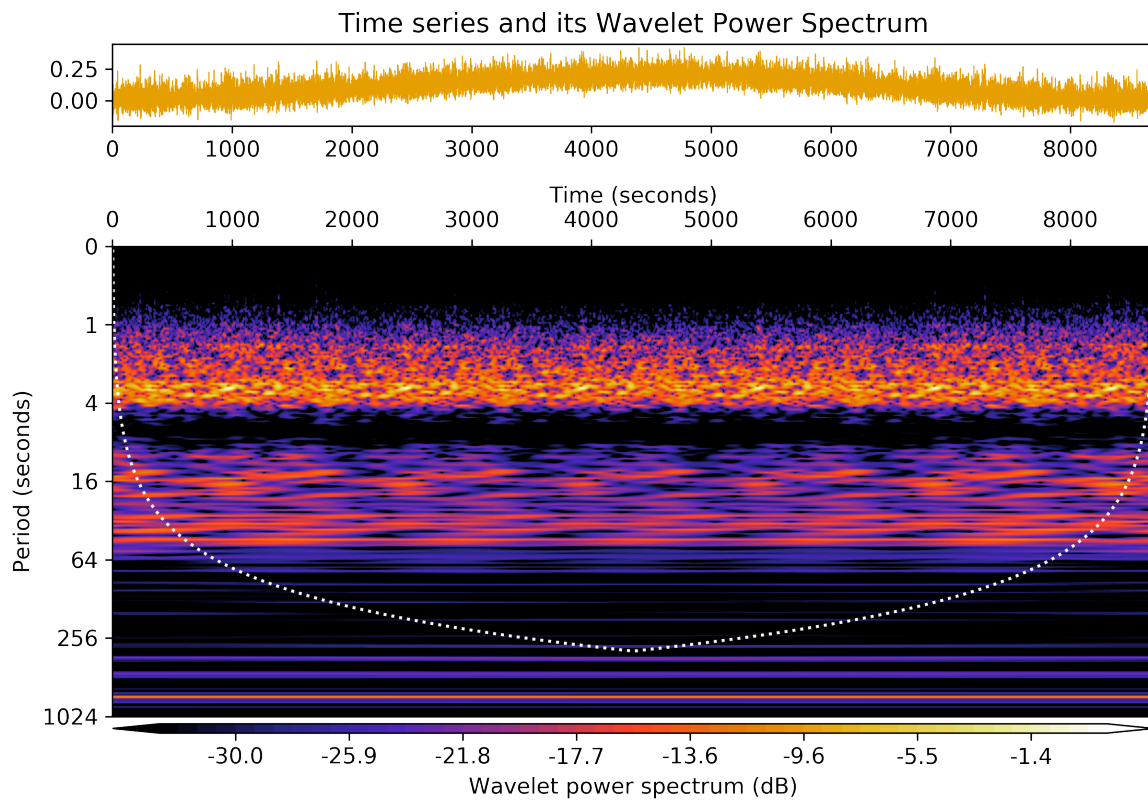


Figure 5.2: Wavelet power spectrum of deviation of water level at first water height meter using the Morlet 60 wavelet.

Averaging

The signal used to separate waves is shown in Figure 5.2. The wavelet power spectrum shows high power in the periods of 1-4 and 8-64 seconds. The first band, 1-4 Hz, is dictated by the settings of the wave maker. In the band between 8 to 64 periods is relative much power compared to the periods between 4 to 8 seconds. This power is assumed to be the result of the pumps that actively regulate the mean water level in the flume during the experiment. These two bands are also distinct in the global wavelet spectrum shown in Figure 5.3a. In this figure the global wavelet spectrum is compared to the regular Fourier spectrum. In general the GWS is a good approximation of the underlying Fourier spectrum [53], however note that in this case the wavelet power decreases after a period of 256 seconds and the Fourier power increases. This discrepancy is the result of the non-stationary water level and will cause low frequency effects in the separation in the algorithm of Zelt and Skjelbreia [62].

Cross-wavelet Applications

Furthermore we have a look at the cross wavelet spectrum and wavelet coherence of two neighbouring measurements. These are shown in Figure 5.3b and Figure 5.3c. It is clear that the power in both period bands is present in both signals. From the wavelet coherence plot the coherence between the two signals is not directly clear. From the averages over time and scale it becomes clearer that the coherence in the 8-64 period band is high.

Separated Waves

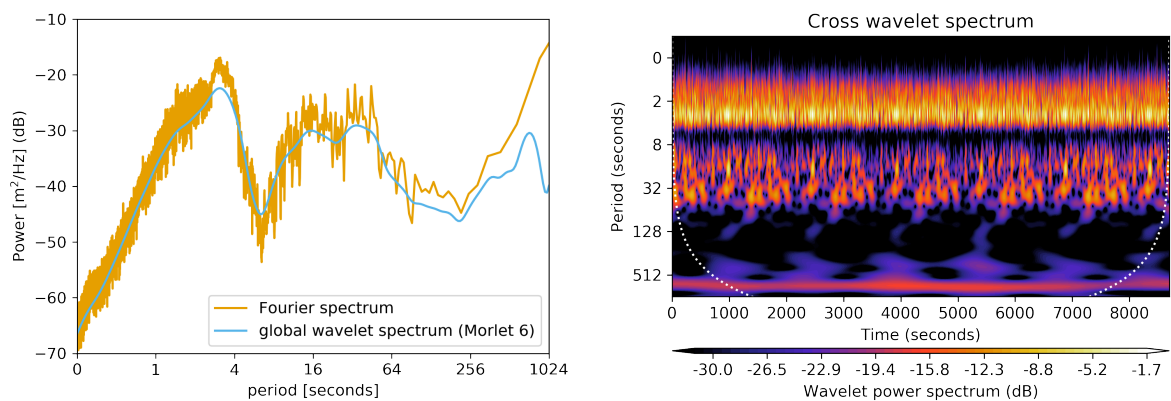
The waves are separated using both Fourier and wavelet coefficients. In the Fourier case, the mean water level over the whole experiment is used to determine the wave number. Three cases are compared: no determinant

limiter, a determinant limiter of 0.1 and the case without determinant limiter and without all frequencies below 1/10 Hz. The results of these cases are presented in Section H.2.1.

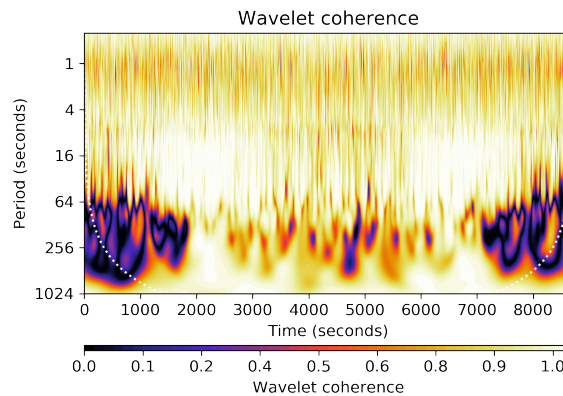
When no determinant limiter is used, the Fourier based reflection coefficient is 1. As expected, it is plagued by especially low frequency disturbance. The Wavelet based reflection coefficient is around 0.45. This is pretty high because a reflection coefficient $\leq 1/3$ is expected.

Both methods find a reflection coefficient of about 0.25, when the determinant limiter of 0.1 is used. The reconstructed waves do not overlap exactly, but their wave characteristics are comparable. When the limiter is used, energy that is in the waves, is not taken into account in the reconstruction. If instead of a limiter, only the frequencies below 1/10 Hz are not taken into account, the Fourier reflection coefficient is about 0.5. The wavelet based reflection coefficient however becomes 0.26, slightly higher than the limited one: less energy is filtered out.

So the difference between 0.26 and 0.42 can be assigned to the frequencies below 1/10 Hz. These were assumed to be the result of the active water level regulation. Looking back at the cross wavelet spectrum shown in Figure 5.3b, a lot of energy is present in the periods above 10 seconds. Moreover, the coherence of these periods is large as well.



(a) Comparison of Fourier spectrum and GWS using the Morlet 6 wavelet. (b) Cross wavelet spectrum for the first and second water height meter (Morlet 6 wavelet).



(c) The wavelet coherence for the first and second water height meter (Morlet 6 wavelet, using code of Grinsted et al. [23]).

Figure 5.3: Cross-wavelet analysis of waves for WL657585e (more information: Section H.1.2)

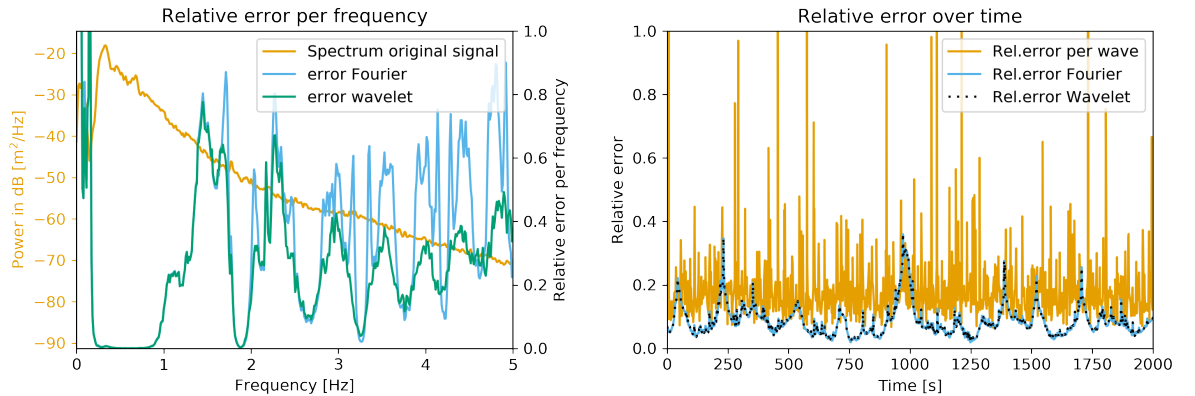
Residual Analysis

Residual analysis is performed on the case with a minimum frequency of 1/10 Hz, without determinant limiter (Figure H.3). This analysis is done for the separation based on Fourier coefficients and based on wavelet coefficients. In Figure 5.4a the spectra of the residual for both methods are shown. As is expected from the

results in Figure H.3 the relative error per frequency deviates between the wavelet and Fourier based separation near the frequencies affected by the gauge spacing. Note that this relative error is mostly high at low power frequencies, therefore the contribution to the absolute error is low.

This also becomes clear from the error of the separated waves over time. In Figure 5.4b three different errors are displayed for the first 2000 seconds of the measurement. The error based on the wave height distance between two down-crossings of the original signal minus the water level is plagued by a lot of spikes. This is due to the fact that the down-crossings of the original signal are not at the same places as the down-crossings of the residual signal. The other two errors are based on the scale averaged wavelet spectrum (SWAP) of the residual signal, as defined in equation 3.24. The error of the Fourier and the wavelet based solutions are almost equal. Note that this method of analysing the residual error is thus not flawless. From the results (Figure H.3) it is clear that the estimate based on the wavelet coefficients is much better than the one based on the Fourier coefficients. The error in the incident and reflected wave often cancel each other, resulting in a comparable residual signal.

In Figure 5.4c the error and the wave height are both shown in time. There is a clear correlation visible between a high relative error and high waves, i.e. for larger waves the relative error is larger. Sorting the waves from high to low, does indeed show that the correlation is true. Thus the absolute error for large waves is even larger. So the separation of waves is less accurate for larger waves, i.e. the largest incident and reflected waves are underestimated or overestimated most. This effect was predicted based on the fact that higher waves are subject to non-linear processes that are not taken into account due to the linearity assumption at the basis of the separation algorithm.



(a) Relative error per frequency of separated waves.

(b) Relative error in time, based on difference between crest and trough per wave and based on SAWP.

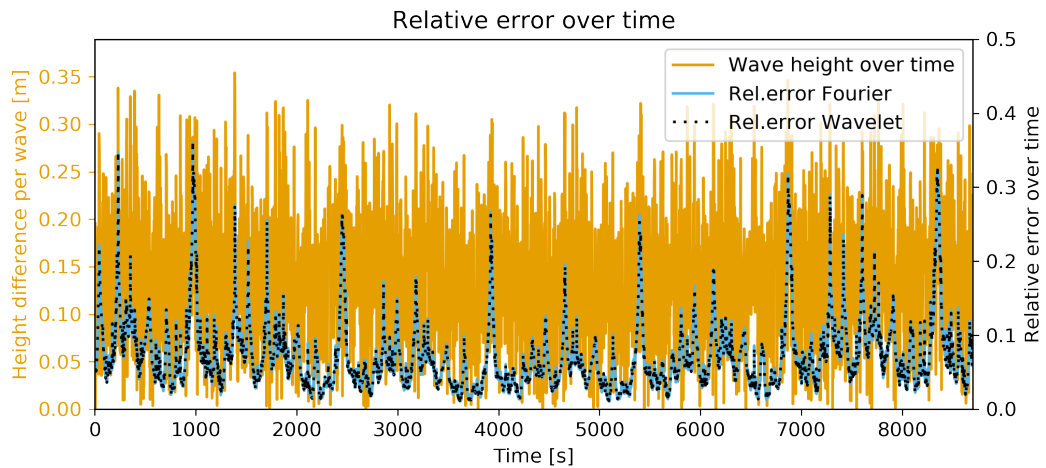
(c) On the left: height difference per wave in time. On the right: $\epsilon_{rel}(t)$ from (3.24) for both methods.

Figure 5.4: Residual analysis of separated waves case WL657585e (more information: Section H.1.2). The relative errors based on the SAWP are filtered using a moving average filter with a length of an average wave (i.e. 43). The Morlet 6 wavelet is used to determine wavelet power.

5.2. Discrete Wavelet Decomposition Filtering

There are numerous applications of filtering in Coastal Engineering. In this section two different applications will be presented. The first one is filtering in general. Often data analyst filter signals based on gut feelings, lacking a justification of the used filter. The first example shows that these gut feelings are correct in his case. However, comparable results can be obtained through reasoning based on the discrete wavelet decomposition. The second example will show the added value of filtering with respect to non-stationary signals and the brought spectrum of discrete wavelets. The last example shows the filtering of a transient from the rest of the signal.

Filter Force

The first example discussed here, is a force measurement from the measurement A3W1T304 (see Section H.1.3). The goal of the filtering is to reconstruct the peak forces in the signal. Due to effects such as resonance and noise, the peak can be over or underestimated. Both these errors have their effects on designs based on these measurements.

These signals are normally filtered using the Savitsky-Golay(x, y) filter. This filter bases the filtered data point on the fitting of a y^{th} order polynomial through x data points [40]. The setting used in this case is based on 'gut feelings' and is set on $x = 201$ and $y = 5$. This will be compared to two wavelet filters and a low-pass filter with a cut off frequency of 16 Hz. The wavelet used in both filters is the Symmlets 8 wavelets, based on its result in Chapter 4. The objective of the filtering is to find the peak force of the signal.

The first DWD filter is based on noise in the 10 first seconds of the measurement (Figure H.5). The result of this filter is shown in Figure 5.5a. Noise is clearly filtered off, but the resonance frequency is still in the signal. If the moments of impact are studied more carefully (Figure H.4), the approximation coefficients show that the resonance frequency is mainly caught in the sixth and seventh detail levels. The second filter (Figure H.6) therefore omits all detail coefficients from these levels. Resulting the signals shown in Figure 5.5b.

Both wavelet filters have also been applied in shifted mode. The peak values of the different filters are:

- For the Savitsky-Golay(201,5) a peak value of 20.8 is recovered,
- the low-pass filter recovered 20.5 at the peak,
- the wavelet filter (with detail levels 6 and 7 omitted) without shifting 20.9 and
- the shifted one 20.3.

Note that these values are relatively close together, but that the wavelet transform has recovered the lowest value. However, in many application some resonance is expected, but this may be not as much as in the model in the flume. By soft thresholding, the analyst can damp the resonance. This is much easier in wavelet analysis than for any other filter type.

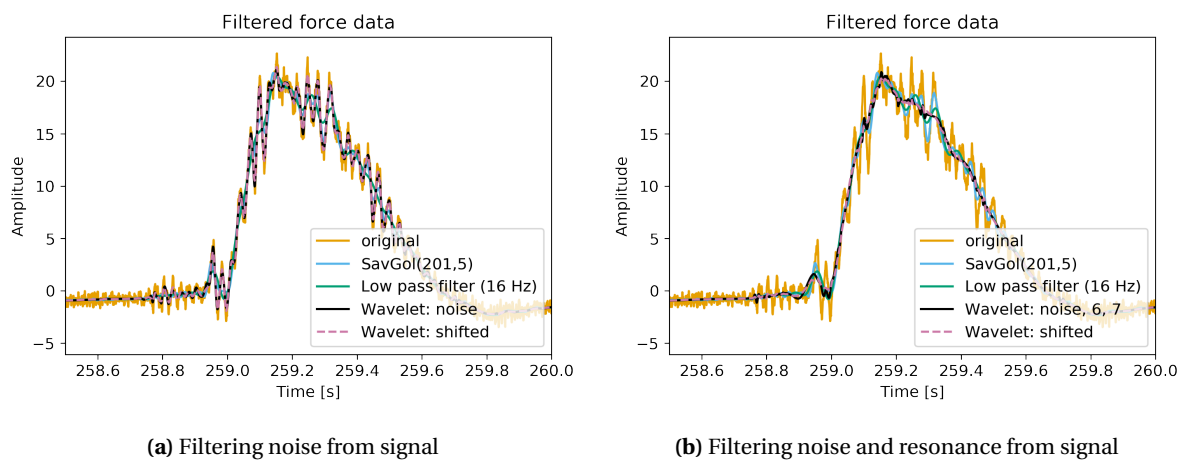


Figure 5.5: Filtering force signal from A3W1T304 (see Section H.1.3).

Over-topping Reservoir

In this second example, we consider a water height measurement from the over-topping reservoir. In order to learn more about the forces on the structure, the water slamming over the structure is captured in the over-topping reservoir. The goal is to determine the volume of water that is filling this reservoir. This can be done by multiplying the water height with the area of the reservoir. However, due to non-stationary effects such as sloshing this water level is quite hard to read. To reconstruct the underlying signal with jumps and without these vibrations a wavelet filter based on the Haar wavelet can be used (Section E.1). A standard frequency filter would be completely useless, because filtering would lead to a smoothing of the jumps.

The Haar wavelet in general is not much used, however for this application it is perfectly fit. There will not be a delicate filter design as discussed above, only the reconstruction of the approximation levels will be used. In Figure 5.6a the reconstruction of a number of different levels is shown. The level 15 and 16 reconstruction appear to be too fine to use as estimator for the water height after a pulse. The level 17 and 18 reconstruction on the other hand are too coarse. This is illustrated in Figure 5.6b. The width of the Haar wavelet these levels is too large to catch the jumps on a smaller scale.

Here the level 16 or 17 approximation level would be advised. Jumps are reconstructed very clearly, however they do not all appear on the time at which the largest difference in the original signal is observed. This is the result of the dyadic structure of the discrete wavelet decomposition. By shifting the signal, the jumps can be shifted so that they occur at the same time as the original jump. By decreasing the sampling interval the problem cannot be solved, i.e. the problems lie within other scales. For jumps close to each other, lower level approximation coefficients will have to be used to reconstruct the jumps at that scale.

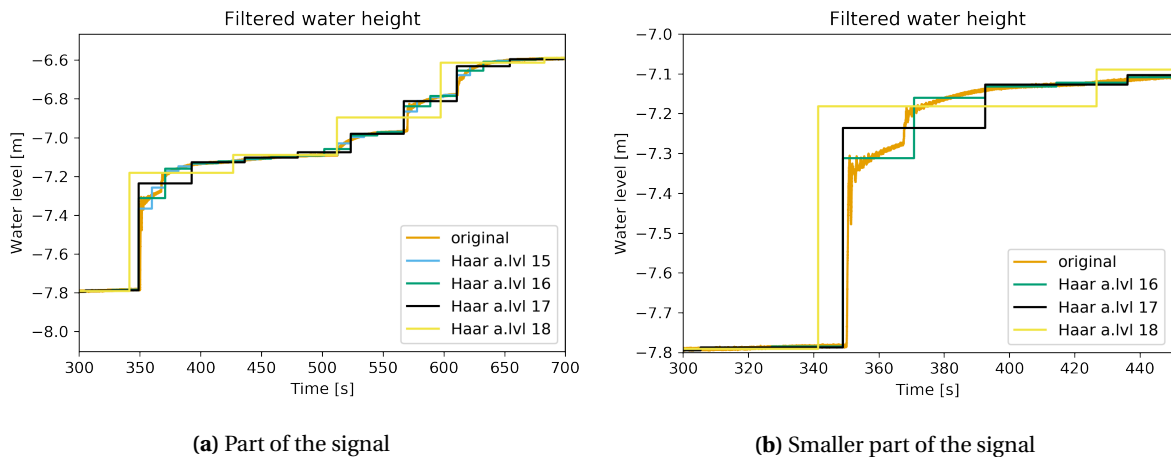


Figure 5.6: Reconstructing jumps in signal using the approximation levels of the Haar wavelet decomposition.

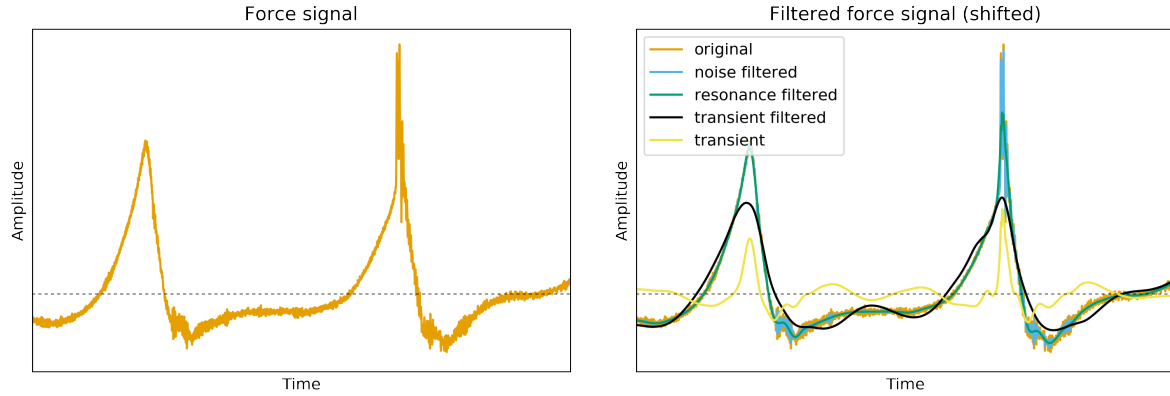
Transient

Another useful application of filters in the discrete wavelet domain is the ability to extract transients from a signal. Transients are signal elements of short duration and of unpredictable nature. A transient decays fast, has a unknown frequency content, and has a unknown arrival time [43]. For instance when forces on structures in breaking wave conditions are investigated transient-like signal elements appear in coastal engineering research. Such a signal is considered in this final example. Due to the confidentiality of this recording, no background or dimensions regarding this signal are given.

In Figure 5.7 two consecutive wave impact are presented. The first hit is a non-breaking wave, the second one is due to a breaking wave. The force exerted on the structure by such a breaking wave is in general described as the sum of a regular wave force and a 'triangle' on top of it. This signal is filtered using the Symmlet 8 wavelet. The filtering is done in a number of steps, all these steps are presented in Figure 5.7b. In this figure presents the result of a shifted algorithm, because the filtering without shifting has less desirable results. First the noise was filtered, followed by the resonance of the structure.

The next step is to filter the transient. This is done by carefully adjusting the filter. The assumption of the sum of a regular wave and a 'triangle' on top was tried to reconstruct. As can be observed in Figure 5.7b, a clear triangular shape is present in the transient at the time of the second wave peak. The peak without the transient shows some sharp edges, this is due to the shifted filter. The first peak of the 'transient filtered'

signal also is decreased in height. This is because the wavelet content of the transient overlaps the wavelet content of the entire signal. This form of transient filtering is a local operation. Especially because the wave heights differ and therefore the shape of the transient. To design a discrete wavelet filter to extract transients from many waves in one time series is very hard and should use non-stationary thresholds. The final filter (for the 'transient filtered' line in Figure 5.7b) is presented in the Appendix, Figure H.7.



(a) Two hits of waves on the structure. The first hit was a regular wave, the second a breaking wave. (b) Filtering the transient from the original signal in multiple steps. Final filter in Figure H.7.

Figure 5.7: Filtering transient in a coastal engineering force measurement. Dimensions are left out for confidentiality. The thin dotted line indicated the 0 force level.

5.3. Computation

The last comparison between the two techniques is the difference in computing capacity. In this chapter two important facets of the computation will be addressed. The first is the number of floating point operations (flops) needed to perform a given task. The second one is the amount of memory needed to store the results. This is expressed in the number of floats. Assume there are G gauges, recording signals consisting of N data points (i.e. floats). Complex valued floats need twice as much space to save as real valued floats. The computation time for the wavenumber is not taken into account.

Fourier

As discussed on page 8, the Fourier Transform needs $\mathcal{O}(N \log N)$ flops to compute. A multiplication in the Fourier domain with a filter takes N flops. A Fourier transformed signal can be stored in the same amount of floats as the original signal. The wave separation technique by Zelt and Skjelbreia [62] uses four sums that sum over the number of gauges G . Therefore solving the system of equations uses $\mathcal{O}(G)$ flops per frequency. From time domain to time domain this takes $\mathcal{O}(GN^2 \log N)$ operations.

CWT

The CWT (2.20) results cannot be stored in the same amount of floats as the original signal. Assume the CWT is performed over A number of scales, then the resulting wavelet coefficients consist of AN complex floats. Due to the computation through the FFT, it only takes $AN \log N$ flops to compute these coefficients (see ??). The reconstruction formula (2.24) uses $\mathcal{O}(AN)$ flops if the coefficients C_δ is already known. Assume this is not known, then the reconstruction is of $\mathcal{O}(AN^2)$. For stationary waves therefore the separation of waves takes $\mathcal{O}(AGN^3)$ flops. For non-stationary waves the algorithm has to be looped in time, leading to $\mathcal{O}(AGN^4)$ flops. The cone of influence needs little space to be saved, A floats. The zones of influence are very costly to store compared to the COI, with AN floats.

DWT

The discrete wavelet coefficients can be computed very effectively through the fast wavelet transform algorithm. This algorithm is of $\mathcal{O}(N^2 \log N)$ flops. The result can be stored in $\mathcal{O}(N)$ floats, the same as for amount as for the original signal. Determining thresholds depends on the techniques used. General denoising methods use $\mathcal{O}(N \log N)$ operations [50]. So denoising discrete wavelet coefficients takes $\mathcal{O}(N^2 \log N)$ flops, which is an order N higher than filtering using discrete Fourier coefficients.

Considerations

All work in this thesis has been applied on a 4 GB RAM personal computer. On such a machine the difference in computation time between the FFT and DWT is not noticeable. The PyWavelets [52] package uses the FWT algorithm and computes the results very fast. The continuous wavelet transform on the other hand takes more time to compute. The used basis code by Torrence, C [54] is less optimised. Further more there are side processes running, for instance to calculate the wavelets and the COI.

However, especially the non-stationary wave separation is most time consuming. This is also expected from the theoretical computation time. The developed code can be optimised to speed up the computations. Down-sampling reduces N , which can reduce the Often the most time consuming part is the creation of figures. Contour plots are much more computational intensive to create than line plots.

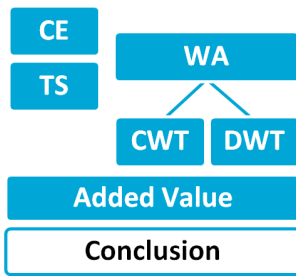
5.4. Discussion

The results presented in this chapter offer some opportunities. However, the results are not a major improvement with respect to the current method. The (discretised) continuous wavelet transform is a powerful tool in time-frequency analysis. By choosing the correct signal extension method and use the zone of influence to cope with the effects of gaps in the data, the effectiveness of the time-frequency analysis has been expanded.

In many applications the wavelet coefficients can be used instead of Fourier coefficients. The example addressed in Section 5.1.2 discussed a lot of applications of the wavelet coefficients. The signal used has a non-stationary mean, theoretically better suitable for wavelet analysis than Fourier analysis. The global wavelet spectrum does not have added value over the Fourier spectrum for stationary signals. In this non-stationary case is clear that the global wavelet spectrum expresses the power distribution of the signal better than the spectrum.

The scale averaged wavelet power, on the other hand, allows insight in the power distribution of a signal in time. This is used to show that the separation algorithms have a larger relative error for large waves than for small waves. The separation of waves using wavelet or Fourier coefficients often result in separated waves that are very similar. Import differences between the solutions is that wavelet transform has a lower density in the frequency domain which results in less disturbance due to critical gauge spacing. The introduction of the determinant limiter improves the result of the Fourier coefficient based algorithm much more. On the other hand the lower density is a downside, because the wavenumber is frequency dependant. Resulting in less accurate reconstruction of waves above certain frequencies.

For waves in the field of coastal engineering this often is not a problem because high frequencies are of very low power. The near and far shore waves have a more narrow range of wavenumbers, so a larger set of frequencies can be separated in these conditions. When a signal has non-stationary elements such as a changing mean water level, the wavelet coefficients are more suitable for separating the waves.



6

Conclusion and Recommendations

The goal of the research was to create guidelines to guide analysts in applying this technique on time-series from the field of coastal engineering. The wavelet transform is divided into two domains: the continuous wavelet transform and the discrete wavelet transform. Specific guidelines regarding these transforms are discussed at the ends of respectively Chapter 3 and Chapter 4. In Chapter 5 the added value is shown of both transforms in time-frequency analysis and digital signal processing in coastal engineering. In this last chapter the answer to the research questions and the conclusions of this work will be shared, followed by some recommendations and suggestions for future research.

6.1. Conclusions

[How to improve the \(discretised\) continuous wavelet transform to improve time-frequency analysis for time series in the field of coastal engineering?](#)

The discretised continuous wavelet transform based on the work of Torrence and Compo [53] has been expanded by the addition of different signal extension modes. The right choice of extension mode increases the reliability of the wavelet power spectrum outside the cone of influence. In Figure 3.2 some recommendations regarding the right choice are presented. In order to improve time-frequency analysis of signals with missing data points, the zones of influences have been developed. These zones indicate the disturbance of the wavelet coefficients, based on the wavelets mass distribution. These improvements allow better time-frequency analysis for time-series from the field of coastal engineering.

[Does the separation of incident and reflected waves based on wavelet coefficients for \$N\$ gauges perform better than the separation based on Fourier coefficients?](#)

The results of Ma et al. [35] and Zelt and Skjelbreia [62] have been combined to create an algorithm to separate incident and reflected waves for more than two gauges. These waves do only travel in one direction. Due to the increasing bandwidth of wavelets for higher frequencies, the algorithm using Fourier coefficients shows better results than the one based on wavelet coefficients for high frequencies. However, this effect can be minimised by choosing a small bandwidth wavelet. For relative low frequencies, that occur frequent in coastal engineering problems (< 5 Hz), there is almost no difference between the solution based on wavelet or Fourier coefficients. The determinant limiter that was introduced reduces the amount of energy in the reconstructed signals based on wavelet coefficients more than those based on Fourier coefficients. This is due to the resolution difference in the frequency domain of both methods. Conversely, the wavelet algorithm is less plagued by the close to zero determinant, resulting in more reliable separation without limiter.

When a non-stationary mean is introduced, the Fourier algorithm is plagued by low frequency noise. Furthermore, the wavenumber changes over time, which cannot be included in the Fourier algorithm. Because the wavelet coefficients depend on time, the change of the wavenumber can be incorporated, decreasing the error of the separation with respect to the Fourier separated waves. All in all is concluded that the separation based on wavelet coefficient is as better applicable to coastal engineering time series as the one based on Fourier coefficients. In particular for signals with a changing mean water level, for stationary signals the solutions do not differ significantly.

Which discrete wavelet based algorithm is best suited to remove noise from coastal engineering signals?

The results of four discrete wavelet based algorithms were compared to the results of a low pass Fourier filter. The low pass filter showed better results in filtering stationary signals. This is also clear from the theory. As is the fact that the wavelet based algorithms performed better on the non-stationary signal cases. The Srivastava based thresholds did not work out as well as predicted. The thresholds based on an idle period were much more effective in suppressing noise, both environmental and measurement noise. The thresholds based on the MAD combined with the soft thresholding did show the best results in recovering the sum of the basis signal and the measurement noise.

The choice of wavelet also influences the output of the filter. Comparing five different ones, lead to the conclusion that symmetric wavelets are better fit to filter stationary signals, than non-symmetric wavelets. Natural non-stationary signals are better denoised if the discrete wavelet decomposition is constructed using wavelets that mimic natural frequency behaviour. The Symmlets 8 and the Coiflet 3 outperformed the Haar, Daubechies and biorthogonal wavelet, as predicted by their spectra and literature.

What is the added value of wavelet analysis over current time series analysis methods in coastal engineering?

The added value of wavelet analysis is the addition of an extra dimension. Instead of observing signal behaviour in time or frequency, the wavelet coefficients are dependent on both time and frequency. Methods allowing similar insights exist, such as the short term Fourier transform, but are not optimal. The downside of any time-frequency method is that a trade off has to be made between the resolution in time and frequency. The resolution cannot be the same as in only the time or frequency domain.

This trade off is most clear in the separation of waves, where the wavelet based separation performs worse than the Fourier based separation for high frequencies. In the field of coastal engineering, however, these high frequencies do not arise very frequent, and therefore the wavelet and Fourier based separation methods can be used interchangeably. However, when the mean water level changes over time, the wavenumber in the wavelet based separation can be adapted in order to separate the waves better. For the Fourier based method this is impossible; here lies the added value of the wavelet coefficients with respect to the current method based on Fourier coefficients [22, 39, 62].

The limited time support of the wavelets ensures that local signal elements, for instance a discontinuity, only affects coefficients near that jump. This is in contrast to the Fourier coefficients, which are affected globally by a local event. Filling missing data points leads to discontinuities which affect all Fourier coefficients. The disturbance of the wavelet coefficients can be estimated using the wavelet mass distribution. This allows analysis of frequencies that are not possible in current methods. In coastal engineering long term measurements are very common and these often show defects like missing data points. The zones of influence allow time-frequency analysis for these signals.

The examples in Section 5.2 show the wide employability of filtering signal elements in the discrete wavelet domain. The best example of this wide applicability is the reconstruction of jumps using the Haar wavelet. This reconstruction is not possible in any other domain than the wavelet domain. The large number of wavelets available (Figure 2.4) leads to many opportunities. If this is not even enough, wavelets can be created to better fit the objective. The filtering in the wavelet domain has most added value in separating non-stationary signal elements from the rest of the signal. It is a much more powerful than current time or Fourier based methods.

How can wavelet analysis improve time-series analysis and processing in the field of coastal engineering?

All in all, wavelet analysis offers many improvements with respect to currently used time and Fourier based methods. The wavelet power spectrum and cross-wavelet applications can be applied to signals that are disturbed by missing or incorrect datapoints. The effect of these can be estimated based on the wavelet mass distribution. This allows quantitative analysis of different frequency components in time.

The separation of waves for signal with a changing mean water level can be solved without dividing the signal in parts. A continuous separated solution is a major improvement with respect to the non-continuous solution based on the Fourier separation currently in use. Furthermore, many challenges can be solved using the discrete wavelet transform. The discrete wavelet decomposition gives more insight into the behaviour of a signal and its noise. This allows analysts to justify the filter applied, which is a major improvement with respect to the empirically based filters that are currently in use.

The use of the wavelet transform, however, often is more time consuming. On one hand, the number of arithmetic operations for most applications is an $\mathcal{O}(N)$ more than the Fourier based analyses. On the other

hand, there is more information to process, which also takes more time. However, this quantity of information is what allows wavelet analysis to improve current methods. It provides more information about the signals behaviour, and is better able to cope with non-stationary signal elements. This results in a better separation of waves in non-stationary conditions, mathematically justified filters for all sorts of signal elements and better insight in the time-frequency behaviour of a signal.

6.2. Recommendations and Future Research

In this section some recommendations and suggestions for future research will be shared. These are split into three items. The first concerns the time-frequency analysis based on the results from Section 3.1, the second item concerns the separation of waves based on the continuous wavelet coefficients. Concluding with some suggestions regarding the added value of the discrete wavelet transform.

The largest recommendation regarding time-frequency analysis based on the continuous wavelet coefficients is to apply it. The physical interpretation of the signals using the scaling proposed by Liu et al. [33] improves the added value of wavelet analysis in time-frequency analysis. It has proven to be an effective analysis tool in other fields of research, especially for signals with non-stationary elements which occur frequent in coastal engineering. The extension of the cone of influence to the zones of influence allows time-frequency analysis for signals with missing data points. This extension is based on the wavelet mass distribution. Another measure could be based on the window function that is present in most continuous wavelets. The statistical significance of the wavelet power spectrum was not addressed in this thesis, but is important in the time-frequency analysis. Monte Carlo simulations can always offer good results, however, these are very time consuming. Analytical descriptions of background spectra can speed up time-frequency analysis using wavelets.

The separation of waves based on wavelet coefficients is as effective as the method based on Fourier coefficients for waves considered in coastal engineering. Future research could focus on the use of the chosen set of scales in order to evade the critical points where $\sin(k\Delta x)$ is (close to) zero. Therefore the reconstruction (2.24) has to be adjusted. There is more to gain regarding the reconstruction; the used reconstruction equation has quite a large reconstruction error in comparison to the discrete Fourier and wavelet reconstructions. By implementing a reconstruction using the analysing wavelet, this error might be decreased, which affects the separated waves. The design of a wavelet for the specific goal of separating non-linear waveforms (for instance as presented by Lykke Andersen et al. [34]), could improve separation results as well. Finally, the wavelet based algorithm can be expanded to sloping bathymetry [35] and oblique incident waves [36], possible even waves travelling in two dimensions.

With respect to the discrete wavelet transform, only the tip of the ice berg has been shown. There are many expansion such as wavelet packets, multiwavelets and the use of different dilation factors that could improve filter results [29]. This however will not benefit the user experience. The thresholding will become much more complicated, especially for those with little background in discrete wavelet theory. To improve the discrete wavelet filtering as applied in this thesis, a wavelet can be designed that complies to the characteristics of the signal to filter. Additionally, a (wavelet based) filter resulting in the desired filtered signal has not been found yet for the presented coastal engineering signals. The development of such an algorithm is of much added value for the filtering of much repeated measurements.

List of Demonstrations

3.1	Demonstration (Down-sampling)	25
3.2	Demonstration (Effect of missing data points on spectrum)	29
3.3	Demonstration (Cones of influence)	30
3.4	Demonstration (Zones of influence 1.0)	30
3.5	Demonstration (Zones of influence 2.0)	31
3.6	Demonstration (Accuracy of the zones)	33
3.7	Demonstration (Separate coastal engineering time series)	40
3.8	Demonstration (Wave number)	40
3.9	Demonstration (Critical gauge placement, number of gauges)	41
3.10	Demonstration (Different wavelets)	41
3.11	Demonstration (Number of scales)	41
3.12	Demonstration (Determinant limiter, p_{\max})	42
3.13	Demonstration (Weighing)	42
3.14	Demonstration (Change reflection coefficient over time)	43
3.15	Demonstration (Sloping signal)	43
3.16	Demonstration (Jumps)	43
3.17	Demonstration (Noise)	44
4.1	Demonstration (Test signal and discrete wavelet coefficients)	49
4.2	Demonstration (Srivastava filtering)	50

Bibliography

- [1] Luís Aguiar-Conraria and Maria Joana Soares. The Continuous Wavelet Transform: Moving beyond Uni- and Bivariate analysis. *Journal of Economic Surveys*, 28(2):344–375, apr 2014. ISSN 09500804. doi: 10.1111/joes.12012. URL <http://doi.wiley.com/10.1111/joes.12012>.
- [2] Luís Aguiar-Conraria, Nuno Azevedo, and Maria Joana Soares. Using wavelets to decompose the time-frequency effects of monetary policy. *Physica A: Statistical Mechanics and its Applications*, 387(12): 2863–2878, 2008. ISSN 03784371. doi: 10.1016/j.physa.2008.01.063.
- [3] Anestis Antoniadis. Wavelet methods in statistics: some recent developments and their applications. *Statistics Surveys*, 1:16–55, 2007. ISSN 1935-7516. doi: 10.1214/07-SS014. URL <http://arxiv.org/abs/0712.0283>
<http://dx.doi.org/10.1214/07-SS014>
<http://projecteuclid.org/euclid.ssu/1196693422>.
- [4] Ilker Bayram and Ivan W. Selesnick. Overcomplete Discrete Wavelet Transforms With Rational Dilation Factors. *IEEE Transactions on Signal Processing*, 57(1):131–145, jan 2009. ISSN 1053-587X. doi: 10.1109/TSP.2008.2007097. URL <http://ieeexplore.ieee.org/document/4663893/>.
- [5] Alex Bellos. Abel Prize 2017: Yves Meyer wins 'maths Nobel' for work on wavelets | Science | The Guardian. <https://www.theguardian.com/science/alex-adventures-in-numberland/2017/mar/21/abel-prize-2017-yves-meyer-wins-maths-nobel-for-work-on-wavelets>, 2017. Date accessed: 24-3-2017.
- [6] Richard E Blahut. *Algebraic Codes for Data Transmission*. Cambridge University Press, 2003. ISBN 978-0-521-55374-2. doi: 10.1017/CBO9780511800467. URL <http://www.amazon.com/Algebraic-Codes-Transmission-Richard-Blahut/dp/0521553741>.
- [7] Christian Blatter. *Wavelets: A Primer*. A K Peters, Ltd, 1998. ISBN 9781568811956.
- [8] Judith Bosboom and Marcel J.F. Stive. *Coastal Dynamics I*, lecture notes. VSSD, Delft, 2011.
- [9] Peter Brockwell and Richard Davis. *Introduction to Time Series and Forecasting*. Springer, 2002. ISBN 0387953515. doi: 10.2307/1271510. URL <http://scholar.google.com/scholar?hl=en&btnG=Search&q=intitle:Introduction+to+Time+Series+and+Forecasting>
<http://www.jstor.org/stable/1271510?origin=crossref>.
- [10] B. Cazelles, Kévin Cazelles, and Mario Chavez. Wavelet analysis in ecology and epidemiology: impact of statistical tests. *Journal of The Royal Society Interface*, 11(91):20130585–20130585, 2013. ISSN 1742-5689. doi: 10.1098/rsif.2013.0585. URL <http://rsif.royalsocietypublishing.org/content/11/91/20130585.abstract>
<http://rsif.royalsocietypublishing.org/cgi/doi/10.1098/rsif.2013.0585>.
- [11] Bernard Cazelles, Mario Chavez, Guillaume Constantin de Magny, Jean-Francois Guégan, and Simon Hales. Time-dependent spectral analysis of epidemiological time-series with wavelets. *Journal of the Royal Society, Interface / the Royal Society*, 4(15):625–36, 2007. ISSN 1742-5689. doi: 10.1098/rsif.2007.0212. URL <http://rsif.royalsocietypublishing.org/content/4/15/625.short>.
- [12] Leon W. Couch. *Digital and Analog Communication Systems*. Pearson Prentice Hall, 7th edition, 2007. ISBN 0-13-203794-7.
- [13] creativecommons.org. *Time-Frequency Dictionaries*. <http://archive.cnx.org/contents/4a47d3df-bfe5-428c-8bb6-e5b738077caa@2/time-frequency-dictionaries>, 2017. Date accessed: 20-2-2017.

- [14] Ingrid Daubechies. Orthonormal bases of compactly supported wavelets. *Communications on Pure and Applied Mathematics*, 41(7):909–996, oct 1988. ISSN 10970312. doi: 10.1002/cpa.3160410705. URL <http://doi.wiley.com/10.1002/cpa.3160410705>.
- [15] Ingrid Daubechies. *Ten Lectures on Wavelets*. Society for Industrial and Applied Mathematics, Pennsylvania, 1992. ISBN 0-89871-274-2.
- [16] M. P. C. de Jong. Low-frequency sea waves generated by atmospheric convection cells. *Journal of Geophysical Research*, 109:1–18, 2004. ISSN 0148-0227. doi: 10.1029/2003JC001931.
- [17] M. P C de Jong and J. A. Battjes. Seiche characteristics of Rotterdam Harbour. *Coastal Engineering*, 51(5-6):373–386, 2004. ISSN 03783839. doi: 10.1016/j.coastaleng.2004.04.002.
- [18] Jaidev Deshpande. PyHHT Tutorials – pyhht 0.0.1. documentation. <http://pyhht.readthedocs.io/en/latest/tutorials.html>, 2017. Date accessed: 29-3-2017.
- [19] Dennis Gabor. *Theory of Communication*, 1946. ISSN 09252312. URL citeulike-article-id: 4452465.
- [20] Z. Ge. Significance tests for the wavelet power and the wavelet power spectrum. *Annales Geophysicae*, 25(11):2259–2269, 2007. ISSN 1432-0576. doi: 10.5194/angeo-25-2259-2007.
- [21] Bernd Girod, Rudolf Rabenstein, and Alexander Stenger. *Signals and systems*. John Wiley & Sons, inc., 2001. ISBN 0-471-98800-6.
- [22] Yoshimi Goda and Yasumasa Suzuki. Estimation of Incident and Reflected Waves in Random Wave Experiments. In *Coastal Engineering 1976*, pages 828–845, New York, NY, nov 1977. American Society of Civil Engineers. ISBN 9780872620834. doi: 10.1061/9780872620834.048. URL <http://ascelibrary.org/doi/10.1061/9780872620834.048>.
- [23] a. Grinsted, J. C. Moore, and S. Jevrejeva. Application of the cross wavelet transform and wavelet coherence to geophysical time series. *Nonlinear Processes in Geophysics*, 11(5/6):561–566, 2004. ISSN 1607-7946. doi: 10.5194/npg-11-561-2004. URL <http://www.nonlin-processes-geophys.net/11/561/2004/>.
- [24] S. A P Haddad, J. M H Karel, R. L M Peeters, Ronald L. Westra, and Wouter A. Serdijn. Analog complex wavelet filters. *Proceedings - IEEE International Symposium on Circuits and Systems*, pages 3287–3290, 2005. ISSN 02714310. doi: 10.1109/ISCAS.2005.1465330.
- [25] Leo H. Holthuijsen. *Waves in Oceanic and Coastal Waters*. Cambridge University Press, New York, 2007. ISBN 978-0-511-27021-5.
- [26] Norden E. Huang and Sauuel S. P. Shen. *Hilbert Huang Transform and Its Applications*, volume 16. World Scientific Publishing Co. Pte. Ltd., second edition, 2014. ISBN 978-9814508230. doi: 10.1007/s13398-014-0173-7.2. URL <http://www.worldscientific.com/worldscibooks/10.1142/8804>.
- [27] Norden E Huang and Zhaohua Wu. A Review on Hilbert-Huang Transform: Method and Its Applications to Geophysical Studies. *Reviews of Geophysics*, 46(2007):1–23, 2008. ISSN 87551209. doi: 10.1029/2007RG000228.1.INTRODUCTION. URL <http://rcada.ncu.edu.tw/reference010.pdf>.
- [28] Norden E Huang, Zheng Shen, and Steven R Long. A new view of nonlinear water waves: The Hilbert Spectrum. *Annual Review of Fluid Mechanics*, 31(1):417–457, 1999. ISSN 0066-4189. doi: 10.1146/annurev.fluid.31.1.417. URL <http://www.annualreviews.org/doi/abs/10.1146/annurev.fluid.31.1.417>.
- [29] Fritz Keinert. *Wavelets and Multiwavelets*. Chapman & Hall/CRC, 2004. ISBN 1-58488-304-9.
- [30] Byungil Kim, Hoyoung Jeong, Hyoungkwan Kim, and Bin Han. Exploring wavelet applications in civil engineering. *KSCSE Journal of Civil Engineering*, 21(4):1076–1086, 2017. ISSN 19763808. doi: 10.1007/s12205-016-0933-3.
- [31] J. F. Kirby. Which wavelet best reproduces the Fourier power spectrum? *Computers and Geosciences*, 31(7):846–864, 2005. ISSN 00983004. doi: 10.1016/j.cageo.2005.01.014.
-

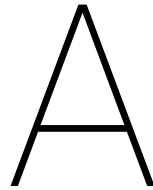
- [32] Chun-Liu Liu. A Tutorial of the Wavelet Transform. National Taiwan University, Department of Electrical Engineering (NTUEE), pages 1–72, 2010. ISSN 0166526X. doi: 10.1111/j.1600-0404.1995.tb01711.x. URL <http://disp.ee.ntu.edu.tw/tutorial/WaveletTutorial.pdf>.
- [33] Yonggang Liu, X. San Liang, and Robert H. Weisberg. Rectification of the bias in the wavelet power spectrum. *Journal of Atmospheric and Oceanic Technology*, 24(12):2093–2102, 2007. ISSN 07390572. doi: 10.1175/2007JTECHO511.1.
- [34] Thomas Lykke Andersen, Mads Røge Eldrup, and Peter Frigaard. Estimation of incident and reflected components in highly nonlinear regular waves. *Coastal Engineering*, 119:51–64, 2017. ISSN 03783839. doi: 10.1016/j.coastaleng.2016.08.013. URL <http://dx.doi.org/10.1016/j.coastaleng.2016.08.013>.
- [35] Yuxiang Ma, Guohai Dong, Xiaozhou Ma, and Gang Wang. A new method for separation of 2D incident and reflected waves by the Morlet wavelet transform. *Coastal Engineering*, 57(6):597–603, 2010. ISSN 03783839. doi: 10.1016/j.coastaleng.2010.01.002. URL <http://dx.doi.org/10.1016/j.coastaleng.2010.01.002>.
- [36] Yuxiang Ma, Guohai Dong, and Xiaozhou Ma. Separation of obliquely incident and reflected irregular waves by the Morlet wavelet transform. *Coastal Engineering*, 58(8):761–766, 2011. ISSN 03783839. doi: 10.1016/j.coastaleng.2011.03.014. URL <http://dx.doi.org/10.1016/j.coastaleng.2011.03.014>.
- [37] S.G. Mallat. A theory for multiresolution signal decomposition: the wavelet representation. *IEEE Transactions on Pattern Analysis and Machine Intelligence*, 11(7):674–693, jul 1989. ISSN 01628828. doi: 10.1109/34.192463. URL <http://ieeexplore.ieee.org/document/192463/>.
- [38] Stéphane Mallat. *A Wavelet Tour of Signal Processing*. Academic Press, 2nd edition, 1999. ISBN 0-12-466606-X.
- [39] E.P.D. Mansard and E.R. Funke. The Measurement of Incident and Reflected Spectra Using a Least Squares Method. In *SEVENTEENTH COASTAL ENGG. CONE*, pages 154–172, Sydney, Australia, 1980. Am. Soc. Civ. Engrs.
- [40] MathWorks Benelux. Signal Smoothing - MATLAB & Simulink Example - MathWorks Benelux. <https://nl.mathworks.com/help/signal/examples/signal-smoothing.html>, 2017. Date accessed: 7-4-2017.
- [41] MathWorks Benelux. Wavelet Toolbox - MATLAB. <https://nl.mathworks.com/products/wavelet.html>, 2017. Date accessed: 27-2-2017.
- [42] Gene Mosca and Paul A. Tipler. *Physics for Scientists and Engineers*. W.H. Freeman and Company, New York, sixth edition, 2009. ISBN 978-0-7167-8964-2.
- [43] SV Narasimhan, N Basumallick, and S Veena. *Introduction to wavelet transform: a signal processing approach*. Alpha Science International Ltd., 2011. ISBN 978-1-84265-629-7.
- [44] Radomír Pavlík. Binary PSK/CPFSK and MSK bandpass modulation identifier based on the complex shannon wavelet transform. *Journal of Electrical Engineering*, 56(3-4):71–77, 2005. ISSN 13353632.
- [45] Z. K. Peng, Peter W. Tse, and F. L. Chu. A comparison study of improved Hilbert-Huang transform and wavelet transform: Application to fault diagnosis for rolling bearing. *Mechanical Systems and Signal Processing*, 19(5):974–988, 2005. ISSN 08883270. doi: 10.1016/j.ymsp.2004.01.006.
- [46] Roger Peyret. *Spectral Methods for Incompressible Viscous Flow*. Springer Science+ Business Media, New York, 2002. ISBN 978-1-4419-2913-6. doi: 10.1007/978-1-4757-6557-1.
- [47] John G. Proakis and Dimitri G. Manolakis. *Digital Signal Processing*. Pearson Prentice Hall, 2007. ISBN 0-13-228731-5.
- [48] Tristan Rouyer, Jean Marc Fromentin, Nils Chr Stenseth, and Bernard Cazelles. Analysing multiple time series and extending significance testing in wavelet analysis. *Marine Ecology Progress Series*, 359 (Daubechies 1992):11–23, 2008. ISSN 01718630. doi: 10.3354/meps07330.

- [49] Kinhong Shin and Joseph K. Hammond. *Fundamentals of Signal Processing for Sound and Vibration Engineers*. John Wiley & Sons, inc., 2007. ISBN 978-0-470-51188-6.
- [50] Madhur Srivastava, C. Lindsay Anderson, and Jack H. Freed. A New Wavelet Denoising Method for Selecting Decomposition Levels and Noise Thresholds. *IEEE Access*, 4:3862–3877, 2016. ISSN 21693536. doi: 10.1109/ACCESS.2016.2587581.
- [51] G. Strang and T. Nguyen. *Wavelets and Filter Banks*. Wellesley-Cambridge Press, 2003. ISBN 0961408871.
- [52] The PyWavelet Developers. *Wavelets – PyWavelets Documentation*. <http://pywavelets.readthedocs.io/en/latest/ref/wavelets.html>, 2017. Date accessed: 17-3-2017.
- [53] Christopher Torrence and Gilbert P. Compo. A Practical Guide to Wavelet Analysis. *Bulletin of the American Meteorological Society*, 79(1):61–78, 1998. ISSN 00030007. doi: 10.1175/1520-0477(1998)079<0061:APGTWA>2.0.CO;2. URL <http://atoc.colorado.edu/research/wavelets/>.
- [54] Compo, Gilbert P. Torrence, C. Wavelet analysis; significance levels; confidence intervals;. paos.colorado.edu/research/wavelets/, 2017. Date accessed: 8-5-2017.
- [55] M van Berkel. *Wavelets for Feature Detection; Theoretical background*. Technical report, Eindhoven University of Technology, 2010.
- [56] J van Kan, A Segal, and F Vermolen. *Numerical methods in scientific computing*. Delft Academic Press / VSSD, second edition, 2014. ISBN 97890-6562-3638. URL <https://scholar.google.nl/scholar?hl=nl&q=vermolen+numerical+methods+in+scientific+computing&btnG={&}lr=>.
- [57] David F. Walnut. *An Introduction to Wavelet Analysis*. Birkhauser, 2002. ISBN 0-8176-3962-4.
- [58] Filip Wasilewski. Discrete Meyer (FIR Approximation) wavelet (dmey) properties, filters and functions - Wavelet Properties Browser. <http://wavelets.pybytes.com/wavelet/dmey/>, 2017. Date accessed: 17-3-2017.
- [59] Langford B. White and Boualem Boashash. Cross Spectral Analysis of Nonstationary Processes. *IEEE Transactions on Information Theory*, 36(4):830–835, 1990. ISSN 15579654. doi: 10.1109/18.53742.
- [60] Peter Wilders and W.A. Heemink. *Transport Modelling and Data Assimilation - WI4054*. Delft University of Technology, 2016.
- [61] Y Xia and Q Wei. An effective Kalman filtering method for enhancing speech in the presence of colored noise. *Audio, Language and Image Processing (ICALIP)*, 2016. URL <http://ieeexplore.ieee.org/abstract/document/7846530/>.
- [62] J A Zelt and James Skjelbreia. Estimating Incident and Reflected Wave Fields Using an Arbitrary Number of Wave Gauges. *Coastal Engineering Proceedings*, 1:777–789, 1992. ISSN 2156-1028. doi: 10.9753/icce.v23.%p. URL <http://journals.tdl.org/icce/index.php/icce/article/view/4736>.
- [63] Z. Zhang and J. C. Moore. Comment on "significance tests for the wavelet power and the wavelet power spectrum" by Ge (2007). *Annales Geophysicae*, 30(12):1743–1750, 2012. ISSN 09927689. doi: 10.5194/angeo-30-1743-2012.
-

Appendices

A	MSc thesis assignment	A3
B	Fourier transforms	A5
B.1	Continuous Fourier transforms	A5
B.1.1	Important functions	A5
C	Sampling theory	A7
C.1	Sampling Theorem	A7
C.1.1	Filtering	A7
C.1.2	Fourier transform requirements	A8
C.2	Regularity and decay	A8
C.2.1	Uncertainty principle	A8
D	Multi resolution analysis	A11
D.1	Fine details	A13
D.2	DWT - Discrete Wavelet Transformation	A14
D.3	Requirements for wavelet transform	A15
D.3.1	From CWT to DWT.	A15
D.4	The design equations	A16
D.4.1	Cascade algorithm	A16
D.5	Biorthogonal wavelets	A16
D.6	Discrete moments	A17
D.7	DWT algorithm	A18
D.8	The algorithm.	A18
D.8.1	Convolution implementation	A19
D.8.2	Programming the routine	A19
D.9	Filter formulation.	A20
D.10	Pre- and postprocessing	A20
D.11	Boundaries: different approaches.	A21
D.12	Formulations	A23
D.12.1	Modulation formulation	A23
D.12.2	Polyphase formulation.	A24
E	Wavelets	A27
E.1	Continuous Wavelets	A27
E.1.1	Example: Morlet wavelet.	A29
E.2	Discrete Wavelets	A29
F	Separation of incident and reflected waves	A31
F.1	Wavenumber	A31
F.2	Derivation for 2 gauges	A31
F.3	Reading the results	A32
F.4	Results	A33
G	Filter results	A51
G.1	Numbers	A51
G.2	Examples of other filters	A53
G.3	Five different wavelets and their spectra	A55
G.4	Comparison of wavelets in filtering	A58
G.5	Periodic signal extension	A63
G.6	Signals	A64

H	Compare techniques	A67
H.1	SignalsA67
H.1.1	WesterscheldeA67
H.1.2	WL657585e.A67
H.1.3	A3W1T304A67
H.2	FiguresA68
H.2.1	Separating waves.A68
H.2.2	FiltersA72



MSc thesis assignment

MSc-thesis assignment

Wavelets



Figure 1 Example of obtaining wave field information near trunk of a breakwater

The FBI uses wavelet techniques for image compression of digital fingerprints to save storage space. In geophysics wavelets are being used to analyse seismic signals for detecting e.g. earthquakes and oil layers. In finance the wavelet is used to analyse stock markets due to their dynamic and non-linear nature. These are just a few examples to highlight the applicability of the wavelet techniques.

The same techniques are potentially very interesting for Deltares as coastal engineers have to deal with complex time dependent physical processes as for example illustrated in the figures included.

To improve the understanding of these physical processes associated with waves, wave structure interaction, stability of structures or the influence on morphology various measurements techniques like time sampling, lasers scanning, photography are employed to capture instant information on wave conditions, forces, currents, erosion and accretion for further detailed analysis.



Figure 2 Example of measuring wave field

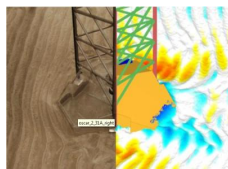


Figure 3 Example Stereophotography

This assignment is related to the part of detailed analysis of time series containing the time evolution of wave heights, forces, etc. Currently, the analysis is performed through Fourier analysis combined with filtering techniques to remove e.g. noise. However, the Fourier analysis has its limitations.

The purpose of this assignment is to look into the added value of applying existing wavelets and the related techniques compared to Fourier type of analysis.

The question is: can we improve our analysis by employing wavelet instead of Fourier technique? To answer this question, the following tasks have been defined for this assignment.

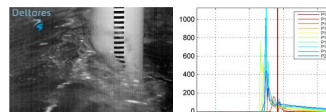


Figure 4 Example wave impact on a pile and measured pressure

Tasks

1. Provide a summary/overview on how wavelets are being used in other fields of expertise, including background information on the mathematical aspects of wavelets.
2. Verify the added value of wavelets by comparing results obtained through wavelet techniques with Fourier analysis by using different type of measured of time series (e.g. pressure due to wave impact, wave height, etc.) which representative for Deltares. Important aspects related to this task are:
 - a. Use wavelets to detect and filter different components (e.g. noise) from the signal by using for example thresholding methods.
 - b. Use wavelets to detect, if possible, the influence of wave basin characteristics on measured signals.

- c. Use wavelets to detect non-stationary properties in a signal, which is not possible by using standard Fourier analysis.
3. Research the sensitivity of wavelet specific parameters, e.g. type of wavelet, on the output of a wavelet analysis, including using statistical techniques to be able to interpret results.
4. Make wavelet analysis accessible in projects through scripts on top of an existing wavelet toolbox (yet to be selected). One important aspect for this task is the presentation of results.

Requirements

- Programming skills in either Matlab and/or Python.

This assignment is your chance to start a new era in coastal engineering with respect to time series analysis and also create added value to your own skills as wavelets are used in various fields of expertise. The only difference is jargon as the mathematics stays the same! If you are interested, please contact me.

Indication start date: After August 2016

Company: Deltares

Name : Jan Kramer

Email address: jan.kramer@deltares.nl

Figure A.1: The MSc thesis proposal as subjected by Deltares via <http://ta.twi.tudelft.nl/nw/users/vuik/numanal/rooij.html>.

B

Fourier transforms

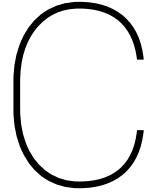
B.1. Continuous Fourier transforms

Property	Time signal $f(t)$	Fourier transform $\mathcal{F}\{f\}(\omega) = F(\omega)$	
Linearity	$c_1 f_1(t) + c_2 f_2(t)$	$c_1 F_1(\omega) + c_2 F_2(\omega)$	(B.1)
Translation	$f(t - h)$	$e^{-i\omega h} F(\omega)$	(B.2)
Modulation	$e^{i\xi t} f(t)$	$F(\omega - \xi)$	(B.3)
Scaling	$f\left(\frac{t}{a}\right)$	$ a F(a\omega)$	(B.4)
Convolution	$f_1 * f_2(t)$	$F_1(\omega) F_2(\omega)$	(B.5)
Multiplication	$f_1 f_2(t)$	$\frac{1}{2\pi} F_1 * F_2(\omega)$	(B.6)
Inversion	$F(t)$	$f(-\omega)$	(B.7)
Time differentiation	$\frac{df(t)}{dt}$	$i\omega F(\omega)$	(B.8)

more needed? [38, p.25]

B.1.1. Important functions

Time signal $f(t)$	Fourier transform $\mathcal{F}\{f\}(\omega)$	
$\delta(t - \tau)$	$e^{-i\tau\omega}$	(B.9)
$H(x)$	$\frac{1}{2} \left(\delta(\omega) - \frac{i}{\pi\omega} \right)$	(B.10)



Sampling theory

C.1. Nyquist-Shannon Sampling Theorem

As mentioned before the sampling of a signal can be seen as multiplying the sampled signal $x(t)$ by a set of Delta impulses (??). The Nyquist-Shannon theorem relates properties of the signal to the properties of the sampling frequency and vice versa. This theorem mainly has effect in the Fourier approach used in both the Fourier transform as the short term Fourier transform. For a signal of an interval T , we find the sampling frequency as $f_{\text{sampling}} = 2\pi/T$ [43], resulting in the DFT (??). The spectrum of the original signal $x(t)$, $X(\omega)$, repeats at every frequency interval of f_{sampling} in the spectrum of the sampled signal $X_{\text{sampled}}(\omega)$ [43]. These repetitions are called *images*. However if the original spectrum $X(\omega)$ is not limited by a maximum frequency (also known as *bandwidth*) $f_{\text{max}} \leq f_{\text{sampling}}/2$, the repetitions of $X(\omega)$ result in overlapping. The high frequency components of $X(\omega)$ are added to its low frequency components, resulting in a distorted $X_{\text{sampled}}(\omega)$. The repetitions of the spectrum can be cut out by using a *low pass* filter. In this case the choice for a filter selecting the domain $[-f_{\text{sampling}}/2, f_{\text{sampling}}/2]$ is made. This however does not remove the overlapping components.

This distortion of the recovered signal due to insufficient sampling frequency is known as *aliasing* [43]. A clear illustration of aliasing is given in ???. Signals with sudden transitions or noticeable noise often contain frequency components of which $\omega \rightarrow \infty$, these are therefore impossible to catch by any sampling frequency and will always lead to aliasing effect. These might be small however. To recover an analog signal properly from the sampled signal, $f_{\text{sampling}} \geq 2f_{\text{max}}$ [12, 43]. This minimum sampling frequency for a signal is known as the *Nyquist frequency*, defined as $f_N = 2f_{\text{max}}$ [12]. Sampling a signal under the Nyquist frequency is called *undersampling*, sampling with a frequency over the Nyquist frequency is called *oversampling*. Is oversampling a problem? No it is not, but working with an oversampled signal, results in doing computations that are not strictly necessary. However, when the Nyquist rate is based on the bandwidth of the sampled signal, oversampling could reduce noise, aliasing and improves the resolution of your signal. These effects are all explained by a theorem called the Nyquist-Shannon or Sampling Theorem. A nice proof of this theorem is given by Couch [12].

C.1.1. Filtering

The images of a spectrum can be taken out of the spectrum using a gate function $G(\omega)$. This function in signal analysis is referred to as a filter. Filters can be applied using computers, but often also *analogue filtering* (in the form of electronics) is used. An audio amplifier for instance often contains a set of analogue filters to determine the audio signals for the low, mid and high speakers. Often measurement equipment apply filtering effects to the measurements. A *low pass filter* is a filter that passes all frequencies under the cutoff frequency ω_m , for instance $G(\omega) = \mathbb{1}_{[-\omega_0, \omega_0]}(\omega)$. In this same way, *bandpass* and *high pass* filters are used to respectively pass signals in a certain bandwidth and above a certain cutoff frequency. This filtering can be interpreted as a multiplication in the frequency domain: $X_{\text{filtered}}(\omega) = X_{\text{sampled}}(\omega)G(\omega)$. If cut off windows are used, the *Gibbs phenomenon* or *ripple effect* arises [43]. This is best shown with an example.

By truncating the spectrum of the signal as in ??, a lot of relative large ripples appear. Choosing a longer window leads to increased ripple frequency, with no effect on the ripples magnitude [43]. A solution to this problem is choosing smoother windows, however, this results in loss of frequency resolution. The filter de-

termines the quality of the signal approximation [43]. Because the DFT is done using a computer, the signal is of finite length T . This can be interpreted as multiplying the original infinite signal with a block window $w(t) = \mathbb{1}_{[0,T]}$. By the inversion property of the Fourier transform (B.7), this will result in rippling effects in the spectrum, as observed in the in ??.

C.1.2. Fourier transform requirements

The Fourier transform cannot just be applied to all functions existing. In mathematical terms the CWT only exists for functions in the L^2 space [21]. This ensures the convergence of the integral in ??. In physical terms one would speak of functions with a finite energy [12]. Discrete signals can be interpreted as truncated signals, which will thus always be of finite energy. For these, the Fourier transform should be restricted to the representation of smooth, 2π -periodic functions [46]. When used to represent non-periodic functions, or functions with discontinuities, the Gibbs-effect will be present in the spectrum, and convergence around the boundaries will be non-uniform. There are efficient ways to weaken this effect [46], but this is a large disadvantage of the Fourier transform. Vice versa, when signals in the Fourier domain are truncated, the Gibbs effect shows in the time domain.

C.2. Regularity and decay

Till thus far the Fourier transform and the short term Fourier transform have been addressed. We have seen some nice results using the different transforms. There are some limitations however, especially for the STFT. These limitations are dependent on the regularity and decay of the chosen window function. The regularity of a signal $x(t)$ affects the decay of its Fourier transform $|X(\omega)|$ and vice versa [38]. The decay depends completely on the worst singular behaviour of $x(t)$. If there exists a constant K and $\epsilon > 0$ such that

$$|X(\omega)| \leq \frac{K}{1 + |\omega|^{p+1+\epsilon}}, \quad \text{then } x \in C^p. \quad (\text{C.1})$$

For instance a step function, which is in C^0 , results in a decay of $\mathcal{O}(1/|\omega|)$.

C.2.1. Uncertainty principle

equation C.1 shows that for a fast decaying spectrum $|X(\omega)|$ the signal $x(t)$ has regular variations in time. The energy of the signal $x(t)$ therefore has to be spread over a relatively large domain. The *uncertainty principle* relates the localization of energy in time with the localization in frequency. This principle is known to many as the *Heisenberg uncertainty principle*, for its implications in quantum mechanics which were discovered by Werner Heisenberg in the late 1920's. Assume a signal $x(t)$ of which the time spread is reduced, but the total energy is kept constant:

$$x_s(t) = \frac{1}{\sqrt{s}} x\left(\frac{t}{s}\right), \quad (\text{C.2})$$

then its Fourier transform (use Appendix B) is $\mathcal{F}x_s(\omega) = \sqrt{s}X(s\omega)$. So the increased localization in the temporal domain ($s < 1$) has led to a decreased localization in the frequency domain. These concentrations of energy in time and frequency are therefore restricted.

This restriction is mathematically described by the uncertainty principle. The simplest explanation of this principle is that if one wants to detect a frequency, one has to observe at least one period of the signal. So for low frequencies, this takes a lot of time. For high frequencies, very small time ranges have to be considered. The uncertainty principle knows a number of different mathematical formulations [7, 21, 29, 38]. The principle [38] states that the product of the temporal variance σ_t^2 and the frequency variance σ_ω^2 of a signal $x(t)$ and its Fourier transform respectively are restricted by

$$\sigma_t^2 \sigma_\omega^2 \geq \frac{1}{4}. \quad (\text{C.3})$$

The equality only holds for special cases of the signal. In addition, if a function $f \neq 0$ has a compact support (the signal is of finite length), then its FT $\mathcal{F}f(\omega)$ cannot have a compact support and vice versa [38].

Heisenberg boxes

The so called *Heisenberg box* is the result of this principle. This box limits the temporal and frequency precision of the STFT. The temporal and frequency variance are determined by the choice of the window function

$g(t)$. Assume $g(t)$ real and symmetric, with $g_{s,\xi}(t) = e^{i\xi t} g(t-s)$. Then the variances are only dependent on time and frequency, and therefore independent of the translation s and the modulation ξ (see equation C.4). Hence $g_{s,\xi}(t)$ corresponds to a Heisenberg box of area $\sigma_t \sigma_\omega$, centered around (s, ξ) [38], this is illustrated in Figure C.1. Because the window function does not change, the STFT is of identical resolution across the whole time-frequency plane.

$$\sigma_t^2 = \int_{-\infty}^{\infty} t^2 |g(t)|^2 dt, \quad \sigma_\omega^2 = \int_{-\infty}^{\infty} \omega^2 |\mathcal{F}\{g(t)\}(\omega)|^2 dt. \quad (\text{C.4})$$

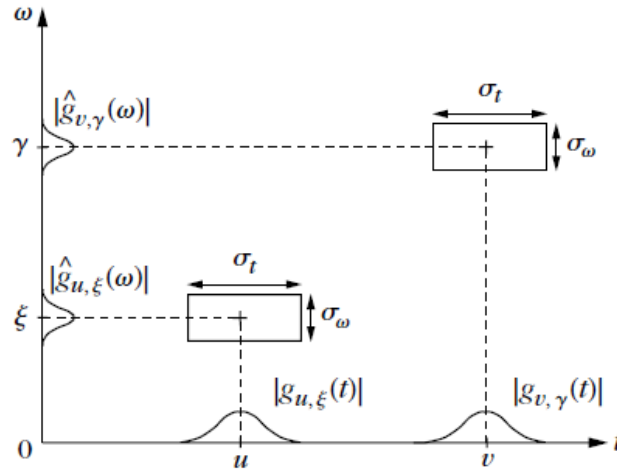


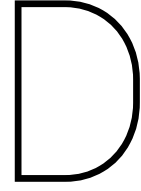
Figure C.1: Heisenberg boxes of two windowed Fourier transforms, where $\hat{f} := \mathcal{F}f$ [13, 38].

Choice of windows

From the above, we may conclude that the resolution in time and frequency of the STFT is dependent on the spread of the window in time and frequency. Notice that from the Heisenberg uncertainty principle (C.3) follows that the minimal area of an Heisenberg box is $1/2$. Mallat [38] shows that this can only be reached if g is a Gaussian window function. However, the organization of this box, width vs. height, can be arranged, to match a specific temporal or frequency resolution. This can be done by scaling the window $g(t)$ as in (C.2).

$g(t)$ finite?

For numerical applications, $g(t)$ must have a compact support, for it is finite. However, this results in an infinite support of the window function in the frequency domain [38]. The frequency resolution of the transform is maximized by concentrating the energy of $\mathcal{F}g(\omega)$ near $\omega = 0$. Then the temporal and frequency variance σ_t and σ_ω are not to deviating. If we for instance choose to shrink σ_ω to 0 (i.e. by choosing $g(t) = \delta(t)$), this results in the normal Fourier transform: high frequency resolution, but no temporal resolution.



Multi resolution analysis

The *multi resolution analysis* or *multi resolution approximation* (MRA) is another way of defining wavelets. In the first part of this chapter the CWT was defined from the theory of the STFT. The *discrete wavelet transform* (DWT) theory can be approached from the definition of the CWT, with addition of the notion of frames in Hilbert spaces [7, 15, 38]. Here however, the MRA approach of the DWT will be followed, which has two main advantages. The first advantage is that the MRA theory is discrete to begin with, resulting in a more natural derivation of the DWT, which is easier to implement as a computer algorithm [7, 29, 43]. Secondly, the MRA structure allows for convenient, fast and exact calculation of wavelet coefficients by providing a recursion relation, for both the discrete and the continuous case. This recursion relation is a relation between scaling coefficients at a given scale 2^{-n-1} and the scaling and wavelet coefficients at the next coarser scale 2^{-n} [57]. This section starts with the definition of a refinable function and an MRA and it ends with the definition of the DWT. This is followed by the covering of biorthogonal MRAs, in addition to the orthogonal ones discussed here. Through out this section the example of the Haar wavelet will be used. First we start with a *refinable function*, which is a function $\phi : \mathbb{R} \rightarrow \mathbb{C}$ which satisfies a two-scale refinement equation, or *recursion relation* of the form

$$\phi(t) = \sqrt{2} \sum_{k=k_0}^{k_1} h_k \phi(2t - k). \quad (\text{D.1})$$

The $h_k \in \mathbb{C}$ are known as the *recursion coefficients*. A refinable function ϕ is called orthogonal if for $k \in \mathbb{Z}$ [7, 29]

$$\langle \phi(t), \phi(t - k) \rangle = \delta_{0k} \quad \text{holds.} \quad (\text{D.2})$$

Haar function An example of such an orthogonal refinable function is the *Haar function*, defined as

$$\phi_{\text{Haar}}(t) := \mathbb{1}_{[0,1]} = \begin{cases} 1 & 0 \leq t \leq 1 \\ 0 & \text{elsewhere} \end{cases}. \quad (\text{D.3})$$

The Haar function is orthogonal and refinable with $h_0 = h_1 = 1/\sqrt{2}$, as shown in Figure G.5.

The set $\{V_j\}_{j \in \mathbb{Z}}$ is called a orthogonal *multi resolution analysis* (MRA) of L^2 , where $V_j, j \in \mathbb{Z}$ is a sequence of subspaces of L^2 , if it complies to six conditions [29]:

$$V_j \subset V_{j+1} \quad (\text{nested subsets}) \quad (\text{D.4a})$$

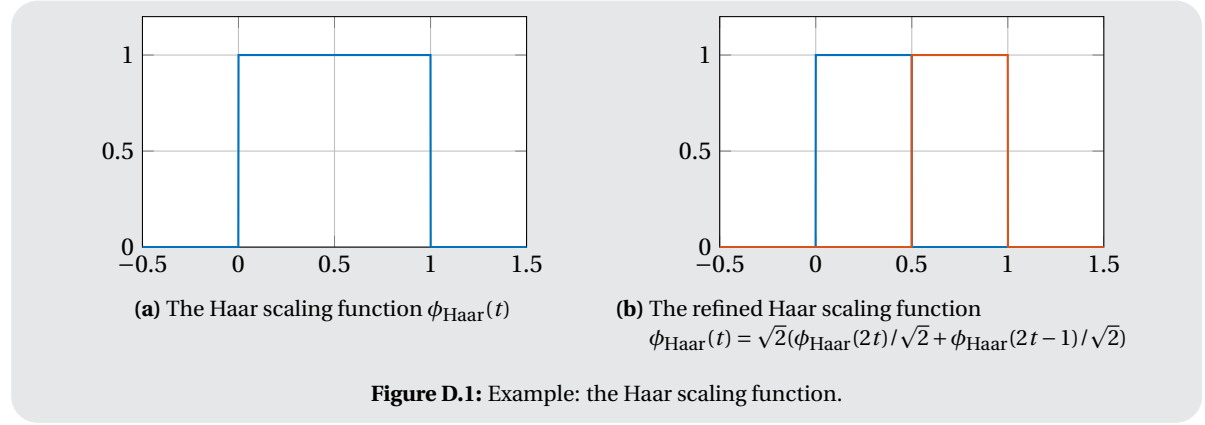
$$\cup_{j \in \mathbb{Z}} V_j = L^2 \quad (\text{density axiom}) \quad (\text{D.4b})$$

$$\cap_{j \in \mathbb{Z}} V_j = \{0\} \quad (\text{separation axiom}) \quad (\text{D.4c})$$

$$f(t) \in V_n \iff f(2x) \in f(2t) \in V_{n+1} \quad \forall n \in \mathbb{Z} \quad (\text{scaling property}) \quad (\text{D.4d})$$

$$f(t) \in V_n \iff f(2x) \in f(t - 2^{-n}k) \in V_n \quad \forall n, k \in \mathbb{Z} \quad (\text{scaling property}) \quad (\text{D.4e})$$

$$\exists \phi(t) \in L^2 \text{ such that } \{\phi(t - k) : k \in \mathbb{Z}\} \text{ forms an orthogonal basis of } V_0 \quad (\text{scaling function}) \quad (\text{D.4f})$$



There also exist MRAs built on non orthogonal scaling functions, these will be discussed later (Section D.5). Orthonormalizing an existing scaling function is possible, but the resulting new ϕ often does not have compact support anymore, losing its function for practical applications [29]. The fourth condition (D.4d) expresses the main property of an MRA: each subspace V_n consists of the functions in V_0 compressed by a factor 2^n , therefore spanning V_0 . From this can be concluded that a stable basis of V_n is given by $\{\phi_{nk}(t) : n \in \mathbb{Z}\}$, where

$$\phi_{nk}(t) = 2^{n/2} \phi(2^n t - k), \quad k \in \mathbb{N}. \quad (\text{D.5})$$

The last condition (D.4f) implies that any function $f \in V_0$ can be written uniquely as a sum of coefficients f_k multiplied with a scaling function

$$f(t) = \sum_{k \in \mathbb{Z}} \overline{f_k} \phi(t - k), \quad (\text{D.6})$$

converging in L^2 . The essential characteristic of the MRA is that $\phi(t) \in V_0$ can be written in the terms of the basis of V_1 as

$$\phi(t) = \sum_k h_k \phi_{1k}(t) = \sqrt{2} \sum_k h_k \phi(2t - k), \quad (\text{D.7})$$

for some coefficients h_k . This is called the *refinement equation*. From this follows that ϕ is a refinable function, for ϕ complies to the recursion relation (D.1). This refinement equation can be an infinite sum, but for now we will continue assuming a finite sum. The orthogonality condition (D.2) in this form becomes

$$\sum_k h_k \overline{h_{k-2\ell}} = \delta_{0\ell}. \quad (\text{D.8})$$

The orthogonal projection onto the subspace V_n , denoted with P_n , of an arbitrary function $f \in L^2$ is given by

$$P_n f = \sum_k \langle f, \phi_{nk} \rangle \phi_{nk}. \quad (\text{D.9})$$

Note that the projection $P_n f$ cannot represent details smaller than 2^{-n} . Therefore we say that functions in V_n have *resolution* or *scale* 2^{-n} . An MRA provides a sequence of approximations $P_n f$ of increasing accuracy to a given function f .

Orthogonal projection Lets continue with the Haar example. We are going to approximate the function $\cos(t)$ on the interval $[0, 10]$. We start with the function ϕ_{Haar} (D.3), then

$$P_0 f(t) = \sum_k \langle f, \phi_{0k} \rangle \phi_{0k} = \sum_k \langle \cos t, \phi_{\text{Haar}}(t - k) \rangle \cdot \phi_{\text{Haar}}(t - k).$$

And so the same can be applied to $P_1 f(t)$:

$$P_1 f(t) = \sum_k \langle f, \phi_{1k} \rangle \phi_{1k} = \sum_k \langle \cos t, \sqrt{2} \phi_{\text{Haar}}(2t - k) \rangle \cdot \sqrt{2} \phi_{\text{Haar}}(2t - k).$$

The result of this approximation is given in Figure D.2. Note that the Haar function produces an orthogonal MRA.

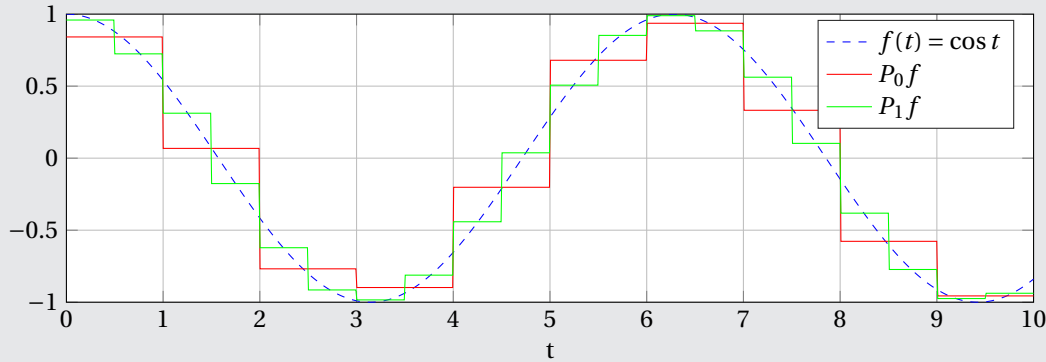


Figure D.2: Orthogonal projection of the function $\cos t$ using the Haar function (D.3).

D.1. Fine details

Orthogonal components In Example D.2 we have seen that we can approximate a function using the scaling function ϕ . The representation of, for instance, a function $x(t) \in V_1$ can be done by the space V_1 , but also by all spaces V_j , $j > 1$ [43]. This representation however is not very efficient, because more parameters than necessary are needed. How do you use less parameters? Note we used the functions in V_1 only to represent the part of $x(t)$ which could not be represented by V_0 . If we only use the difference between the spaces V_1 and V_0 to describe $x(t)$, less parameters are needed. Therefore the space W_0 will be explicitly designed. This space W_0 is in V_1 , but not in V_0 and therefore is called the *orthogonal component* of V_0 in V_1 . A more mathematical description follows.

When this difference between two approximations at different levels is considered, the applicability of the MRA rises. The difference between two levels of resolution 2^{-n} and 2^{-n-1} is also called the *fine detail at resolution 2^{-n}* , denoted as Q_n :

$$Q_n f = P_{n+1} f - P_n f. \quad (\text{D.10})$$

Note that Q_n is also an orthogonal projection [29] and that its range W_n is orthogonal to V_n , so the direct sum of the function space V_n and W_n is V_{n+1} :

$$V_n \oplus W_n = V_{n+1}.$$

This is the final step that brings us to another definition of the wavelet, approached discretely instead of continuous (??). Wavelets are an element of an orthogonal MRA. For any orthogonal MRA with scaling function ϕ [29]

$$\bigoplus_n W_n = L^2 \text{ dense} \quad (\text{D.11a})$$

$$W_k \perp W_n \text{ if } k \neq n \quad (\text{D.11b})$$

$$f(t) \in W_n \iff f(2t) \in W_{n+1} \forall n \in \mathbb{Z} \quad (\text{D.11c})$$

$$f(t) \in W_n \iff f(t - 2^{-n}k) \in W_n \forall n, k \in \mathbb{Z} \quad (\text{D.11d})$$

$$\exists \psi \in L^2, \text{ called a wavelet, such that } \{\phi(t - k) : k \in \mathbb{Z}\} \text{ forms an orthogonal basis of } W_0 \text{ and } \{\psi_{nk} : n, k \in \mathbb{Z}\} \text{ forms a stable basis of } L^2. \quad (\text{D.11e})$$

Since $\psi \in V_1$, it can be represented as

$$\psi(t) = \sum_k g_k \phi_{1k} = \sqrt{2} \sum_k g_k \phi(2x - k), \text{ with } g_k = (-1)^k h_{N-k}, \text{ with } N \text{ odd.} \quad (\text{D.11f})$$

Here ψ is known as the *mother wavelet*. In terms of the wavelet function, the projection Q_n is given, in the same way as P_n (D.9):

$$Q_n f = \sum_k \langle f, \psi_{nk} \rangle \psi_{nk}. \quad (\text{D.12})$$

This projection is the final step to the *discrete wavelet transform* DWT.

The Haar wavelet Now we will apply this to the example of the Haar function from Example D.1, to introduce our first wavelet build using MRA: the Haar wavelet (see Figure D.3). The coefficients g_k from (D.11f) to create the Haar wavelet are $\{g_0, g_1\} = \{h_1, -h_0\} = \{1/\sqrt{2}, -1/\sqrt{2}\}$, resulting in the function $\psi_{\text{Haar}}(t) = \mathbb{1}_{[0;0.5)}(t) - \mathbb{1}_{[0.5;1)}(t)$.

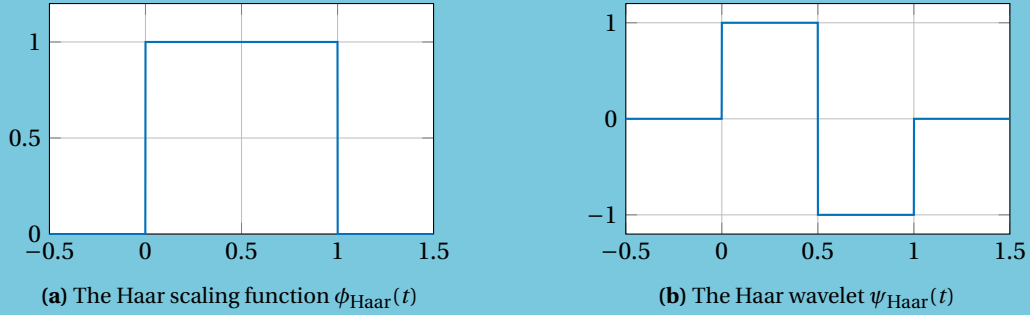


Figure D.3: The Haar scaling function and wavelet.

D.2. DWT - Discrete Wavelet Transformation

We have seen that given a function $f \in L^2$ we can represent it as a complete decomposition in terms of detail at all levels:

$$f = \sum_{k=-\infty}^{\infty} Q_k f.$$

As an alternative one can choose to start at a level ℓ and use the approximation at resolution $2^{-\ell}$ together with the detail at finer resolution, to decompose f as:

$$f = P_\ell f + \sum_{k=\ell}^{\infty} Q_k f.$$

An infinite sum is not practical applicable, so the sum is reduced to a finite sum: therefore we assume $f \in V_n$ for some $n > \ell$. Then the *discrete wavelet transform* (DWT) is described by

$$f = P_n f = P_\ell f + \sum_{k=\ell}^{n-1} Q_k f. \quad (\text{D.13})$$

The DWT approach is similar to the CWT approach, except of using continuous scale a and translation b , these are chosen discretely as scale n and translation k . The mother wavelet $\psi(t)$ is chosen and the daughter wavelets are

$$\psi_{nk}(t) = 2^{n/2} \psi(2^n t - k). \quad (\text{D.14})$$

The nk Heisenberg box has size $2^{-n} \sigma_t \times 2^n \sigma_\omega$, with different spacings for different frequencies, as for the continuous case. The inverse operation of the DWT will be discussed in Section D.7.

DWT This is the last time the Haar example will be discussed. For the Haar example $P_0 f$ and $P_1 f$ have been computed, following the DWT (D.13) we should find that $P_1 f = P_0 f + Q_0 f$. Therefore we use (D.12) to find

$$Q_0 f = \sum_k \langle f, \psi_{0k} \rangle \psi_{0k} = \sum_k \langle \cos t, \mathbb{1}_{[0;0.5)}(t-k) - \mathbb{1}_{[0.5;1)}(t-k) \rangle \cdot (\mathbb{1}_{[0;0.5)}(t-k) - \mathbb{1}_{[0.5;1)}(t-k)).$$

The result is shown in Figure D.4.

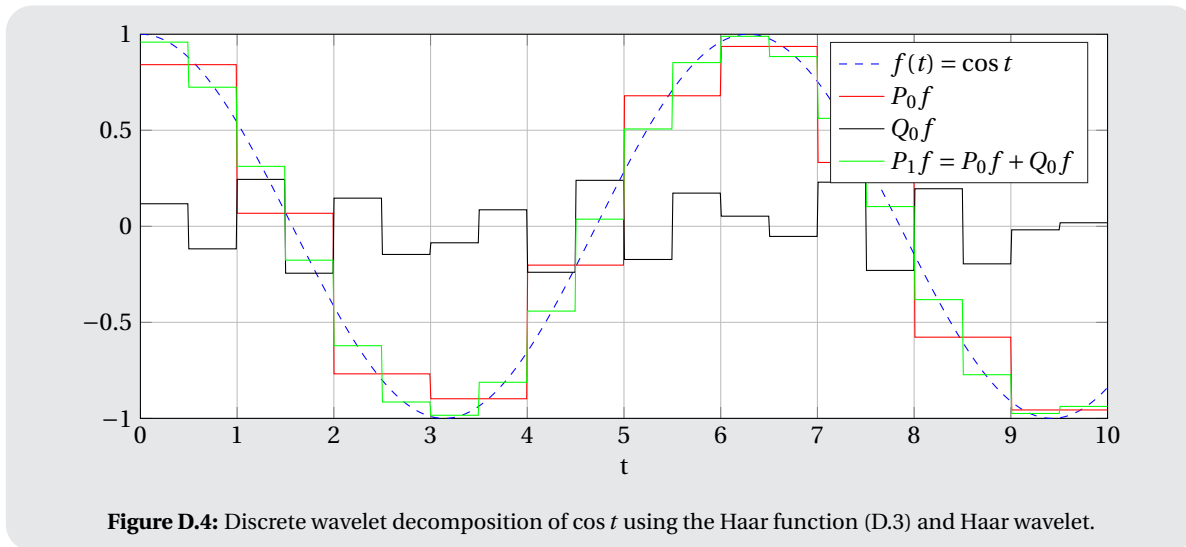


Figure D.4: Discrete wavelet decomposition of $\cos t$ using the Haar function (D.3) and Haar wavelet.

D.3. Requirements for wavelet transform

As for the Fourier transform, the integral defining the coefficients should converge. So, just like for the Fourier transform, only functions in the L^2 space are theoretically suitable for wavelet transformation [38]. For discrete signals some requirements will be discussed in Section D.7. However effects such as the Gibbs effect are not present in the wavelet transform. This makes the wavelet transform much more suitable to use for signals with discontinuities. The Fourier transform can also show unwanted effects in the reconstruction of non periodic functions, for instance a linear function. The reconstruction of the wavelet transform for both non periodic as periodic functions is close to perfect [61]. Because the wavelet transform (up to a certain scale) only catches local effect, the wavelet transform is also better applicable to non stationary signals.

The downside of the wavelet transform is the time-frequency representation in the form of the scalogram. The scalograms shown in ?? are hard to read and do not necessarily contain better information than the spectrograms of these signals (??, ?? and ??.) The discrete version of the scalogram, which will be presented in Figure D.7b is even harder to read. There is not necessarily a one to one coupling of wavelet scales to frequency. When complex wavelets are used this is determined most easy. Because of these downsides the scalogram is not much used in time-frequency domain analysis; especially the discrete version is almost never used.

D.3.1. From CWT to DWT

As mentioned before, there are two ways to derive the DWT. Following the MRA theory, we have found an expression for the (discrete) wavelet coefficient belonging to wavelet ψ_{nk} (from (D.12)): $\langle f, \psi_{nk} \rangle$. The definition of the inner product on L^2 in (??) shows the similarity with the continuous wavelet coefficient from (??). The CWT and DWT coefficients are defined through the same integral. Therefore a large set of functions is suitable for both continuous and discrete wavelet transform. However the most are better suited for one or the other; an overview will be given in ???. The DWT cannot be derived directly from the CWT expression (??), because the set of discrete scales and translations cannot be chosen arbitrarily. The justification of this choice can be made through the notion of frames from the Hilbert space theory [7, 15, 38]. This a very theoretical approach, where the MRA approach is less theoretical. They however result in the same expression for the DWT. A mayor advantage of the MRA approach is that an efficient algorithm of the DWT is easily derived, for both orthogonal and non orthogonal wavelets (see Section D.5). This algorithm will be explained to the reader in Section D.7.

D.4. The design equations

The Fourier transforms of the scaling function and the wavelet are indispensable in the design of wavelets. Here they are shortly reviewed. $H(\omega)$ and $G(\omega)$ are known as the *symbol* of respectively the refinable function and the wavelet[29]:

$$\Phi(\omega) = \mathcal{F}\phi(\omega) = H(\omega/2)\Phi(\omega/2), \quad \text{with } H(\omega) = \frac{1}{\sqrt{2}} \sum_k h_k e^{-ik\omega}, \quad (\text{D.15})$$

$$\Psi(\omega) = \mathcal{F}\psi(\omega) = G(\omega/2)\Psi(\omega/2), \quad \text{with } G(\omega) = \frac{1}{\sqrt{2}} \sum_k g_k e^{-ik\omega}. \quad (\text{D.16})$$

The orthogonality condition (D.8) in the Fourier domain becomes

$$|H(\omega)|^2 + |H(\omega + \pi)|^2 = 1. \quad (\text{D.17})$$

Relationship (D.15) can be substituted recursively, to find the formal limit

$$\Phi(\omega) = \left[\prod_{k=1}^{\infty} H(2^{-k}\omega) \right] \Phi(0). \quad (\text{D.18})$$

This approach is effective in the creation of wavelets. This relation can also be used to calculate the refinement equation corresponding to a certain low pass filter [32]. If convergence of this infinite product is assumed, this expression provides a way to compute $\phi(t)$ theoretically. $\Phi(0)$ can be chosen arbitrarily: solutions of the refinement equation (D.7) are only defined up to a constant factor. Choose $\Phi(0) \neq 0$ to find solutions other than $\phi(t) = 0$. Multiples of the solution of the equation are also solutions to the equation.

D.4.1. Cascade algorithm

The *cascade algorithm* is a more suitable way than (D.18) to approximate point values of $\phi(t)$ [29]. This algorithm applies a fixed point iteration applied to the refinement equation. Starting by choosing a suitable scaling function $\phi^{(0)}(t)$, and define

$$\phi^{(n)}(t) = \sqrt{2} \sum_k h_k \phi^{(n-1)}(2t - k), \quad (\text{D.19})$$

which will converge in many cases.

D.5. Biorthogonal wavelets

In the derivation of the DWT we used the existence of orthogonal MRAs. These orthogonal MRAs however are not very common [29] and therefore the *biorthogonal* MRA will be discussed (sometimes referred to as *semi orthogonal*). We first start with an example from linear algebra, to explain the concept of biorthogonality.

Biorthogonal system Consider two independent vectors \mathbf{b}_1 and $\mathbf{b}_2 \in \mathbb{R}^2$. By independence, \mathbf{b}_1 and \mathbf{b}_2 are a basis for \mathbb{R} . If $\mathbf{b}_1 \perp \mathbf{b}_2$, this basis is called orthogonal, if also both vectors are unit vectors, the basis is called orthonormal. Any vector $\mathbf{x} \in \mathbb{R}^2$ can be written as $\mathbf{x} = \alpha \mathbf{b}_1 + \beta \mathbf{b}_2$. If we choose $B = [\mathbf{b}_1, \mathbf{b}_2]$, then we can solve for the coefficients:

$$\mathbf{x} = B \begin{bmatrix} \alpha \\ \beta \end{bmatrix} = B \mathbf{c} \quad \Rightarrow \quad \mathbf{c} = B^{-1} \mathbf{x}.$$

This however is not as easily solved for a nonorthogonal set as for an orthogonal set of basis vectors. Therefore the *dual* base $\{\tilde{\mathbf{b}}_1, \tilde{\mathbf{b}}_2\}$ is introduced. These vectors comply to [43]

$$\langle \mathbf{b}_1, \tilde{\mathbf{b}}_1 \rangle = 1, \quad \langle \mathbf{b}_2, \tilde{\mathbf{b}}_2 \rangle = 1, \quad \langle \mathbf{b}_2, \tilde{\mathbf{b}}_1 \rangle = 0, \quad \langle \mathbf{b}_1, \tilde{\mathbf{b}}_2 \rangle = 0,$$

such that we can use the relation $\mathbf{c} = B^{-1} \mathbf{x} = \tilde{B} \mathbf{x}$, to determine the coefficients α and β . This matrix \tilde{B} is chosen $\tilde{B} = [\tilde{\mathbf{b}}_1, \tilde{\mathbf{b}}_2]^T$ such that

$$\mathbf{x} = (\tilde{\mathbf{b}}_1^T \mathbf{x}) \mathbf{b}_1 + (\tilde{\mathbf{b}}_2^T \mathbf{x}) \mathbf{b}_2. \quad (\text{D.20})$$

E.g. we choose two non orthogonal vectors, spanning \mathbb{R}^2 and a vector \mathbf{x} :

$$\mathbf{b}_1 = \begin{bmatrix} 1 \\ 0 \end{bmatrix}, \quad \mathbf{b}_2 = \begin{bmatrix} 1/2 \\ \sqrt{3}/2 \end{bmatrix}, \quad \mathbf{x} = \begin{bmatrix} 1 \\ 1 \end{bmatrix}.$$

The dual base for the given \mathbf{b}_1 and \mathbf{b}_2 is given by

$$\tilde{\mathbf{b}}_1 = \begin{bmatrix} 1 \\ -1/\sqrt{3} \end{bmatrix} \quad \text{and} \quad \tilde{\mathbf{b}}_2 = \begin{bmatrix} 0 \\ 2/\sqrt{3} \end{bmatrix}.$$

Then

$$\tilde{\mathbf{b}}_1^\top \mathbf{x} = 1 - 1/\sqrt{3}, \quad \tilde{\mathbf{b}}_2^\top \mathbf{x} = 2/\sqrt{3}, \quad \Rightarrow \quad (1 - 1/\sqrt{3}) \begin{bmatrix} 1 \\ 0 \end{bmatrix} + 2/\sqrt{3} \begin{bmatrix} 1/2 \\ \sqrt{3}/2 \end{bmatrix} = \begin{bmatrix} 1 \\ 1 \end{bmatrix} = \mathbf{x}.$$

The sets $\{\mathbf{b}_1, \mathbf{b}_2\}$ and $\{\tilde{\mathbf{b}}_1, \tilde{\mathbf{b}}_2\}$ are a biorthogonal system of \mathbb{R}^2 .

As the word *bi* in biorthogonal implies, the biorthogonal MRA has not one but two refinable functions as a basis. Refinable functions in general are relatively easy to find, but a lot of them do not result in orthogonal MRAs, so the orthogonality conditions will be replaced by milder biorthogonality conditions [29]. Two refinable functions ϕ and $\tilde{\phi}$ are called *biorthogonal* if

$$\langle \phi(x), \tilde{\phi}(x - k) \rangle = \delta_{0k}.$$

$\tilde{\phi}$ then is referred to as the *dual* of ϕ . This dual however is not unique [29], dual lifting, a process discussed later, will produce numerous other duals of the same ϕ . These two scaling functions define two MRAs: $\{V_n\}_{n \in \mathbb{Z}}$ and $\{\tilde{V}_n\}_{n \in \mathbb{Z}}$. Then the construction of the projections follows the same line of reasoning as in Example D.5: there are two projections, P_n (D.21a) and \tilde{P}_n (D.21b) to project a function from L^2 to $\{V_n\}_{n \in \mathbb{Z}}$ and $\{\tilde{V}_n\}_{n \in \mathbb{Z}}$ respectively.

The projections Q_n (D.21c) and \tilde{Q}_n (D.21d) are defined as before, spanning the spaces $\{W_n\}_{n \in \mathbb{Z}}$ and $\{\tilde{W}_n\}_{n \in \mathbb{Z}}$ respectively. The space W_n is now orthogonal to \tilde{V}_n , such that the fine detail relation (D.10) still holds. The same hold for \tilde{W}_n and V_n . Now note that $V_n \oplus W_n = V_{n+1}$ still holds, but now as a nonorthogonal direct sum instead of an orthogonal one. Keinert [29] states that finding wavelet functions ψ and $\tilde{\psi}$ which span the spaces W_n and \tilde{W}_n is not that hard, but stability is not guaranteed. How to find these functions is further elaborated in ??.

$$P_n f = \sum_k \langle f, \tilde{\phi}_{nk} \rangle \phi_{nk}, \quad (\text{D.21a})$$

$$\tilde{P}_n f = \sum_k \langle f, \phi_{nk} \rangle \tilde{\phi}_{nk}, \quad (\text{D.21b})$$

$$Q_n f = P_{n+1} f - P_n f, \quad (\text{D.21c})$$

$$\tilde{Q}_n f = \tilde{P}_{n+1} f - \tilde{P}_n f. \quad (\text{D.21d})$$

When an orthogonal wavelet is used for decomposition, the representation of the signal is the most compact: the number of convolutions at a scale is proportional to the size of a scale [53]. This will result in a relative sparse representation of the signal. This is characteristic is very desirable in signal compression [29]. An aperiodic shift in time series produces a different wavelet spectrum, this is often not beneficial in time series analysis. When a biorthogonal wavelet is used, the large scales are highly redundant, the wavelet coefficients at adjacent times are highly correlated. This makes the biorthogonal wavelets better applicable to time series analysis where smooth, continuous variations in wavelet coefficients are expected [53].

D.6. Discrete moments

In ?? the importance of the number of vanishing moments for the wavelet transform has been addressed. The discrete wavelet do have vanishing moments, just like the continuous case. They however can be defined by their coefficients: the k th discrete moment of the refinement function ϕ and the wavelet ψ are defined by their coefficients h_k and g_k . The m denotes the moment of the refinable function, the n the moment of the

wavelet [29].

$$\begin{aligned} m_k &= \frac{1}{\sqrt{2}} \sum_{\ell} \ell^k h_{\ell}, & n_k &= \frac{1}{\sqrt{2}} \sum_{\ell} \ell^k g_{\ell}, \\ m_k &= i^k \frac{d^k h}{d\omega^k}(0), & n_k &= i^k \frac{d^k g}{d\omega^k}(0). \end{aligned}$$

If in particular $m_0 = h(0) = 1$, the zeroth moment of a refinement function is 1. These discrete moments are uniquely defined and easy to calculate. They can be computed using the relation between the discrete and continuous moments:

$$\mu_k = 2^{-k} \sum_{p=0}^k \binom{k}{p} m_{k-p} \mu_p, \quad \nu_k = 2^{-k} \sum_{p=0}^k \binom{k}{p} n_{k-p} \nu_p.$$

D.7. Discrete wavelet transform algorithmic

In this section of the chapter the two or three steps of the algorithm performing the DWT are explained. Some different formulations of the DWT algorithm are discussed, which are essential to the building of wavelets. The resulting algorithm needs $\mathcal{O}(N \log_2 N)$ operations, which as fast as the DFT, however it is asymptotically faster than the STFT algorithm, using $\mathcal{O}(N^2 \log_2 N)$ operations. The two or three steps to do a complete DWT for a 1D signal of finite length are [29]:

1. Optional: preprocessing of the signal (Section D.10);
2. Handling the boundary conditions (Section D.11); and
3. Applying the algorithm (Section D.8).

Finally there are different ways of formulation and implementation of the algorithm. These will be discussed at the end of this section. This section is started with the final step of the DWT: the algorithm. Note we assume the use of biorthogonal wavelets, if one uses a orthogonal wavelets the tildes in this explanation can be dropped. The DWT is based on the decomposition of the space V_n :

$$V_n = V_{\ell} \oplus W_{\ell} \oplus \dots \oplus W_{n-1}.$$

D.8. The algorithm

We start with a function $s \in V_n$ (or signal), which by the theory can be represented by its coefficient vector $\mathbf{s}_n = \{s_{nk}\}_{k=1, \dots, N}$:

$$s(t) = \sum_k \bar{s}_{nk} \phi_{nk}(t). \quad (\text{D.22})$$

The function can also be expanded into two parts:

$$s(t) = \sum_k \bar{s}_{\ell k} \phi_{\ell k}(t) + \sum_{j=\ell}^{n-1} \sum_k \bar{d}_{jk} \psi_{jk}(t).$$

The notations s and d originate from the Haar wavelet, where s denotes the sum and d the difference. For regular wavelets, it is easier to remind s as the smooth part and d as the (fine) detail [29]. The complex conjugate notation of the coefficients comes from the multiwavelet theory. The DWT and inverse DWT (IDWT) convert the coefficients s_{nk} to $s_{\ell k}$ and d_{jk} , $j = \ell, \dots, n-1$ and vice versa. Signals consisting of equally spaced samples of the signal s frequently are in the form $s(2^{-n}k)$. The conversion of $s(2^{-n}k)$ to s_{nk} is called *preprocessing*, the reverse processes *postprocessing*. Both are explained later. So the signal s is *decomposed* in its components in V_{n-1} and W_{n-1} by

$$\begin{aligned} s &= P_{n-1} s + Q_{n-1} s = \sum_k \langle s, \tilde{\phi}_{n-1,j} \rangle \phi_{n-1,j} + \sum_k \langle s, \tilde{\psi}_{n-1,j} \rangle \psi_{n-1,j} \\ \Rightarrow \mathbf{s}_n &= \sum_k \bar{s}_{n-1,j} \phi_{n-1,j} + \sum_k \bar{d}_{n-1,j} \psi_{n-1,j}. \end{aligned}$$

By this the (discrete) signal s , \mathbf{s}_n in vector notation, is *decomposed* in two pieces: \mathbf{s}_{n-1} (D.23a) and \mathbf{d}_{n-1} (D.23b) [29]. From this the signal can be reconstructed following (D.23c).

$$s_{n-1,j} = \sum_k \tilde{h}_{k-2j} s_{nk}, \quad (\text{D.23a})$$

$$d_{n-1,j} = \sum_k \tilde{g}_{k-2j} s_{nk}, \quad (\text{D.23b})$$

$$s_n k = \sum_j (\bar{h}_{k-2j} s_{n-1,j} + \bar{g}_{k-2j} d_{n-1,j}) \quad (\text{D.23c})$$

Where we define

$$\langle \phi_{n-1,j}, \tilde{\phi}_{nk} \rangle = h_{k-2j}, \quad \langle \phi_{n-1,j}, \tilde{\psi}_{nk} \rangle = g_{k-2j}, \quad \langle \tilde{\phi}_{n-1,j}, \phi_{nk} \rangle = \tilde{h}_{k-2j}, \quad \langle \tilde{\psi}_{n-1,j}, \phi_{nk} \rangle = \tilde{g}_{k-2j}.$$

D.8.1. Convolution implementation

The decomposition step can be written as two discrete convolutions, of computation time $\mathcal{O}(N \log_2 N)$ using the same improvement as the FFT algorithm. These convolutions are¹

$$((-)\tilde{\mathbf{h}} * \mathbf{s}_n)_j = \sum_k \tilde{h}_{-(j-k)} s_{nk}, \quad ((-)\tilde{\mathbf{g}} * \mathbf{s}_n)_j = \sum_k \tilde{g}_{-(j-k)} s_{nk}, \quad (\text{D.24a})$$

which are followed by downsampling to determine \mathbf{s}_{n-1} and \mathbf{d}_{n-1} (assume computation time of $\mathcal{O}(1)$):

$$\mathbf{s}_{n-1} = (\downarrow 2)((-)\tilde{\mathbf{h}} * \mathbf{s}_n), \quad \mathbf{d}_{n-1} = (\downarrow 2)((-)\tilde{\mathbf{g}} * \mathbf{s}_n). \quad (\text{D.24b})$$

This is only one step of the algorithm, in practice these steps often repeated several times:

$$\begin{aligned} \mathbf{s}_n &\rightarrow \mathbf{s}_{n-1}, \mathbf{d}_{n-1} \\ \mathbf{s}_{n-1} &\rightarrow \mathbf{s}_{n-2}, \mathbf{d}_{n-2} \\ &\vdots \\ \mathbf{s}_{\ell+1} &\rightarrow \mathbf{s}_{\ell}, \mathbf{d}_{\ell}. \end{aligned}$$

Because in every step, the length of the components \mathbf{s}_{n-1} , \mathbf{d}_{n-1} is half the length of the components \mathbf{s}_n , \mathbf{d}_n , the algorithm has to compute $\mathcal{O}(N) + \mathcal{O}(N/2) + \mathcal{O}(N/4) + \dots = \mathcal{O}(N)$ convolutions. This results in $\mathcal{O}(N^2 \log_2 N)$ arithmetic operations to determine the discrete wavelet transform of a signal. The reconstruction of the signal from the DWT is opposite to the decomposition: first upsampling, followed by two convolutions:

$$\mathbf{s}_n = \bar{\mathbf{h}} * (\uparrow 2)\mathbf{s}_{n-1} + \bar{\mathbf{g}} * (\uparrow 2)\mathbf{d}_{n-1}. \quad (\text{D.24c})$$

D.8.2. Programming the routine

When we start with a signal \mathbf{s}_n of length N , the first step produces \mathbf{s}_{n-1} and \mathbf{d}_{n-1} , which are both of length $N/2$. These signals are most of the time stored in the same place as the original signal \mathbf{s}_n . So the output of the DWT routine after several steps becomes then

$$\begin{bmatrix} \mathbf{s}_{\ell} \\ \mathbf{d}_{\ell} \\ \mathbf{d}_{\ell+1} \\ \vdots \\ \mathbf{d}_{n-1} \end{bmatrix}.$$

This vector can be stored in the same space as \mathbf{s}_n with which the routine started. This representation results in an ugly programmable routine. The *matrix formulation* of the DWT results in a more appealing matrix-vector product notation.

¹For notation, see ??.

Both the decomposition as the reconstruction can be implemented as infinite matrix-vector products [29]. Here $(\mathbf{sd})_n = [\dots, s_{n,-1}, d_{n,-1}, s_{n,0}, d_{n,0}, s_{n,1}, d_{n,1}, \dots]^\top$, such that the decomposition step can be written as

$$(\mathbf{sd})_{n-1} = \tilde{L} \mathbf{s}_n, \quad \text{with } \tilde{L} = \begin{bmatrix} \dots & \dots & \dots & & \\ \dots & \tilde{L}_0 & \tilde{L}_1 & \dots & \\ & \dots & \tilde{L}_0 & \tilde{L}_1 & \dots \\ & & \dots & \dots & \dots \end{bmatrix}, \quad \text{for } \tilde{L}_k = \begin{bmatrix} \tilde{h}_{2k} & \tilde{h}_{2k+1} \\ \tilde{g}_{2k} & \tilde{g}_{2k+1} \end{bmatrix}. \quad (\text{D.25})$$

The reconstruction step can thus be written as

$$\mathbf{s}_n = L^* (\mathbf{sd})_{n-1},$$

where the perfect reconstruction condition is expressed as $L^* \tilde{L} = I$. The finite, and therefore applicable versions will be derived when the boundaries are discussed.

D.9. Filter formulation

The filter formulation of this algorithm will be discussed shortly for it is widely used [41, 43, 52]. In the algorithm the decomposition is given by a convolution and a down sampling. The recomposition is given as a up sampling step follow by a convolution with the same signal. These steps are shown in Figure D.5. From these figures it is clear that both filters $g[n]$ and $h[n]$ have different properties. The filter $g[n]$ is a high pass filter, whereas the filter $h[n]$ is a low pass filter. The down sampled low pass filter output is then treated as an input for the next stage, passing through the same analyzing filters. From this follows that admissible wavelets are either high pas or band pass filters [43]. This process can be repeated until the desired number of stages is achieved. An example for three stages is found in Figure D.6. In the recomposition it is clear why only the most coarse smooth part and all fine details are saved. By omitting the finest details, a signal can for instance be compressed. The representation in Figure D.6 is known as the dyadic implementation. The recomposition filters are known as *interpolating filters*. If wavelet packets are used, not only the smooth part is fed into the decomposition again, but also the detail parts are decomposed. If not all detail parts are decomposed, this can lead to interesting distributions of the time frequency plane (such as ??). They are almost nowhere used to display data, but have different applications in mostly compression and noise reduction [43].

Wavelets can be designed from this filter perspective, where $h[n]$ can be seen as high pass filter and $g[n]$ as a low pass filter. This design perspective will not be addressed much in this literature thesis. However, note that the choice of filter $h[n]$ has impact on the vanishing moments, the regularity and the decay of the accompanied wavelet. The choice of the coefficients of $h[n]$ that lead to maximum regularity differs from the choice of a maximum number of vanishing moments [15]. The filter implementation of the DWT algorithm is also known as the Fast Wavelet Transform (FWT) and was first proposed by Mallat in 1988. It finds its strength in using the Fourier transform of the signals and the convolution property (5) [38]. This will be elaborated further in Section D.12.

D.10. Pre- and postprocessing

As mentioned in the begin of Section D.7, the data, mostly in the form of a signal $s(2^{-n}k)$, has to be converted to the coefficients s_{nk} from (D.22). Keinert [29] discusses a few options to find the coefficients s_{nk} (assume the signal $s(t)$ is real for simplification):

- Use for the coefficients their exact values: $s_{nk} = \int_{-\infty}^{\infty} s(t) \tilde{\phi}_{nk}(t) dt$. This is only feasible for continuous signals $s(t)$.

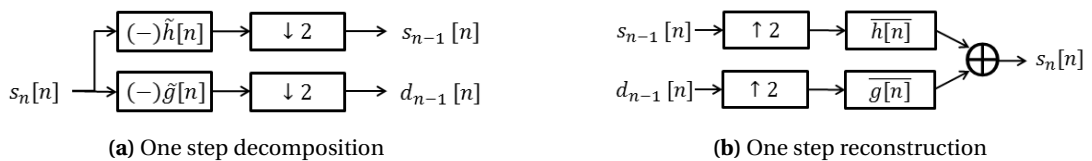


Figure D.5: Filter formulation of the DWT algorithm.

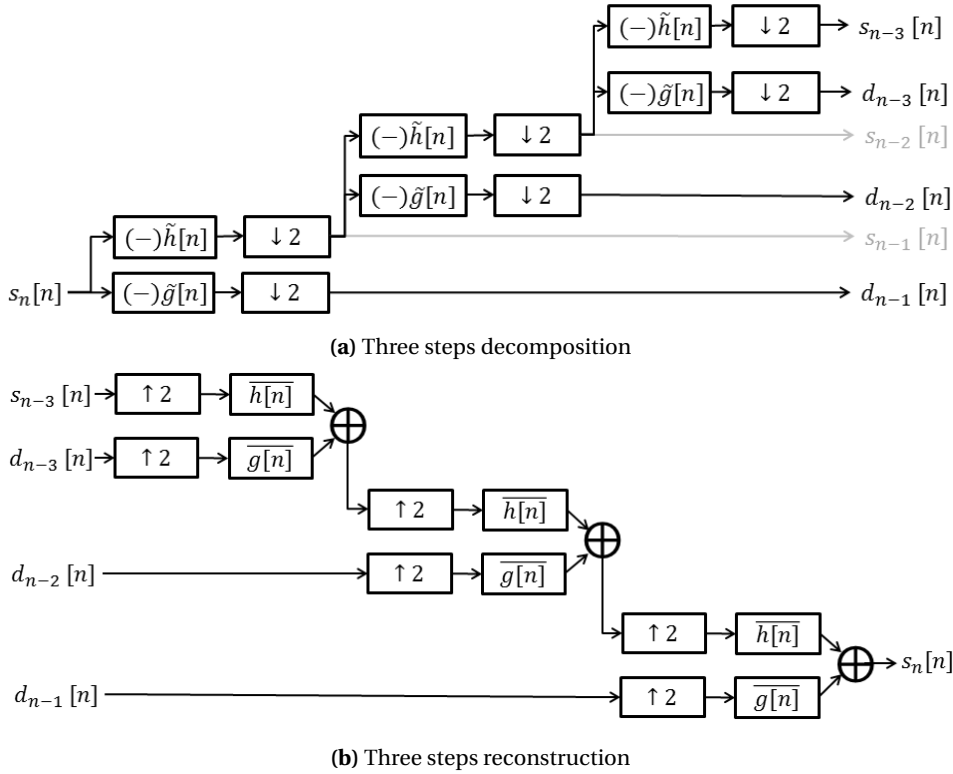


Figure D.6: Filter formulation of the algorithm for a three step algorithm

- For discrete signals, for instance the trapezoidal rule can be used: $s_{nk} \approx 2^{-n/2} \sum_{\ell} s(2^{-n}\ell) \tilde{\phi}(\ell - k) dt$. It is important to note that the point values of $\tilde{\phi}$ at the integer points are known. Higher order quadrature rules can be used too. The trapezoidal rule is one of the many quadrature rules, in general form written as [56]

$$\int_{t_1}^{t_2} f(t) dt \approx \sum_{k=1}^K w_k f(v_k),$$

where K is the number of quadrature points, w_k the weights and v_k the quadrature points in $[t_1, t_2]$. The Gaussian rules are a special type of these quadrature rules, where the integration points and weights are chosen such that the highest order of accuracy is reached for a particular number of integration points v_k .

- Keinert [29] suggests to use $s_{nk} \approx s(2^{-n}k)$. Both Walnut [57] and Keinert [29] refer to the book of Strang and Nguyen [51], where this assumption is called a *wavelet crime*. However Keinert [29] shows that for smooth s (at least two times differentiable) the truncation error is smaller than the coefficients by a factor of order 2^{-n} .

Postprocessing is the above described process in reverse: the conversion from s_{nk} to $s(t)$. There are two main approaches for postprocessing:

- Adding up scaling function expansions in between sampling points to retrieve the continuous signal $s(t)$. Because many scaling functions are not smooth, this might lead to a non continuous reconstruction [29].
- The alternative is finding intermediate points using interpolation.
- Other approaches from papers or books, a start point is given by Keinert [29].

D.11. Boundaries: different approaches

In Section D.8 the infinite approach of the algorithm and the corresponding implementation (D.25) has been discussed. Of course this infinite approach is not implementable, therefore boundaries are introduced to

abbreviate the infinite approach to a finite implementation. As for the infinite length DWT the finite length algorithm will be assumed linear, where the form of \tilde{L}_n is changed to:

$$(\mathbf{s}\mathbf{d})_{n-1} = \tilde{L}_n \mathbf{s}_n, \quad \text{with } \tilde{L}_n = \begin{bmatrix} \tilde{L}_b & & \emptyset \\ & \tilde{L}_i & \\ \emptyset & & \tilde{L}_e \end{bmatrix}. \quad (\text{D.26})$$

Here the subscript b , i and e stand for begin, interior and end. In the begin and end parts of the matrix, the boundaries will be handled. Generally the size of L_b and L_e are small with respect to the size of L_n and they both remain constant at all levels. The interior \tilde{L}_i is a segment of the infinite matrix \tilde{L} from (D.25). This part makes up the most of the matrix, approximately doubling in size when going from n to $n+1$. For the IDWT to exist, the matrix \tilde{L}_n has to be invertible. In the orthogonal case $L_n^{-1} = L_n^*$, for the biorthogonal case the 'inverse' L_n^* has an analogous structure, being

$$L_n^* = \begin{bmatrix} \tilde{L}_b^* & & \emptyset \\ & \tilde{L}_i^* & \\ \emptyset & & \tilde{L}_e^* \end{bmatrix}.$$

There are three main ways to implement boundaries [29]. These boundary methods often do require some preprocessing. The choice for a specific method is data dependent. This will be discussed in the following enumeration. If one has non-periodic, non-symmetric data, and the boundary function approach is too hard, Keinert [29] advises to use linear extension for it is easy to implement and does not introduce artificial jumps in the data. For signals with enough zeros at the begin and end of the signal, the boundary handling is irrelevant.

- **The data extension approach.** This method extends the signal across the boundaries, such that each extended coefficient is a linear combination of known coefficients. The resulting \tilde{L}_n can be singular, though most of the times it is not. The inverse L_n^* might not have the correct form such that reconstruction is possible. In this method several extension methods, known as modes in Matlab and Python:
 - Periodic extension: the signal is assumed to be periodic, so the h - and g -coefficients disappearing on the left side of the matrix appear at the right and vice versa. This extension always works, preserving orthogonality and approximation $\mathcal{O}(h)$. Matlab and Python also know an extension method called periodization [41, 52]. Periodization is virtually the same as periodic extension, however it ensures the smallest length wavelet decomposition. When the data is not truly periodic, the jump at the boundary leads to large d -coefficients [29].
 - Zero extension, also known as zero padding (see ??) is done by truncating the infinite matrix \tilde{L} . The non-existing infinite part of the signal is observed as 0's. This also introduces jumps, as the periodic extension, and this method does not preserve orthogonality or approximation orders [29].
 - Symmetric extension mirrors the data in the endpoints, resulting in the coefficients in \tilde{L} that disappear at the ends, get mirrored back. There are three ways of reflection: whole-sample symmetry, half-sample symmetry and antisymmetric reflection (only useful in the case $s_0 = 0$). If the data extension type matches the type of symmetry of the scaling function, the finite DWT will be equivalent to an infinite DWT [29].
 - Extrapolation does not conserve the orthogonality condition. Constant extrapolation leads to approximation $\mathcal{O}(2^{-n})$, linear approximation (also known as smooth-padding [52]) to order $\mathcal{O}(2^{-2n})$ [29].
- **The matrix completion approach** guarantees $\tilde{L}_n L_n^* = I$, approaching the problem from a linear algebra view. The downside is that this approach generally does not conserve approximation order.
- **The boundary function approach** is the most time-consuming approach, preserving both orthogonality and approximation order. This approach introduces special functions at the boundaries of the interval which, unlike ϕ_0 , do not extend over the border. The decomposition and reconstruction algorithm have to be worked out newly. The hardest part is to derive boundary wavelets which have the same number of vanishing moments as the original [38].

- Instead of assuming the periodicity of the signal, **periodic wavelets** can be used. Wavelets that cross one border of the domain are made periodic [38]. These wavelets create high amplitude wavelet coefficients in the neighborhood of the borders of the domain and do not have vanishing moments. The method is mathematically the same as extending the data periodically [38].

DWT decomposition An example of a DWT decomposition: the signal at the bottom is decomposed four times. Note that the length of the detail coefficient vector is half the length of its predecessor and that the resulting smooth part and the fourth detail coefficients vector have the same length. The coefficients on the right have been translated to their contribution to the signal (left). The sum of the contributions results in the original signal. The error is negligible: in the order of 10^{-15} (see Figure D.7c)

D.12. Formulations

Till now we have seen the so called matrix notation of the DWT. This notation is very convenient for those used to linear algebra. There are two different formulations of the DWT. The first is the *modulation formulation*, which is a way of looking at the DWT from Fourier analysis. This way is not implementable, but this is useful in the creation of new wavelets bases, for instance by using the *lifting* method which will be discussed in ???. The *polyphase formulation* arranges the calculation of the DWT in such a way that convolutions are used without wasting computations. The direct implementation of the DWT in terms of the convolutions throws away the half of the computed values in the downscaling step. This is very regrettable, therefore the polyphase formulation uses convolutions without wasting computations [29].

D.12.1. Modulation formulation

Here we use the symbol formulation. For the discrete sequence $\mathbf{a} = \{a_k\}$ the symbol is defined as $a(\omega) = \sum_k a_k e^{-ik\omega}$. Remember that $c = a * b$, then $c(\omega) = a(\omega)b(\omega)$. Down- and upsampling are also defined for the Fourier domain as

$$\begin{aligned} (\downarrow 2)a(\omega) &= \frac{1}{2} [a(\omega/2) + a(\omega/2 + \pi)], \\ (\uparrow 2)a(\omega) &= a(2\omega). \end{aligned}$$

The full DWT algorithm in terms of the symbols is the modulation formulation. The original signal is $s_n(\omega)$, then the decomposition in s_{n-1} and d_{n-1} becomes

$$\begin{aligned} s_{n-1}(2\omega) &= \frac{1}{\sqrt{2}} [\tilde{h}(\omega)s_n(\omega) + \tilde{h}(\omega + \pi)s_n(\omega + \pi)], \\ d_{n-1}(2\omega) &= \frac{1}{\sqrt{2}} [\tilde{g}(\omega)s_n(\omega) + \tilde{g}(\omega + \pi)s_n(\omega + \pi)]. \end{aligned}$$

In this we recognize the convolution step from (D.24a) and the sampling step from (D.24b). The reconstruction is the same as (D.24c):

$$s_n(\omega) = \sqrt{2}[\overline{\tilde{h}(\omega)}s_{n-1}(2\omega) + \overline{\tilde{g}(\omega)}d_{n-1}(2\omega)].$$

This formulation can also be given in the matrix form. For the decomposition equation as

$$\begin{bmatrix} s_{n-1}(2\omega) \\ d_{n-1}(2\omega) \end{bmatrix} = \tilde{M} \cdot \frac{1}{2\sqrt{2}} \begin{bmatrix} s_n(\omega) \\ s_n(\omega + \pi) \end{bmatrix}, \quad \text{with } M(\omega) = \begin{bmatrix} h(\omega) & h(\omega + \pi) \\ g(\omega) & g(\omega + \pi) \end{bmatrix}. \quad (\text{D.27})$$

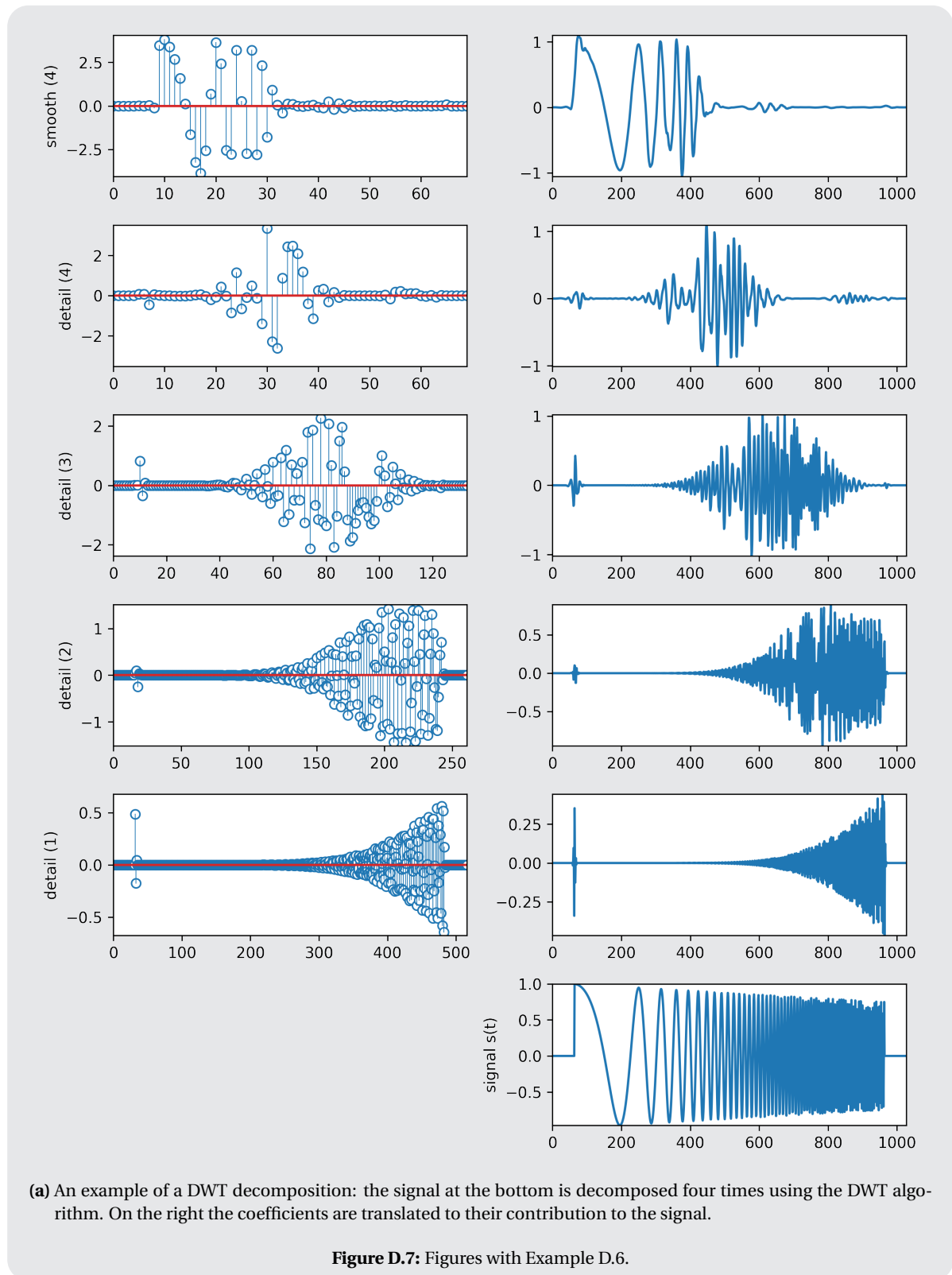
This matrix M is called the *modulation matrix*. For the reconstruction equation a redundant statement has to be added, which is the second row of the matrix formulation:

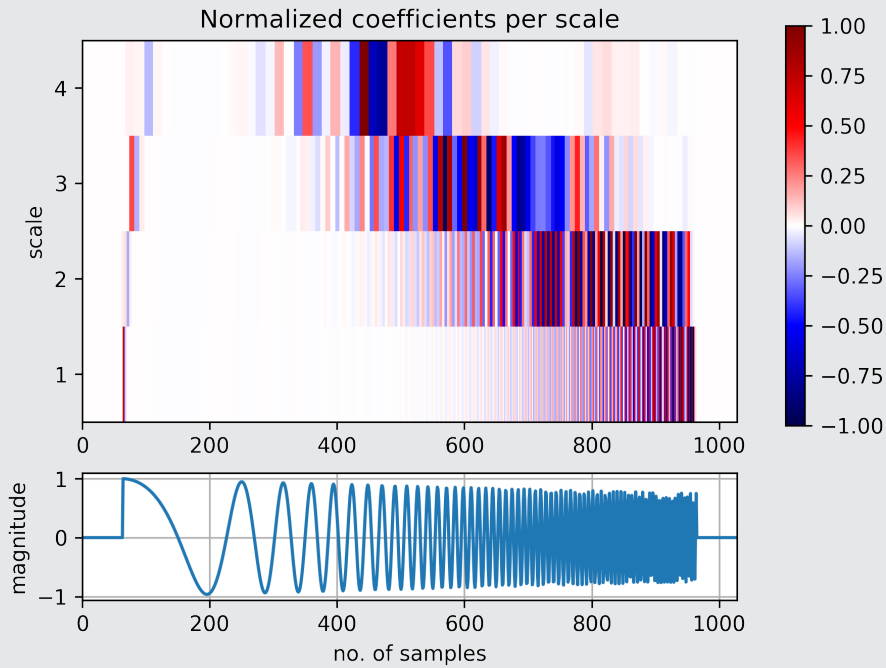
$$\begin{bmatrix} s_n(\omega) \\ s_n(\omega + \pi) \end{bmatrix} = M^* \cdot \sqrt{2} \begin{bmatrix} s_{n-1}(2\omega) \\ d_{n-1}(2\omega) \end{bmatrix}.$$

From these expressions another biorthogonality condition can be derived: $M(\omega)^* \tilde{M}(\omega) = I$. Note again that for the orthogonal MRA case, the tildes can be eliminated. The condition $M(\omega)^* M(\omega) = I$ is then called *paraunitary*.

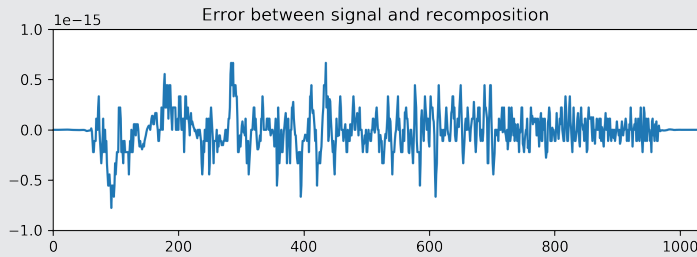
D.12.2. Polyphase formulation

The polyphase formulation begins by splitting the signal and the recursion coefficients into odd and even phases. The notation used for the even and odd phases \mathbf{a}_0 and \mathbf{a}_1 of a sequence $\mathbf{a} = \{a_k\}$ is defined by $a_{0,k} =$





(b) The detail coefficients from (a) depicted differently.



(c) The error between the reconstruction and the original signal from Example D.6, in numerical terms is the error 0.

Figure D.7: Figures with Example D.6.

a_{2k} and $a_{1,k} = a_{2k+1}$. Using this notation, the convolution (D.24a) to find s_{n-1} can be written as [29]

$$s_{n-1} = (-)\tilde{h}_0 * s_{n,0} + (-)\tilde{h}_1 * s_{n,1}.$$

The odd and even phases are computed separately and finally recombined. Note that the number of floating point operations is unchanged from the direct implementation.

The polyphase symbols of the sequence \mathbf{a} are given by

$$a_0(\omega) = \sum_k a_{0,k} e^{-ik\omega} = \sum_k a_{2k} e^{-ik\omega}, \quad a_1(\omega) = \sum_k a_{1,k} e^{-ik\omega} = \sum_k a_{2k+1} e^{-ik\omega}.$$

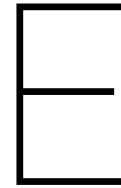
Then the decomposition of the signal \mathbf{s} can be written as

$$\begin{bmatrix} s_{n-1}(\omega) \\ d_{n-1}(\omega) \end{bmatrix} = \tilde{P} \begin{bmatrix} s_{n,0}(\omega) \\ s_{n,1}(\omega) \end{bmatrix} \quad \text{with } P(\omega) = \begin{bmatrix} h_0(\omega) & h_1(\omega) \\ g_0(\omega) & g_1(\omega) \end{bmatrix}.$$

Where $P(\omega)$ is called the *polyphase matrix*. As for the modulation approach, the tildes can be dropped when an orthogonal MRA is used. The reconstruction step then is

$$\begin{bmatrix} s_{n,0}(\omega) \\ s_{n,1}(\omega) \end{bmatrix} = P^* \begin{bmatrix} s_{n-1}(\omega) \\ d_{n-1}(\omega) \end{bmatrix}.$$

The biorthogonality condition in this formulation becomes $P(\omega)^* \tilde{P}(\omega) = I$. For the orthogonal MRA the polyphase matrix is paraunitary, as for the modulation formulation.



Wavelets

E.1. Continuous Wavelets

This appendix contains different continuous wavelets and their known, analytic values.

Name	Wavelet $\psi(t)$	$\mathcal{F}\{\psi(t)\} = \Psi(\omega)$	e -folding time τ_a	Fourier wave-length λ
Complex Morlet [43, 53]	$\pi^{-1/4} e^{-i\omega_0 t} e^{-t^2/2}$	$\pi^{-1/4} H(\omega) e^{-(\omega-\omega_0)^2/2}$	$\sqrt{2}$	$\frac{4\pi}{\omega_0 + \sqrt{2 + \omega_0^2}}$
Morlet [43]	$e^{t^2/2} \cos(5t)$	-	$\sqrt{2}$	-
Paul, order m [53]	$\frac{2^m i^m m!}{\sqrt{\pi(2m)!}} (1 - it)^{-(m+1)}$	$\frac{2^m}{\sqrt{m(2m-1)!}} H(\omega) \omega^m e^{-\omega}$	$1/\sqrt{2}$	$\frac{2\pi}{\sqrt{m+1/2}}$
(Derivative of) Gaussian, order m [53]	$\frac{(-1)^{m+1}}{\sqrt{\Gamma(m+1/2)}} \frac{d^m}{dt^m} (e^{-t^2/2})$	$\frac{-i^m}{\sqrt{\Gamma(m+1/2)}} \omega^m e^{-\omega^2/2}$	$\sqrt{2}$	$\frac{2\pi}{\sqrt{m+1/2}}$
Complex (Derivative of) Gaussian, order m [24]	$C \cdot \frac{d^m}{dt^m} (e^{-i\omega_0 t} e^{-t^2/2})$	-	-	idem
Complex Shannon, order m [44]	$\sqrt{f_b} \left(\text{sinc} \left(\frac{f_b t}{m} \right) \right)^m e^{i\omega_0 t}$	-	-	-
Shannon [43]	$\text{sinc} \left(\frac{t}{2} \right) \cos \left(\frac{3\pi t}{2} \right)$	-	-	-
Meyer [14]	-	see (E.3)	-	-

Table E.1: Continuous wavelets, summarized in Figure ??.

- The **Complex Morlet** wavelet is described as a complex wave $e^{i2\pi\omega_0 t}$ within the Gaussian envelope $e^{-t^2/2}$. The term in front of the expression ensures unit energy. For values of $\omega_0 \gg 0$ this wavelet has the property that it minimizes the error [43]. Often $\omega_0 = 6$ is chosen [53].
- The **Morlet** wavelet is the real part of the complex Morlet wavelet [43]. The example given in Table ?? is used in the Mathworks Toolbox.
- The **(derivative of) Gaussian** wavelet family is a set of wavelets, derived from the derivatives of the Gaussian function, e^{-t^2} . This function can be derived infinitely many times, therefore there are a lot of Gaussian wavelets. The best known is the Mexican Hat wavelet, which is described next. The Mexican

Hat wavelet is an example of a nice wavelet, with compact support and mean value zero [43]. Not all derivatives lead to wavelet with these nice characteristics. For a n -times differentiated Gaussian, the number of vanishing moments is n too. Moreover, if n is even the wavelet is symmetric, for odd n it is anti symmetric.

- The **Mexican hat** wavelet is probably the best known continuous wavelet. It is defined by [43]:

$$\psi_{\text{mexh}}(t) = K(1 - t^2)e^{-(t^2/2)}, \quad K = \frac{2}{\sqrt{3\pi}^{1/4}}. \quad (\text{E.1})$$

The factor K normalizes the Mexican hat wavelet. If $K = 1$ the wavelet is known as the unnormalized Mexican hat [43]. The wavelet is named after its shape, however it is originally known as the **Ricker** wavelet.

- The **complex (derivative of) Gaussian** wavelet family, also known as the **Hermitian** or **Gabor** wavelet family, has the same properties as the Gaussian wavelet family, the only difference is that this is a complex wavelet. It is made complex by multiplying the Gaussian window with a complex exponential function $e^{-i\omega_0 t}$. The C in the formula from Table ?? is the normalizing term.
- The **complex Shannon** wavelet is defined by a set of complex waveform within a sinc() function envelope [44], where

$$\text{sinc}(t) = \frac{\sin(\pi t)}{\pi t}. \quad (\text{E.2})$$

It has integer order m , a bandwidth parameter f_b controlling the width of the main lobe of the sinc() function and wavelet centre frequency ω_0 . The centre frequency also determines the number of oscillations within the main lobe. The imaginary part of the complex Shannon wavelet is shifted $\pi/4$ from the real part. This wavelet has *infinite* support and is therefore not much used.

- The **Shannon** wavelet as defined in Table ?? is *real* and *symmetric* but does not have a finite support [43], however it is infinitely differentiable and $\Psi(\omega)$ is zero in the neighbourhood of $\omega = 0$, as are all its derivatives [38]. We may conclude that it has infinitely many vanishing moments. It is therefore not a good wavelet to apply wavelet analysis with [43]. The Shannon wavelet is a specific case of the spline wavelets [38].

The Morlet, Gaussian and Shannon wavelets are also known as crude wavelets [TB]. These wavelets only have minimal properties. Their downsides are that their scaling functions $\phi(t)$ do not exist, the analysis is not orthogonal or biorthogonal and $\psi(t)$ is not of compact support. Therefore reconstruction is not insured and there are no fast algorithms to do calculations with. These wavelets are only useful for a (complex) continuous decomposition. Good properties are the symmetry and explicit declaration of the wavelet $\psi(t)$ [TB]. Complex wavelets can have a spectrum for which $\Psi(\omega)|_{\omega < 0} = 0$, such that a wavelet transform for only positive frequencies is possible.

- The **Meyer** wavelet is a *symmetric* and *orthogonal* wavelet invented by Meyer in 1990 [15]. It is a *band-limited* wavelet, limited to $2\pi/3 \leq |\omega| \leq 8\pi/3$, which results in an *infinite support* in the time domain [43]. Its amplitude in time decays rapidly, making it suitable for wavelet analysis. The Meyer scaling function satisfies [15]

$$\Psi(\omega) = \begin{cases} \frac{1}{\sqrt{2\pi}} e^{i\omega/2} \sin \left[\frac{\pi}{2} v \left(\frac{3}{2\pi} |\omega| - 1 \right) \right] & \text{for } \frac{2\pi}{3} \leq |\omega| \leq \frac{4\pi}{3}, \\ \frac{1}{\sqrt{2\pi}} e^{i\omega/2} \cos \left[\frac{\pi}{2} v \left(\frac{3}{4\pi} |\omega| - 1 \right) \right] & \text{for } \frac{4\pi}{3} \leq |\omega| \leq \frac{8\pi}{3}, \\ 0 & \text{elsewhere.} \end{cases} \quad (\text{E.3})$$

where

$$v(x) = \begin{cases} 0 & x \leq 0, \\ \sin^2 \left(\frac{\pi}{2} x \right) & 0 \leq x \leq 1, \\ 1 & x \geq 1. \end{cases}$$

The Meyer wavelet has infinite vanishing moments [38]. The Meyer wavelet is known as an infinitely regular wavelet. It can be applied in both continuous and discrete wavelet analysis. Its filter implementation however is not a FIR filter. The analysis of the pair ψ_{Meyer} and ϕ_{Meyer} is orthogonal. Both functions are infinitely differentiable and have compact support. The symmetry and infinite regularity are its most important properties. The difficulty of this wavelet lies within the filter implementation: there is no fast algorithm available for the filter is of infinite impulse response.

- The **Discrete Meyer** wavelet is the finite filter approximation of the Meyer wavelet [58]. It remains *orthogonal* and *symmetric*. By the truncation it is the FIR implementation of the Meyer wavelet. Technically this thus is a *discrete* wavelet.

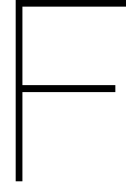
E.1.1. Example: Morlet wavelet

hier graag figuur morlet wavelet met

E.2. Discrete Wavelets

Wavelet family	Filter length	Orth.	Biorth.	Sym.	Extra information
Haar	2	Yes	No	No	Same as Daubechies 1 wavelet Discontinuous: little number of applications
Daubechies x	$2x$	Yes	Yes	No	$x \geq 1$
Symmlet x	$2x$	Yes	Yes	Near	$x \geq 2$ Derived from Daubechies wavelet to be near symmetric
Coiflet x	$6x$	Yes	Yes	Near	$x \geq 1$ Derived from Daubechies wavelet, scaling functions have vanishing moments
Bi orthogonal	≥ 6	No	Yes	Yes	Also known as Spline wavelet. Exception: bi orthogonal 1.1 wavelet is the Haar wavelet.
Reverse bi orthogonal	≥ 6	No	Yes	Yes	Dual set of the bi orthogonal wavelets
Discrete Meyer	62	Yes	Yes	Yes	FIR approximation of Meyer wavelet

Table E.2: An overview of the FWT applicable wavelets available in the PyWavelets package [52]. x is the number of vanishing moments, if specified.



Separation of incident and reflected waves

F.1. Wavenumber

Korte samenvatting hoe het golfgetal in elkaar zit [25].

$$\text{hier alles invoeren aub} \tag{F.1}$$

F.2. Derivation for 2 gauges

Assume there are two gauges in the channel, one on a distance of x_1 from the wave maker and the second one at a distance $x_2 > x_1$. Define $x_2 - x_1 = \Delta x$. The situation is depicted in Figure 3.6. The surface elevation as recorded at point x_1 then will be:

$$\eta_1(x_1, t) = a_I \cos(\omega t - kx_1 + \theta_I) + a_R \cos(\omega t + kx_1 + \theta_R) \tag{F.2a}$$

and so at x_2 we find the following expression:

$$\begin{aligned} \eta_2(x_2, t) &= \eta_1(x_2, t) = a_I \cos(\omega t - kx_2 + \theta_I) + a_R \cos(\omega t + kx_2 + \theta_R) \\ &= a_I \cos(\omega t - kx_1 - k\Delta x + \theta_I) + a_R \cos(\omega t + kx_1 + k\Delta x + \theta_R). \end{aligned} \tag{F.2b}$$

Reconstructing the incident and reflected waves through these equations directly is hard, therefore their analytic forms are being used:

$$\zeta_1(x_1, t) = a_I e^{i(\omega t - kx_1 + \theta_I)} + a_R e^{i(\omega t + kx_1 + \theta_R)} \text{ and} \tag{F.3a}$$

$$\begin{aligned} \zeta_2(x_2, t) &= a_I e^{i(\omega t - kx_1 - k\Delta x + \theta_I)} + a_R e^{i(\omega t + kx_2 + k\Delta x + \theta_R)} \\ &= a_I e^{i(\omega t - kx_1 + \theta_I)} e^{-ik\Delta x} + a_R e^{i(\omega t + kx_2 + \theta_R)} e^{ik\Delta x}. \end{aligned} \tag{F.3b}$$

Note that the real part of ζ_1 is η_1 and the same holds for ζ_2 and η_2 . In general the wave number k and the distance between the two gauges, Δx , is known. Using the exponential form of the sine function,

$$\sin(x) = \frac{e^{ix} - e^{-ix}}{2i}, \tag{F.4}$$

the analytic form of the incident and reflected waves at point x_1 can be obtained as follows.

$$\begin{aligned} \zeta_1(x_1, t) e^{ik\Delta x} - \zeta_2(x_1, t) &= a_I e^{i(\omega t - kx_1 + \theta_I)} e^{ik\Delta x} + a_R e^{i(\omega t + kx_1 + \theta_R)} e^{ik\Delta x} \\ &\quad - a_I e^{i(\omega t - kx_1 + \theta_I)} e^{-ik\Delta x} - a_R e^{i(\omega t + kx_2 + \theta_R)} e^{ik\Delta x} \\ &= a_I e^{i(\omega t - kx_1 + \theta_I)} e^{ik\Delta x} - a_I e^{i(\omega t - kx_1 + \theta_I)} e^{-ik\Delta x} \\ &= a_I e^{i(\omega t - kx_1 + \theta_I)} \left(e^{ik\Delta x} - e^{-ik\Delta x} \right) \end{aligned}$$

Divide this result by $2i \cdot \sin(ik\Delta x)$ to find:

$$a_I e^{i(\omega t - kx_1 + \theta_I)} = \frac{\zeta_1(x_1, t) e^{ik\Delta x} - \zeta_2(x_1, t)}{2i \sin(k\Delta x)}. \tag{F.5a}$$

In the same manner the analytic expression of the reflected wave is found as:

$$a_R e^{i(\omega t + kx_1 + \theta_R)} = \frac{\zeta_1(x_1, t) e^{-ik\Delta x} - \zeta_2(x_1, t)}{-2i \sin(k\Delta x)}. \quad (\text{E5b})$$

The real parts of the solutions will result in the incident and reflected wave.

Instead of the analytic expression given in (E.3), continuous wavelet coefficients at scale a are used, i.e.

$$\zeta_{a,1}(x_1, t) = \mathcal{W}\{\eta_1(x_1, t)\}(a, t), \quad \zeta_{a,2}(x_2, t) = \mathcal{W}\{\eta_2(x_2, t)\}(a, t).$$

The wavelet transform using complex wavelets results in a set of complex coefficients $W(a, t)$. These coefficients contain the the amplitude and the phase shift of the transformed signal: $W = |W|e^{i \arg(W)}$. This characteristic makes the wavelet coefficient a suitable candidate for the analytic expression. So, instead of using the analytical expressions of the waves in (E.5), the wavelet coefficients are used. When these two equations are solved, the coefficients of respectively the incident and reflected wavelet transformed waves are recovered. The time series of the incident and reflected waves can then be reconstructed through the reconstruction equation (??). Ma et al. [35] use numerical examples, simulations with large numbers of waves in stationary and non-stationary situations, to show that the method is independent of $\Delta x/L$. They find a reflection coefficient error of 3.3%. This case has been verified and can be found in .

E.3. Reading the results

$$|Z^I + Z^R + Z^N - (\widetilde{Z}^I + \widetilde{Z}^R)|_{\text{watdenk jevanhoed jevoordereconstructies?}} \quad (\text{E6})$$

F.4. Results

Signal	90 waves from JONSWAP spectrum with f in [0.3,2]		
Wavelet	Morlet	Parameter	6
Sampling freq	25	Duration	480.0 sec = 8.0 min
Determined at gauge	11.0		
Using gauges	[11. 12.]		
with distances	[0. 1.]		
Wavenumber	dispersion	with water depth	-1
Noise	no	Weights	no
No of steps CWT	200		
p_min	8.000667E-02	p_max	4E+00
Error CWT reconstruction and original			1.062284E-02
Error CWT reconstruction and sum			4.540368E-17
Error CWT reconstruction incident and original incident			1.407499E-02
Error CWT reconstruction reflected and original reflected			1.105085E-02

	Original	Wavelet filtering	% difference
Reflection coeff	4.989225E-01	5.085815E-01	1.93595454481
m0_incident	5.672494E-03	7.398267E-03	30.4235262141
m0_reflected	1.412018E-03	1.913599E-03	35.5222882748

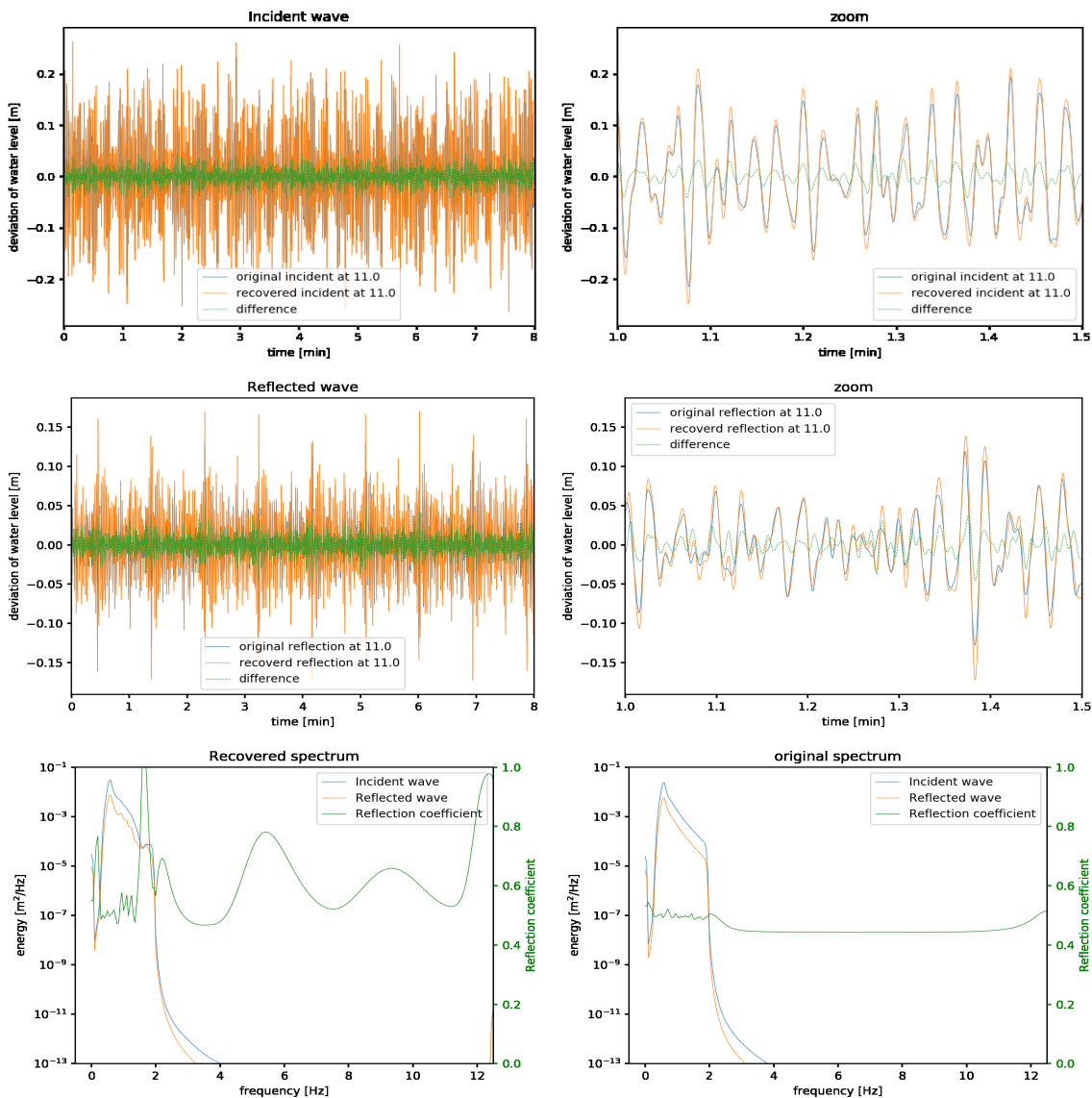


Figure F.1: Verification of error study by Ma et al. [35]. Water depth: 1 meter shallow water.

Signal	200 waves from JONSWAP spectrum with f in $[0.01, fs/2]$				
Wavelet	Morlet	Parameter	60.0		
Sampling freq	12	Duration	480.0 sec = 8.0 min		
Determined at gauge					
Using gauges			39.382		
Wavenumber	dispersion	with water depth	[39.382 40.1]		
Noise	no	Weights	no		
No of steps CWT			200		
Determinant limit			0		
p_min	1.666956E-01	p_max	1.777215E+01		
RMSE reconstruction	Fourier	Wavelet			
sum	1.714063E-16	1.03757E-03			
incident	2.02122E-14	3.626032E-16			
reflected	1.282526E-01	1.398801E-02			
		1.397111E-02			
Ref.cff.	Original	Fourier	% diff	Wavelet	% diff
m0_in	5.013296E-01	8.994054E-01	79.4	5.272067E-01	5.16
m0_ref	5.5754E-03	2.209132E-02	296.23	5.878451E-03	5.44
	1.401273E-03	1.787033E-02	1175.29	1.633897E-03	16.6

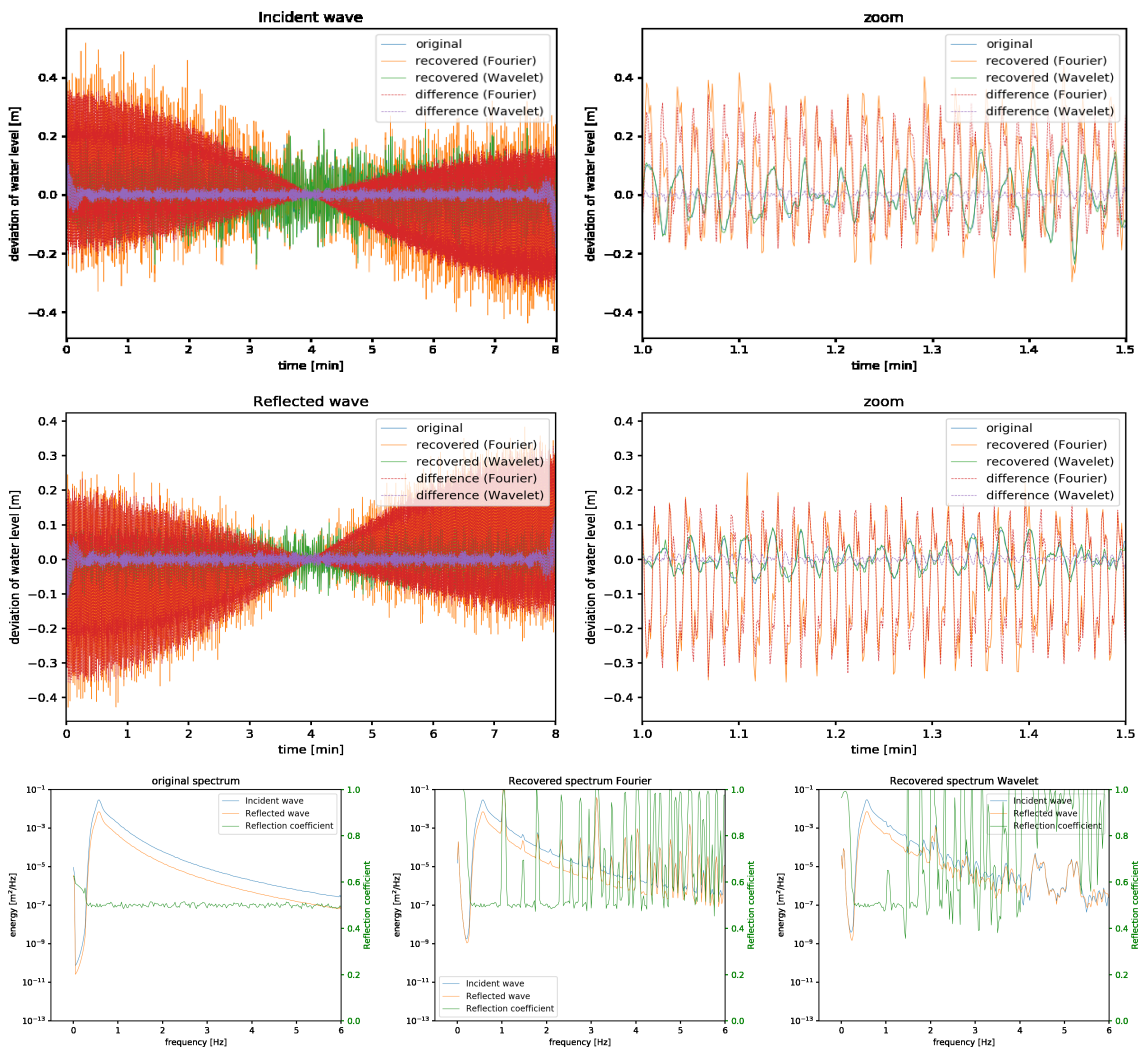


Figure E.2: Separating waves using 2 gauges

Signal	200 waves from JONSWAP spectrum with f in $[0.01, f_s/2]$				
Wavelet	Morlet	Parameter	60.0		
Sampling freq	12	Duration	480.0 sec = 8.0 min		
Determined at gauge	39.382				
Using gauges	[39.382 40.1]				
Wavenumber	equal	with water depth	1		
Noise	no	Weights	no		
No of steps CWT	200				
Determinant limit	0.0				
p_{min}	1.666956E-01	p_{max}	1.777215E+01		
RMSE reconstruction sum	Fourier	Wavelet			
incident	1.945462E-16	1.156294E-03			
reflected	2.731964E-17	6.464717E-17			
	3.507527E-02	1.398079E-03			
	3.507528E-02	1.211011E-03			
Ref.cff.	Original	Fourier	% diff	Wavelet	% diff
$m0_{in}$	5.017083E-01	1E+00	99.32	5.016081E-01	-0.02
$m0_{ref}$	5.599747E-03	2.274359E-03	-59.38	5.725979E-03	2.25
	1.409519E-03	2.274359E-03	61.36	1.440717E-03	2.21

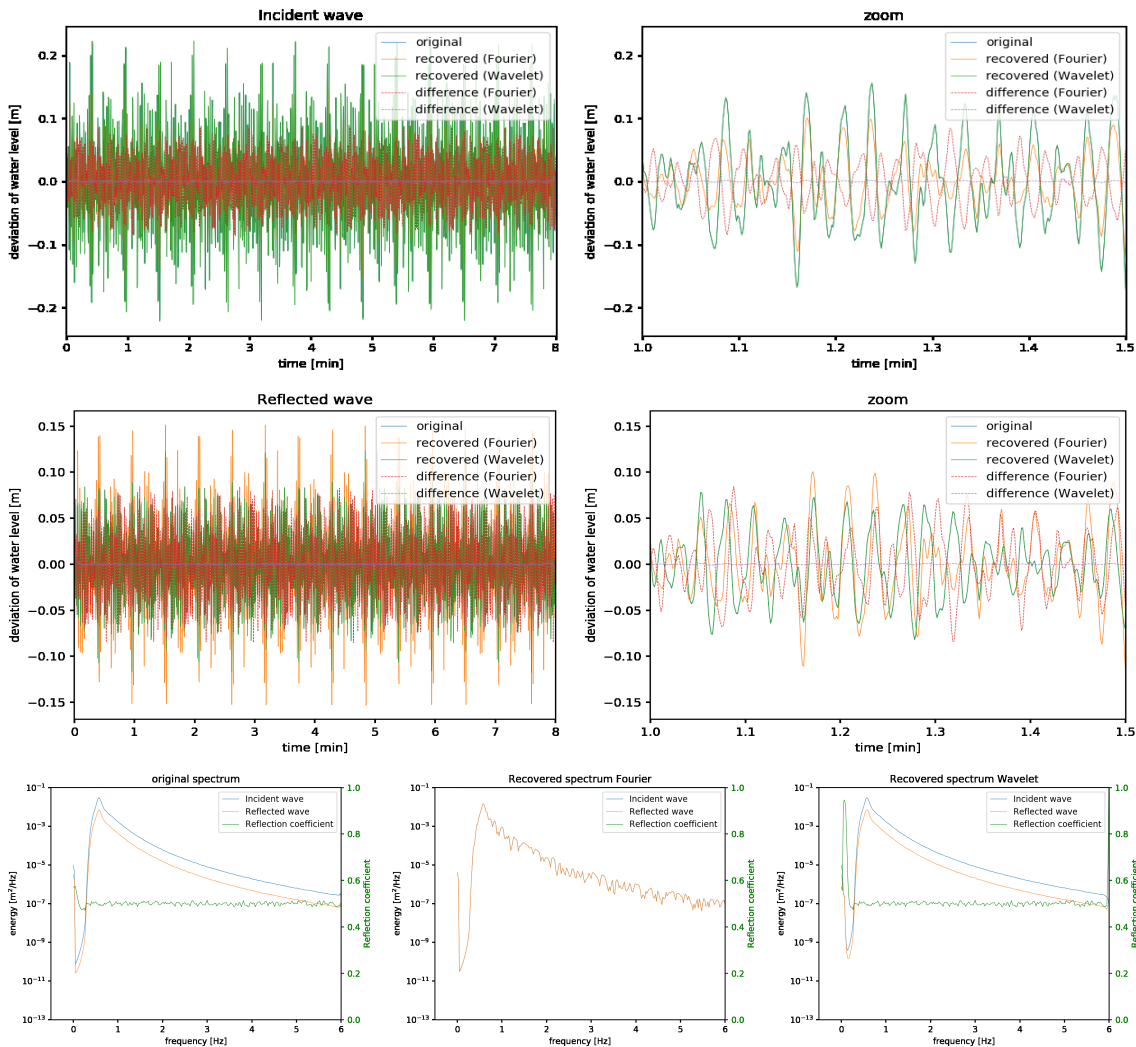


Figure E.3: Separating waves using 2 gauges, using an equal wave number for all frequencies. The Fourier algorithm was disabled in this example.

Signal	200 waves from JONSWAP spectrum with f in $[0.01, fs/2]$				
Wavelet	Morlet	Parameter	60.0		
Sampling freq	12	Duration	480.0 sec = 8.0 min		
Determined at gauge			39.382		
Using gauges			[39.382 39.83 40.1]		
Wavenumber	dispersion	with water depth	1		
Noise	no	Weights	no		
No of steps CWT			200		
Determinant limit			0		
p_min	1.666956E-01	p_max	1.777215E+01		
RMSE	Fourier	Wavelet			
reconstruction	1.793458E-16	1.045626E-03			
sum	1.579025E-03	1.701242E-03			
incident	1.585319E-02	3.387655E-03			
reflected	1.572349E-02	2.58678E-03			
Ref.cff.	Original	Fourier	% diff	Wavelet	% diff
m0_in	5.029976E-01	5.335495E-01	6.07	5.039578E-01	0.19
m0_ref	5.598901E-03	5.844593E-03	4.39	5.716851E-03	2.11
	1.416559E-03	1.66381E-03	17.45	1.451928E-03	2.5

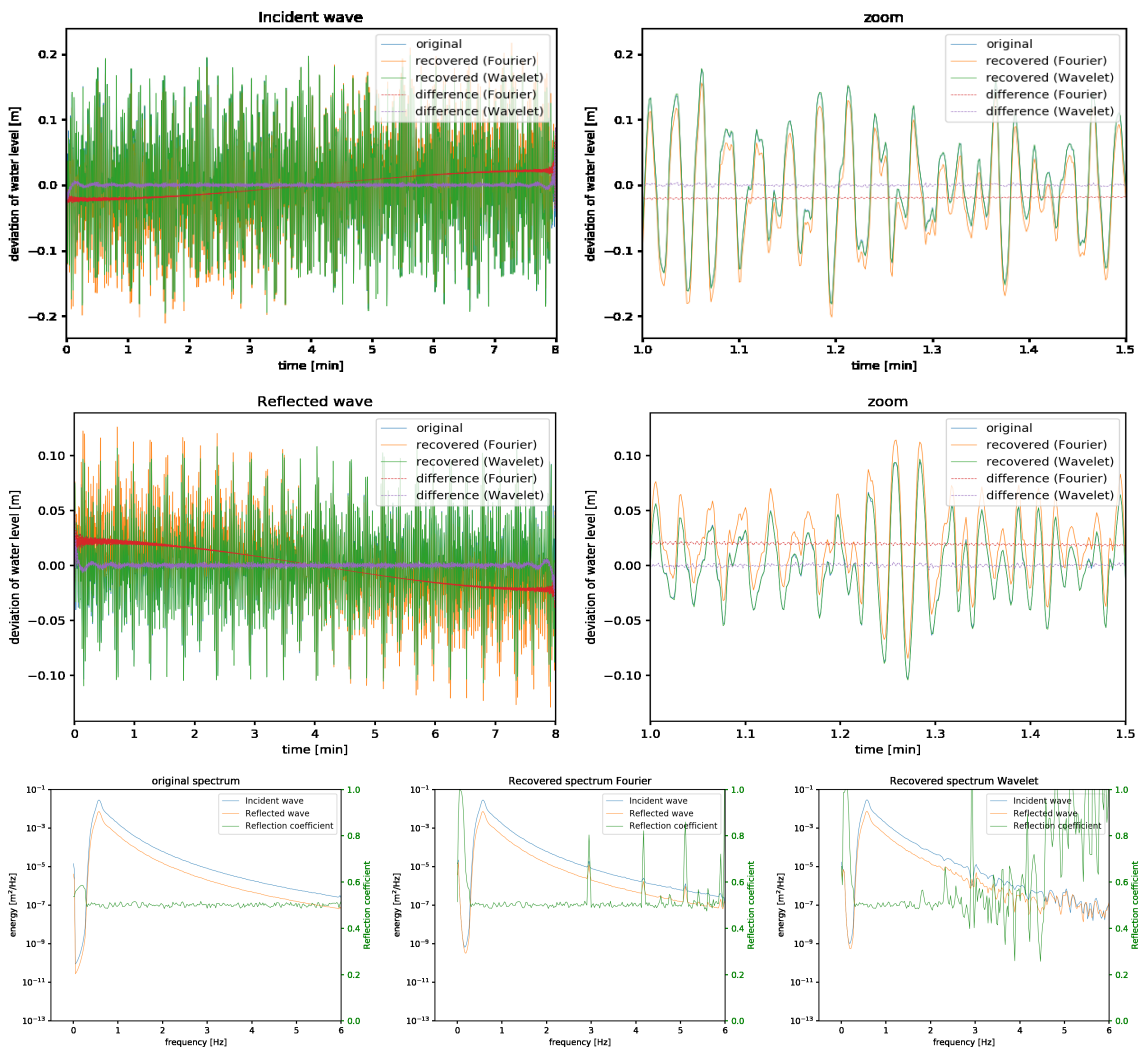


Figure E.4: Separating waves using 3 gauges

Signal	200 waves from JONSWAP spectrum with f in [0.01,fs/2]				
Wavelet	Morlet	Parameter	60.0		
Sampling freq	12	Duration	480.0 sec = 8.0 min		
Determined at gauge			35.742		
Using gauges			[35.742	38.726	39.382 39.83 40.0
Wavenumber	dispersion	with water depth	1		
Noise	no	Weights	no		
No of steps CWT			200		
Determinant limit			0		
p_min	1.666956E-01	p_max	1.777215E+01		
RMSE reconstruction	Fourier	Wavelet			
sum incident	1.513282E-16	9.131862E-04			
reflected	4.853375E-03	7.743863E-03			
	7.782599E-03	9.207705E-03			
	6.376457E-03	5.471597E-03			
Ref.cff.	Original	Fourier	% diff	Wavelet	% diff
m0_in	5.024461E-01	5.051175E-01	0.53	5.006965E-01	-0.35
m0_ref	5.612317E-03	5.646311E-03	0.61	5.364472E-03	-4.42
	1.416841E-03	1.440621E-03	1.68	1.344857E-03	-5.08

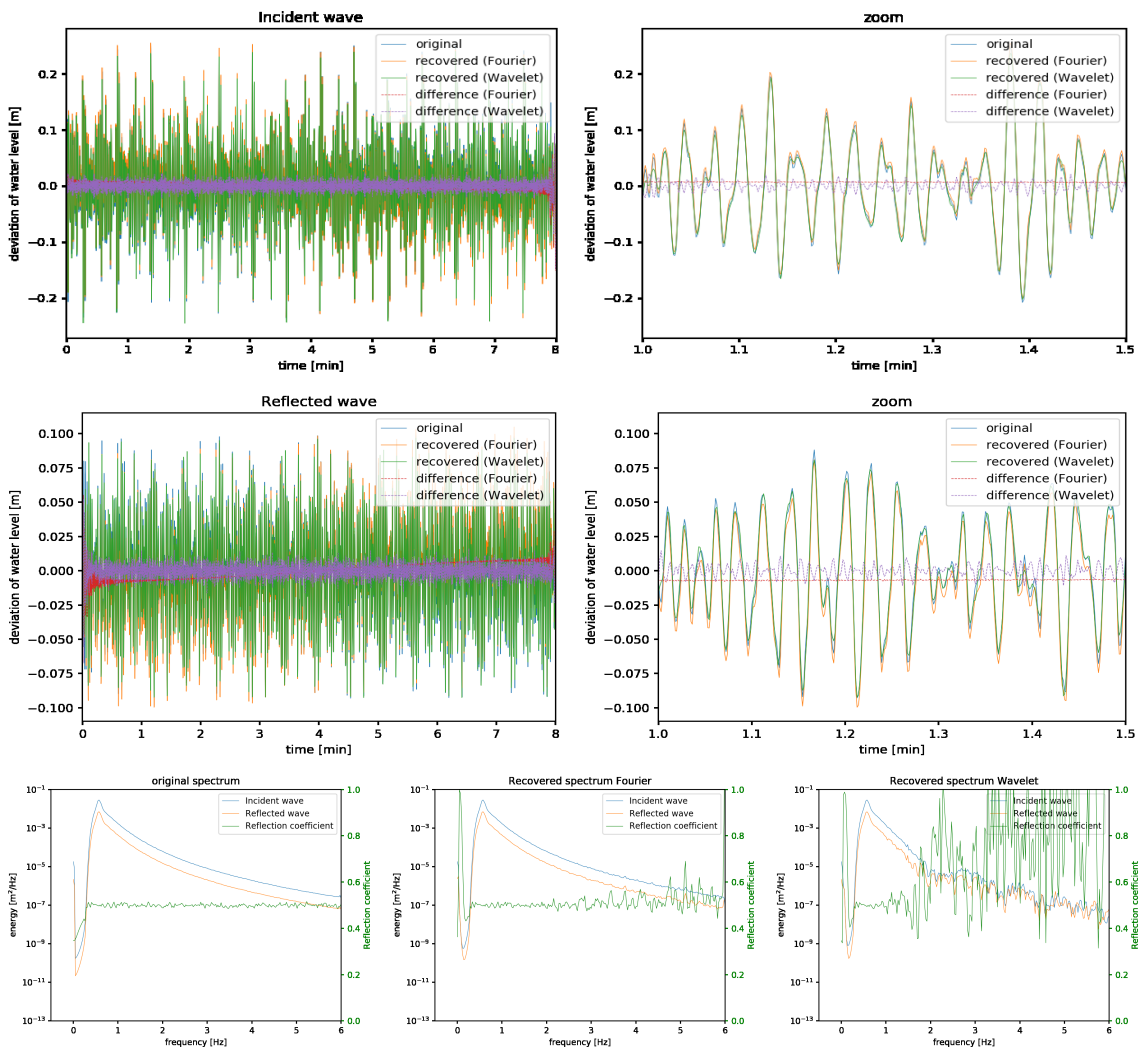


Figure E.5: Separating waves using 5 gauges

Signal	200 waves from JONSWAP spectrum with f in $[0.01, fs/2]$				
Wavelet	Morlet	Parameter	60.0		
Sampling freq	12	Duration	480.0 sec = 8.0 min		
Determined at gauge			39.382	[39.382 40.1]	
Using gauges					
Wavenumber	dispersion	with water depth	1		
Noise	no	Weights	no		
No of steps CWT			200		
Determinant limit			0.1		
p_min	1.666956E-01	p_max	1.777215E+01		
RMSE	Fourier	Wavelet			
reconstruction	1.714063E-16	1.03757E-03			
sum	1.396335E-02	1.158056E-02			
incident	1.234553E-02	1.150164E-02			
reflected	7.85703E-03	7.384558E-03			
Ref.cff.	Original	Fourier	% diff	Wavelet	% diff
m0_in	5.013296E-01	5.064333E-01	1.02	5.065781E-01	1.05
m0_ref	5.5754E-03	5.457513E-03	-2.11	5.554474E-03	-0.38
	1.401273E-03	1.399714E-03	-0.11	1.425397E-03	1.72

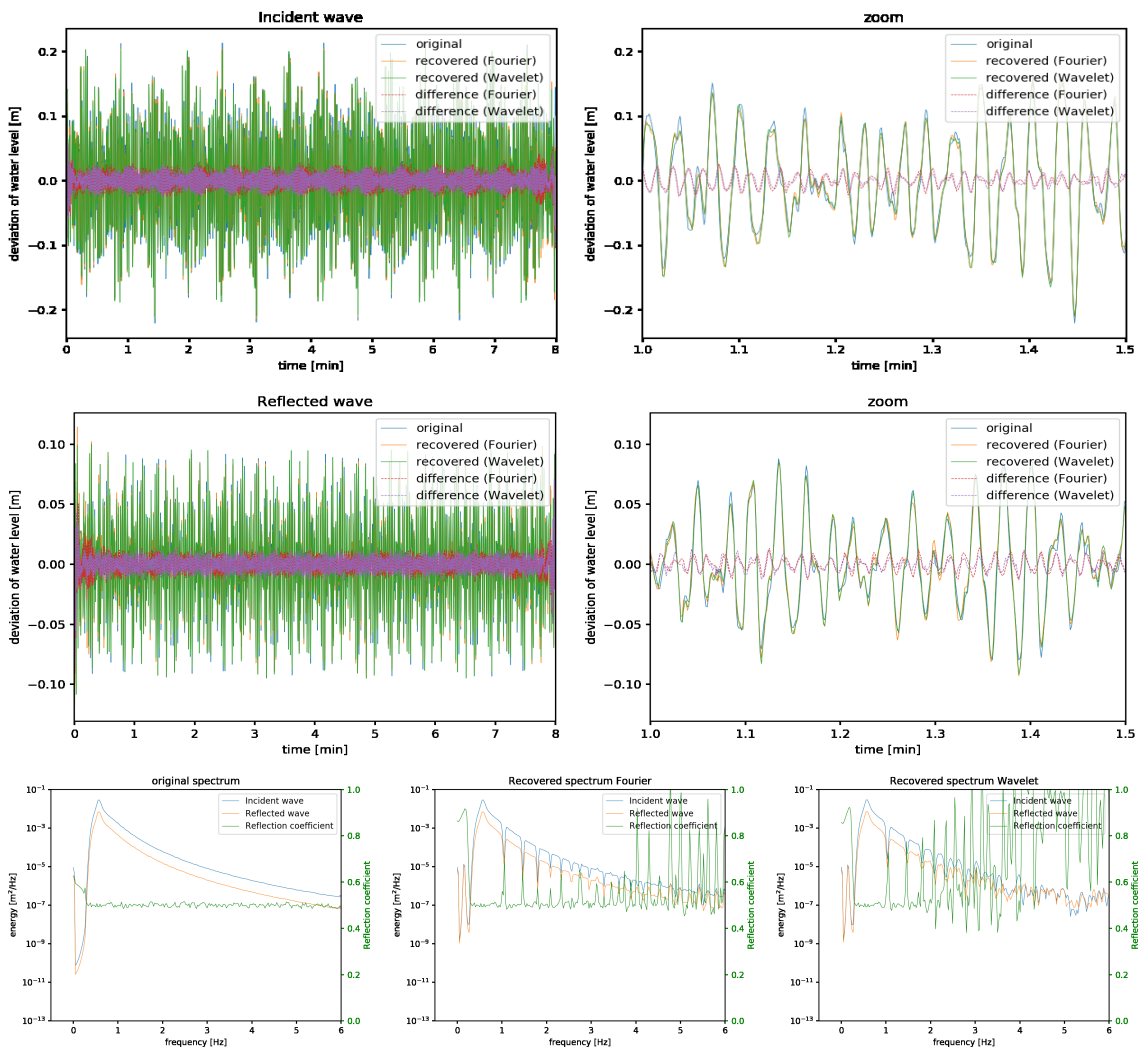


Figure E6: Separating waves using 2 gauges, a determinant limiter of 0.1 has been added.

Signal	200 waves from JONSWAP spectrum with f in [0.01,fs/2]				
Wavelet	Morlet	Parameter	6.0		
Sampling freq	12	Duration	480.0 sec = 8.0 min		
Determined at gauge			39.382		
Using gauges			[39.382 40.1]		
Wavenumber	dispersion	with water depth	1		
Noise	no	Weights	no		
No of steps CWT			200		
Determinant limit			0		
p_min	1.666956E-01	p_max	1.753438E+02		
RMSE reconstruction	Fourier	Wavelet			
sum	1.754694E-16	8.094903E-03			
incident	4.151245E-14	2.427245E-15			
reflected	1.864212E-01	9.062197E-02			
	1.864213E-01	9.219416E-02			
Ref.cff.	Original	Fourier	% diff	Wavelet	% diff
m0_in	5.039467E-01	9.472165E-01	87.96	9.468592E-01	87.89
m0_ref	5.55159E-03	4.028092E-02	625.57	9.806519E-03	76.64
	1.409894E-03	3.614081E-02	2463.37	8.791959E-03	523.59

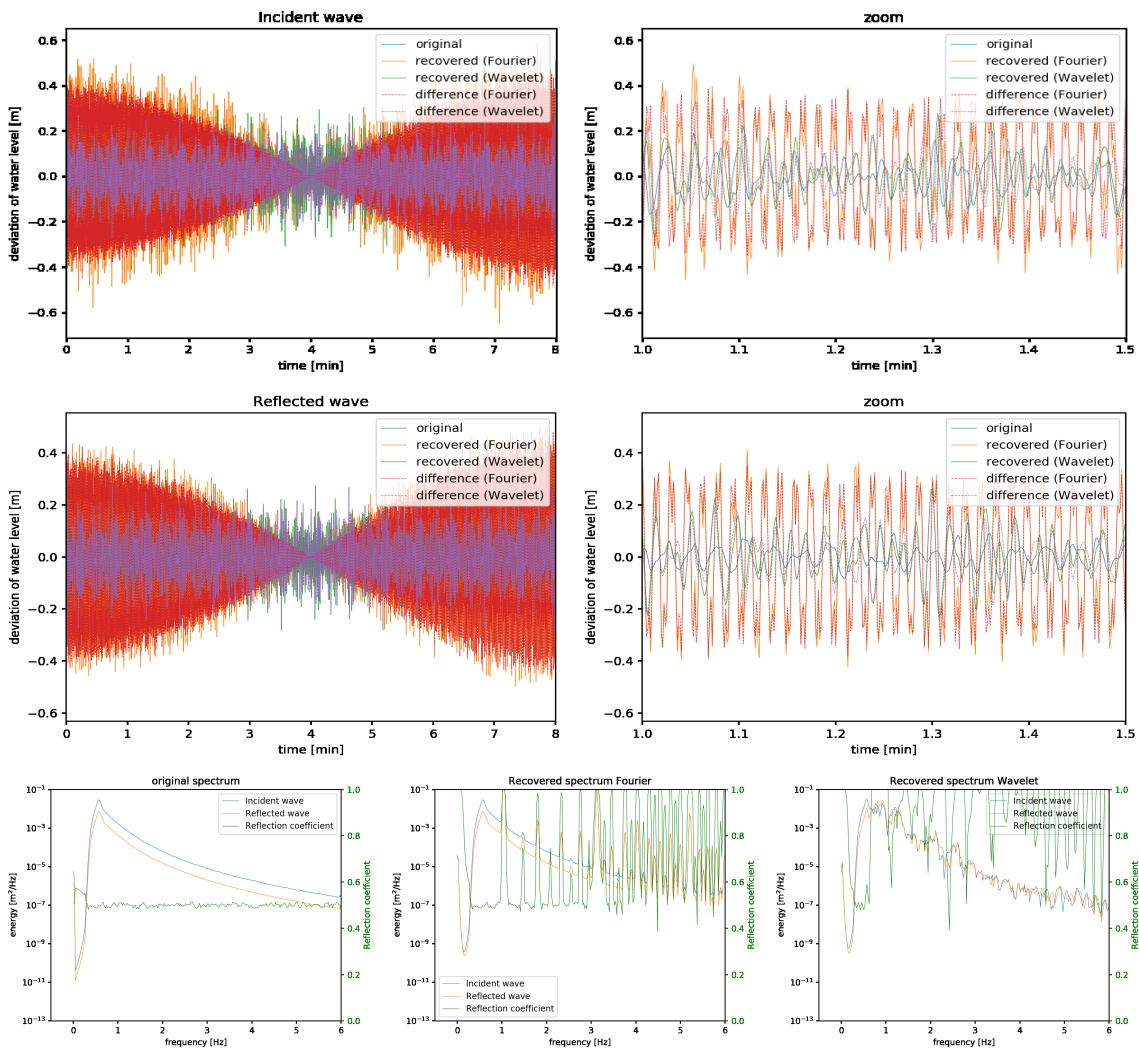


Figure E7: Separating waves using 2 gauges, the Morlet 6 wavelet is used.

Signal	200 waves from JONSWAP spectrum with f in [0.01,fs/2]				
Wavelet	Morlet	Parameter	6.0		
Sampling freq	12	Duration	480.0 sec = 8.0 min		
Determined at gauge			35.742	38.726	39.382
Using gauges			[35.742	38.726	39.382
Wavenumber	dispersion	with water depth	1	39.83	40.0
Noise	no	Weights	no		
No of steps CWT			200		
Determinant limit			0		
p_min	1.666956E-01	p_max	1.753438E+02		
RMSE reconstruction	Fourier	Wavelet			
sum	1.49919E-16	7.131343E-03			
incident	6.033238E-03	4.20067E-02			
reflected	8.564489E-03	4.358948E-02			
	5.884976E-03	2.517018E-02			
Ref.cff.	Original	Fourier	% diff	Wavelet	% diff
m0_in	4.997987E-01	5.058063E-01	1.2	5.687812E-01	13.8
m0_ref	5.631724E-03	5.615814E-03	-0.28	1.328323E-03	-76.41
	1.406798E-03	1.43675E-03	2.13	4.297284E-04	-69.45

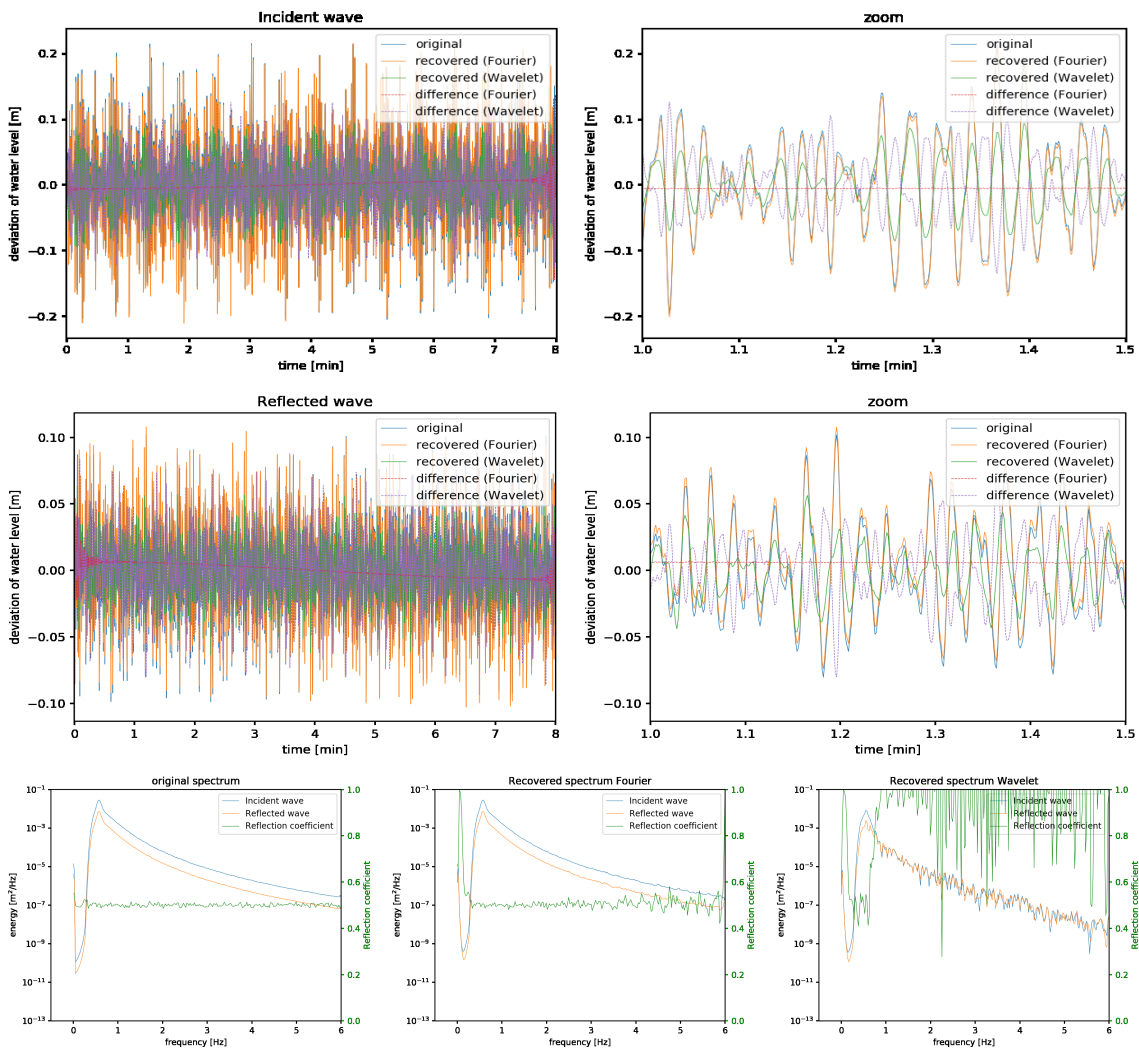


Figure F.8: Separating waves using 2 gauges, the Morlet 6 wavelet is used.

Signal	200 waves from JONSWAP spectrum with f in [0.01,fs/2]				
Wavelet	Morlet	Parameter	6.0		
Sampling freq	12	Duration	480.0 sec = 8.0 min		
Determined at gauge	39.382				
Using gauges	[39.382 40.1]				
Wavenumber	equal	with water depth	1		
Noise	no	Weights	no		
No of steps CWT	200				
Determinant limit	0.0				
p_min	1.666956E-01	p_max	1.753438E+02		
RMSE reconstruction sum	Fourier	Wavelet			
incident	1.690193E-16	7.587509E-03			
reflected	2.633091E-17	7.19489E-17			
	4.182334E-02	7.042717E-03			
	4.182334E-02	3.89677E-03			
Ref.cff.	Original	Fourier	% diff	Wavelet	% diff
m0_in	4.967628E-01	1E+00	101.3	4.966376E-01	-0.03
m0_ref	5.678219E-03	1.790534E-03	-68.47	6.737207E-03	18.65
	1.401233E-03	1.790534E-03	27.78	1.661724E-03	18.59

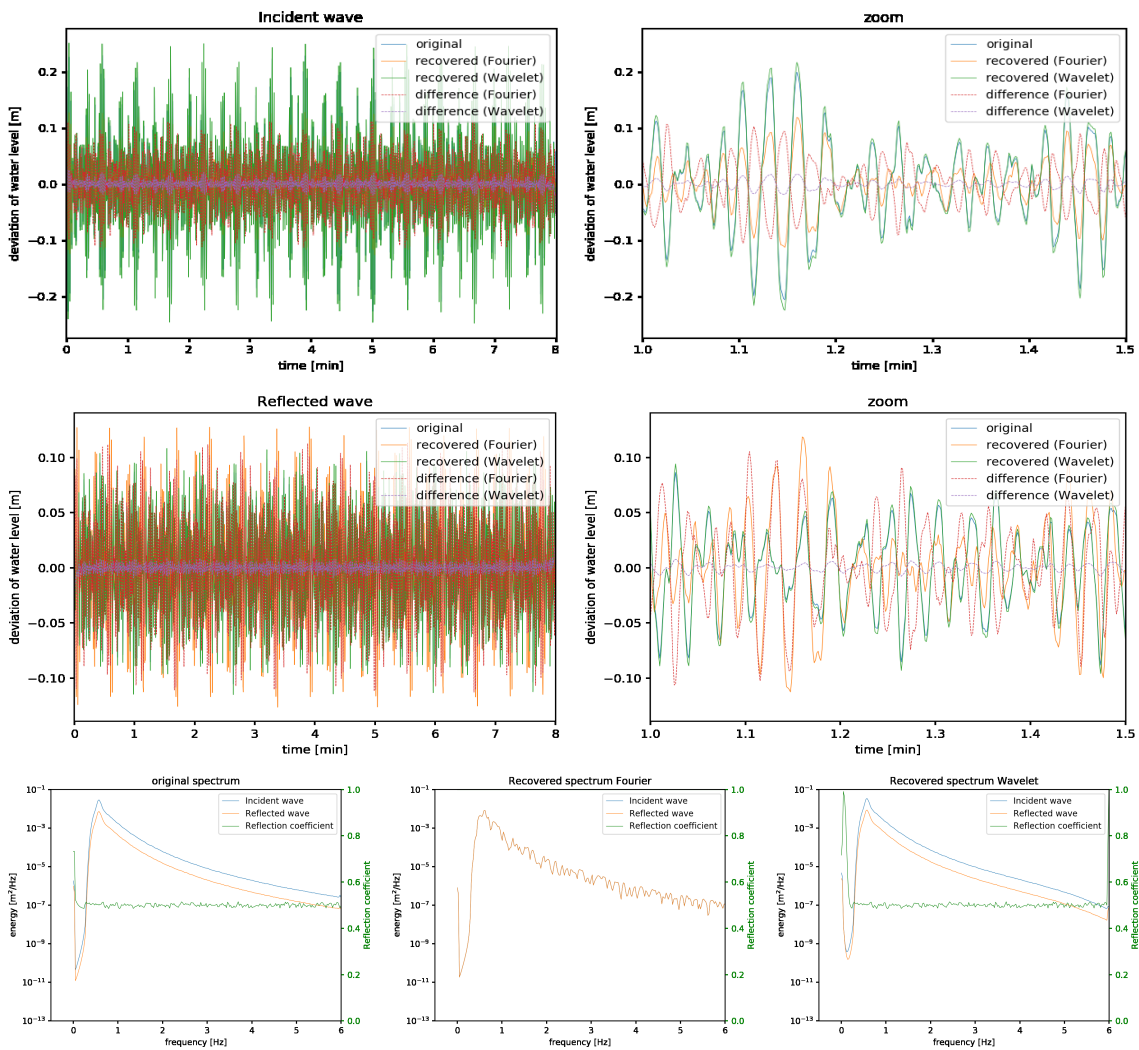


Figure F9: Separating waves using 2 gauges, using the same wave number for all frequencies and the Morlet 6 wavelet.

Signal	200 waves from JONSWAP spectrum with f in [0.01,fs/2]				
Wavelet	Morlet	Parameter	60.0		
Sampling freq	12	Duration	480.0 sec = 8.0 min		
Determined at gauge	35.742				
Using gauges	[35.742 38.726 39.382 39.83 40.1]				
Wavenumber	disperion	with water depth	1		
Noise	no	Weights	no		
No of steps CWT	20				
Determinant limit	0.0				
p_min	1.666956E-01	p_max	1.777215E+01		
RMSE reconstruction	Fourier	Wavelet			
sum	1.513282E-16	1.242043E-01			
incident	4.853375E-03	2.701533E-02			
reflected	7.782599E-03	1.107794E-01			
	6.376457E-03	5.617696E-02			
Ref.cff.	Original	Fourier	% diff	Wavelet	% diff
m0_in	5.024461E-01	5.051175E-01	0.53	5.028802E-01	0.09
m0_ref	5.612317E-03	5.646311E-03	0.61	1.537792E-02	174.0
	1.416841E-03	1.440621E-03	1.68	3.888897E-03	174.48

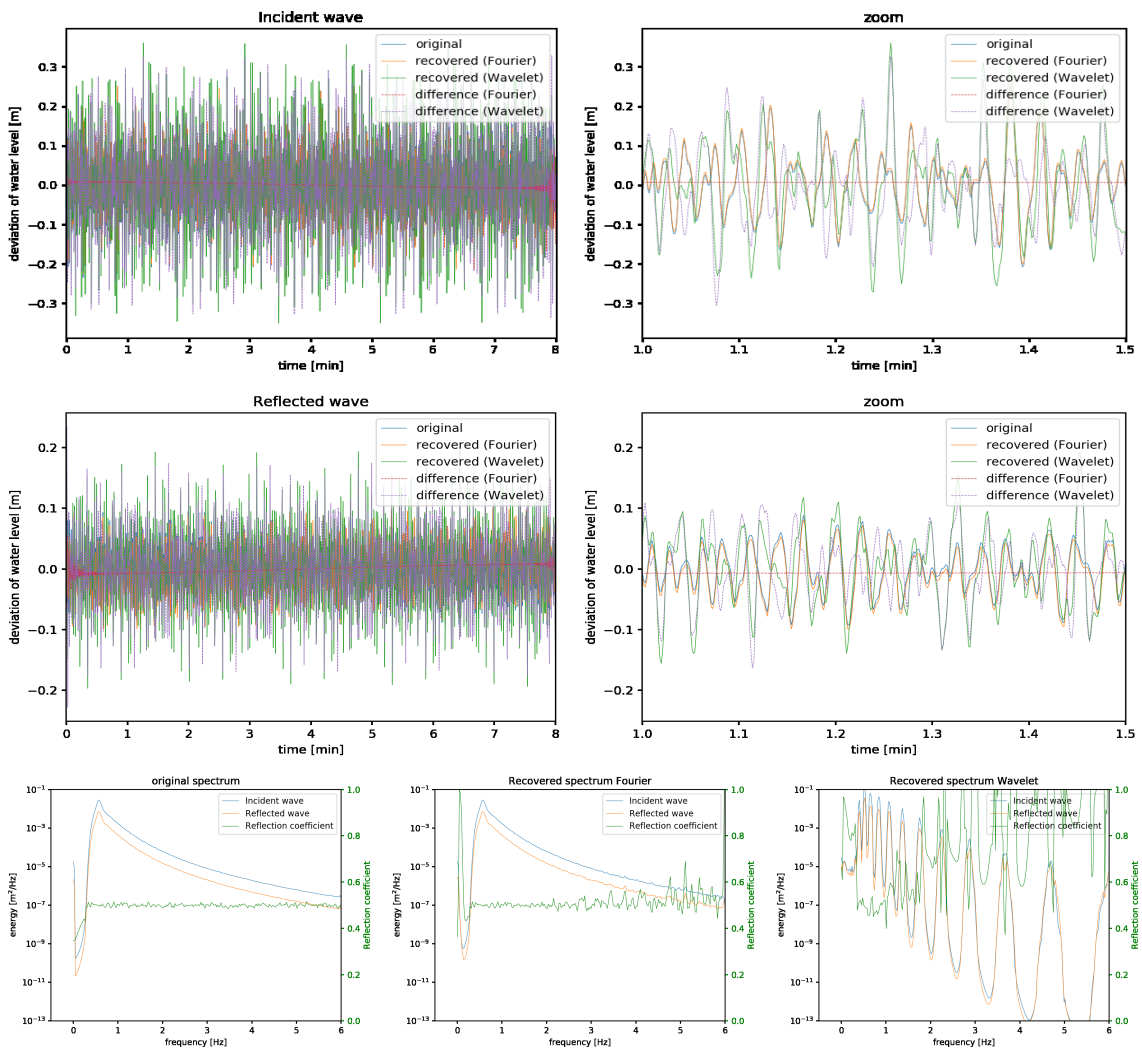


Figure F.10: Separating waves using 5 gauges, using too little scales; 20 scales.

Signal	200 waves from JONSWAP spectrum with f in $[0.01, fs/2]$				
Wavelet	Morlet	Parameter	60.0		
Sampling freq	12	Duration	480.0 sec = 8.0 min		
Determined at gauge	35.742				
Using gauges	[35.742 38.726 39.382 39.83 40.1]				
Wavenumber	dispersion	with water depth	1		
Noise	no	Weights	no		
No of steps CWT	1000				
Determinant limit	0.1				
p_min	1.666956E-01	p_max	1.777215E+01		
RMSE reconstruction	Fourier	Wavelet			
sum incident	1.528517E-16	1.290062E-03			
reflected	5.55671E-03	8.300589E-03			
	6.854045E-03	9.622151E-03			
	3.155962E-03	4.936339E-03			
Ref.cff.	Original	Fourier	% diff	Wavelet	% diff
m0_in	5.012965E-01	5.041818E-01	0.58	5.051833E-01	0.78
m0_ref	5.593016E-03	5.571197E-03	-0.39	5.370117E-03	-3.99
	1.405515E-03	1.416194E-03	0.76	1.370508E-03	-2.49

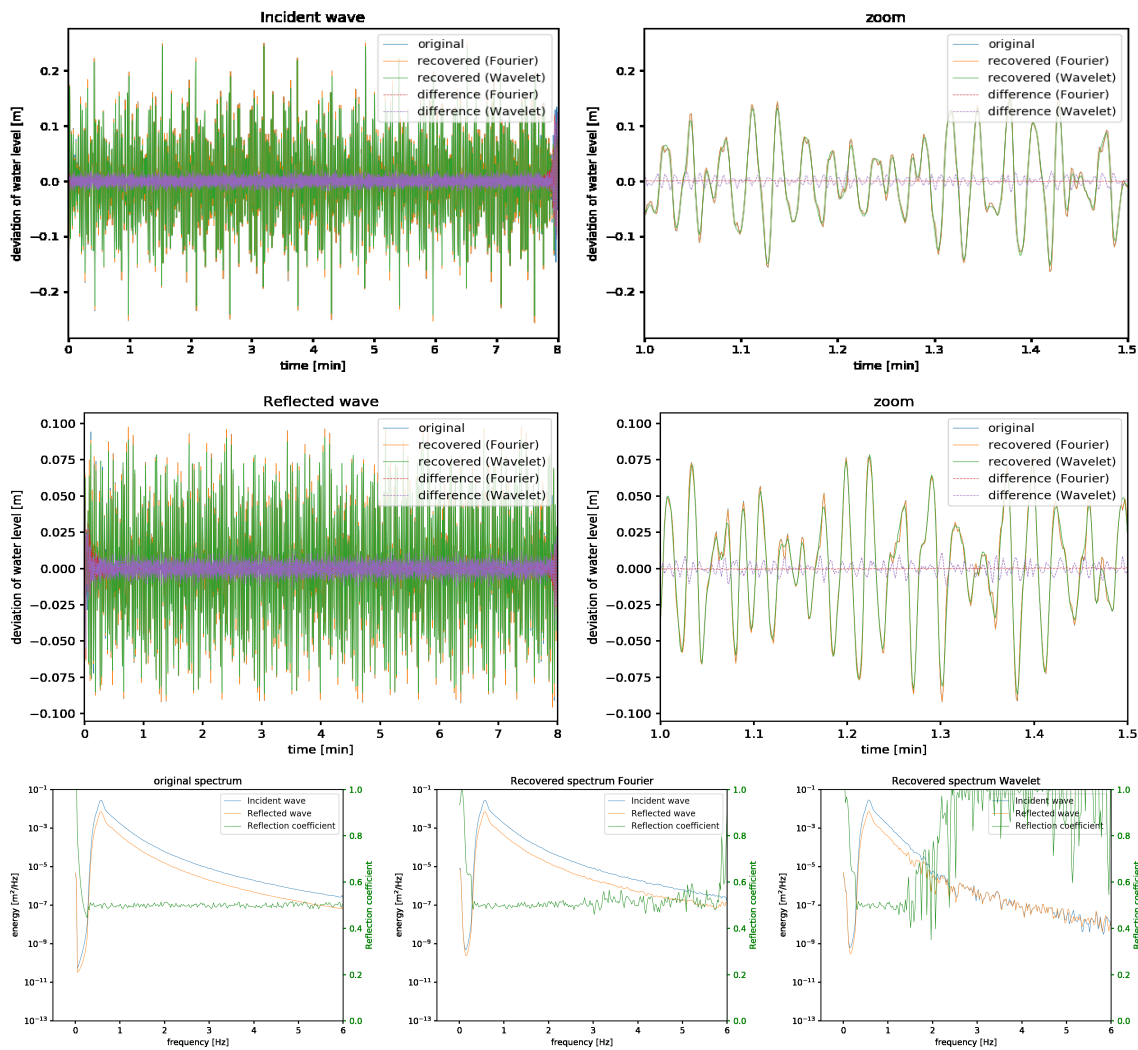


Figure F.11: Separating waves using 5 gauges, using many scales; 1000 scales.

Signal	200 waves from JONSWAP spectrum with f in [0.01,fs/2]				
Wavelet	Morlet	Parameter	60.0		
Sampling freq	12	Duration	480.0 sec = 8.0 min		
Determined at gauge					
Using gauges			39.382		
Wavenumber	dispersion	with water depth	[39.382 40.1]		
Noise	no	Weights	no		
No of steps CWT			200		
Determinant limit			0.5		
p_min	1.666956E-01	p_max	1.777215E+01		
RMSE reconstruction	Fourier	Wavelet			
sum	1.714063E-16	1.03757E-03			
incident	2.151178E-02	1.977146E-02			
reflected	1.806545E-02	1.676688E-02			
	9.452914E-03	8.831368E-03			
Ref.cff.	Original	Fourier	% diff	Wavelet	% diff
m0_in	5.013296E-01	5.039098E-01	0.51	5.046765E-01	0.67
m0_ref	5.5754E-03	5.254034E-03	-5.76	5.343346E-03	-4.16
	1.401273E-03	1.334131E-03	-4.79	1.360941E-03	-2.88

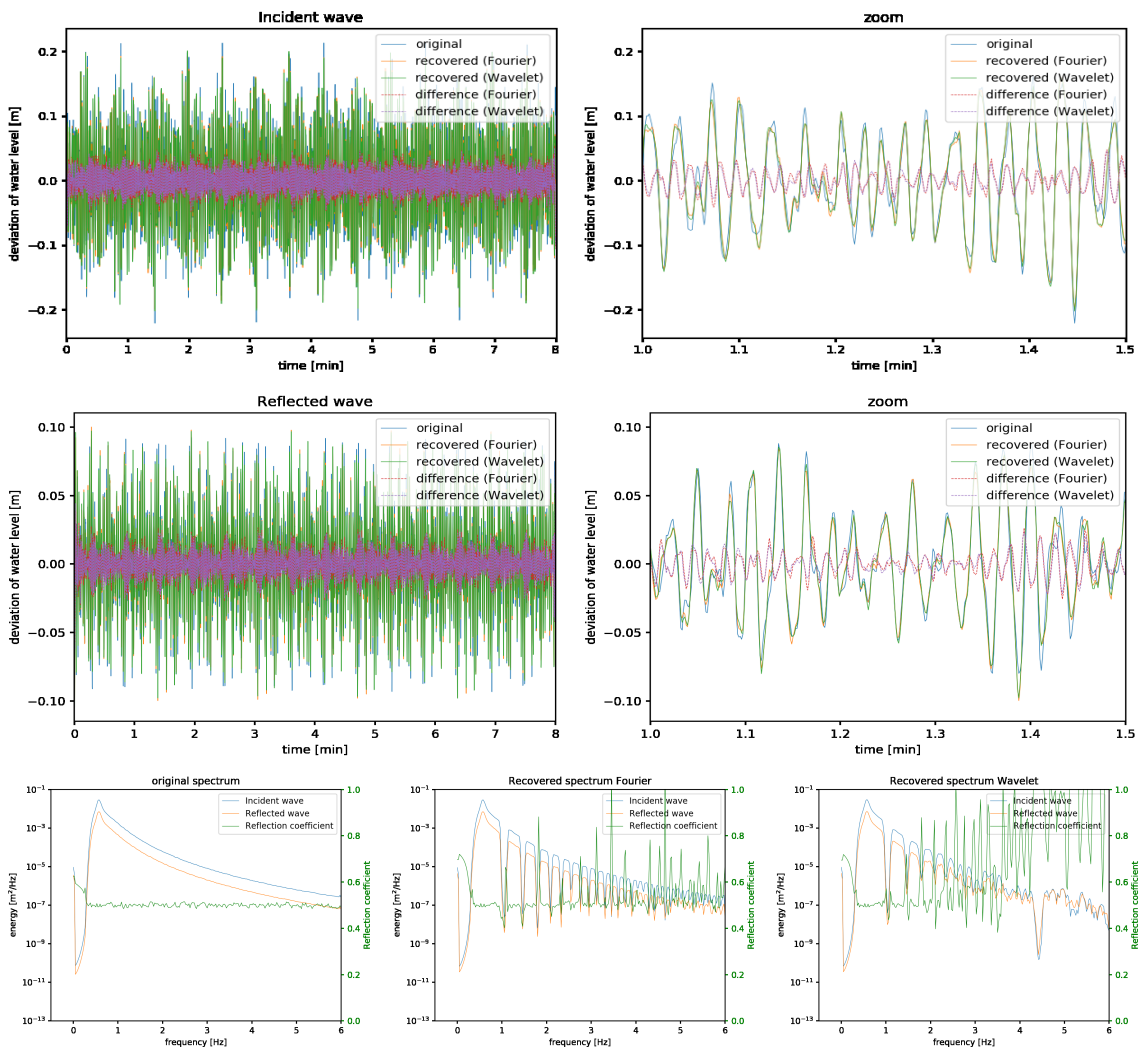


Figure F.12: Separating waves using 2 gauges, a determinant limiter of 0.5 has been added.

Signal	200 waves from JONSWAP spectrum with f in [0.01,fs/2]				
Wavelet	Morlet	Parameter	60.0		
Sampling freq	12	Duration	480.0 sec = 8.0 min		
Determined at gauge			39.382		
Using gauges			[39.382 39.83 40.1]		
Wavenumber	dispersion	with water depth	1		
Noise	no	Weights	zelt		
No of steps CWT			200		
Determinant limit			0		
p_min	1.666956E-01	p_max	1.777215E+01		
RMSE reconstruction	Fourier	Wavelet			
sum incident	1.378247E-16	8.438111E-04			
reflected	1.177983E-03	1.331431E-03			
	1.005492E-02	2.675956E-03			
	1.005925E-02	2.519676E-03			
Ref.cff.	Original	Fourier	% diff	Wavelet	% diff
m0_in	4.989154E-01	5.117766E-01	2.58	4.996177E-01	0.14
m0_ref	5.698587E-03	5.801439E-03	1.8	5.821553E-03	2.16
	1.418473E-03	1.519486E-03	7.12	1.453164E-03	2.45

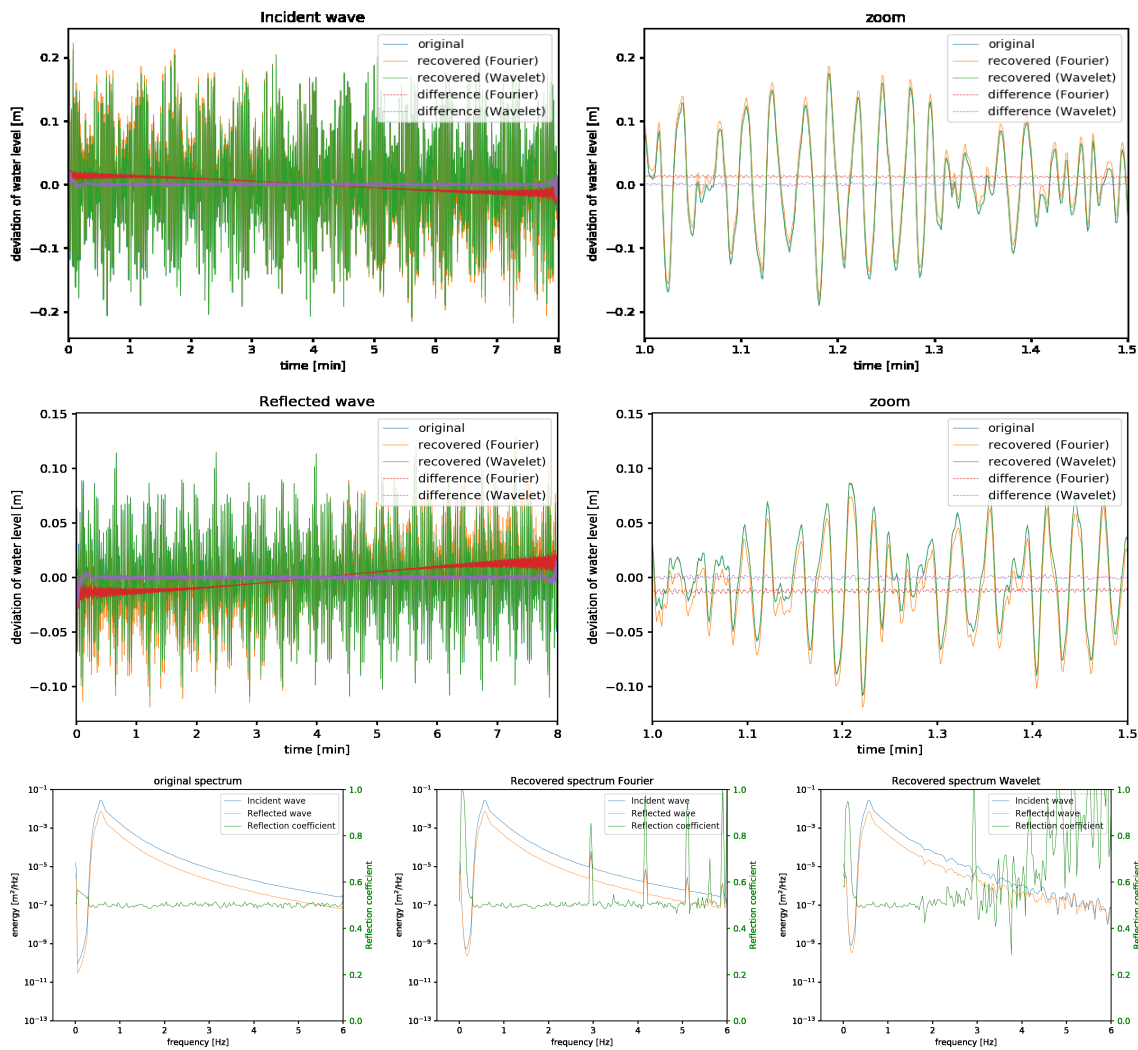


Figure E.13: Separating waves using 3 gauges, added the weightings described in equation 3.22.

Signal	200 waves from JONSWAP spectrum with f in [0.01,fs/2], refl.cff changes				
Wavelet	Morlet	Parameter	60.0		
Sampling freq	12	Duration	480.0 sec = 8.0 min		
Determined at gauge	35.742				
Using gauges	[35.742 38.726 39.382 39.83 40.1]				
Wavenumber	disperion	with water depth	1		
Noise	no	Weights	no		
No of steps CWT	200				
Determinant limit	0.0				
p_min	1.666956E-01	p_max	1.777215E+01		
RMSE reconstruction sum	Fourier	Wavelet			
incident	1.845117E-16	2.893224E-03			
reflected	4.703134E-03	8.699147E-03			
	6.176124E-03	9.499821E-03			
	3.143778E-03	6.266618E-03			
Ref.cff.	Original	Fourier	% diff	Wavelet	% diff
m0_in	7.092311E-01	7.118718E-01	0.37	7.121914E-01	0.42
m0_ref	5.593476E-03	5.568218E-03	-0.45	5.324922E-03	-4.8
	2.813567E-03	2.821758E-03	0.29	2.700888E-03	-4.0

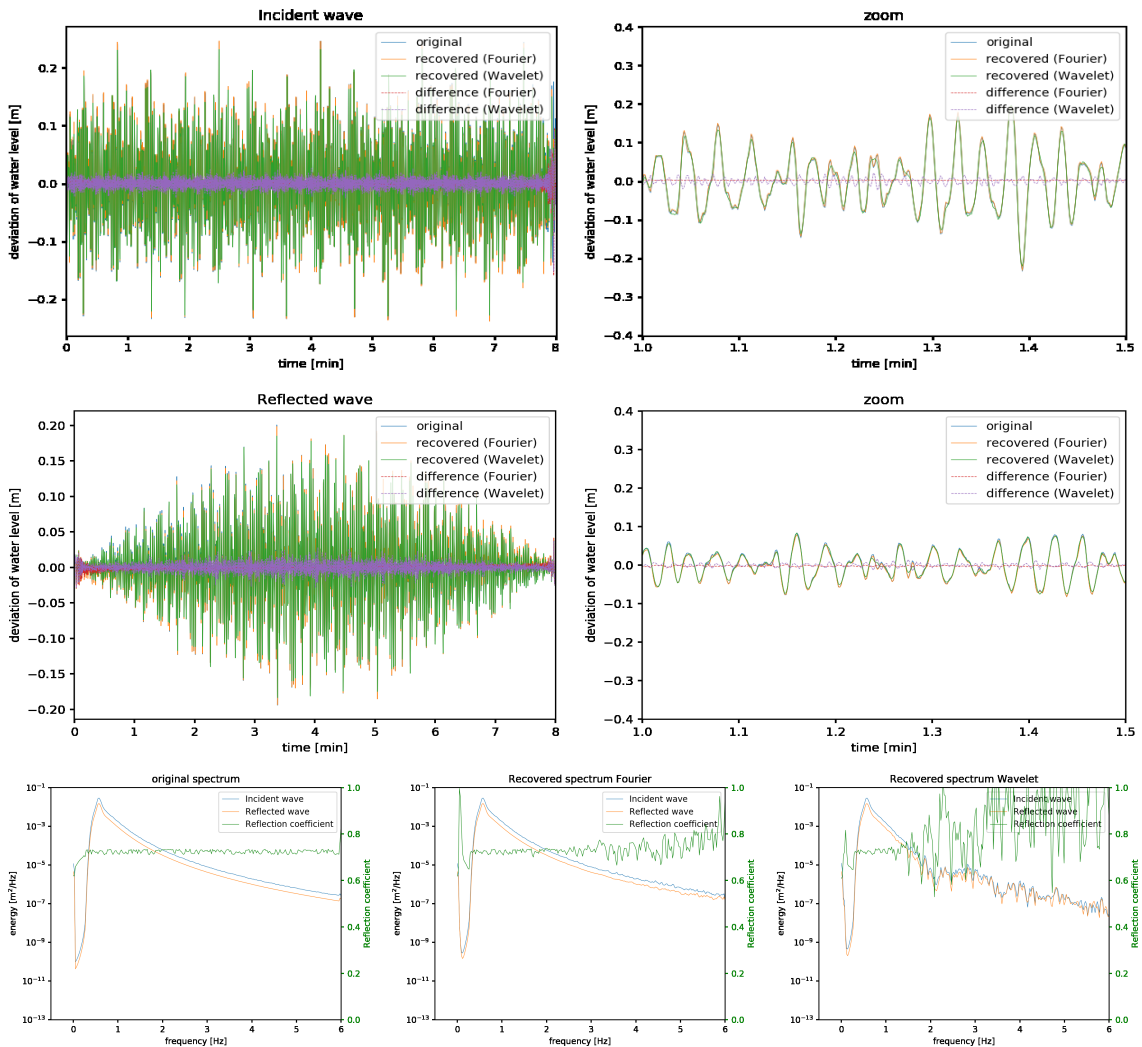


Figure F.14: Separating waves using 5 gauges, reflection coefficient changes over time; following a half a sine over the entire interval.

Signal	200 waves from JONSWAP spectrum with f in $[0.01, fs/2]$, slope in signal				
Wavelet	Morlet	Parameter	60.0		
Sampling freq	12	Duration	480.0 sec = 8.0 min		
Determined at gauge	35.742				
Using gauges	[35.742 38.726 39.382 39.83 40.1]				
Wavenumber	disperion	with water depth	1		
Noise	no	Weights	no		
No of steps CWT	200				
Determinant limit	0.0				
p_min	1.666956E-01	p_max	1.777215E+01		
RMSE reconstruction sum	Fourier	Wavelet			
incident	2.729379E-16	1.448473E-01			
reflected	1.749256E-02	2.389889E-02			
	7.997851E-02	1.546532E-02			
	6.664183E-02	1.266747E-02			
Ref.cff.	Original	Fourier	% diff	Wavelet	% diff
m0_in	5.016754E-01	7.03346E-01	40.2	5.185117E-01	3.36
m0_ref	5.627654E-03	1.17803E-02	109.33	5.518058E-03	-1.95
	1.416358E-03	5.827664E-03	311.45	1.483554E-03	4.74

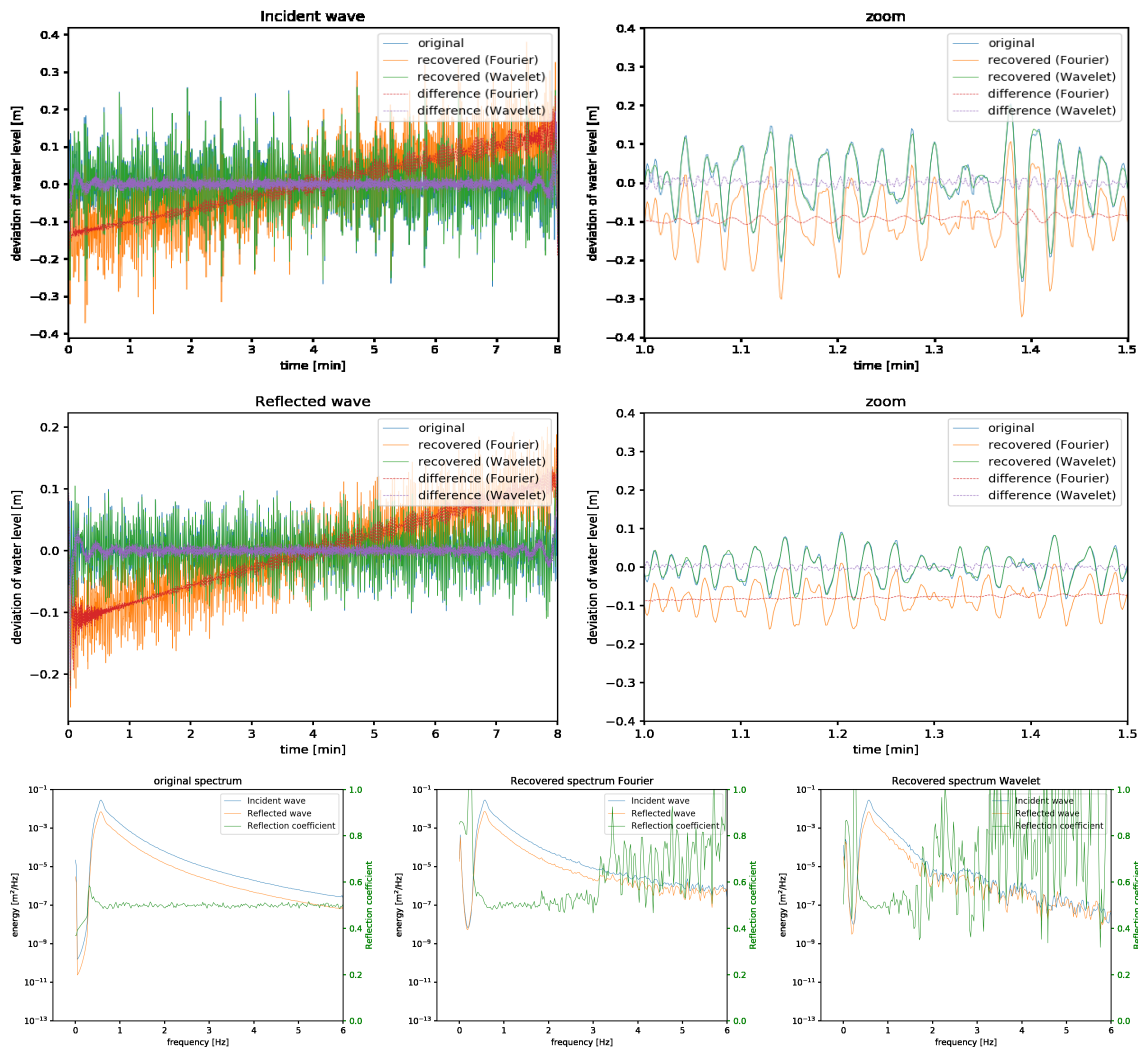


Figure F.15: Separating waves using 5 gauges, slope added to the signal. Increase of water level of 0.5 meter in 8 minutes. The sum of the wavelet separated incident and reflected wave is not close to the original signal because the slope is not present in the separated waves.

Signal	200 waves from JONSWAP spectrum with f in $[0.01, fs/2]$, non stationary reflec				
Wavelet	Morlet	Parameter	60.0		
Sampling freq	12	Duration	480.0 sec = 8.0 min		
Determined at gauge	35.742				
Using gauges	[35.742 38.726 39.382 39.83 40.1]				
Wavenumber	disperion	with water depth	1		
Noise	no	Weights	no		
No of steps CWT	200				
Determinant limit	0.0				
p_min	1.666956E-01	p_max	1.777215E+01		
RMSE reconstruction	Fourier	Wavelet			
sum	6.919914E-16	4.038558E-01			
incident	4.705659E-02	4.721172E-02			
reflected	1.216143E-01	2.353307E-01			
	1.217744E-01	2.353185E-01			
Ref.cff.	Original	Fourier	% diff	Wavelet	% diff
m0_in	9.527674E-01	9.554861E-01	0.29	7.129344E-01	-25.17
m0_ref	4.91902E-02	5.000326E-02	1.65	8.91487E-03	-81.88
	4.465318E-02	4.565066E-02	2.23	4.531209E-03	-89.85

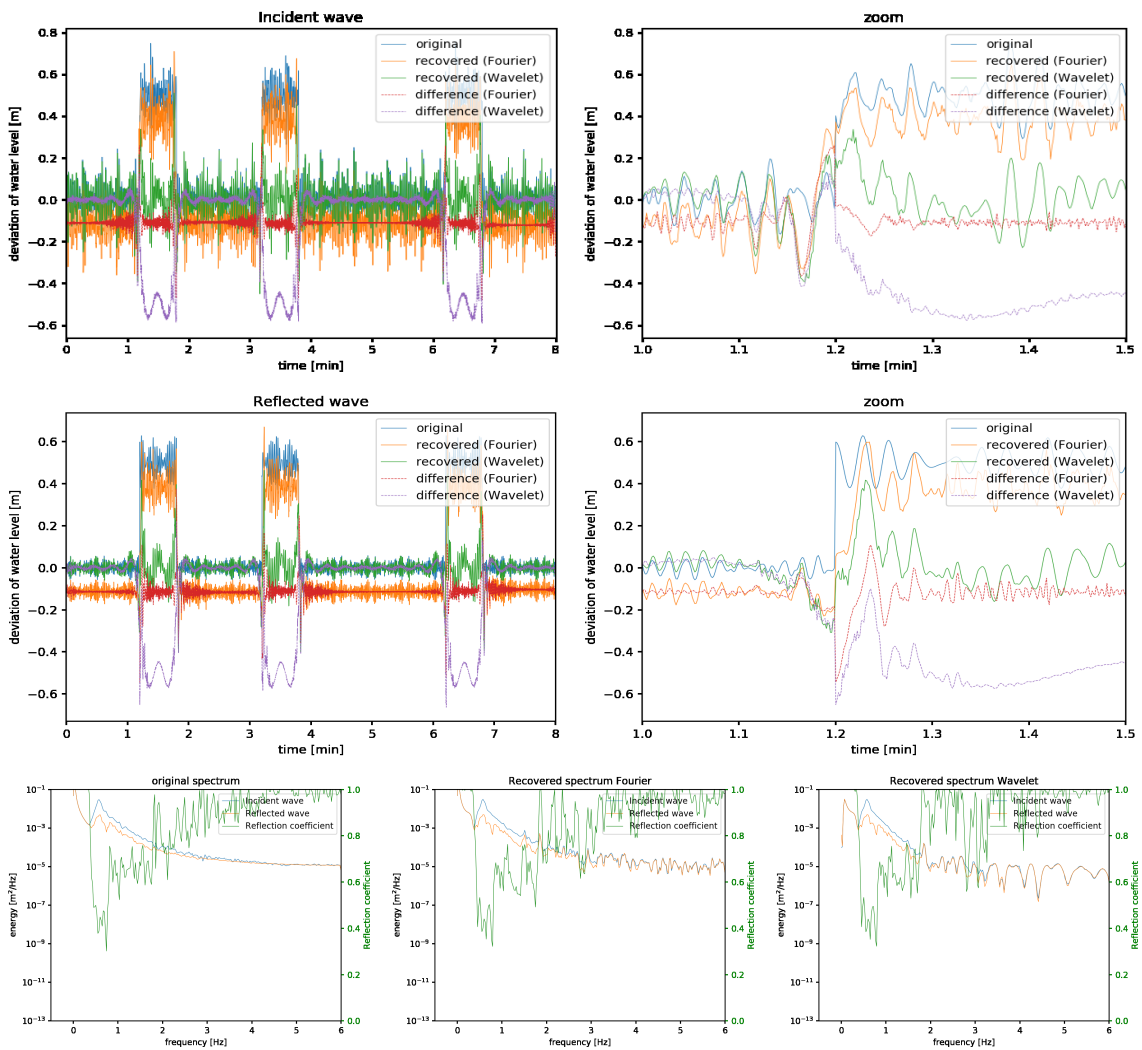


Figure F.16: Separating waves using 5 gauges, jumps added to signal.

Signal	200 waves from JONSWAP spectrum with f in $[0.01, fs/2]$				
Wavelet	Morlet	Parameter	60.0		
Sampling freq	12	Duration	480.0 sec = 8.0 min		
Determined at gauge	39.382				
Using gauges	[39.382 40.1]				
Wavenumber	dispersion	with water depth	1		
Noise	var/0.1	Weights	no		
No of steps CWT	200				
Determinant limit	0.1				
p_min	1.666956E-01	p_max	1.777215E+01		
RMSE reconstruction	Fourier	Wavelet			
sum	1.960715E-16	1.136034E-02			
incident	2.415382E-02	1.953535E-02			
reflected	6.855018E-02	5.332024E-02			
	6.747686E-02	5.228281E-02			
Ref.cff.	Original	Fourier	% diff	Wavelet	% diff
m0_in	5.008078E-01	7.649991E-01	52.75	6.99347E-01	39.64
m0_ref	5.626912E-03	1.014042E-02	80.21	8.431024E-03	49.83
	1.411277E-03	5.934415E-03	320.5	4.123497E-03	192.18

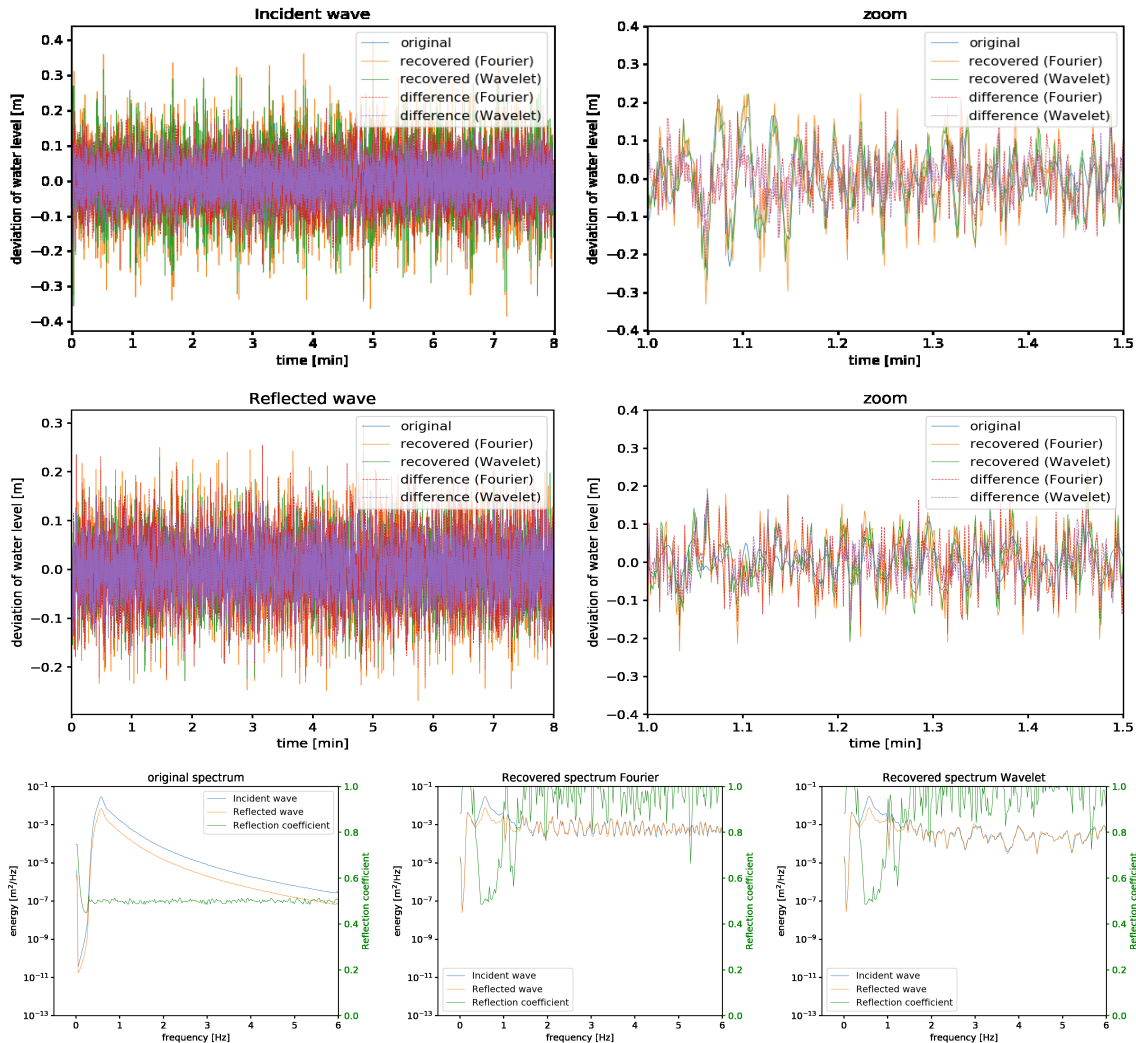


Figure F.17: Separating waves using 2 gauges, noise added to the signal of 10 times the incident wave power. Solved using a determinant limiter of 0.1.

Signal	200 waves from JONSWAP spectrum with f in [0.01,fs/2]				
Wavelet	Morlet	Parameter	60.0		
Sampling freq	12	Duration	480.0 sec = 8.0 min		
Determined at gauge	35.742				
Using gauges	[35.742 38.726 39.382 39.83 40.1]				
Wavenumber	disperion	with water depth	1		
Noise	var/0.1	Weights	no		
No of steps CWT	200				
Determinant limit	0.1				
p_min	1.666956E-01	p_max	1.777215E+01		
RMSE reconstruction	Fourier	Wavelet			
sum	2.147517E-16	8.35714E-03			
incident	4.258662E-02	3.904357E-02			
reflected	3.093711E-02	2.371355E-02			
	3.099383E-02	2.300432E-02			
Ref.cff.	Original	Fourier	% diff	Wavelet	% diff
m0_in	5.016262E-01	6.05833E-01	20.77	5.699105E-01	13.61
m0_ref	5.564055E-03	6.380366E-03	14.67	5.700034E-03	2.44
	1.400077E-03	2.341809E-03	67.26	1.851359E-03	32.23

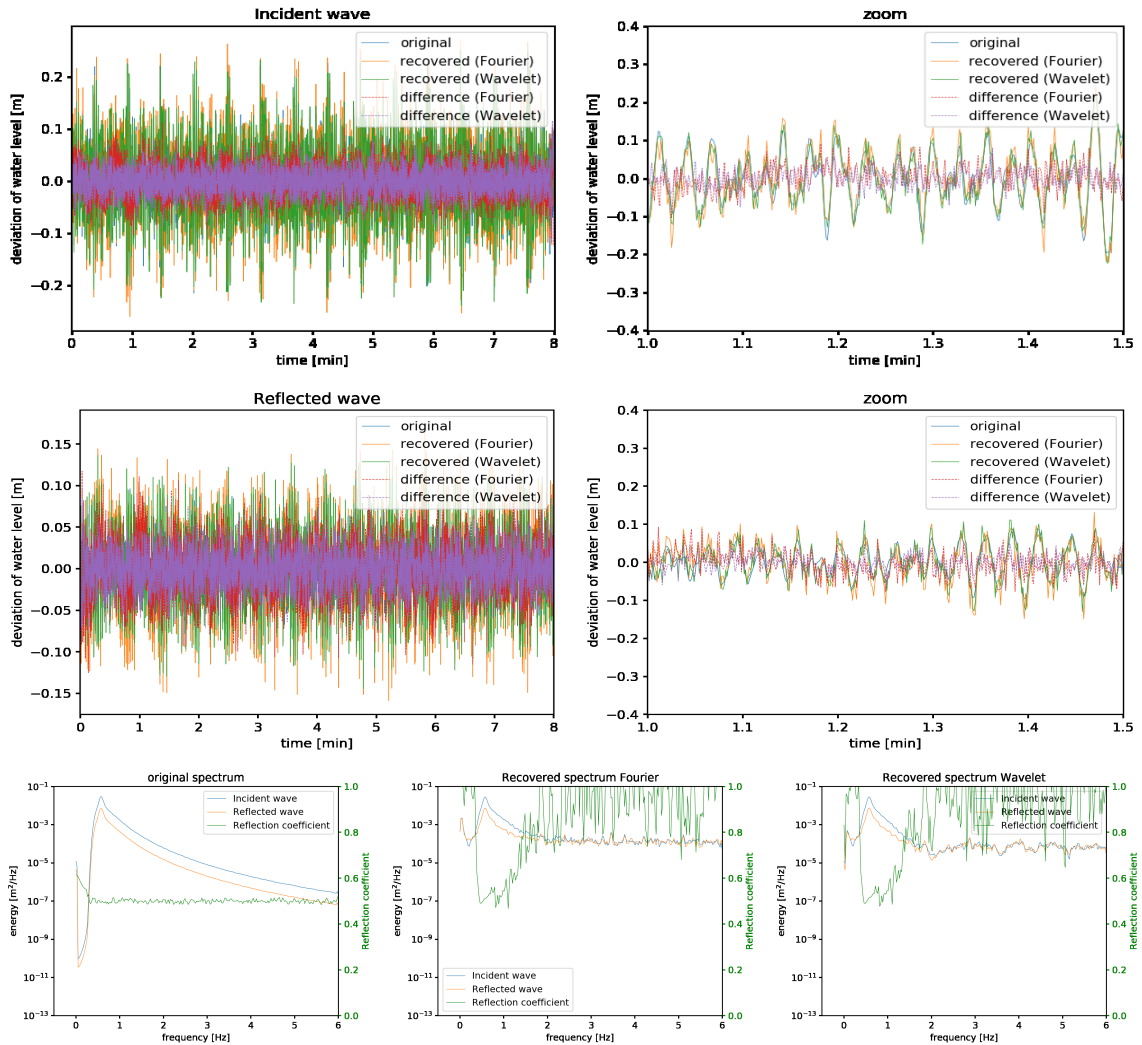


Figure F.18: Separating waves using 5 gauges, noise added to the signal of 10 times the incident wave power. Solved using a determinant limiter of 0.1.

Signal $s = x + w + v$				Wavelets							Wavelets							
x: stationarity	w	v: noise color	v: noise power (dB)	v: power supply + mirrors	RMSE(f - x)							RMSE(f - (x + w))						
					No Filter	Haar	Sym8	Coif3	Bior2.8	Db20	No Filter	Haar	Sym8	Coif3	Bior2.8	Db20		
Yes	White	-10	0	Yes	0.00	6.01	6.46	6.49	7.23	6.53	0.00	8.46	8.82	8.81	8.99	8.77		
				No	0.00	6.10	6.52	6.52	7.28	6.42	0.00	8.55	8.88	8.89	9.04	8.81		
				Yes	0.00	3.87	5.54	5.41	6.08	6.00	0.00	4.65	5.28	5.28	6.01	5.21		
				No	0.00	3.95	5.53	5.42	6.12	5.91	0.00	5.22	5.94	5.95	6.58	5.91		
				Yes	0.00	2.37	5.21	5.25	5.94	5.24	0.00	3.16	5.59	5.53	5.78	5.66		
				No	0.00	2.28	5.12	5.19	5.97	5.11	0.00	2.32	4.41	4.42	4.93	4.37		
No	White	-10	0	Yes	0.00	11.02	12.56	12.31	11.79	12.32	0.00	8.46	8.82	8.81	8.99	8.77		
				No	0.00	11.38	12.75	12.88	11.48	12.42	0.00	8.55	8.88	8.89	9.04	8.81		
				Yes	0.00	6.15	5.63	5.65	4.92	5.68	0.00	4.65	5.28	5.28	6.01	5.21		
				No	0.00	5.76	5.37	5.38	4.93	5.38	0.00	5.22	5.94	5.95	6.58	5.91		
				Yes	0.00	1.46	1.22	1.23	1.19	1.21	0.00	3.16	5.59	5.53	5.78	5.66		
				No	0.00	1.41	1.14	1.14	1.08	1.14	0.00	2.32	4.41	4.42	4.93	4.37		
No	White	0	0	Yes	0.00	11.22	12.69	12.74	12.85	12.54	0.00	8.46	8.82	8.81	8.99	8.77		
				No	0.00	11.21	12.93	12.95	13.03	12.69	0.00	8.55	8.88	8.89	9.04	8.81		
				Yes	0.00	10.07	12.20	12.26	12.43	12.03	0.00	4.65	5.28	5.28	6.01	5.21		
				No	0.00	9.54	11.90	11.94	12.14	11.34	0.00	5.22	5.94	5.95	6.58	5.91		
				Yes	0.00	8.31	11.30	11.38	11.87	10.73	0.00	3.16	5.59	5.53	5.78	5.66		
				No	0.00	8.48	11.38	11.51	12.00	10.68	0.00	2.32	4.41	4.42	4.93	4.37		
				ND														

Figure G.2: The results of the different wavelets in hard thresholding for the white noise cases

G.2. Examples of other filters

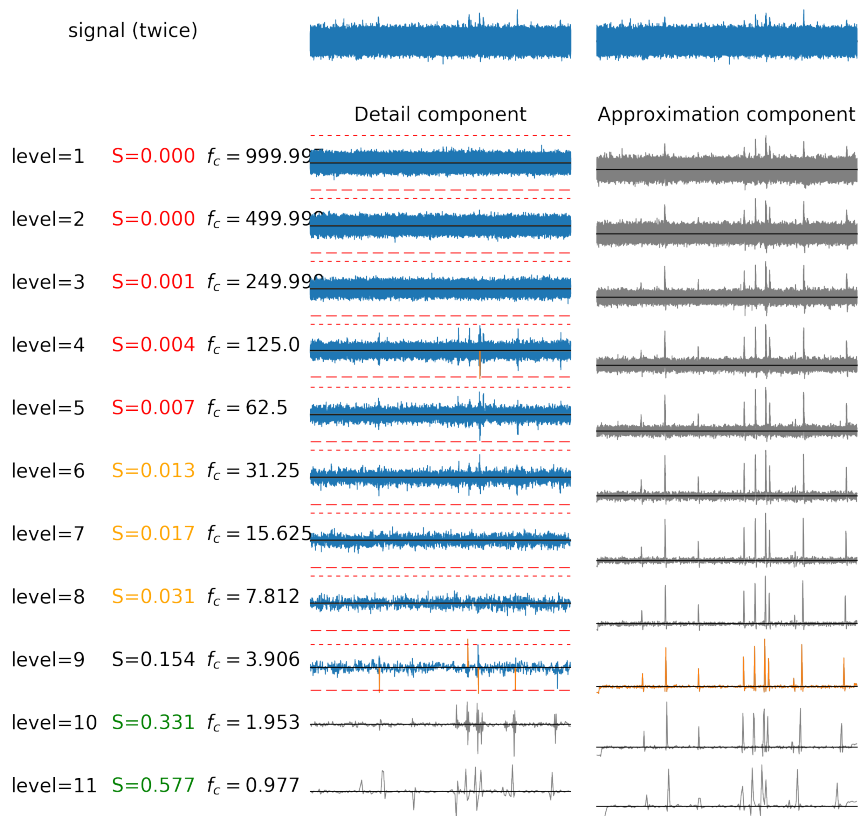


Figure G.3: The approximation and detail coefficients and their thresholds, based on the hard thresholding methods. The colours correspond with the colours in Figure 3e) of the original file. The S denotes the peak-to-sum ratio (or sparsity) of the detail coefficients at that level.

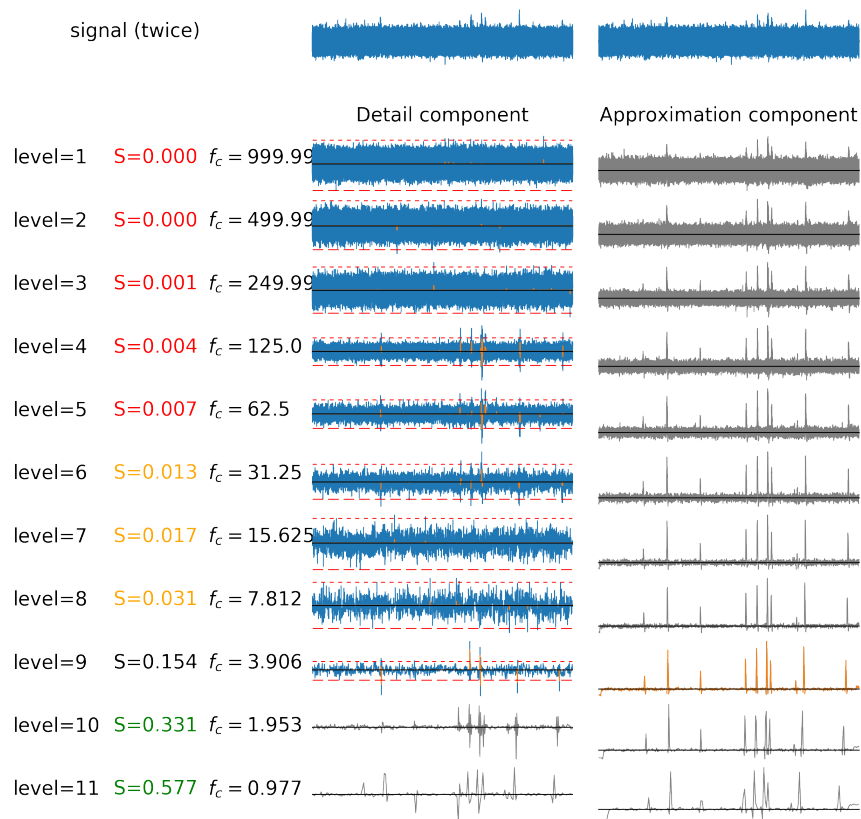


Figure G.4: The approximation and detail coefficients and their thresholds, based on the first 30 seconds being signal free. The colours correspond with the colours in Figure 3e) of the original file. The S denotes the peak-to-sum ratio (or sparsity) of the detail coefficients at that level.

G.3. Five different wavelets and their spectra

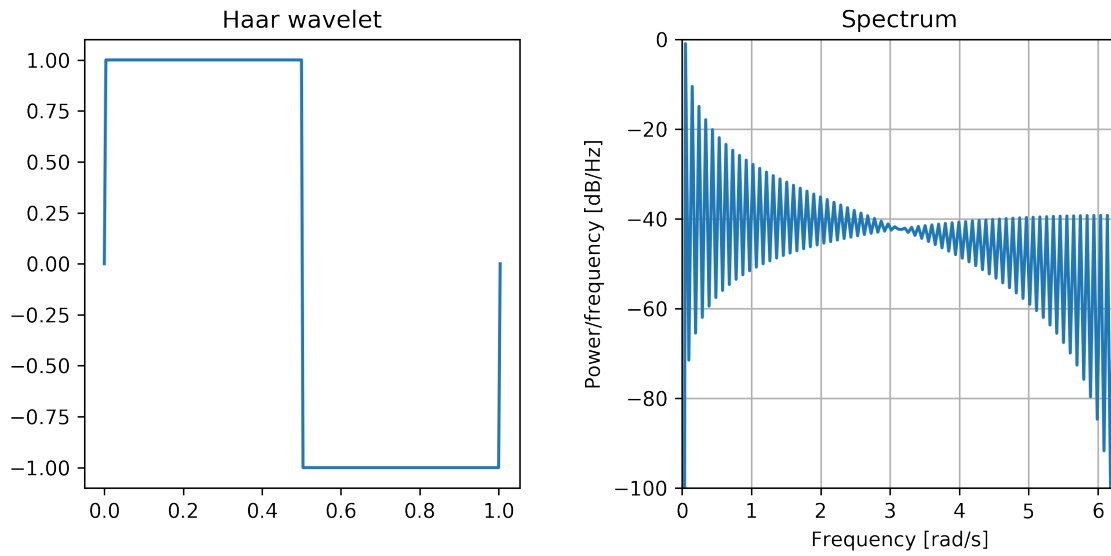


Figure G.5: The Haar wavelet

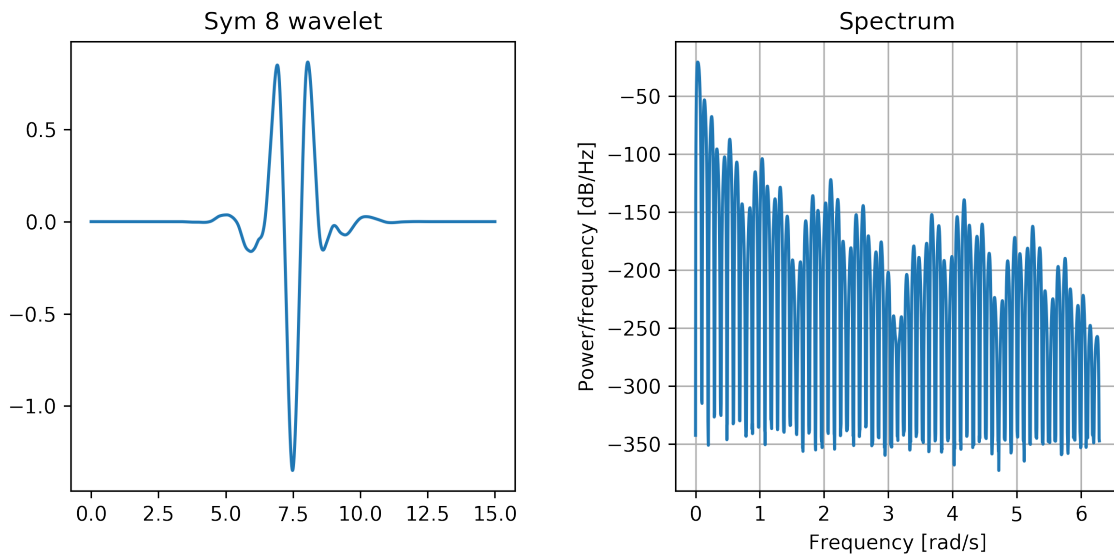


Figure G.6: The Symmlet 8 wavelet

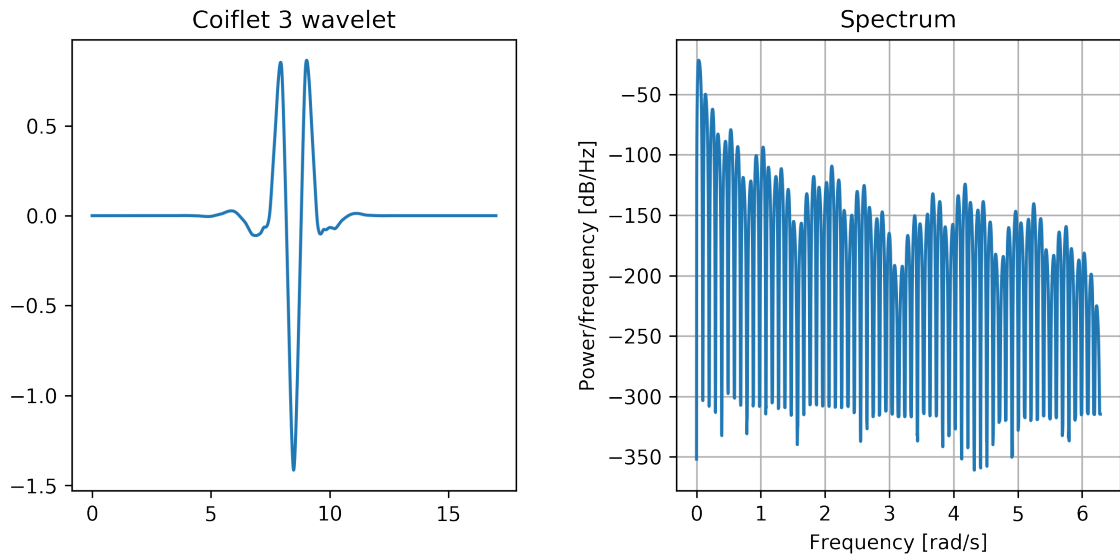


Figure G.7: The Coiflet 3wavelet

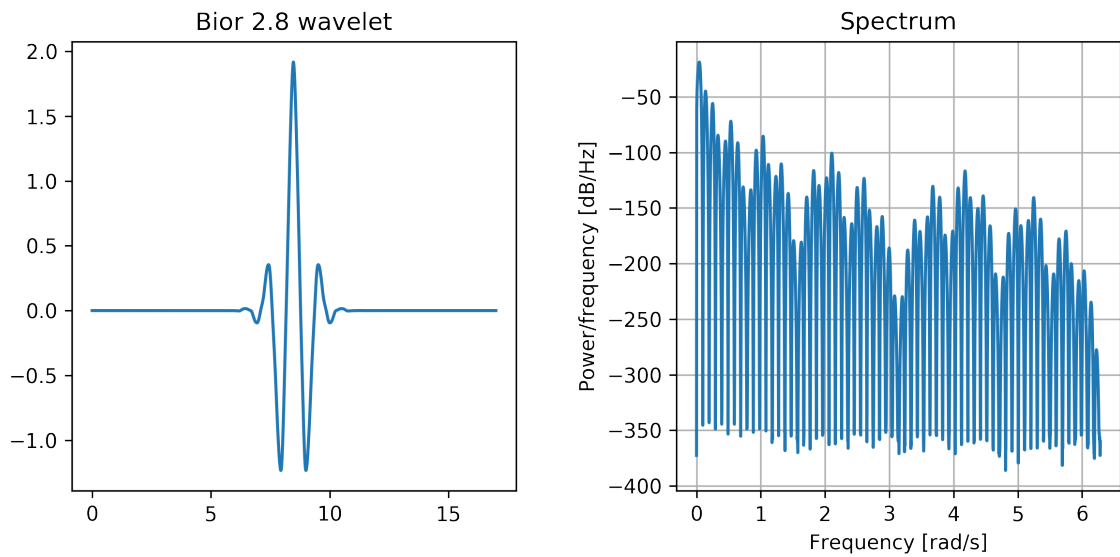


Figure G.8: The Biorthogonal 2.8 wavelet

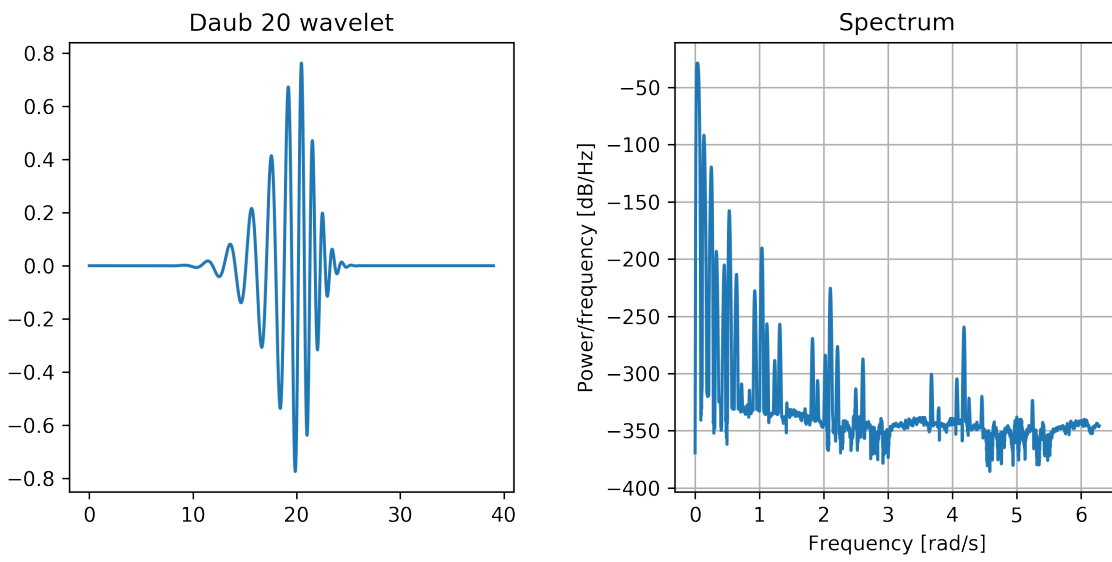


Figure G.9: The Daubechies 20 wavelet

G.4. Comparison of wavelets in filtering

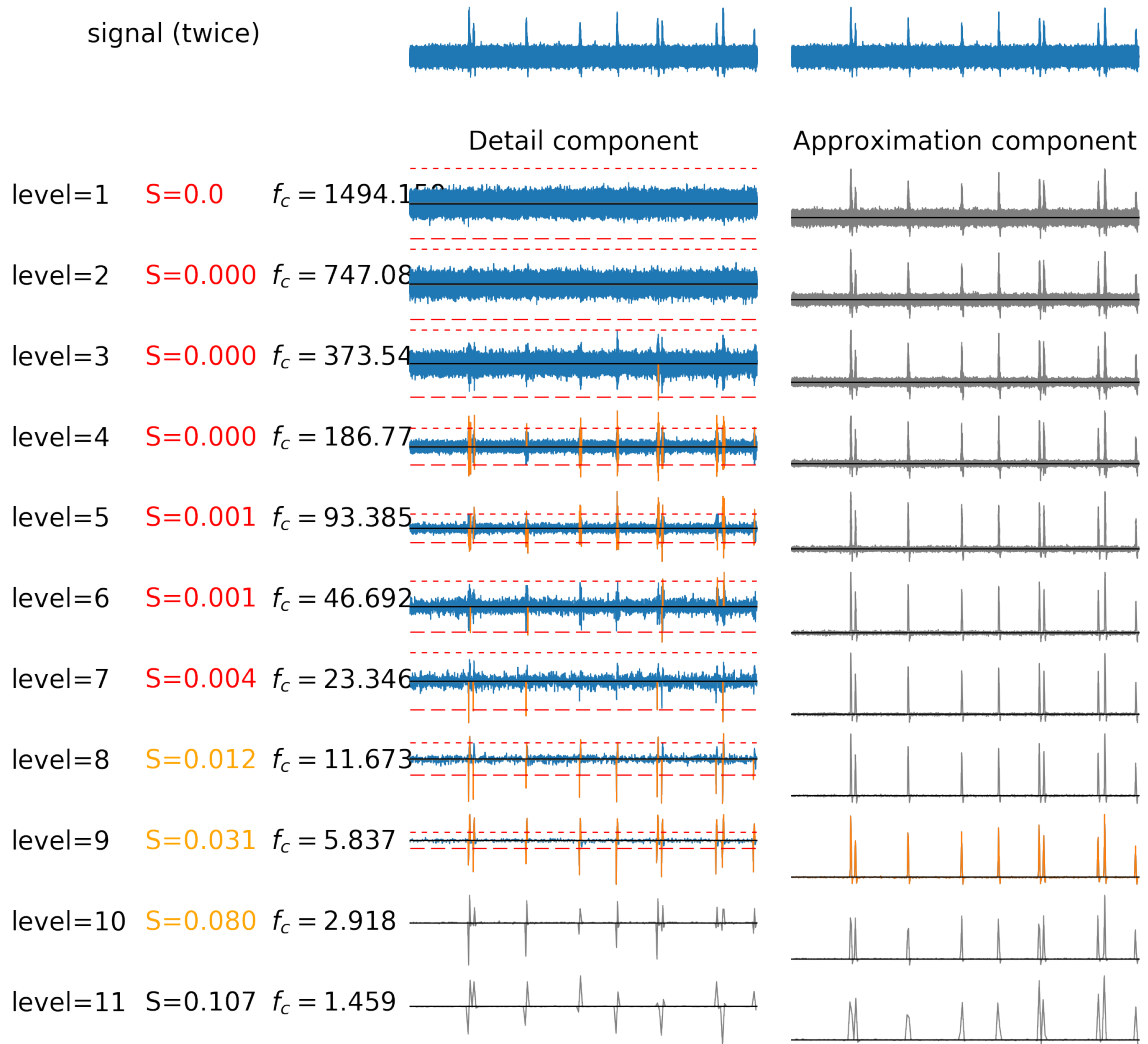


Figure G.10: The hard filtering algorithm applied with the Haar wavelet for the non stationary signal with w and a SNR of 0 dB.

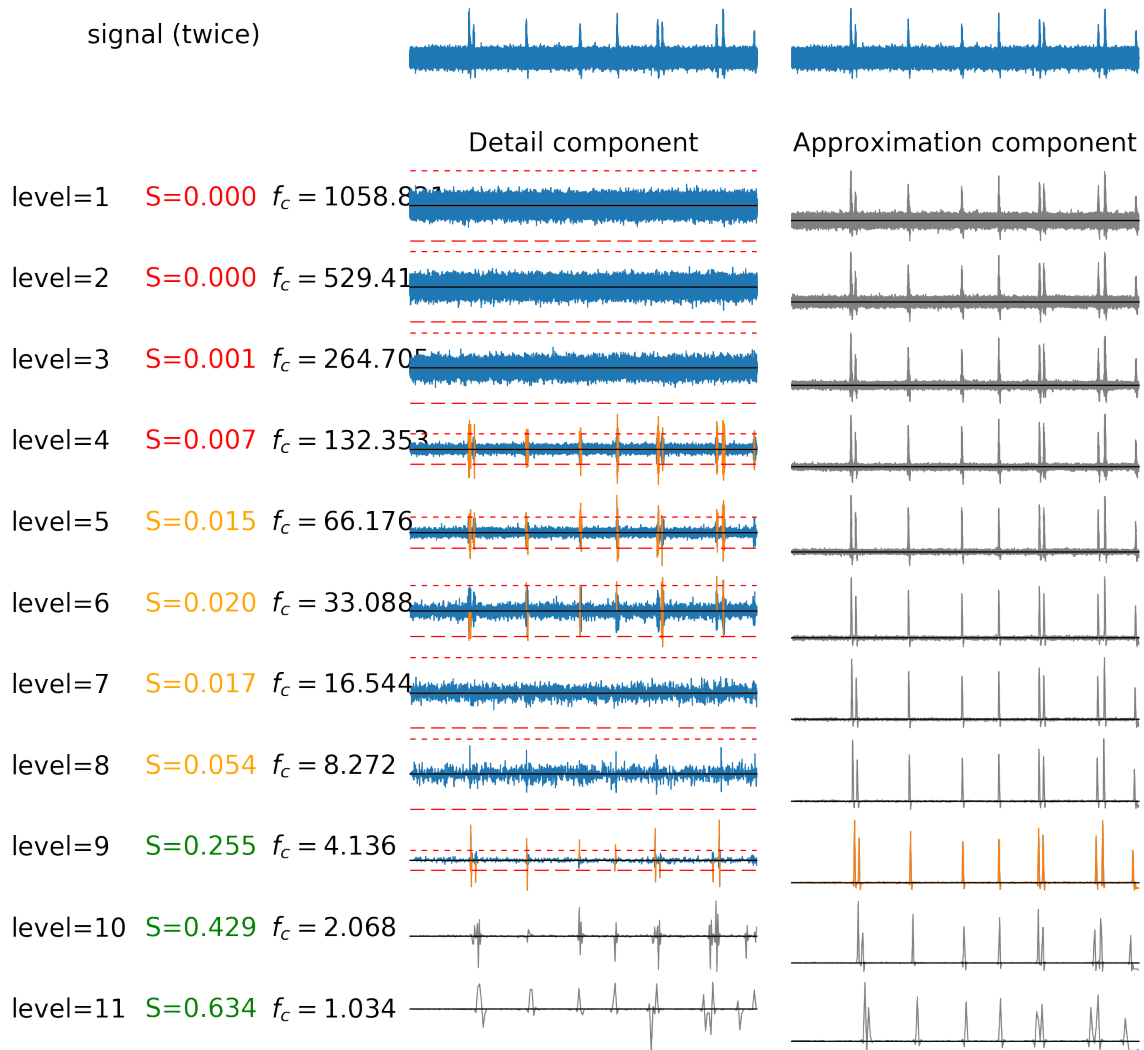


Figure G.12: The hard filtering algorithm applied with the Coiflet 3 wavelet for the non stationary signal with w and a SNR of 0 dB.

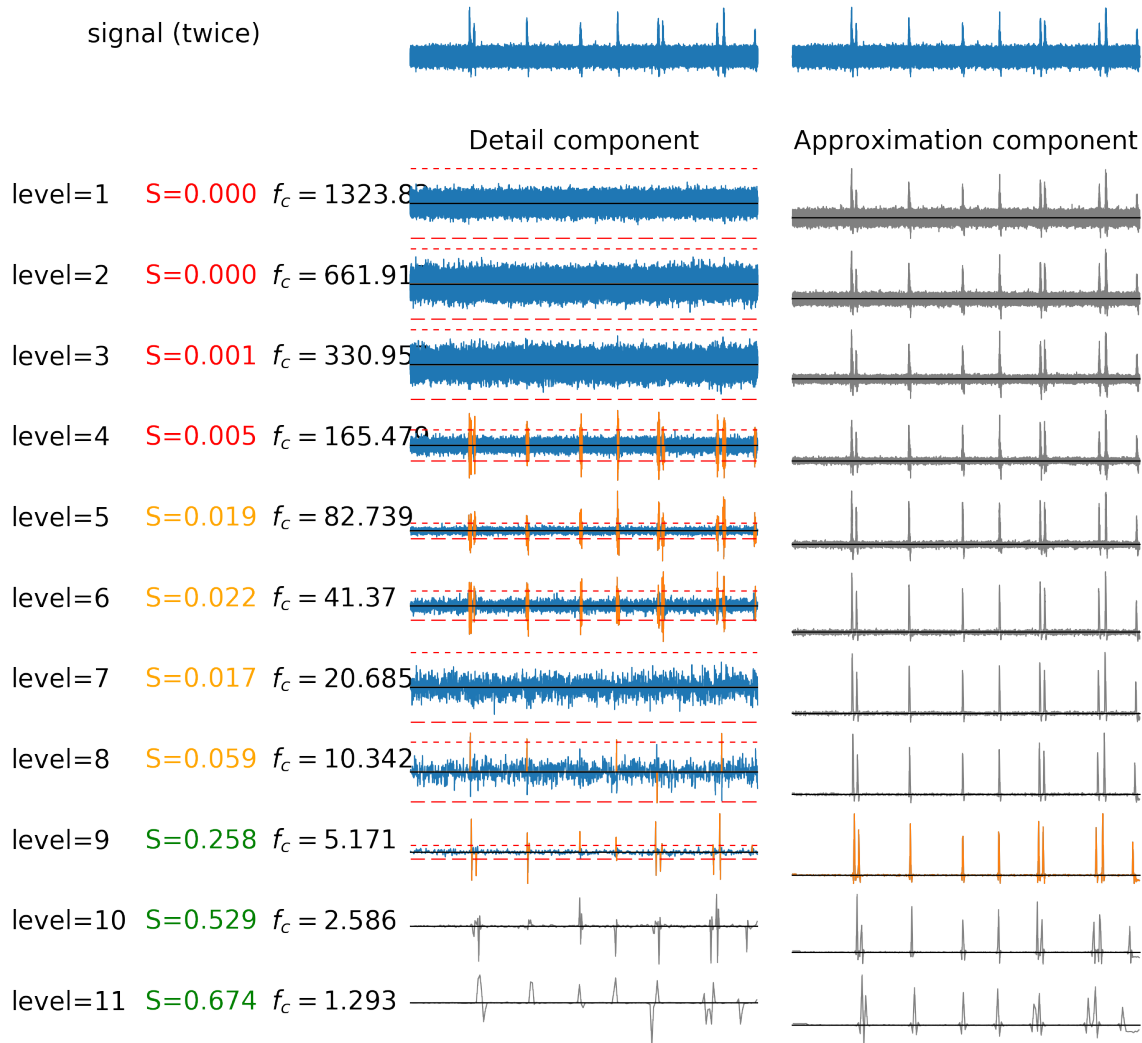


Figure G.13: The hard filtering algorithm applied with the Biorthogonal 2.8 wavelet for the non stationary signal with w and a SNR of 0 dB.

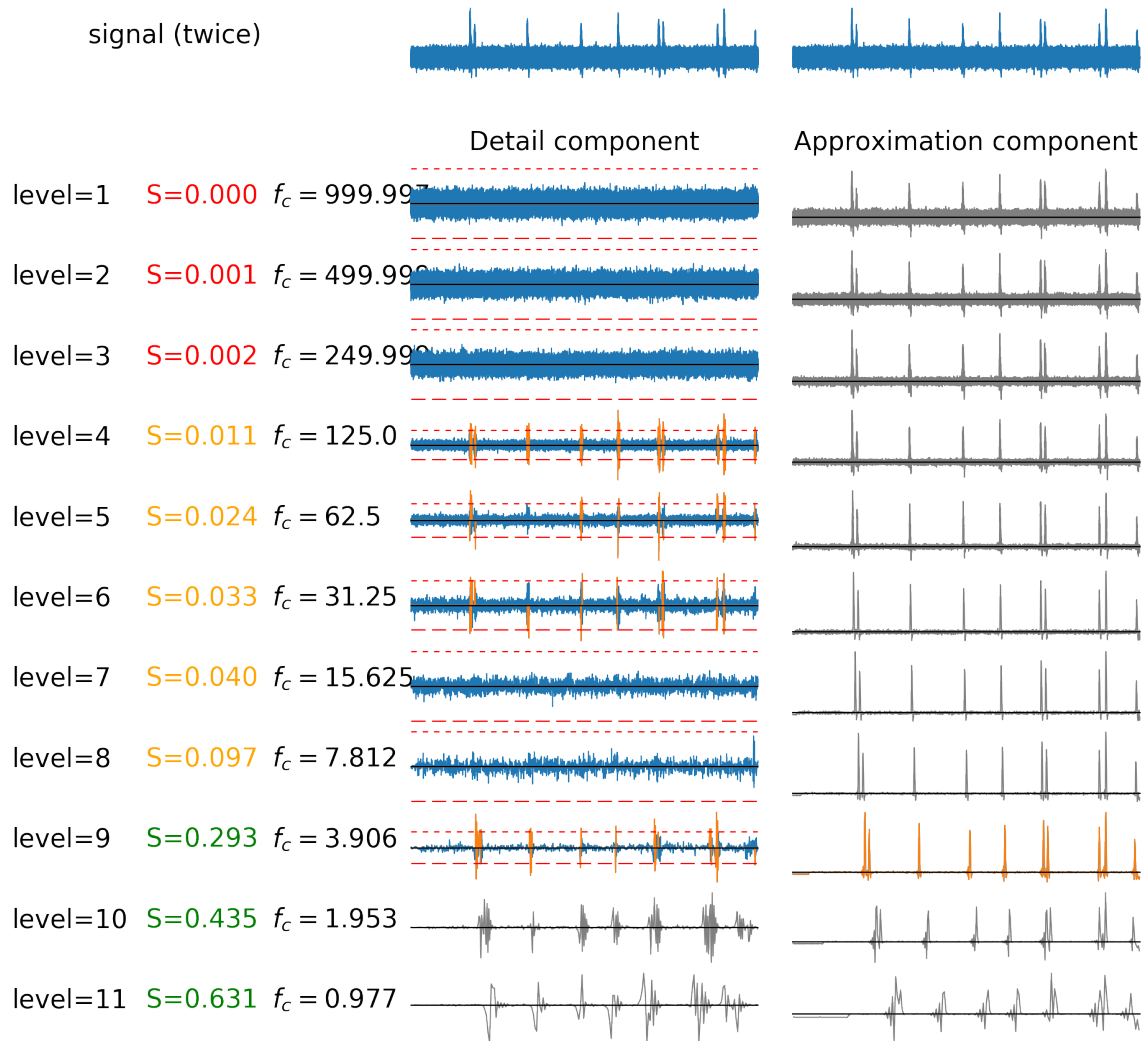


Figure G.14: The hard filtering algorithm applied with the Daubechies 20 wavelet for the non stationary signal with w and a SNR of 0 dB.

G.5. Periodic signal extension

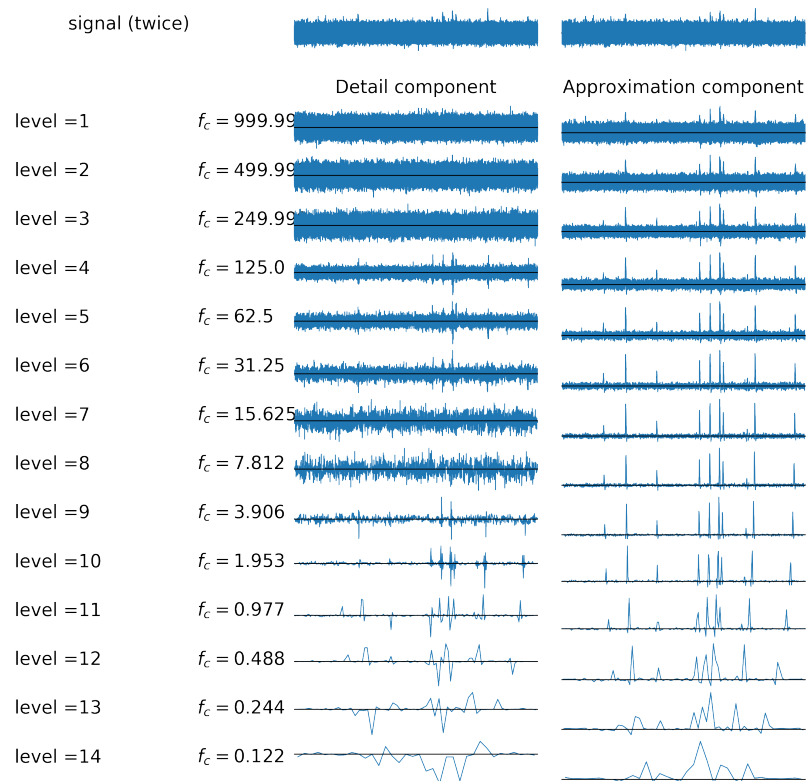


Figure G.15: Figure 5 from original, now using periodic signal extension instead of symmetric signal extension.

G.6. Signals

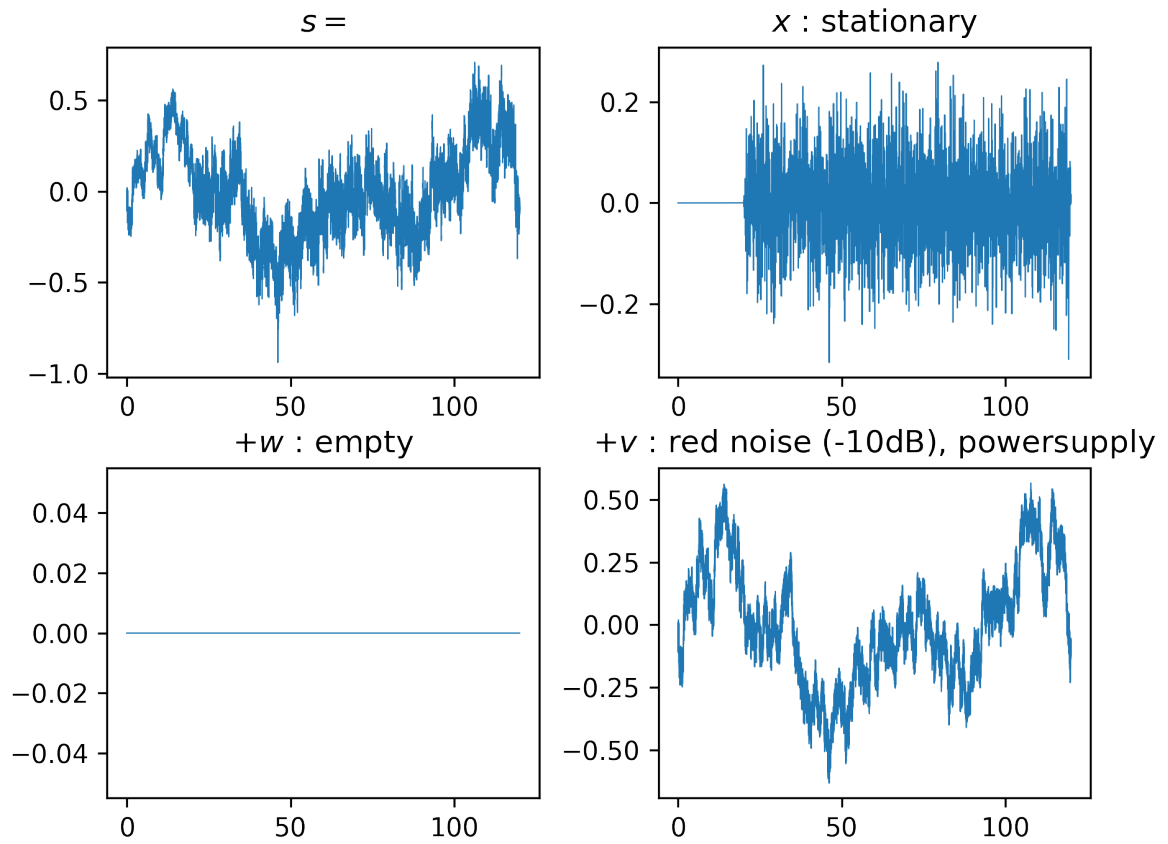


Figure G.16: Non stationary signal, with red noise.

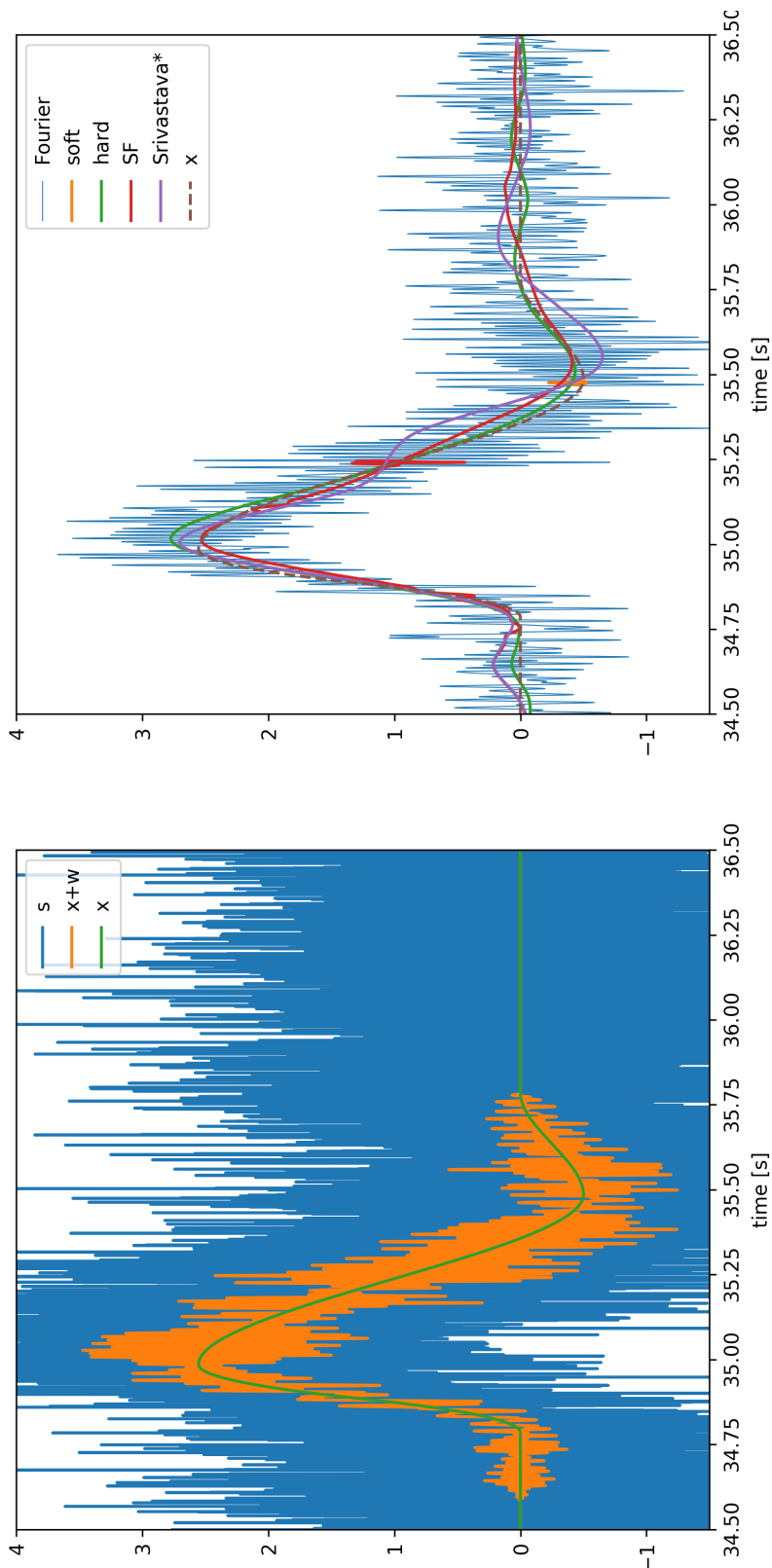
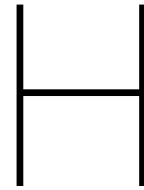


Figure G.17: A peak in the non-stationary noise case, with SNR=-10 dB, measurement noise and power supply noise. On the left the original signals, on the right the filtered results.



Compare techniques

This appendix supports the result in Appendix 5. The signals used to compare the different techniques are presented in the first section of this chapter. In the second section some supporting figures are shown.

H.1. Signals

H.1.1. Westerschelde

This set of measurements comes from the Westerschelde, a river in the Netherlands. This are the values over the year 2016, from the gauge at Walsoorden. This data is made available via <https://waterberichtgeving.rws.nl/water-en-weer/dataleveringen>.

H.1.2. WL657585e

Hier uitleg over signaal Data van Jan, golf onder spectrum

H.1.3. A3W1T304

Hier uitleg over signaal Data van Alex, eerste signaal gekregen

H.2. Figures

H.2.1. Separating waves

Signal	WL657585e	
Wavelet	Morlet	Parameter
Sampling freq	20.0	Duration
Determined at gauge	35.92	60
Using gauges	[35.92 36.47 36.69]	8699.95 sec = 144.9991666
Wavenumber	dispersion	with water depth
No of steps CWT	150	[0.6602 0.6618 0.6616 ...,
Determinant limit	0.1	p_max
p_min	1E-01	3.220643E+02
RMSE reconstruction sum	Fourier 2.676379E-16 1.201751E-01	Wavelet 1.200836E-01 1.292706E-02
Ref.cff.	Fourier 2.553696E-01 2.883003E-03 1.880111E-04	Wavelet 2.562337E-01 3.009569E-03 1.975953E-04

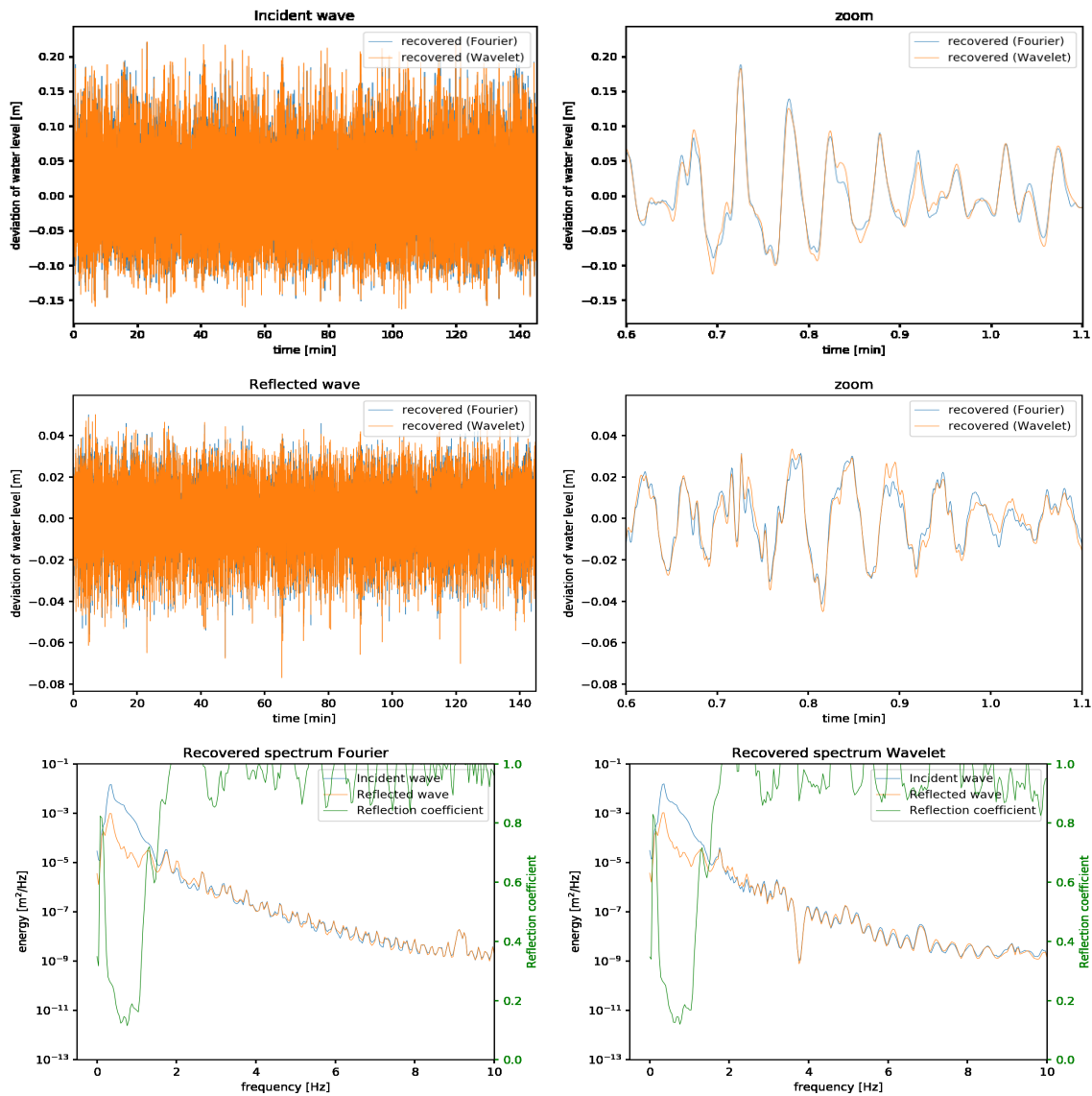


Figure H.1: Separating waves for non-stationary signal from coastal engineering, determinant limiter 0.1 (Morlet 60 wavelet)

Signal	WL657585e_250steps		
Wavelet	Morlet	Parameter	60
Sampling freq	20.0	Duration	8699.95 sec = 144.9991666
Determined at gauge	35.92		
Using gauges	[35.92 36.47 36.69]		
Wavenumber	dispersion	with water depth	[0.6602 0.6618 0.6616 ...,
No of steps CWT	300		
Determinant limit	0		
p_min	1E-01	p_max	3.220643E+02
RMSE reconstruction sum	Fourier 2.676379E-16 5.083595E-03	Wavelet 1.19493E-01 5.025583E-03	
Ref.cff.	Fourier 9.991147E-01 2.789107E+01 2.784171E+01	Wavelet 4.26688E-01 3.348221E-03 6.09586E-04	

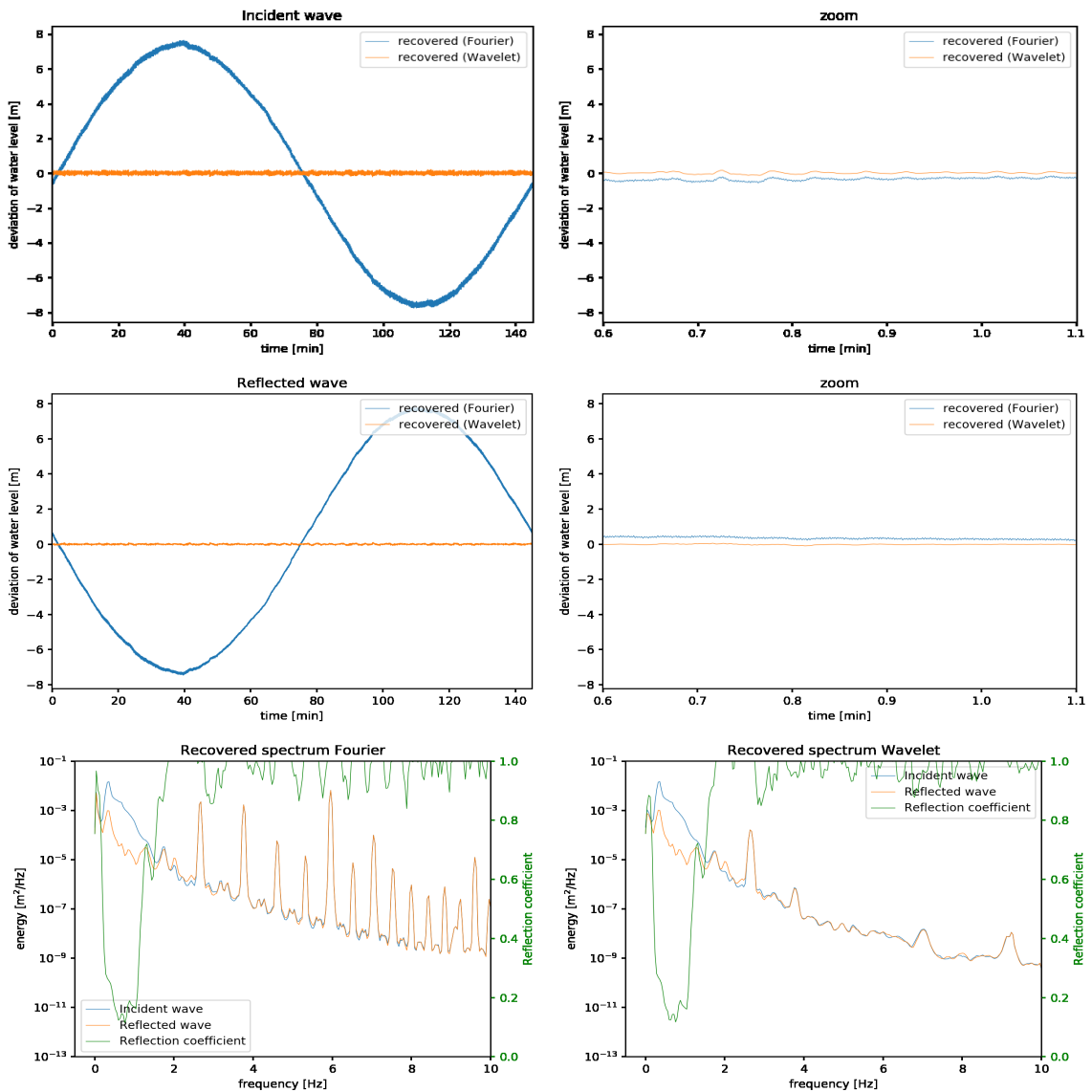


Figure H.2: Separating waves for non-stationary signal from coastal engineering, without determinant limiter. (Morlet 60 wavelet)

Signal	WL657585e_250steps		Parameter	60
Wavelet	Morlet		Duration	8699.95 sec = 144.9991666
Sampling freq	20.0			
Determined at gauge	35.92			
Using gauges	[35.92 36.47 36.69]			
Wavenumber	dispersion		with water depth	[0.6602 0.6618 0.6616 ...,
No of steps CWT	300			
Determinant limit	0			
p_min	1E-01		p_max	1E+01
RMSE reconstruction sum	Fourier 2.676379E-16 1.201393E-01		Wavelet 1.200272E-01 5.084425E-03	
Ref.cff.	Fourier 4.962071E-01 3.579397E-03 8.813242E-04		Wavelet 2.627414E-01 2.973176E-03 2.052475E-04	

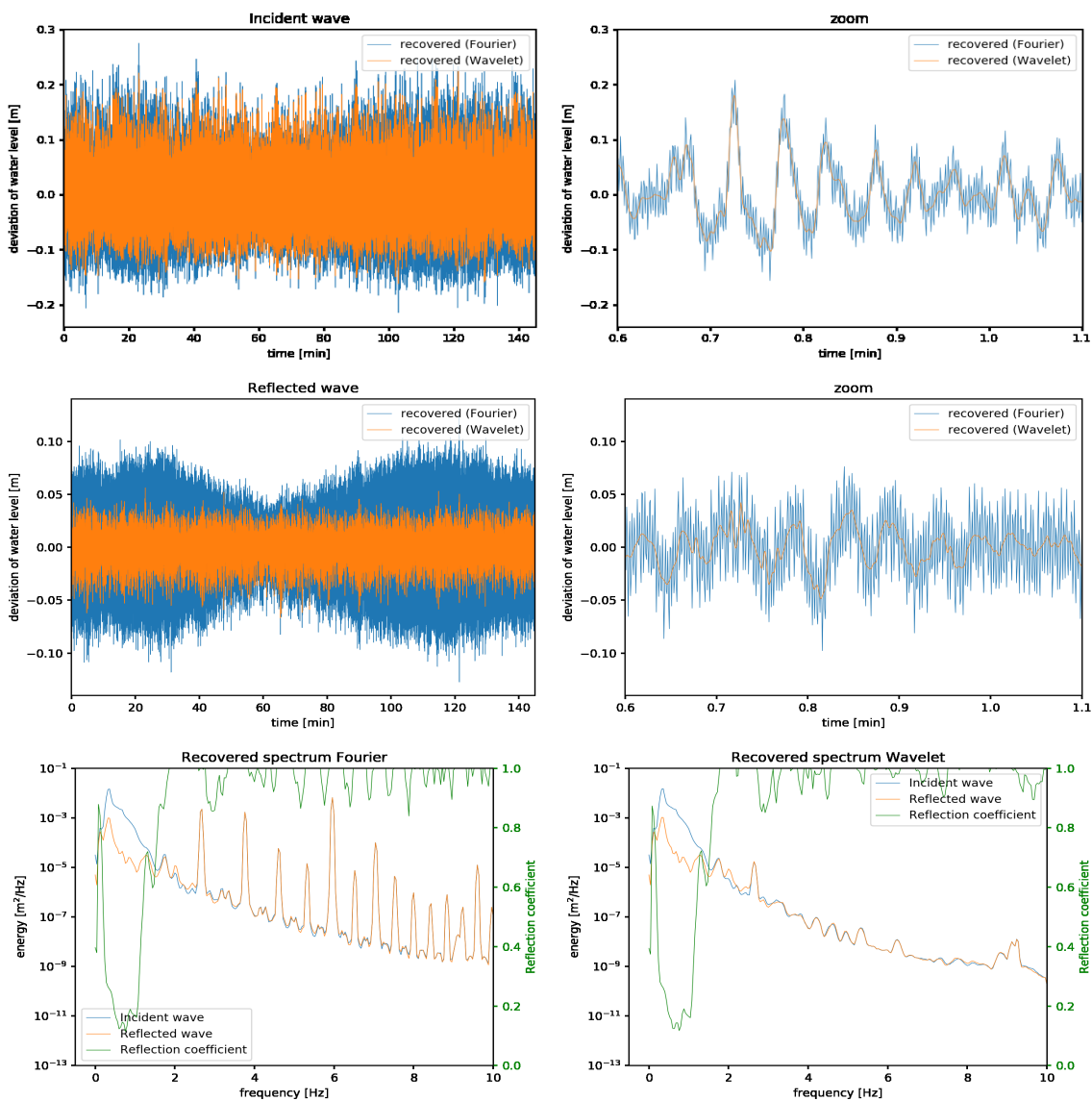


Figure H.3: Separating waves for non-stationary signal from coastal engineering, without determinant limiter. Maximum period of 10 seconds imposed. (Morlet 60 wavelet)

H.2.2. Filters

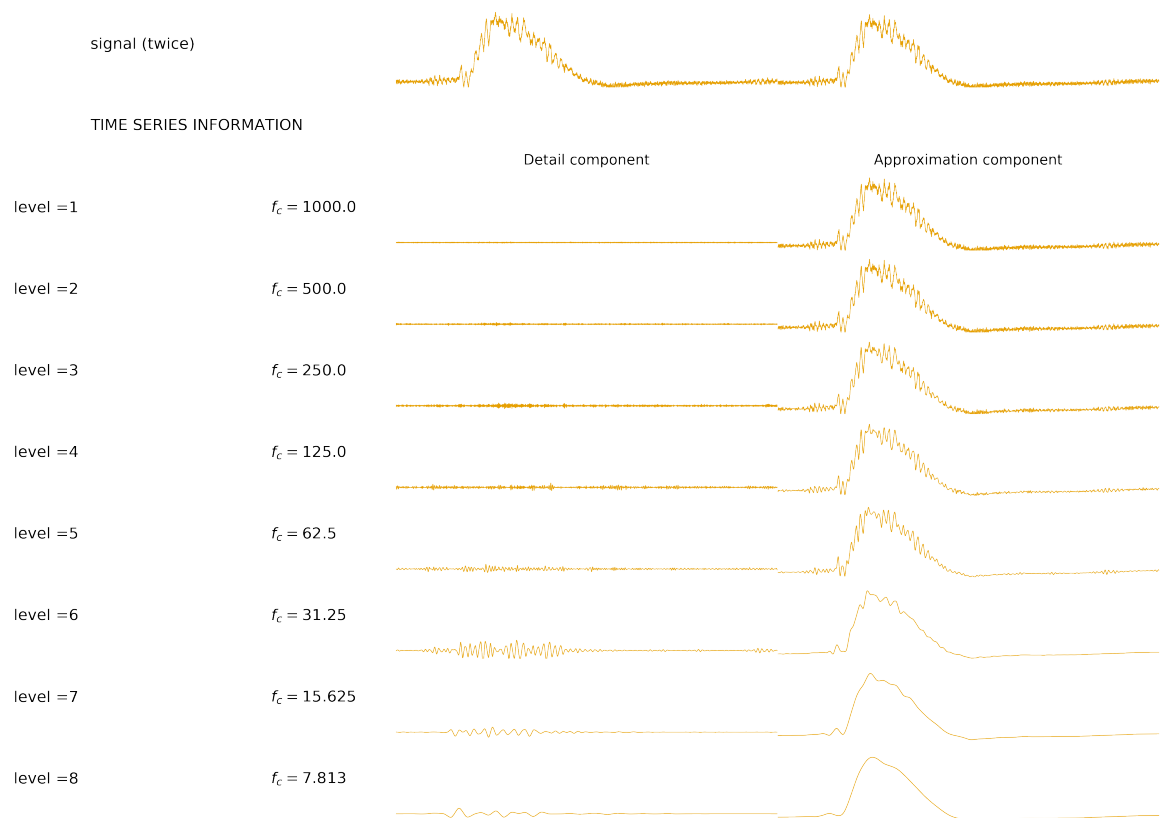


Figure H.4: The approximation and detail levels transformed to signals for force measurement. Note that the resonance frequency on the peak is mostly contained in detail level 6 and 7. (Discrete Wavelet Decomposition using the Symmlets 8 wavelet, upto level 8)

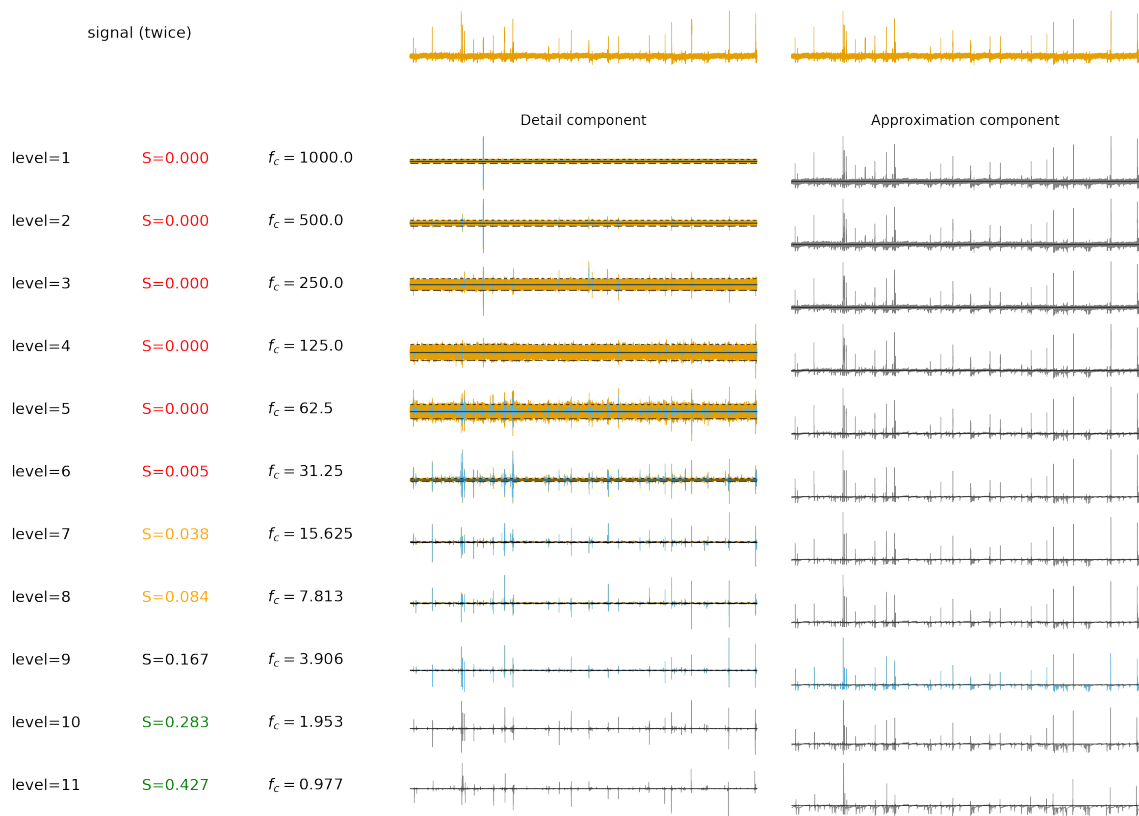


Figure H.5: Discrete wavelet filter based on noise in first 10 seconds of signal. (Discrete Wavelet Decomposition using the Symmlets 8 wavelet, upto level 11)

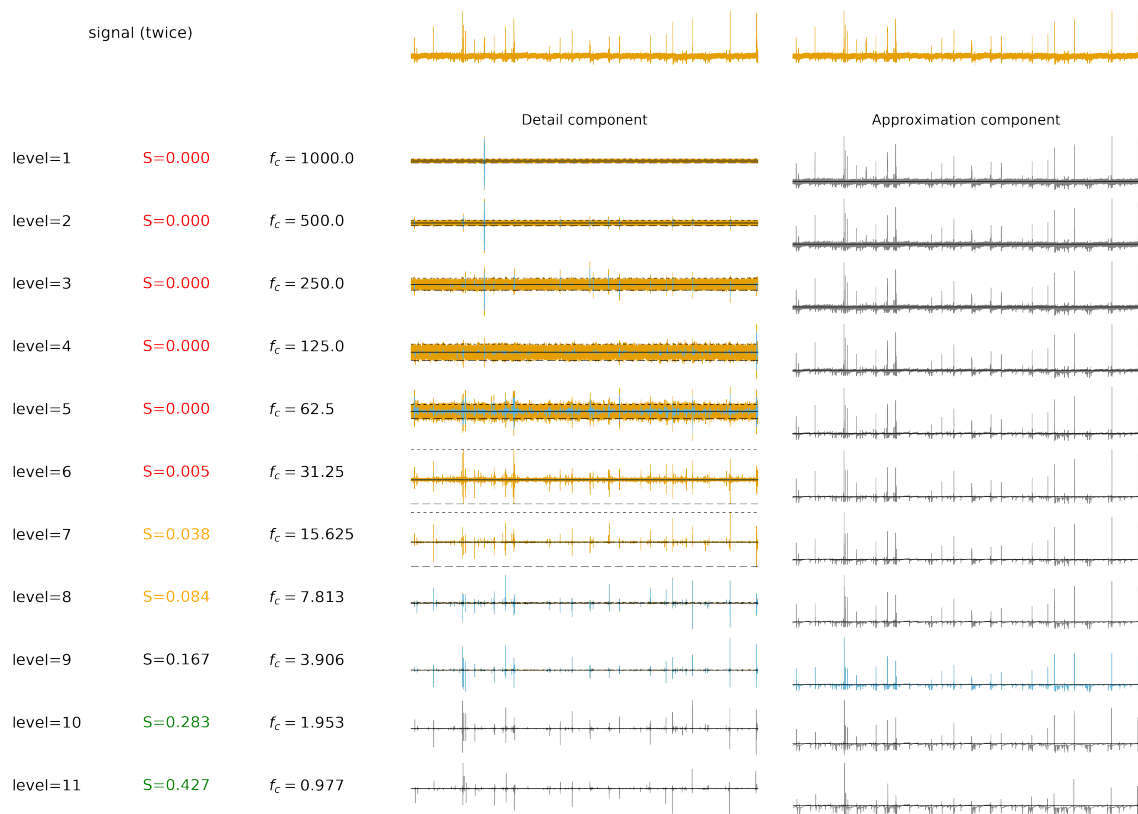


Figure H.6: Discrete wavelet filter based on noise in first 10 seconds of signal. Detail level 6 and 7 are filtered out (see Figure H.4). (Discrete Wavelet Decomposition using the Symmlets 8 wavelet, upto level 11)



Figure H.7: Discrete wavelet filter to filter transient for signal presented in Figure 5.7a. (Discrete Wavelet Decomposition using the Symmlets 8 wavelet, upto level 9)